Phonon transport in the quantum regime

Adib Tavakoli-Ghinani

Communauté
UNIVERSITÉ Grenoble Alpes

THÈSE

Pour obtenir le grade de

DOCTEUR DE LA COMMUNAUTÉ UNIVERSITÉ DE GRENOBLE ALPES

Spécialité : **Physique de la Matière Condensée et du Rayonnement**

Arrêté ministériel : 25 mai 2016

Présentée par

Adib TAVAKOLI-GHINANI

Thèse dirigée par **Olivier BOURGEOIS,** Directeur de recherche**, Institut Néel / CNRS**

Préparée au sein de l'institut Néel
dans **l'École Doctorale de Physique de Grenoble**

Transport de phonons dans le régime quantique

Phonon transport in the quantum regime

Thèse soutenue publiquement le **14 Décembre 2017**,
devant le jury composé de :

Monsieur Hervé Courtois
Professeur, Institut Néel / CNRS, Président
Monsieur Ilari Maasilta
Professeur, University of Jyväskylä, Rapporteur
Monsieur, Sébastian Volz
Directeur de Recherche, University of Tokyo, Rapporteur
Monsieur Eddy Collin
Chercheur, Institut Néel / CNRS, Examinateur
Monsieur Jean-François Robillard
Maître de Conférences, ISEN / IEMN, Examinateur
Monsieur Olivier Bourgeois
Directeur de Recherche, Institut Néel / CNRS, Directeur de thèse

To my parents, to whom I owe everything...

Dieu nie le monde, et moi je nie Dieu! Vive rien puisque c'est la seule chose qui existe!
— Albert CAMUS

Acknowledgements

After almost four years of adventure, there are plenty of people I would like to thank. The people without who this PhD could not have been done. First of all I would like to express my sincere gratitude to my supervisor Pr. Olivier Bourgeois, for giving me the opportunity to carry out my PhD project within your group. You weren't only a thoughtful supervisor, but also my best friend during these years. I admire the way you manage the TPS group, your vision to solve the problems, your kindness and sense of humor, and your encouragement and advice. I owe you all things I learned in my professional life and it has been a honor for me to have worked with you. I also appreciate each of our philosophical debates, book exchange, and our struggle to find the meaning of life. At least we know that "we can imagine *ourself* happy !"

I would like to thank Jean-luc Garden, for being always like a friend to me and support me. I appreciate all these moments with you, your sense of humor and your willing to do sports. As you always said: Il faut rien Lâcher, RIEN !!

I would like to thank Jacques Richard, I was always impressed about your personality and your knowledge. I really enjoyed discussing with you about scientific, cultural, historical, or political subjects. The TPS group is lucky to have such a scientist. Thanks to Dimitri Tainoff (*big daddy*). Your professional behavior in your work, and your friendly attitude to gather people together were always remarkable to me.

Regarding to the fabrication process, I should really thank Thierry Crozes. All I can say is that all these processes that we did over and over finally worth it. Thanks for being always available to help me especially for nanobeam lithography. I should thank Thierry Fournier, Jean-Francois Motte, Sébastien Dufresnes, Bruno Fernandez, Gwénaelle Julie and Latifa Abbasi (Nanofab group) for their technical help and friendly behavior. I should mention that working with you was one the most joyful part of my PhD. I owe you a huge thank you for having tolerated me with all the wrong things I did (developing in Acetone, using the wrong resist, over etching the sample, etc.); Of course this is not the part that I'm proud of. I would like to thank Emmanuel André for always being available and helping me for evaporation process. I always endorse the quality of your work and your technical abilities. Thank also to Gael Moiroux as a members of pole Capteurs.

I should thank the whole group of TPS (*Teuf, Physique, Sport*). I have to confess that nothing just to see you, discuss with you was my biggest motivation to come to laboratory everyday (specially on Fridays). I would like to say that I am grateful to all of those with whom I have had the pleasure to work during these years. Each of the members of TPS group has provided me extensive personal and professional guidance and taught me a great deal about both scientific research and life in general. I know leaving you will be one the most difficult thing I'm gonna encounter. I'll miss every second we past together, searching for an excuse to gather together or celebrate some events. I would like you to know that you are more than just a simple collaborator to me.

I should thank the UBT group members specially Eddy Collin. Eddy, I'm really impressed about your social and scientific attitude. I really enjoyed talking with you and mostly use your very constructive ideas related to our project. For the publications and my thesis you always gave me innovative suggestions.

One of the most important part of my project is done thank to the technical facilities. I would like to thank each member of the pôle Cryogénie and Mécanique for helping me to solve any problem related to cryostat. Finally we found the leakage of my dilution after six months. All I can say is that God bless you. A huge thank to Pierre Brosse for his attitude. Even if I didn't directly worked with you, your advices helped me a lot. I admire you behavior and the way you are. It was an honor for me knowing you and of course seeing you every Wednesday at 11h in musculation room. For me you will be always the one who broke Jean-Luc's record (I know this discussion will never ends). I would like to thank Jean-Seb Roch and Bernard Maire-Amiot and other members of pôle informatique. Each time I had any kind of problem you solved in the earliest delay. A big thank to Olivier Exshaw, and Christophe Guttin and any other members of the pôle electronique. Without the low noise electronic equipments they have developed, it was absolutely impossible to do such precise measurements. Every time I had a problem with electronic signals or Labview program, you were always present. I am really lucky to be in such environment equipped with all these high quality technical facilities.

I would like to express my gratitude to Mathilde Berard. You always helped me for all the documents we should provide before and after each mission, in the earliest delay and always having a smile. Thanks to Cécile for her constructive advice for poster presentation, and interesting cultural discussion we had. A big thank to Christine and Élodie for your infinite kindness and helping me for administrative documents. Thank to Pascal Lejay, Abdel and Joel for your friendly behavior full of interesting discussion. Thank to Aviad for your friendly behavior with your attitude that is a passionate scientist. Thank to Pierre Lachkar for your sympathy and humanism behavior.

During this PhD, the life in laboratory was just half of the time; It's somehow unfair not to speak about the magnificent moments that we had with the best dudes in the best bars. I would like to give a special thank to Tiphaine, Clothilde and Olivier. We started all together, and now one after another we are finishing our PhD. It seems that it was just yesterday we were gathering together to celebrate the beginning of our PhD (*beauté de la science*), and now we are celebrating its end. But the good point about friendship is that there is no end in it. I would like to thank all my best dudes, Jessy, Céline, Anaïs, Antoine, Ibo, Hugo, Kevin, Rahul, Laure, Pierre, Dhruv, Tuyen and everyone else that I has passed some memorable moment. I can say thank to the whole generation of *RASACA*. You made me feel what does it mean to have real friends. I own you guys. Respectively, I should thank our third houses as well: Emile, Korner pub, le Hasard, Loco Mosquito, and Barberouse.

I owe my deepest gratitude to my parents. I owe you everything I have. Thank you for being here, thank you for believing in me while I didn't believe in myself. You made me what I am now. You are my everything. I must express my emotions to my lovely wife Azadeh for her continued support and encouragement. I must say that you are the only one who experienced all of the ups and downs of my PhD; my countless experiments, my endless headaches, working during the weekends. I would like to confess that you gave

me unending inspiration. Thanks for being with me. I cannot even imagine how my life will be without you. I would like to thank the one who was with me during this last five years since I came to France, my big brother Iman. From the first day I came to France until now, you supported me in any condition. I own you a lot brother.

There are plenty of people who are far from here, but they mean a lot to me. Thank to all my family and friends in Iran. A special thank to Misagh, Mona, Omid, Mohamad reza (*daaanaaa*), Samira and Farhad for regularly calling me, thinking about me, and giving the feeling that I'm not forgotten. Thank to our new family member Baran. A huge thank to every member of the *Ch.T* group. I should thank also Marie-Claude and Henriette for their continuous support during all these years.

Thank to my loyal dude Farzad. Even thought we didn't see each other that much, but that was enough to realize how close we are, that at least another person think like you, and help you to evaluate your thoughts. Thank to my adventuress friend Tony (*... T.Rex*). The most interesting thing about you is that we can do endless crazy stuff together at any time, at any age.

I want also thank Klaus HASSELBACH director of MCBT departement for his serious and supportive attitude. I would like to acknowledge the financial support from the European project MERGING.

I finally want to thank my hero, *Albert Camus.* The most amazing thing that happened to me during these years was finding myself. Albert Camus showed me the line and faced me to what I really am.

I think it's over. One big beautiful adventure full of ups and downs with memorable sensory emotions, friendship and happiness is coming to its end; and some others are just beginning.

Adib TAVAKOLI
Grenoble, Janvier 2018

Résumé

Ce travail de thèse est consacré à la mesure de *transport de chaleur par les phonons dans le régime quantique* dans des systèmes confinés à très basse température. Le contexte de ce sujet est de soumettre ces systèmes à deux conditions extrêmes : basse température et faibles dimensions et de comprendre les propriétés thermiques fondamentales issues de ces limites. Les échantillons étudiés sont des structures suspendues (membrane ou nanofil) ; elles sont élaborées à partir de nitrure de silicium amorphe (SiN).

En abaissant la température, les longueurs caractéristiques des phonons comme le libre parcours moyen ou la longueur d'onde dominante des phonons augmentent. Lorsque ces longueurs caractéristiques dépassent les dimensions latérales du système, la diffusion sur les surfaces (boundary scattering) régira les propriétés thermiques. Dans cette limite de diffusion, le transport des phonons va de la diffusion aux surfaces (régime de Casimir) au régime balistique (limite quantique). Dans ce régime balistique, le courant de chaleur peut être exprimé en utilisant le modèle de Landauer. La conductance thermique est alors exprimée par: $K = N_\alpha q \mathcal{T}$ où, N_α est le nombre de modes vibratoires peuplés, $q = (\pi^2 k_B^2 T/3h)$ est la valeur universelle du quantum de conductance thermique et $\mathcal{T}$ est le coefficient de transmission. Dans ce travail, les mesures de conductance thermique de nanofils suspendus ont été effectuées jusqu'á très basse température. Une plate-forme de mesure ayant une sensibilité sans précédent a été développée pour mesurer la variation d'énergie inférieure à l'attojoule. Ces nouveaux capteurs permettent de mesurer les propriétés thermiques du guide d'onde de phonon 1D dans le régime quantique du transport de chaleur. Nous montrons que le coefficient de transmission est le facteur dominant qui définit la valeur de conductance thermique. Ce coefficent dépend de la dimension et de la forme des réservoirs ainsi que de la nature du matériau utilisé ce qui rend difficile la mesure du quantum de conductance thermique. Nous montrons que dans toutes les structures de SiN mesurées, le transport thermique pourrait être dominé par des excitations de faible énergie qui existent dans les solides amorphes (a-solides).

Le deuxième ensemble important d'expériences concerne la chaleur spécifique. Nous avons étudié les propriétés thermiques de membranes suspendues très minces de SiN que (des cavités de phonon 2D). Nous montrons que la dépendance en température de la chaleur spécifique s'écarte du comportement quadratique comme prévu á très basse température. La présence de systèmes à deux niveaux dans les matériaux amorphes pourrait être une explication possible de la valeur absolue élevée de la chaleur spécifique observée.

Abstract

This PhD entitles *Phonon transport in the quantum regime* is based on the analysis of the thermal properties of confined systems at very low temperature. The objectives of this subject are to put the systems (membrane or nanowire) in two extreme conditions (low temperature and low dimensions) and understand the fundamental thermal properties coming from these criteria. By lowering the temperature, the phonon characteristic lengths like the mean free path (MFP) or the phonon dominant wavelength increase. When these characteristic lengths exceed lateral dimensions of the system, the boundary scattering will govern the overall thermal properties.

In 1D channel between two reservoirs, when the phonon MFP is bigger than the length of the system ($\Lambda_{ph} > l$), and the phonon wavelength is bigger than the section ($\lambda_{ph} > d$), the phonon transport is ballistic. In such case, the phonons are transmitted from one reservoir to the other one when they are kept at different temperatures. The thermal conductance is then expressed as: $K = N_\alpha q \mathcal{T}$ where N_α is the number of populated vibrational modes, $q = (\pi^2 k_B^2 T/3h)$ is the universal value of the quantum of thermal conductance, and $\mathcal{T}$ is the transmission coefficient. We show that the transmission coefficient is the dominant factor that will set the thermal conductance value. It depends on the dimension and the shape of the reservoirs, and the nature of the material in use.

The measurements of specific heat of 2D suspended phonon cavities with different thicknesses show the transition of specific heat from volumetric to surface effect. Below 1 K, when the phonon dominant wavelength becomes bigger than the thickness of the membranes, the specific heat is only governed by the surfaces. In another experimental achievement the effect of internal stress on specific heat of 2D phonon cavities was investigated. It was found that the internal stress has an inverse relation with the formation of the localized excitations that exist in amorphous solids (a-solids) at very low temperature. By decreasing the internal stress, the formation of these excitations are enhanced, so the heat capacity increases. According to our experiments, we believe when the phonon transport is governed by boundaries, the high contribution of TLSs on the surfaces will dominate the thermal properties.

Contents

Acknowledgements

Résumé

Abstract

Contents

List of tables

Introduction **1**

1 Theory of phonon transport in nanoscales at low temperatures **3**
1.1 Introduction . . . 3
1.2 Notion of phonon . . . 4
1.2.1 Phonons dispersion relations . . . 4
1.2.2 Phonon characteristic lengths . . . 7
1.3 Thermal properties . . . 9
1.3.1 Specific heat . . . 10
1.3.2 Thermal conductivity and thermal conductance . . . 11
1.4 The confinement effects . . . 13
1.5 The effects of confinement on phonon transport at low temperatures . . . 14
1.5.1 The Casimir model . . . 14
1.5.2 The Ziman model . . . 16
1.5.3 Fully ballistic regime and the universal quantum of thermal conductance . . . 19
1.6 The effects of confinement on specific heat at low temperatures . . . 23
1.7 Vibrational excitations of amorphous solids . . . 25
1.7.1 Two-Level Systems . . . 26
1.7.2 Specific heat . . . 27
1.7.3 Thermal conductivity . . . 29
1.8 Nanophononics . . . 31
1.9 Conclusion . . . 33

2 Sample fabrication and experimental techniques for measurement of thermal conductance **35**
2.1 Introduction . . . 35
2.2 State of art of calorimetry . . . 36
2.3 Sample preparation . . . 36

2.4 Fabrication of Si_3N_4 membrane-based nanocalorimeter . . . 37
2.4.1 Current leads . . . 37
2.4.2 Heater . . . 39
2.4.3 Thermometer . . . 39
2.4.4 Etching processes . . . 40
2.5 Bridging Si_3N_4 nanowires between double suspended nanocalorimeter . . . 42
2.5.1 E-beam lithography . . . 42
2.6 Thermometer characterisation . . . 44
2.7 Specificity of NbN thermometry at low temperature . . . 45
2.8 Thermal conductance measurements on nanoscale systems . . . 53
2.8.1 Dynamical method . . . 54
2.8.2 Steady-state method . . . 55
2.8.3 Measurement setup . . . 56
2.8.4 Noise characterisation . . . 61
2.8.5 Measurement of noise . . . 64
2.9 Conclusion . . . 65

3 Phonon heat transport in 1D quantum channel 67
3.1 Introduction . . . 67
3.2 Experimental achievements . . . 69
3.3 Comparison with theoretical models . . . 71
3.3.1 Mean free path analysis . . . 72
3.4 Transmission coefficient . . . 75
3.5 Possible scenarios for the non-perfect transmission coefficient . . . 75
3.5.1 Dependence of the transmission coefficient on the shape of the junctions . . . 76
3.5.2 Thermal contact resistance between 1D nanowire to 2D reservoirs . 77
3.5.3 The cutoff frequencies of transmission coefficient . . . 78
3.5.4 Dependence of the transmission coefficient on the length of nanowire 79
3.5.5 Role of Two-Level Systems on the transmission coefficient . . . 80
3.6 Comparison of the present results to anterior experiment by K. Schwab *et al.* 84
3.7 Conclusion . . . 87

4 Heat capacity of 2D phonon cavities 89
4.1 Introduction . . . 89
4.2 Theoretical prediction for specific heat of 2D phonon cavity . . . 90
4.2.1 Elastic continuum model . . . 90
4.2.2 Low temperature specific heat of amorphous solids . . . 91
4.3 Low temperature measurement of specific heat . . . 92
4.3.1 ac calorimetry . . . 92
4.3.2 Measurement setup . . . 96
4.4 The measurement of low temperature heat capacity . . . 98
4.4.1 Data treatment . . . 99
4.5 Effect of stress on heat capacity . . . 104
4.6 Tunneling states in tetrahedrally bonded materials . . . 107

4.7 Conclusion 108

5 Thermal rectification **111**
5.1 Introduction 111
5.2 Thermal rectification by asymmetric mass gradient 112
5.2.1 Experimental achievement 113
5.3 Thermal rectification by asymmetric nanostructured geometry 116
5.4 Conclusion 116

Conclusion **118**

Bibliography **121**

Contents

List of Tables

1.1 **Classification of the different regimes of phonon transport.** This classification represents possible scenarios of phonon transport in nanoscaled systems, from boundary limited regime to fully ballistic transport of phonon at low temperature. L is the length of the sample, Λ_{ph} is the phonon mean free path, and λ_{dom} is the phonon dominant wavelength. Concerning the Landauer limit, the parameter $\mathcal{T}$ denotes the transmission coefficient between a nanowire and its heat reservoirs [1]. 21

2.1 Noise calculation for the measurement of the thermal conductance of the nanowires between the two nanocalorimeters. 65

3.1 Details of the dimensions of the four different kinds of samples made out of Si_3N_4 thin films: sample types and their width $\mathcal{W}$ and length L and thickness t. . . . 82

4.1 The calculation of the heat capacity of the heater and the thermometer on the nanocalorimeter. The heat capacities and the specific heats are calculated for T=1 K. 101

4.2 Parameters for high-stress (HS), low-stress (LS), and super low-stress (SLS) SiN_x. ρ is the density of material, n_0 is the TLS density of states, and P_c is the temperature exponent of the measured heat capacity below 1 K. 105

5.1 The dimensions and the masses of deposited material on each side of nanowire. The thickness of deposition is estimated $t = 70 \pm 30$ nm. 114

List of tables

Introduction

From the development of micro and nanoscale fabrication techniques a broad scientific and technical revolution has emerged. Miniaturization of macroscopic systems has enabled the scientist (especially in the condensed matter community) to control and manage the properties by designing the structures of one system whose functionality is favored. Furthermore, in terms of fundamental physics, nanoscale systems have broadened the integration between quantum and classical physics. In other words, fabricating devices much larger than the atomic scale (from nanometer to micrometer) exhibiting quantum effects has become possible.

Decades of research have been successfully dedicated to nanoengineering for electronic and optical applications. It is only recently that these concepts are applied to heat transport with envisioned applications of nanostructure to engineered thermal properties. In computer processors for information technology, thermoelectric systems, and even energy performance of almost any kind of electronic device, the thermal properties need to be managed, and may become a dominant factor in energy conversion technology. For instance, perceiving the fundamental effect of quantum confinement on the thermal properties of ceramics or semiconducting materials that are vastly applied in various solid-states applications, can be an effective step toward future advancement. In such materials, the thermal behaviors are generally governed by phonons.

Phonons have a wide variation in their characteristic lengths as a function of temperature and materials: the wavelength, and the mean free path. When the phonon coherent length scales become larger than the microstructural length scales of a material, phonon interference effects lead to modified dispersion relation, group velocity, and spectral density. Hence, understanding the concept of quantum confinement effects on the thermal properties raises important conceptual issues among which is the transition from classical to purely quantum limit of heat conduction, or investigating the predominant factor in specific heat of systems of restricted dimensions. The framework of analyzing the phonon properties within nanostructured systems is called *nanophononics*.

This PhD work focuses on the experimental analysis of the thermal properties of nanoscale systems (1D, 2D) in the quantum limit. The objective is to probe and understand the mysterious aspect of quantum effects on the thermal properties in extreme conditions. In this objective several important criteria should be fulfilled. First of all, in order to do a precise analysis on the thermal properties, the system under study should be thermally isolated. The isolation of small systems can be enhanced if they are me-

chanically suspended. Another important feature is that the quantum limit of thermal properties appears when the dimension of the system is far below of the phonon characteristic lengths. To do so, two extreme conditions should be applied: the system under study should be miniaturized, and the phonon characteristic lengths should be maximized. In order to maximize the coherent length scale of phonons, it is necessary to work at very low temperatures. In addition, the measuring part of the system (sensors), and all the electronic facilities should have a very high sensitivity, and to be adapted to the temperature range of the study.

Here we will present an experimental investigation of the thermal properties of confined structures in the quantum limit: the thermal conductance and the heat capacity. In the first chapter, a theoretical overview on the physics of thermal properties in low dimensions and low temperature is presented. The second chapter is dedicated to the technical aspect of the experiment. The experimental setup for the measurement of thermal conductance and specific heat are explained. The fabrication processes including each step of the fabrication, the design of geometry of the system, and the choice of the used material is detailed.

Chapter 3 presents an in-depth discussion on the experimental achievements of heat conduction through 1D phonon waveguides in a purely quantum regime. The predominant features of heat exchange through a 1D channel between two reservoirs will be discussed. The dependence of ballistic phonon transport on the details of the structure of 1D channel, the shape of the contacts, the coupling of 1D channel to 2D reservoirs, the cutoff phonon frequency, and the nature of the material will be reviewed as well.

In chapter 4, the experimental results of the specific heat of 2D phonon cavities at very low temperature are presented. The effect of confinement on heat capacity with the transition from volumetric to surfaces effects is probed. Finally, the effect of internal stress on enhancement of the absolute value of heat capacity is investigated.

Chapter 5 is focused on the potential applications that exist in terms of thermal management (thermal rectification) in the ballistic limit of heat conduction. A primarily experiment on thermal rectification with asymmetric mass gradient is presented. At the end possible methods to attain a thermal rectifier systems via asymmetric nano-engineered are also presented.

1 CHAPTER

Theory of phonon transport in nanoscales at low temperatures

1.1 Introduction

The potential applications of thermal properties by nanostructures have attracted lots of interests during the last decades. Indeed, the reduction of the size alters the properties of the system if the characteristic length scales of heat carriers are within the dimension of the system. These characteristic lengths are known as the mean free path MFP and/or wavelength of heat carriers (either electron or phonon). The effects coming from a decrease in the size of devices will cause an increase in their operating speeds, frequencies, and will change the density of states related to the heat carriers [2]. The heat carriers in solid state physics are known as electrons, photons, and phonons which their contribution can vary according to the material nature. For instance, in semiconductors and insulators, the dominating heat carriers are the phonons.

The confinement can alter the thermal properties of a system either in the case of heat diffusion, thermal transport or energy storage. These modifications will not be fulfilled by classical laws. In addition, low-temperature nanoscale thermal properties are more complex because of the dependence of the characteristic length scales of heat carriers on temperature. These characteristic lengths can exceed not only the section of the system but also the length of the device. This is where quantum effects of heat carriers will govern the thermal properties [3].

At low temperature, in an insulator, the only heat carriers are phonons. To have a better understanding of phonons within a confined system, especially, at low temperature one needs to have the perceptual insight of nanoscale heat transport at low temperature; from classical to purely quantum effects.

In this chapter, firstly, the concept of phonon will be introduced to study heat transport

and heat storage. Then, a broad explanation on the mechanism of heat transport at low temperature and low dimensions are presented. In the end, the physics of the fundamental properties of disordered structures at low temperature is presented as well.

1.2 Notion of phonon

Phonons are elementary excitations with the quantum of energy $\hbar\omega(\boldsymbol{q})$ ($\hbar$ is the Planck constant, and ω is the frequency of vibration of phonons) arising from collective simple harmonic oscillations of atoms about their equilibrium sites in crystalline solids at wavevector $\boldsymbol{q}$. In fact, a phonon is a quantum of crystal vibration and it is considered as quasi-particle of zero spin. Thus the energy of the normal modes of a crystal are defined as: $U = (n_{BE} + \frac{1}{2})\hbar\omega(\boldsymbol{q})$. n_{BE} is the Bose-Einstein distribution function, which defines the average number of phonons at a given temperature T of the crystal. it is given by [3]:

$$n_{BE} = \frac{1}{\exp\left(\hbar\omega(\boldsymbol{q})/k_B T\right) - 1} \tag{1.1}$$

where k_B is the Boltzmann constant. From the expression, it is clear that at $T = 0$ K there are no phonon in a crystal. At low temperature where $\hbar\omega \gg k_B T$, $n_{BE} \cong \exp(-\hbar\omega/k_B T)$ and there is an exponentially small probability for a phonon to be present. Thus, the number of vibrational channels of phonons is highly reduced at low temperature. At high temperature $\hbar\omega \ll k_B T$, $n_{BE} \cong k_B T/\hbar\omega$ and the number of phonons increases linearly with temperature [2].

1.2.1 Phonons dispersion relations

Phonon dispersion relations establish a relation between the frequency of ω and the wave vector $\boldsymbol{q}$. These relations are essential ingredients for understanding a large number of properties of 3D solids, surfaces, and nanostructured materials [4]. They can either be measured by neutron scattering or to be calculated from lattice dynamics theory.

The description of lattice vibrations starts by considering a monoatomic linear chain on an infinity large number N of identical elementary atoms separated by a distance (see Fig. 1.1). The individual potential energies from each compressed or expanded spring are evaluated as the harmonics potential U^{harm}.

$$U^{harm} = \frac{1}{2} g\Sigma \left\{u[na] - u[(n+1)a]\right\}^2 \tag{1.2}$$

When the atoms vibrate, they move from their equilibrium position. Then from Newton's second law and Hooke's law the equation of displacement for n_{th} atom is described as:

$$F = m\frac{d^2 u_n}{dt^2} = -\frac{\partial U^{harm}}{\partial u(na)} = g\left[(u_{n+1} - u_n) + (u_{n-1} - u_n)\right] \tag{1.3}$$

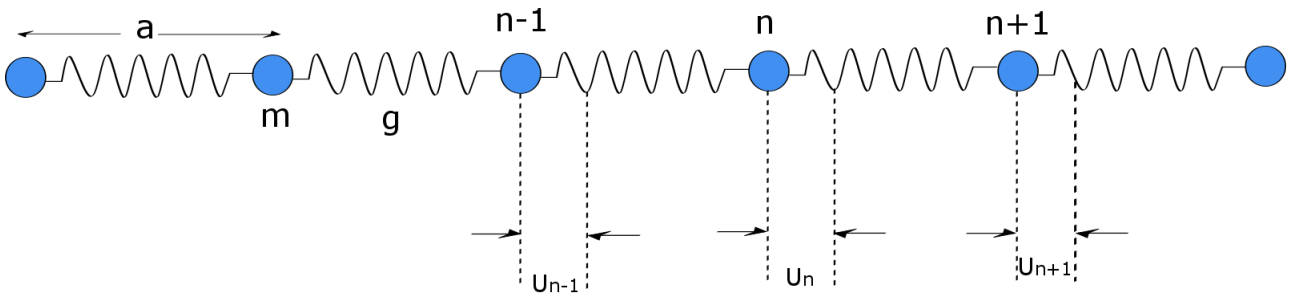

Figure 1.1: **Schematic monoatomic linear chain.** The lattice constant is a, and atomic mass m. For a spring constant g showing the displacement u_{n-1},u_n, u_{n+1} for the $(n\text{-}1)$th, nth, and $(n+1)$th atoms from equilibrium position.

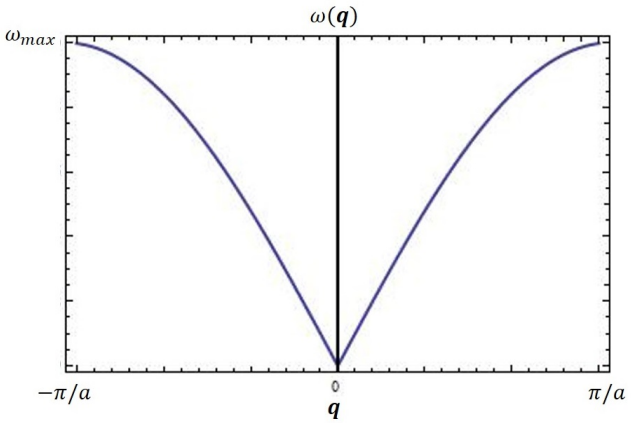

Figure 1.2: **Phonon dispersion relation curve for monoatomic linear chain.** This dispersion relation is presented in the first Brillouin zone between $-\pi/a$ and $+\pi/a$.

The periodic condition of Born-von-Karman that is given by $u_n = u_0$ and $u_{n+1} = u_n$ is applied. Then a plane-wave solution for displacement of harmonic oscillator at location n is considered as:

$$u_n(t) = A\exp\left[i(\boldsymbol{q}x - \omega t)\right] = A\exp\left[i(\boldsymbol{q}na - \omega t)\right] \tag{1.4}$$

Here A denotes the amplitude of the motion of n_{th} atom. By replacing the considered solution in equation 1.3, we have:

$$-m\omega^2 e^{[i(\boldsymbol{q}na-\omega t)]} = -g[2 - e^{-i(\boldsymbol{q}a)} - e^{i(\boldsymbol{q}a)}]e^{[i(\boldsymbol{q}na-\omega t)]} \tag{1.5}$$

$$= -2g\left[1 - \cos(\boldsymbol{q}a)\right] e^{i(\boldsymbol{q}na-\omega t)} \tag{1.6}$$

Therefore we have:

$$\omega^2 = \frac{2g}{m}\left[1 - \cos(\boldsymbol{q}a)\right] \equiv DA \tag{1.7}$$

D is called dynamical matrix and in this case is just a (1×1) matrix. Thus we can extract the dispersion relation as:

$$\omega = 2\sqrt{\frac{g}{m}}\ \mid \sin(\boldsymbol{q}a/2) \mid \tag{1.8}$$

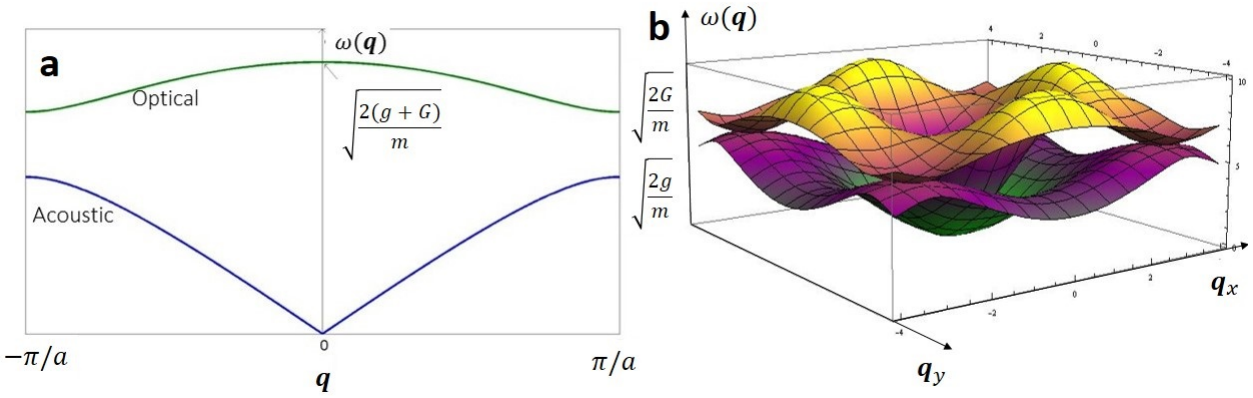

Figure 1.3: **Dispersion relations for a diatomic chain of atoms.** (**a**) The 2D plot that is representing optical (green line) and acoustic modes with Born-von Karman periodic limit (blue line). (**b**) The 3D plot of a dispersion relation of a diatomic chain of atoms.

This is the dispersion relation of the monoatomic chain of atoms with the periodic condition of Born-von-Karman. This dispersion relation has been plotted on Fig. 1.2. From this figure, we notice that the maximum frequency depends quite simply on the spring constant and atomic mass, as $\omega_{max} = 2\sqrt{g/m}$. The essential features of the lattice dynamics of crystals with the basis of more than one atom can be understood most simply by studying the dynamics of a diatomic linear chain, which can be viewed as a linear chain with a basis of two atoms. In this case, with two different interacting energies, the dispersion relation will have another branch. The phonons of this branch have a higher frequency and interact mostly with photons. Therefore the higher branch is referred to as optical phonons, and the lower branch is called acoustic, because it is responsible of the transport of sound.(see Fig. 1.3). The dispersion relation of a material is used to define the velocity of the heat carriers, phonons, or normal vibrational modes (eigenmodes) of the crystals. With use of dispersion relation we can extract three velocities: the group velocity ν_g, the phase velocity ν_ϕ and the sound velocity ν_s; which are:

$$\nu_g = \frac{d\omega}{d\boldsymbol{q}} \qquad \nu_\phi = \frac{\omega}{\boldsymbol{q}} \qquad \nu_s = \lim_{\boldsymbol{q}\to\infty} \frac{d\omega}{d\boldsymbol{q}} \tag{1.9}$$

At very low temperature environment, the phonon group velocity can be assumed constant and taken equal to the speed of sound. Also, in low temperature limit $k_B T \to 0$, so only the lowest vibrational modes are activated because $\hbar\omega \to 0$. This means that at low temperatures the optical branches are not populated. On the other hand, the phonon characteristic lengths depend on the temperature. The next section explains in details the effect of the temperature on these characteristic lengths.

1.2.2 Phonon characteristic lengths

To have a better understanding of phonon physics at low temperature in constricted dimensions, one should know the characteristic length scales of phonon. These characteristic lengths are described as the phonon mean free path (MFP), and the phonon dominant wavelength.

Mean free path

The phonon MFP is the average distance that a phonon travels between two successive inelastic collisions. Differently said, the phonon MFP is the traveled distance in which a phonon keeps its phase coherence. This value can exceed several millimeters below 1 K. In nanoscale systems at low temperature, the scattering is predominated by boundaries. The modification in the phonon MFP will change the thermal properties.

Dominant wavelength

The phonon dominant wavelength is an important parameter to calculate the total energy of phonons. It is also the crucial parameter that will define the regime of boundary scattering at very low temperature.

To calculate this physical parameter an approximation based on blackbody emission is applied to evaluate the spectral density of phonons. The principle is similar to blackbody emission of photons, with an energy density following Planck's law. According to this law, a blackbody emits isotropically all possible electromagnetic radiations at every frequency. It gives a spectral radiance peaked at a certain wavelength, indifferent of shape but determined by temperature only and the sound velocity inside of the material. The Planck's law expressed in term of wavelength λ takes the form:

$$B_\lambda(\lambda, T) = \frac{2h\nu_s^2}{\lambda^5} \frac{1}{e^{\left(\frac{h\nu_s}{\lambda k_B T}\right)} - 1} \tag{1.10}$$

where h the Planck constant, k_B the Boltzmann constant, ν_s is the speed of sound and T is the temperature. Fig. 1.4 shows the spectral density curves of phonons in Si_3N_4 (speed of sound 9900 m/s) at different temperatures. As temperature decreases, the maximum peak shifts toward higher value (red-shifting). This maximum peak is known as the phonon dominant wavelength, and it is given by:

$$\lambda_{dom} = \frac{h\nu_s}{2.82k_B T} \tag{1.11}$$

This length is indeed temperature dependent, increasing as the temperature decreases. It is worth mentioning that, below 1 K the maximum emission is by the wavelengths in

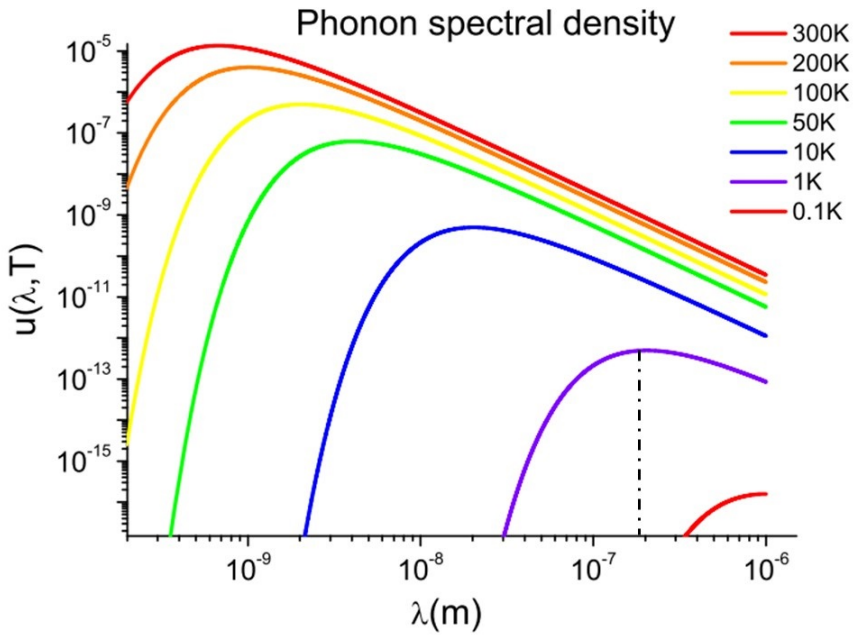

Figure 1.4: **Phonon spectral density as a function of the wavelength.** It is plotted for silicon nitride at different equilibrium temperatures of a black body. The dominant phonon wavelength for each temperature corresponds to the maximum of the curves. Typically, the dominant phonon wavelength is of the order of 1 nm at 300 K and 100 nm around 1 K [1].

order of several hundred nanometers. This means if the size of the section of a device (for example a nanowire) is below the phonon dominant wavelength $\lambda_{dom} > d$ (d is the section of the nanowire) at 1 K, then in the thermal properties, one should observe a transition from 3D to 1D.

Phonon density of states

Phonon density of states $D(\omega)$ is one the most important quantities in the definition of phonon. This quantity evaluates the number of states around a certain frequency (ω and $\omega+d\omega$), or wave vector ($\boldsymbol{q}$ and $\boldsymbol{q}+d\boldsymbol{q}$). The direction of the vibrations in a crystal cover the whole space, and so do the directions of the wavevectors. Thus the density of states in a bulk is proportional to a volume element. In a system with the dimension of d and the periodic condition of Born-Von-Karman $\boldsymbol{q}= 2n\pi/L$, where L represents the length of the system, the density of states in reciprocal space is described as:

$$D(\omega)d\omega = D(\boldsymbol{q})d(\boldsymbol{q}) = \left(\frac{L}{2\pi}\right)^d d\boldsymbol{q} \tag{1.12}$$

$d\boldsymbol{q}$ possesses the dimensionality d and represents the volume in reciprocal space. In the case of 3D geometry, it is a sphere with an internal diameter of q and an external diameter

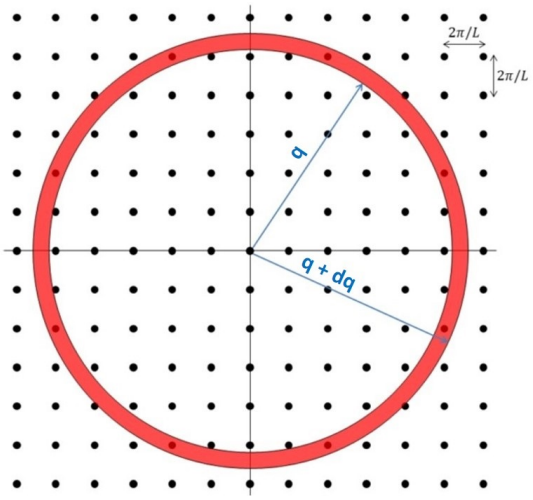

Figure 1.5: ***q*-space in 2D medium**. A square atomic network, the minimum separation between allowable wevevectors is $\left(\frac{2\pi}{L}\right)$. $\boldsymbol{q}$-space spherical volume (circular area for 2D) is depicted by red circles.

of $q+dq$. Fig. 1.5 shows $\boldsymbol{q}$-space in 2D medium, where $d\boldsymbol{q}$ are the allowable wavevectors. So for each dimension we have:

$$d\boldsymbol{q}_{3D} = 4\pi q^2 dq \tag{1.13}$$

$$d\boldsymbol{q}_{2D} = 2\pi q dq \tag{1.14}$$

$$d\boldsymbol{q}_{1D} = dq \tag{1.15}$$

Respectively the density of states for each dimension will be:

$$D(\omega)_{3D} = \frac{V}{2\pi^2} q^2 \left(\frac{d\omega}{dq}\right)^{-1} \tag{1.16}$$

$$D(\omega)_{2D} = \frac{S}{2\pi} q \left(\frac{d\omega}{dq}\right)^{-1} \tag{1.17}$$

$$D(\omega)_{1D} = \frac{L}{2\pi} \left(\frac{d\omega}{dq}\right)^{-1} \tag{1.18}$$

Now based on the DOS of each dimension, we can evaluate the expected thermal properties.

1.3 Thermal properties

The thermal properties of a solid are set by the physics of phonons and electrons. Their contribution to these properties, first of all, is related to the nature of the solid. In a metal

the electrons contribute more in both the heat capacity and the thermal conductivity. However, in dielectric insulators or semiconductors, the thermal properties are governed by phonons. The phonon dispersion relations and the density of states for both electrons and photons are also the important physical parameters that play a crucial role in the thermal properties.

This section presents a theoretical overview of the thermal properties of solids at low temperature. In this thesis, the material under study is an amorphous dielectric silicon nitride, and in such materials, the thermal properties are governed by phonons and not the electrons. Thus, the calculation of the heat capacity and the thermal conductivity of the electrons are neglected.

1.3.1 Specific heat

Microscopic definition of heat capacity is the capacity of a body to rise in temperature following the supply of heat from outside. The calculation of heat capacity is based on two different approaches: Einstein model and Debye model. Einstein model considers that all atoms are independently vibrating with a well-defined frequency. This model is suitable for the calculation of high temperature. Debye model considers a linear dispersion relation ($\omega{=}\nu_s \mid \boldsymbol{q} \mid$) with a cutoff frequency corresponding to interatomic distance [4, 5]. The estimation of Debye model is a better hypothesis for low temperatures calculation of heat capacity.

The heat capacity is given by the variation of the internal energy at constant volume as a function of temperature and it is expressed as:

$$C_V = \frac{dU}{dT}|_V = C_{electron} + C_{phonon} \tag{1.19}$$

The estimation of internal energy for electrons or phonons is completely different. The statistic of electrons is given by Fermi-Dirac distribution, and that of phonons known as bosons is given by Bose-Einstein distribution. Here we only focus on the specific heat of phonons.

Phonon specific heat

The internal energy of a system is described as the sum of the energy of the harmonic oscillators satisfying Bose-Einstein statistics as it is explained in section 1.2.

$$U = \sum \left[\frac{1}{2}\hbar\omega(\boldsymbol{q}) + \frac{\hbar\omega(\boldsymbol{q})}{\exp\left(\hbar\omega(\boldsymbol{q})/k_B T\right) - 1} \right] \tag{1.20}$$

The term of $\frac{1}{2}\hbar\omega$ is the zero point energy. This term will be eliminated in derivation over the whole energy. The system is considered as a continuum, thus one can write this sum

of energies into the form of integral:

$$C_V = \int_{BZ} \frac{\partial}{\partial T} \left(\frac{\hbar\omega(\boldsymbol{q})}{\exp\left(\hbar\omega(\boldsymbol{q})/k_B T\right) - 1} \right) \frac{d\boldsymbol{q}_{3D}}{(2\pi)^3} \tag{1.21}$$

This equation can also be described as:

$$C_V = \int_{BZ} \frac{\partial}{\partial T} \left(\frac{\hbar\omega}{\exp\left(\hbar\omega/k_B T\right) - 1} \right) \quad D(\omega) d\omega \tag{1.22}$$

The integrals are carried out over the first Brillouin zone (BZ). We use the density of states DOS function *D(ω)* (see section 1.2.2), and the Debye assumption of linear dispersion relation $\omega = \nu_s \boldsymbol{q}$. By simplifying the integral the specific heat can be written as:

$$C_V = \frac{6}{\pi^2} \int_0^{\infty} \frac{\partial}{\partial T} \frac{\hbar\nu_s q^3 dq}{\exp\left(\hbar\nu_s q/k_B T\right) - 1} \tag{1.23}$$

with a suitable change of variables $x{=}\hbar\omega/k_B T$, this equation will become:

$$C_V = \frac{3}{2\pi^2} \frac{k_B^4 T^3}{\hbar^3 \nu_s^3} \int_0^{\theta_D/T} \frac{e^x \; x^4 dx}{(e^x - 1)^2} \tag{1.24}$$

θ_D is the Debye temperature of the material under consideration. Now at very low temperature where temperature goes to zero $T \to 0$, respectively we will have $x \to \infty$. The equation 1.24 can be simplified to the following equation.

$$C_V = \frac{2\pi^2}{5} \frac{k_B^4}{\hbar^3 \nu_s^3} \; T^3 \tag{1.25}$$

As we see the final Debye specific heat expression for low temperatures range shows that acoustic phonon specific heat increases as $T^{\,3}$ for a 3D material. In fact, if we assume that the dispersion relations of the system are not changed by the change of the dimension, it can be supposed that the specific heat is proportional to T^d, where d is the dimension of the system. So respectively for a 2D membrane and 1D nanowire, it is expected to see T^2 and T dependence of specific heat on temperature.

1.3.2 Thermal conductivity and thermal conductance

Thermal conductivity is the property of a material to conduct heat. It is evaluated primarily as a coefficient of proportionality between the thermal gradient along with some specific direction. In order to calculate the thermal conductivity, let us consider a one directional system, having temperature gradient along axis x. The heat flux ($\mathrm{W/m^2}$) along axis x can be expressed by Fourier's law:

$$\phi = -\kappa_{ph} \frac{dT}{dx} \tag{1.26}$$

where $-\kappa_{ph}$ (W/m.K) is the thermal conductivity of phonons. According to the kinetic point of view the expression of heat flux can be also described as:

$$\phi = \frac{1}{V}\sum_{q} \nu_x U(q) f(\boldsymbol{r},\boldsymbol{p}) \tag{1.27}$$

V is the volume of the system, ν_s is the particle speed along the relevant axis, $U(q)$ is the energy of the given particle, and f is their distribution function in the phase space $(\boldsymbol{r},\boldsymbol{p})$. One can write down this equation as a continuous form:

$$\phi = \frac{1}{V}\sum_{i} \iiint d\boldsymbol{q}\ \nu_x U(q) f(\boldsymbol{r},\boldsymbol{p})\ \frac{L^3}{2\pi} \tag{1.28}$$

The main missing part in this equation is the determination of the distribution function $f(\boldsymbol{r},\boldsymbol{p})$. To do so, one can use the Boltzmann equation, which describes phonons as a classical particles gas:

$$\frac{\partial f}{\partial t} + \frac{d\mathbf{r}}{dt}.\nabla f + \frac{d\mathbf{p}}{dt}.\nabla f = \left.\frac{\partial f}{\partial t}\right|_{coll} \tag{1.29}$$

The right term of this equation is the so called collision term, in which we can express the collisions within a relaxation time approximation.

$$\left.\frac{\partial f}{\partial t}\right|_{coll} = -\frac{f - f_0}{\tau} \tag{1.30}$$

f_0 is the equilibrium distribution function and τ is the relaxation time. We use equation 1.30 in equation 1.29 with the assumption of stationarity ($\partial f/\partial t = 0$) and no external force ($d\boldsymbol{p}/dt{=}0$), the distribution is then described as:

$$f(r,q) = f_0 + \tau\frac{df}{dT}\mathbf{v}.\nabla T. \tag{1.31}$$

This equation shows that a perturbation as a form of a temperature gradient will create an imbalance between the flows of phonons. This imbalance is resumed in heat flow. By putting this distribution function in equation 1.28 we have:

$$\phi = \sum_{i}\int_0^{\omega_{max}} d\omega \int_0^{2\pi}\int_0^{\pi} d\theta\ \hbar\omega\nu_x\ \left(f_0 + \tau\frac{df}{dT}\mathbf{v}.\nabla T\right)\frac{D(\omega)}{4\pi} \tag{1.32}$$

This equation expresses the heat flow through the direction x. The temperature gradient is along the x axis as well $\nabla T{=}dT/dx$. We can over write this equation in equation 1.26 to find the expression of the heat flux.

$$\phi_{ph} = \sum_{i}\int_0^{\omega_{max}} d\omega \int_0^{2\pi}\int_0^{\pi} d\theta\ \sin\theta\cos^2\theta\hbar\omega\nu_x^2\tau\frac{df_0}{dT}\ \frac{D(\omega)}{4\pi} \tag{1.33}$$

The coefficient of proportionality κ defined as the thermal conductivity is expressed as:

$$\kappa_{ph} = \frac{1}{3}C_{ph}\nu_{ph}\Lambda_{ph} \tag{1.34}$$

This is a very interesting formula that establishes a direct relationship between the specific heat, the thermal conductivity, and the phonon MFP. This equation is known as the kinetic equation. The elastic MFP is defined as $\Lambda = \tau\nu_{ph}$.

The equation 1.34 gives us the first insight of low-temperature behavior of thermal properties. In the case of constant MFP and sound velocity, if the specific heat has a cubic dependence on the temperature, the thermal conductivity will have the same dependence. This kinetic relation is valid at low temperature when collision processes are fully inelastic. Thermal conductance and thermal conductivity are related to each other via the following relation:

$$K = \kappa\frac{S}{L} \tag{1.35}$$

Where S is the section, and L is the length of the system along the heat flow axis. At low temperatures in nanostructures, the phonon MFP depends on the geometry of the system. It is then more appropriate to describe heat transport at the nanoscale with thermal conductance. To compare different geometries a consistent normalization based on the size of the system is needed.

1.4 The confinement effects

When a structure is confined, the populated vibrational modes in each space direction are not equal. This fact shows that the phonon dispersion relations and phonon density of states of low dimensional systems exhibit significant differences compared to bulk materials. Another major effect of low dimensionality appears in the phonon MFP. Indeed, when the size of a system is lower than the phonon MFP, then the MFP is limited by the dimensions and the scattering of phonons are set by the boundaries.

There are at least two features that can be expected to develop due to reduction in dimensionality: modification of dispersion relations and as a consequence reduction of group velocity of phonon modes. In Fig. 1.6 the dispersion relation of (**a**) bulk Si is compared to the dispersion relation of (**b**) Si nanowires [6, 7]. It can be seen that the dispersion relation in Si nanowire (Fig. 1.6 **b**) has a flattened band gap in comparison to the dispersion relation of bulk Si Fig. 1.6 **a**. The finite size of the system can influence the energy transport and energy storage by altering the wave characteristics. For instance, one of these changes is forming standing waves and creating new modes that do not exist in bulk counterparts. In the following sections, the effect of confinement on the phonon MFP and the phonon transport properties and specific heat will be explained in more details.

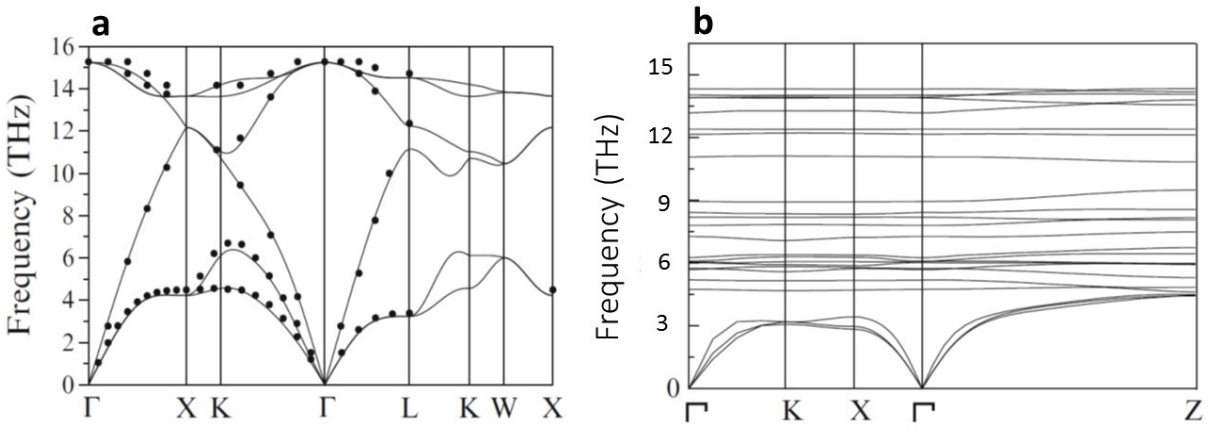

Figure 1.6: **The effect of confinement on dispersion relations.** (**a**)The dispersion relations for bulk Si and (**b**) Si nanowire taken from [6]. The confinement will cause the flattering of the band gap.

1.5 The effects of confinement on phonon transport at low temperatures

In section 1.2.2 it is explained that low temperature has a major impact on phonon transport by increasing the phonon characteristic lengths, consisting of the phonon MFP and the phonon dominant wavelength. In addition, when the size of a system is on the same order of magnitude of the phonon characteristic lengths, the phonon transport (or phonon diffusion) will be affected by boundaries.

There will be two major effects at the boundaries: *coherent* and *incoherent* effects. Both of these effects will happen when the scattering mechanism is only dominated by the boundaries, and other mechanisms (phonon-phonon interaction, electron-phonon interaction, scattering on impurities, etc) do not contribute. Based on the way that phonons are scattered from the surface, one can define each regime of phonon transport. For instance, the regime of phonon transport changes from diffusive boundary (Casimir regime), to fully specular kind of scattering. In this section, a detailed insight of phonon transport with the definition of each regime of phonon transfer will be presented.

1.5.1 The Casimir model

In the Casimir model, it is postulated that the phonon MFP is limited by the boundaries. Assuming the surfaces as black bodies of phonons, all the phonons are absorbed in the surfaces, then they are re-emitted in random directions. This scenario is based on the hypothesis of infinitely rough surfaces, where the scattering of phonons are inelastic. To

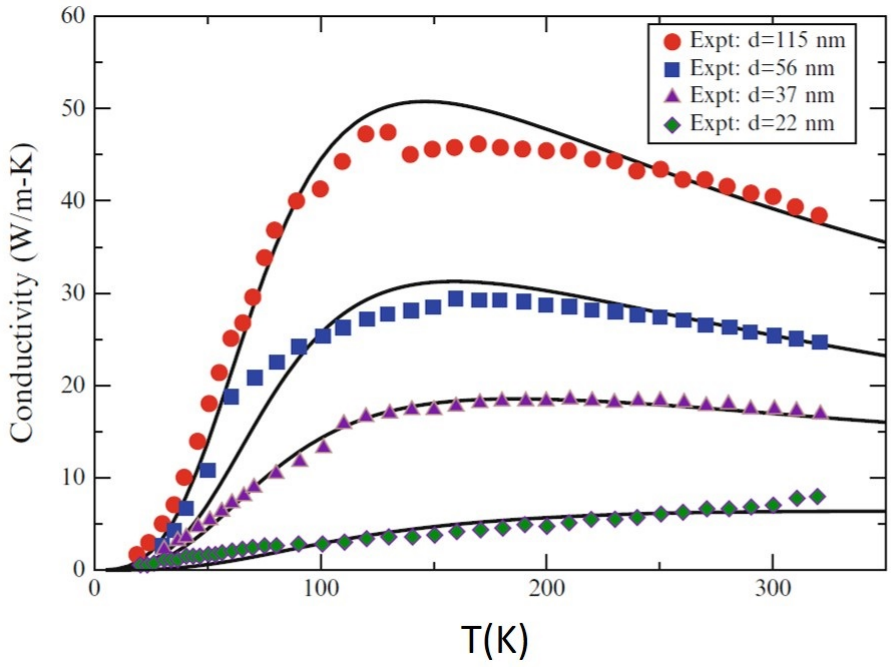

Figure 1.7: **Thermal conductivities of single crystalline of Si nanowires.** Colored symbols are the experimental data obtained by Li D. *et al.* [8], solid lines are theoretical fits taken from [6].

fulfill this hypothesis, the phonon MFP should be limited by the section of the system, and the phonon dominant wavelength much smaller than the roughness of the surfaces.

Due to the Casimir estimation with the kinetic equation (equation 1.34), the thermal conductance is calculated in the form of:

$$K_{Cas} = 3.2 \times 10^3 \left(\frac{2\pi^2 k_B^4}{5\hbar^3 \nu_s^3}\right)^{(2/3)} \frac{e \ \times w\Lambda_{cas}}{L} \ T^3 \tag{1.36}$$

$$= \beta_{cas}\Lambda_{cas}T^3 \tag{1.37}$$

where $\hbar$ is the Planck constant, k_B the Boltzmann constant and ν_s is the speed of sound. $\Lambda_{cas} = 1.12\sqrt{e \times w}$ is the Casimir MFP of phonons in a confined system with thickness of e and width of w. L is the length of the system [9].

As it is shown in Casimir formula (equation 1.37), a size effect is imposed to the phonon transport due to the small cross section area, and thermal conductance will depend on the increased phonon boundary scattering. It was shown experimentally that the thermal conductivity of silicon nanowires shows a strong diameter dependence. The thermal conductivity observed was more than two orders of magnitude lower than the bulk value (see Fig. 1.7) [6, 8, 10, 11].

The Casimir model is quite a simple thermal model that describes a cubic dependence

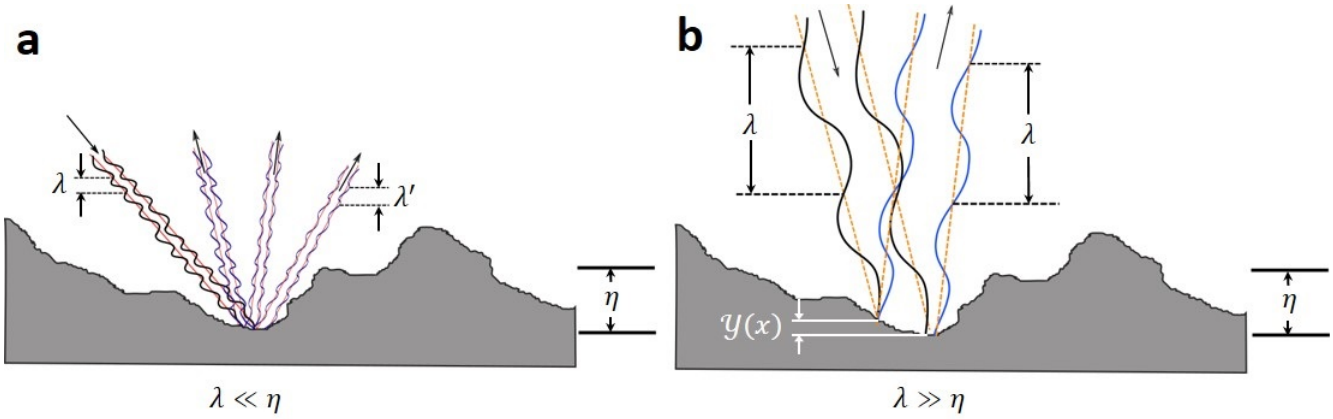

Figure 1.8: **The boundary scattering based on the phonon dominant wavelength.** (**a**) Infinitely rough surface, with inelastic scattering, when the roughness is much bigger than the phonon wavelength $\eta \gg \lambda$. (**b**) Smooth surface with elastic scattering, when the roughness is much smaller than the phonon wavelength $\eta \ll \lambda$.

on temperature and is in good agreement with experiments [10, 11]. This model ascribes only inelastic kind of scattering by the surfaces, although at very low temperature or smooth surfaces the boundary scattering will not be fully inelastic.

1.5.2 The Ziman model

As the temperature is lowered, the dominant phonon wavelength actually grows (based on equation 1.11) and it may become eventually larger than the roughness amplitude η. Then, all the reflections cannot be considered as inelastic scattering like in the Casimir model. In fact, the definition of rough or smooth surface is based on the incoming wavelength. If the incoming wave has a wavelength much smaller than the roughness of the surface $\lambda \ll \eta$, then the surface acts as an infinitely rough one. On the other hand, if on the same surface with the same roughness, the incoming wave has wavelength much bigger than the roughnesses $\lambda \gg \eta$, then the surface acts as a perfectly smooth one.

To take this effect into account, Ziman proposed a phenomenological parameter as the phonon probability of specular reflection p_{spec} [12]. This parameter describes the probability of a phonon of wavelength λ at the temperature T to be specularly reflected. When an incoming phonon reaches the surfaces, there will be two possible kind of scatterings: either the phonon is absorbed in the surface, then it is scattered in a random direction (the Casimir model of perfectly rough surfaces) p_{spec}=0 (Fig. 1.8(**a**)), or every single phonon will be specularly reflected conserving their energy and phases (just like reflection of a photon by a mirror), p_{spec}=1, the case of perfectly smooth surfaces (Fig. 1.8(**b**)).

To calculate this probability of specular reflection, let us consider a plane wave with the

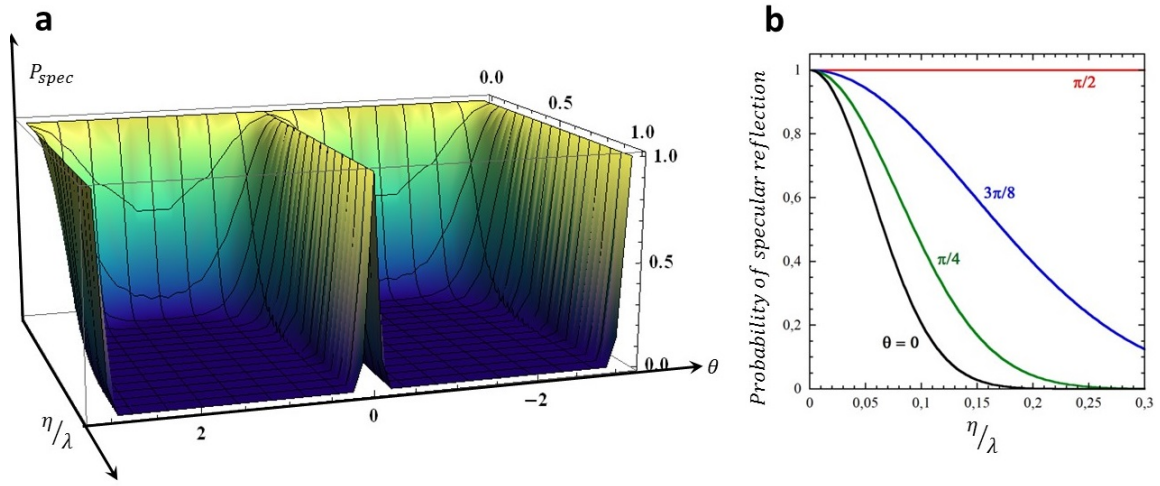

Figure 1.9: **The probability of specular reflection.** (**a**) 3D plot of the probability of specular reflexion as a function of η/λ and incident angle θ. (**b**) The same function with fixed incident angles of phonon to the surface.

wavelength of λ incident on the surface. The reflected waves will have a phase deviation depending on the height *y(x)* of the surface at the position x. This phase shift is described below.

$$\phi(x) = \frac{4\pi y(x)}{\lambda}\cos(\theta) \tag{1.38}$$

What we need to know is the statistical properties of the function $\phi(x)$. The variance of $\bar{\phi^2}$ is proportional to the variance of the height function *y(x)*. This variance is:

$$\bar{\phi^2} = \frac{16\pi^2\eta^2}{\lambda^2}\cos^2(\theta) \qquad\qquad \eta^2 =< y(x)^2 > \tag{1.39}$$

where η is the root mean square deviation of the height of the surface from the reference plane. It is also called *asperity* parameter. The probability of specular reflection is then given as:

$$p_{spec}(\lambda,\eta) = exp(-\pi\bar{\phi^2}) = exp\left(-\frac{16\pi^3\eta^2}{\lambda^2}\cos^2(\theta)\right) \tag{1.40}$$

where θ is the incident angle of phonon to the surface. This formula is simply interpreted by the ratio of η/λ. Fig. 1.9 represents the probability of specular reflection by the equation 1.40.

When the specular reflections become more probable, the phonon MFP is no more totally limited by the section of the system. Ziman proposed that the phonon MFP will be a function of the probability of specular reflection as the equation below:

$$\Lambda_{Ziman} = \frac{1+p}{1-p}\,\Lambda_{Cas} \tag{1.41}$$

The thermal conductance will be the same as the equation 1.37, but the Casimir MFP Λ_{Cas} should be replaced by the Ziman MFP Λ_{Ziman}.

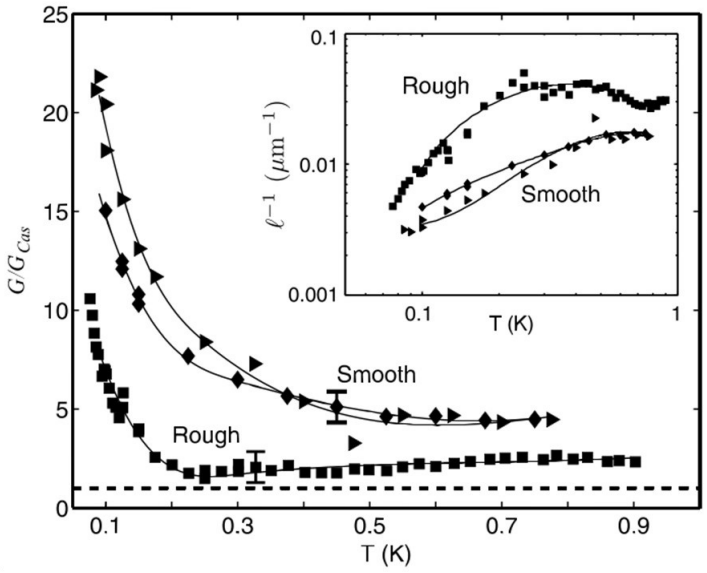

Figure 1.10: **Thermal conductance of silicon beams with rough and smooth surfaces.** The thermal conductances are normalized by the Casimir thermal conductance with a rectangular section. Dashed line represents the Casimir thermal conductance. The square and triangle dots respectively represent the normalized thermal conductance of rough and smooth surfaces. The inset shows the inverse phonon mean free path as a function of temperature [13].

Ziman regime describes an intermediate regime between boundary limited and fully ballistic regime of phonon transport. This stage of phonon transport is highly sensitive to the details of the surfaces of the system. The boundary scattering can be either diffusive-dominated or ballistic-dominated [14]. Indeed, the thermal conductance and the phonon transport regime can be tuned from ballistic to diffusive by varying the surface roughness and the length of the system [11, 15].

In an experimental achievement by Rostem *et al.* [16], resonant phonon scattering has also been observed in beams with highly pitted surfaces with pit depths of order 30 nm at 300 mK. Figure 1.10 represents the experimental measurements of the thermal conductance on silicon beams with rough and smooth surfaces. The inset of Fig. 1.10 represents the inverse of the phonon MFP l^{-1} as a function of temperature. According to their observations, they believe that the peak in l^{-1} in the square dots (the measurement on the rough surface) is due to the resonant phonon scattering that is a signature of the destructive interference between an incoming phonon wave with a reflected one from the same surface.

In the next section, we will explain what happens if in a 1D channel the surface becomes completely smooth ($\lambda \gg \eta$), and all the phonon scattering by the surfaces become specular.

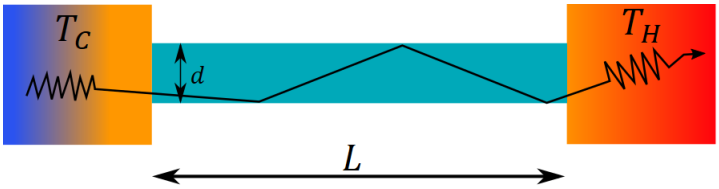

Figure 1.11: **1D quantum channel in a phonon waveguide.** The 1D channel is placed between two reservoirs, and the phonons are transported ballistically along the channel. The only scattering (thermalization) will occur in the two reservoirs.

1.5.3 Fully ballistic regime and the universal quantum of thermal conductance

Consider a 1D system along x axis. The temperature is low enough that the phonon dominant wavelength is not only much bigger than the roughness of the surfaces $\lambda \gg \eta$, but also bigger than the section of the system $\lambda > d$ (d diameter of the system). Moreover, when $\lambda > d$, the transport can be treated as one-dimensional (1D). The surfaces are considered as perfectly smooth for the incident phonons (p_{spec}=*1*), and the phonon MFP exceeds the length of the system $\Lambda > L$ (see Fig. 1.11).

The nanowire will behave exactly like an acoustic waveguide, in the same way as an optical fiber behaves as an optical waveguide. Along the 1D system, there is no thermalization because there is no phonon scattering. Then it is expected that the thermalization occurs only in the reservoirs.

When the two reservoirs are at two different temperatures, the populated phonon vibrational states will travel through the nanowire to reach the other reservoir. The expression of the total heat exchange through the system can be expressed by the Landauer formula:

$$\dot{Q}_x = \sum_{\alpha,\boldsymbol{q}_x} \hbar\omega_\alpha(\boldsymbol{q}_x)\frac{\nu_{s,\alpha}(\boldsymbol{q}_\alpha)}{L}\left\{\frac{1}{\exp[\hbar\omega_\alpha(\boldsymbol{q}_x)/k_BT_H]-1} - \frac{1}{\exp[\hbar\omega_\alpha(\boldsymbol{q}_x)/k_BT_C]-1}\right\}\mathcal{T}_\alpha(\omega) \tag{1.42}$$

where α is the index of populated phonon vibrational modes, $\omega_\alpha(\boldsymbol{q})$ is the dispersion relation for the phonon with wave vector $\boldsymbol{q}$, and the group velocity of $\nu_\alpha(\boldsymbol{q})$. The term $1/(e^{(\hbar\omega/k_BT_i)}-1)$ represents the thermal distribution of phonons in each reservoirs; and $\mathcal{T}$ is the transmission coefficient from the reservoir through the nanowire. The sum of the equation 1.42 over the wave numbers $\boldsymbol{q}_x$ is carried out by going to a continuous limit, introducing the 1D density of states as presented in equation 1.18. The energy flux will then become:

$$\dot{Q}_x = \sum_{\alpha} \int_{\omega_{\alpha,min}}^{\omega_{\alpha,max}} \frac{d\omega_\alpha}{2\pi} \left\{ \frac{\hbar\omega_\alpha}{\exp[\hbar\omega_\alpha(\boldsymbol{q}_x)/k_B T_H] - 1} - \frac{\hbar\omega_\alpha}{\exp[\hbar\omega_\alpha(\boldsymbol{q}_x)/k_B T_C] - 1} \right\} \mathcal{T}_\alpha(\omega) \quad (1.43)$$

At low enough temperature, when only fundamental acoustic modes are occupied in the 1D quantum channel connecting the two reservoirs, then the heat flux can be expressed through:

$$\dot{Q}_x = N_\alpha G_q (T_H - T_C)\mathcal{T} \quad (1.44)$$

where N_α is the number of populated vibrational modes in the quantum wire, and G_q is the quantum of thermal conductance. If the temperature gradient between the reservoirs is very small ($T_H - T_C \to 0$), and the transmission coefficient from the reservoir through the nanowire is equal to unity ($\mathcal{T} = 1$), then the thermal conductance of a 1D channel can reach the quantum of thermal conductance G_q given by:

$$G_q = \frac{\pi^2 k_B^2}{3h} T \quad (1.45)$$

The value of the quantum of thermal conductance represents the maximal contribution of each populated mode to the conductance of a 1D waveguide [17]. It has been calculated that in a pure ballistic phonon transport in 1D channel there exist only four acoustics branches. These four lowest branches arise from one dilatational, one torsional, and two flexural [18]. This value is known as a universal value of energy, entropy and information transport through a 1D quantum channel [19–22], and it is independent of material, and the statistics of the heat carriers (electrons, photons, anyons or phonons) [23–25]. Many theoretical works have been done to calculate this universal feature [26–30]. Several experiments have been done measuring this universal value for electrons [31–33], photons [34, 35], anyons [36], but very few experimental realizations have probed this limit for phonons. It has been measured just once by Schwab and coworkers [37, 38] (see Fig. 1.12), but this measurement has never been reproduced, and the possibility of being able to measure this universal value by phonons is still a subject of debate (more details are explained is chapter 3). Having an experimental access to this quantum regime is highly challenging since not only purely ballistic transport of phonon is required, but also having a perfect transmission coefficient from the junctions to the nanowire is the key point. Several recent experiments have observed a purely ballistic transport inside of nanowires at room [39] and low temperature [40], but there is no sign of the universal value of quantum of thermal conductance.

In table 1.1 a classification of the different regimes of phonon transport is presented, from fully inelastic scattering to purely ballistic regime. In the next section, the optimization of the transmission coefficient is explained.

The junction of nanowires to reservoirs

As it is shown in the Landauer formalism by equation 3.1, in a 1D channel, the maximum of heat current that can be transported from one reservoir to the other one depends on

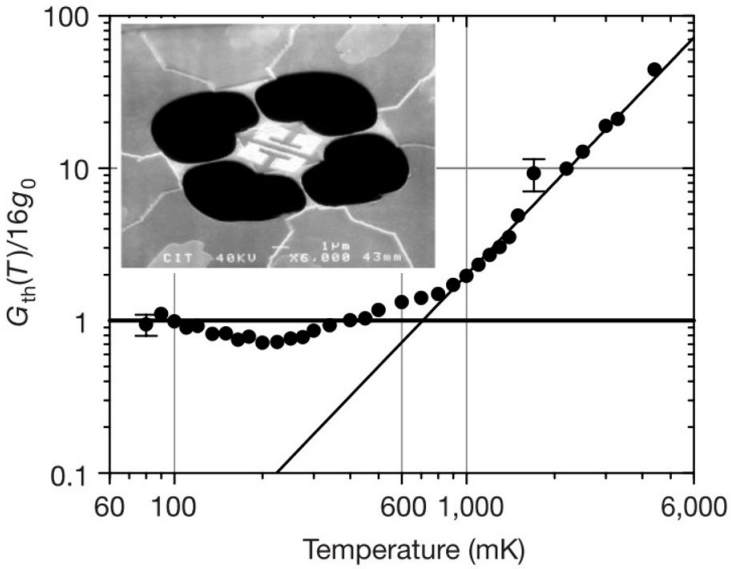

Figure 1.12: **The measurement of the quantum of thermal conductance.** The black dots represent the experimental results of the thermal conductance of a SiN nanowire with rectangular section normalized by the expected low temperature value for 16 conducting modes. Inset represents the suspended mesoscopic device of the experiment. This measurement has been done by Schwab and coworkers [37].

Relevant length scale	transport regime	models	relevant formula
$\lambda_{dom}(T) < \Lambda_{ph}(T) < L$	Diffusive regime (incoherent)	Kinetic model	$K=\frac{1}{3}C\nu_s\Lambda_{ph}$
$\lambda_{dom}(T) < L \sim \Lambda_{ph} < \Lambda_{ph-bulk}$	Casimir regime (incoherent)	Casimir model	$K_{cas}=\beta_{cas}\Lambda_{cas}\ T^3$
$\lambda_{dom}(T) \sim L < \Lambda_{ph}$	Ziman regime (partly coherent)	Ziman model	$\Lambda_{Ziman} = \frac{1+p}{1-p}\Lambda_{Cas}$
$L < \lambda_{dom}(T) < \Lambda_{ph}$	Ballistic regime (coherent)	Landauer model	$\mathcal{T} = \frac{1}{1+3L/4\Lambda_{ph}}$

Table 1.1: **Classification of the different regimes of phonon transport.** This classification represents possible scenarios of phonon transport in nanoscaled systems, from boundary limited regime to fully ballistic transport of phonon at low temperature. L is the length of the sample, Λ_{ph} is the phonon mean free path, and λ_{dom} is the phonon dominant wavelength. Concerning the Landauer limit, the parameter $\mathcal{T}$ denotes the transmission coefficient between a nanowire and its heat reservoirs [1].

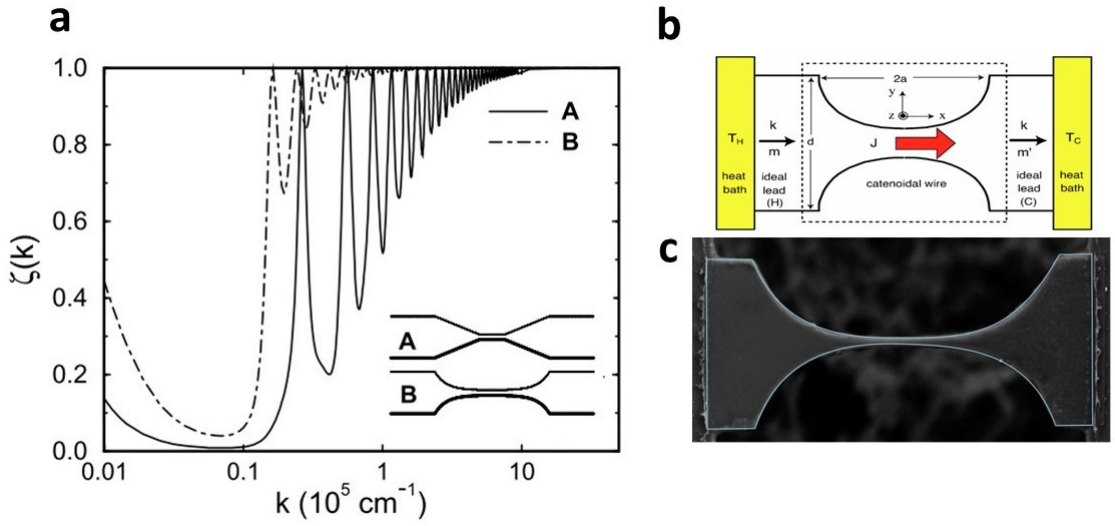

Figure 1.13: **The calculation of transmission coefficient.** (**a**) Calculated transmission coefficient for longitudinal vibrations done by Rego and Kirczenow [17]. (**b**) A representative configuration of catenoïd nanowire [41]. (**c**) Top view of the nanowire that is elaborated by the equation 1.46.

the probability of transmission between the reservoirs. So, if a nanowire is at low enough temperature in the event that all of the internal phonon scatterings by the surface of the nanowire is fully specular (probability of specular reflection p=1), then the dominant factor in the equation 3.1 will be the transmission coefficient. From an experimental point of view, the optimization of this value can be done by adapting the design of the junctions of nanowire to reservoirs. Indeed, the shape of the junctions of reservoirs to nanowire has a direct impact to collect the populated vibrational states [17, 27, 42]. In some theoretical recent works, the transmission coefficients of different design of the junctions of nanowire to reservoirs are compared. It was shown that in an abrupt interface [30, 43–46], the phonon scattering is the strongest, and it exhibits a low value of transmission coefficient. Meanwhile, when the junctions are designed with conical, or catenoidal interfaces [17, 27, 41, 42, 47], the transmission coefficient is optimized.

Based on all theoretical efforts, the catenoidal shape of junctions with a slight curvature will give rise to the largest value of transmission coefficient in comparison to the other geometries (see Fig. 1.13 **a**). In the catenoidal geometry, nanowire's width becomes large and joins smoothly to the thermal reservoirs at the ends. According to the calculation of interface geometry, our nanowires are designed by a catenoidal interfacial function that can be described as:

$$A(x) = A_0 \cosh^2(x/\lambda) \tag{1.46}$$

where $A(x)$ is the cross sectional area of the nanowire to the reservoirs, A_0 is the size of reservoirs, and λ is the characteristic length of the catenoïd.

At low frequencies, the transmission rate of vibrational modes through the wires shows,

in general, complicated behavior including resonances and cutoffs. This means that quantization of thermal conductance relying on perfect phonon transmission should be no longer valid as the temperature goes down to 0 K, where only low-frequency vibrations transport heat inside the wires.

Until now the effect of confinement of the phonon transport and the thermal conductivity have been discussed. However, the confinement has also very noticeable effect on the energy storage (heat capacity) inside of a system. In the following section, the effect of constrained geometry at low temperature on the specific heat of the system will be discussed.

1.6 The effects of confinement on specific heat at low temperatures

In nanostructures, we expect that the specific heat will be different from that of their bulk counterparts. In this work, we are interested mostly in specific heat of 2D phonon cavity. The main differences come from two sources: physical point of view and mathematical one. On one hand, the physical feature is related to the difference of the phonon density of states that exists between a 2D system and 3D bulk. On the other hand, in the mathematical analysis the integration over the total energy of the system is no longer valid, because in confined structure the energy (vibrational modes) in each space direction is not equally distributed. To clarify these physical and mathematical features specifically at low temperatures where the physical characteristic lengths of phonon become bigger than dimensions, there are two main approaches: dynamical lattice theory, and the elastic continuum theory.

Dynamical lattice theory: for systems of the dimensionality of d, the Debye model predicts that at low temperature the lattice specific heat should be proportional to T^d. In this approach, when the dominant phonon wavelength becomes comparable or bigger than the thickness of a 2D membrane, the energy distribution in the direction perpendicular to the surface cannot be considered as continuous one. So the summation over the phonon modes along the plane in parallel to the 2D surface will be an integral, and the summations over the direction perpendicular to the surface becomes discrete.

$$C_{ph} = \frac{3k_B S}{2\pi}\left(\frac{k_B T}{\nu_s \hbar}\right)^2 \times \left[\int_0^\infty \frac{x^3 e^x}{(e^x-1)^2}dx + \sum_{n=1}^{\infty}\int_{nx_0}^\infty \frac{x^3 e^x}{(e^x-1)^2}dx\right] \tag{1.47}$$

S is the section of the membrane and x is a dimensionless parameter $x{=}\pi\hbar\nu_s/k_B T t$, where t is the thickness of the film. The first integration corresponds to a fully 2D phonon cavity [48, 49]. When the phonon dominant wavelength exceeds the thickness of the membrane, the second part of the equation 1.47 tends to zero, then the specific heat of 2D membrane

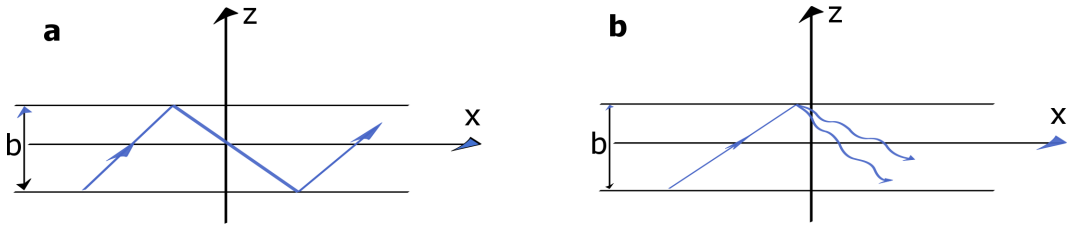

Figure 1.14: **Schematic representation of the reflection of elastic waves from surfaces.** b is the thickness of the membrane. (**a**) Elastic reflection of a horizontal shear waves (SW) with a displacement and wave vector parallel to the plane of the membrane. (**b**) A wave longitudinally or transversally polarized into the xz plane reflects as a superposition of longitudinal and transversal polarized waves.

will become:

$$C_{2D} = \frac{9k_B^3 S}{2\pi\nu_s^2\hbar^2}T^2 \tag{1.48}$$

We immediately notice that specific heat of fully 2D membrane C_{2D} does not depend on the membrane thickness. Also in this analysis, the power of temperature defines the dimensionality of the system.

Elastic continuum model: the main assumption in the calculation of specific heat based on the elastic continuum theory is that the phonons can be described by plane waves with three independent polarizations: one longitudinal and two transverses. In addition, as the dimensions of the structure become sufficiently small, comparable to the phonon MFP, these become standing waves satisfying the appropriate boundary conditions. The boundary conditions will cause different polarization coupled at the surfaces (the total stress should vanish), and create a new set of vibrational modes.

The eigenmodes of these phonons coupled at the surface are classified as dilatational waves (DW), flexural waves (FW), and horizontal shear waves (SW). SW is a transversal wave polarized along the y direction with both displacement and wave vector parallel to the plane of the membrane. The reflection of SW waves by boundaries will be elastic, and they do not mix at the boundaries with waves of different polarizations. The SW mode dispersion law is [48, 50, 51]:

$$\omega_{SW} = c_t\sqrt{\left(\frac{2n\pi}{b}\right)^2 + q_{\|}^2} \tag{1.49}$$

where n is an integer number, and $q_{\|}$ is the wavevector in parallel to the plane of the membrane [52]. DW and FW have an incident wave either longitudinal or transversal, in the plane xz, then the wave will be reflected always in a superposition of longitudinally and transversally polarized waves (see Fig. 1.14.**b**). These two waves have different propagation velocities and different dispersion relations. The dispersion relation for DW is:

$$\omega_{DW} = 2\frac{c_t}{c_l}\sqrt{c_l^2 - c_t^2}\; q_{\|} \tag{1.50}$$

where c_l and c_t respectively are longitudinal and transversal sound velocities. The FW mode dispersion law is:

$$\omega_{FW} = \frac{\hbar}{2m^*} q_{\parallel}^2 \qquad\qquad m^* = \frac{\hbar\ c_l\sqrt{3}}{2c_t b\sqrt{c_l^2 - c_t^2}} \tag{1.51}$$

m^* is the effective mass of massive particles (phonons with large wavelength at low dimensions can be considered as massive particles). Between these three dispersion relations, we can see that ω_{DW} and ω_{SW} have linear dispersion relations, but ω_{FW} has a quadratic dispersion relation. In this formalism, the specific heat is predicted to be [51]:

$$C_V \approx k_B \left(\alpha T^2 + \beta T\right) \tag{1.52}$$

α and β are:

$$\alpha = \frac{3\zeta(3)k_B^3}{\pi\hbar^3}\left(\frac{2}{c_t^2} + \frac{1}{c_l^2}\right) \qquad\qquad \beta = \frac{\zeta(2)k_B m^*}{\pi\hbar^2} \tag{1.53}$$

where ζ is the Riemann zeta function. For temperature below $T \ll (\hbar c_t/2k_B)\, b^{-1}$ the heat capacity of the membrane is dominated by the contribution of the lowest vibrational branches. Between these low vibrational branches, flexural waves will have the highest contribution in specific heat. Due to their quadratic dispersion relation, they will give a rise to quasi-linear specific heat. This approach shows a clear dependence on the thicknesses of the membrane.

In figure 1.15, the calculated specific heat for Si bulk and membranes of different thicknesses are compared. It is clearly showed that by reducing the size, the specific heat become larger than in 3D limits [53].

1.7 Vibrational excitations of amorphous solids

Until now all the formulas were considered for regular crystal lattices. Some fundamental features of amorphous structures will be explained. Amorphous structures have attracted a considerable interest due to their ease of fabrication process and possible potential applications [54–57].

Amorphous solids (a-solids) are considered as isotropic structures. We cannot use the concept of lattice or unit cell because there will be no translational symmetry [58]. In general, a-solids may show both macroscopic structural inhomogeneities (e.g. voids, density fluctuation, etc) and microscopic structural defects (e.g. vacancies, broken bonds, etc) [59]. Detail studies of amorphous structures using inelastic neutron scattering suggest that a-solids exhibit some order on the scale of several interatomic spacings. However, because of the absence of long-range order, it is no longer possible to consider vibrational modes in a-solids as plane waves. Low-frequency vibrational excitation is the equivalent term of phonon for a-solids [3, 60].

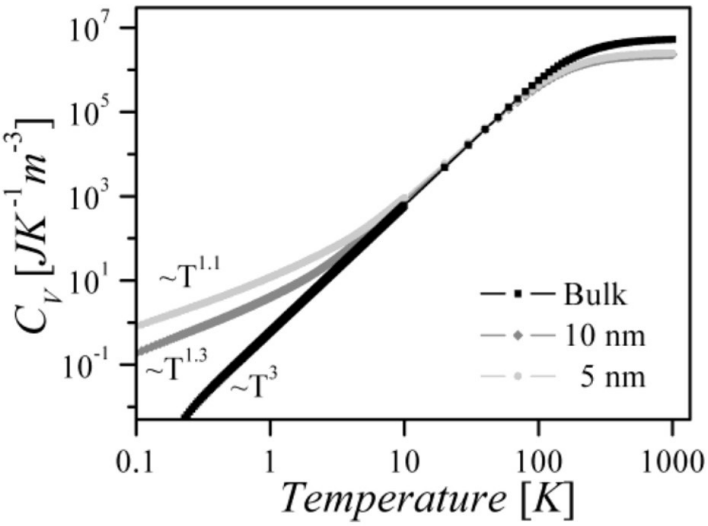

Figure 1.15: **Calculation of the specific heat of thin silicon membranes.** The calculations are done for Si membranes with different thicknesses. Black line represents the specific heat of a bulk Si, dark grey line and grey line show respectively 10 nm and 5 nm of thickness [53].

1.7.1 Two-Level Systems

At very low temperature, one of the most hallmarks of glassy solids is the anomalous thermal and mechanical behavior. Below 1 K the behavior of almost all amorphous materials is qualitatively similar [61, 62]. Almost all the a-solids exhibit a quasi-linear specific heat and thermal conductivity proportional to $T^{1.8}$. In the case of thermal conductivity, this universality is not only qualitative but also quantitative. The thermal conductivity of all amorphous materials lies within a factor of twenty in the same order of magnitude which is called the *glassy range* [61, 63].

To explain these physical features, it was independently proposed by Phillips [64] and Anderson, Halperin and Varma [65] that many low-temperature properties of disorder strutures are related to a phenomenological feature which is known as the *Two-Level Systems* (TLSs). The concept of TLSs is defined as an atom or a group of atoms that can have two stable configurations in their energy landscape at very low temperature. It is like double potential wells with barrier height V_0 and energy separation Δ between the two minima E_0 and E_1 (see Fig. 1.16). At low enough temperatures, these atoms or group of atoms can reach to the lowest energetical states via quantum tunneling between the two minima. Similar tunneling process occurs in doped crystals, but in disordered structures, the spectral distribution is considered as a broad distribution rather than discrete one [63]. These TLSs have recently been reported for the groups of 4−6 atoms on a-Si surfaces [66].

At very low temperature, phonons will interact strongly with the TLSs. The phonon-TLSs inelastic interactions dominate the scattering of the phonons, then defines the prop-

erties of the system. This tunneling effect can explain a wide range of thermal, and mechanical properties of a-solids below 10 K, including the boson peak [60, 67, 68], the plateau of thermal conductivity and internal friction around 10 K [63, 69, 70], and the linearity of specific heat below 1 K [61, 71]. While the TLSs model explains a wide range of experimental results, the true nature of these physical features is still a mystery.

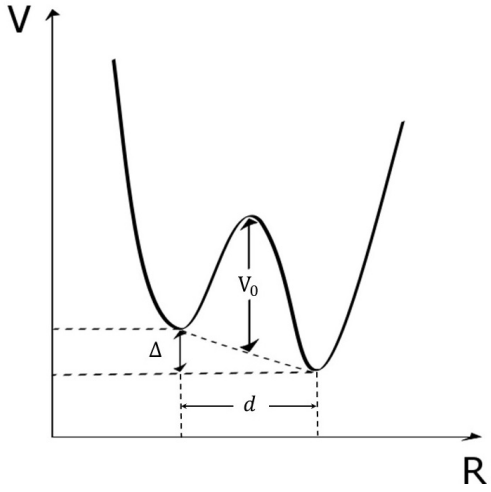

Figure 1.16: **The schematic double-well in the concept of TLSs.** Double-well potential has two lowest stable states of energy as a function of a generalized coordinate. Δ is the energy separation (asymmetry) between the two minima. V_0 is the barrier height between the two potentials.

1.7.2 Specific heat

The specific heat $(J/Kmol)$ of an amorphous dielectric can be described by the equation:

$$C = c_{TLS}T + c_3T^3 \tag{1.54}$$

c_{TLS} is due to the contribution of TLSs in the specific heat, and it is calculated by TLS model [64]. To calculate c_{TLS} we return to the definition of double-well in Fig. 1.16. The difference of energy between the two stable energy states is given by $E = \sqrt{\Delta^2 + W^2}$. W is the tunneling coupling energy, which is defined as:

$$W = \hbar\omega_0 \exp(-\lambda) \qquad \lambda = d(2mV/\hbar^2)^{1/2} \tag{1.55}$$

ω_0 is the frequency of oscillation in an individual well so that $\hbar\omega_0$ is a typical zero-point energy in either well. λ is the tunneling parameter, and m is the particle mass. The

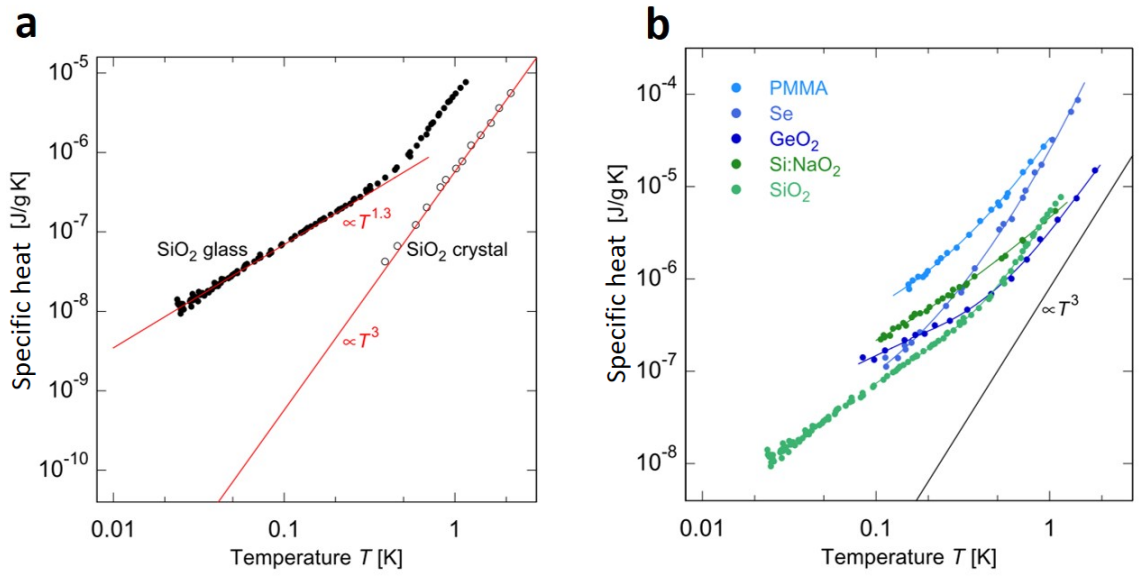

Figure 1.17: **Specific heat of amorphous solids at very low temperatures.** (**a**) Comparison of the specific heat of amorphous and crystalline SiO_2 plotted as a function of temperature, taken from Zeller and Pohl [61]. (**b**) Specific heat of different amorphous solids at low temperatures, in comparison with expected value by Debye model. Below 1K, the specific heat of amorphous solids exceeds for more than one order of magnitude from the one of their crystalline counterparts [62].

contribution of TLSs in specific heat is given by:

$$c_{TLS} = k_B \int_0^\infty n(\omega) \left(\frac{\hbar\omega}{k_B T}\right)^2 \cosh^2\left(\frac{\hbar\omega}{k_B T}\right) d\omega \tag{1.56}$$

$n(\omega)$ is the TLSs density of states, and it is given by:

$$n(\omega) = \bar{P}\ ln\left(\frac{2\hbar\omega}{W}\right) \tag{1.57}$$

$\bar{P}$ is the tunneling distribution function. In general $n_0/\bar{P} \approx 10$, and in the standard model of tunneling the distribution function is associated to constant value $P(W,\lambda) = \bar{P}$ for $\lambda_{min} < \lambda < \lambda_{max}$ and $\Delta_{min} < \Delta < \Delta_{max}$. The specific heat is then given by:

$$c_{TLS} = \frac{\pi^2}{6} k_B^2 n_0 T \tag{1.58}$$

where n_0 is the constant density of TLSs and in most amorphous solids is about $n_0 \approx 10^{-45} - 10^{-47}$ (J^{-1} m^{-3}) [62]. The cubic part of the specific heat c_3 in equation 1.54 is attributed to the Debye specific heat and the excess of specific heat which comes from non-propagating vibrational modes in a-solids [62, 72].

$$c_3 = c_D + c_{ex} \tag{1.59}$$

These non-propagating vibrational modes which can be described by the Soft-Potential-Model (SPM) are mostly responsible for the specific heat of the temperature $T > 1\ K$. They are independent of the elastic properties but depend strongly on density of material [68]. Below 1 K the linear part of specific heat due to TLS dominates the specific heat and gives a linear dependence on temperature. The striking fact is that the glassy state of the same material will give a higher specific heat than its crystalline counterpart (see Fig. 4.4). These tunneling entities are responsible for this excess of specific heat below 1 K in a-solids.

1.7.3 Thermal conductivity

The phonon heat transport in a-solids is characterized by the phonon-TLSs interactions. These interactions are inelastic and dominate the scattering mechanisms in glasses below 1 K. Hence, the phonon MFP is dominated by phonon-TLSs interactions. The bulk phonon MFP, being limited by these interactions lies in the range of $20\ \mu m < \Lambda_{ph-TLS}^{bulk} < 200\ \mu m$ [63, 73]. In the tunneling model, the resonant scattering of phonons (the inverse of phonon MFP) from two-level systems is given by:

$$\Lambda_{\alpha}^{-1}(\omega) = \frac{\pi \gamma_{\alpha}^{2} \omega}{\rho \nu_{\alpha}^{3}} P \tanh\left(\frac{\hbar\omega}{k_B T}\right) \tag{1.60}$$

α is the polarization of phonons, and γ is the phonon-TLS coupling. ρ and ν respectively represent the mass density and the sound velocity. The thermal conductivity $\kappa(T)$ is evaluated on the assumption that heat is carried by non-dispersive sound waves. The kinetic theory prediction for the thermal conductivity, that is described by equation 1.34, seems to be appropriate for glasses. The point is that, in the kinetic equation, C_{ph} is the specific heat of the phonons carrying heat, not the one which comes from the contribution of localized excitations c_{TLS}. The kinetic equation for the a-solids can be expressed as:

$$\kappa(T) = \frac{1}{3} \sum_{\alpha} \int_{0}^{\infty} C_{ph}(\omega) \nu_{\alpha} \Lambda_{\alpha} d\omega \tag{1.61}$$

$$= \frac{\rho k_B^3}{6\pi\hbar^2} \left(\sum \frac{\nu_{\alpha}}{P \gamma_{\alpha}^{2}} \right) T^2 \tag{1.62}$$

This formula gives general agreement with the experimental results below 1 K. The TLSs density of states are assumed to be constant with the coupling constant of $\gamma \approx 1eV$. The experimental results report the temperature dependence of thermal conductivity of a-solids of $T^{1.8}$. This dependence indicates that the distribution function of TLSs is not truly constant [61, 64, 65].

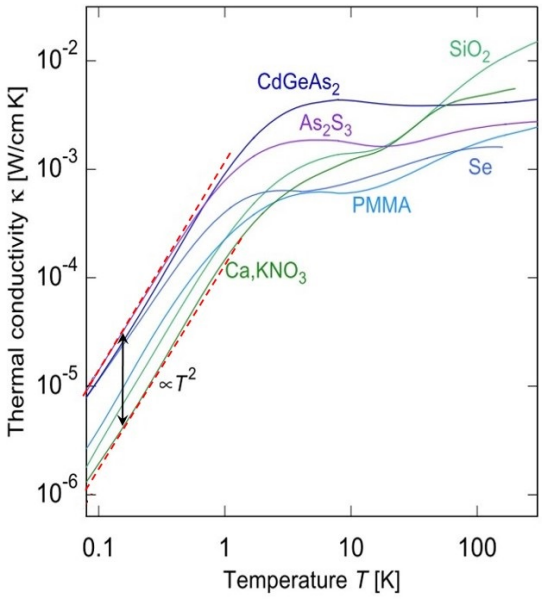

Figure 1.18: **Thermal conductivities of a-solids at low temperature.** All the thermal conductivities lie within one order of magnitude (*glassy range* showed by red dashed lines) and show a T^2 rather than a T^3 dependence like the crystalline solids [61].

TLSs density of states

According to Phillips estimation, TLSs density of states n_0 are independent of elastic properties or chemical compositions, and it was assumed to be constant for any kind of disordered material below 1 K [64].

Some recent experimental results have reported the reduction of TLSs density of states due to the preparation techniques such as growth temperature [72], e-beam evaporation [74, 75], or ionic implantation [76, 77]. On the other hand, some theoretical analysis have pointed out the dependence of TLS density of states on the frequency $n(\omega) \propto \omega^{\mu}$, that leads to $\kappa \propto \mathrm{T}^{2-\mu}$ and $C_{TLS} \propto \mathrm{T}^{1+\mu}$ that have a better matching with experimental data [71, 78–80]. Recently, by investigating dielectric losses in amorphous SiO_2 thin film at different frequencies, Skacel *et al.* [81] found that the TLS density of states is energy dependent.

All these results proves how poorly the tunneling states in amorphous material are known. For instance the dependence of these TLSs on confinement or stress is still a subject of debate. Understanding these TLSs in more details is quite crucial since they are responsible for noise-producing aspects in superconducting resonators [82], and also source of the decoherence of quantum entangled states in Josephson quantum bits [83–86].

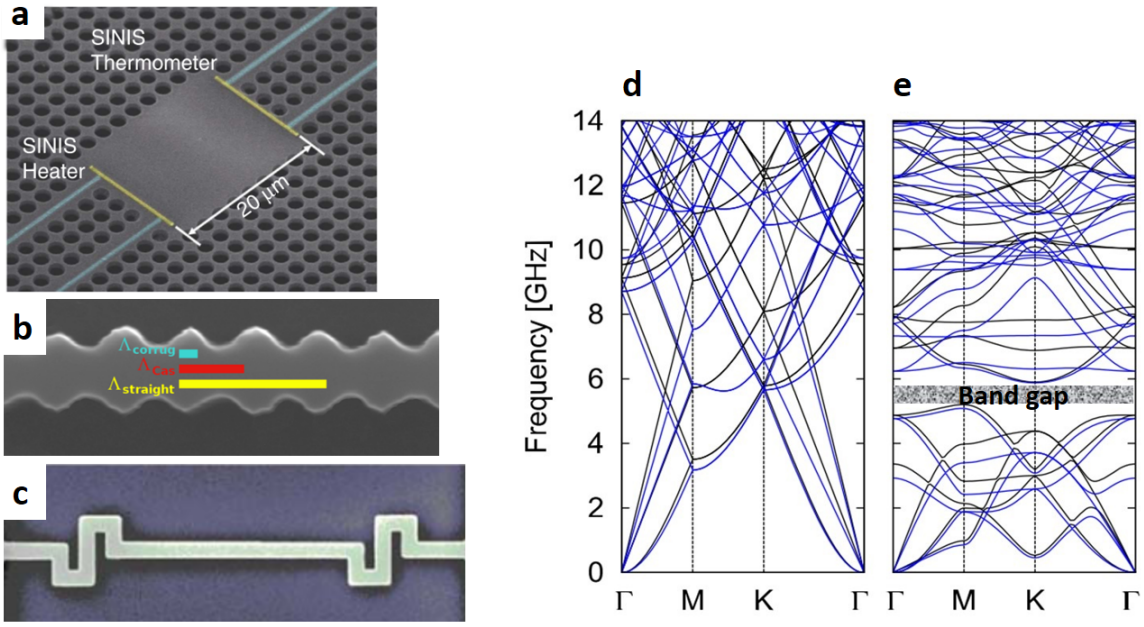

Figure 1.19: **phononic crystals.** (**a**) SEM image of phononic crystal with periodic holes elaborated by Maasilta's group [92]. (**b**) The corrugated Si nanowire that exhibit a thermal conductance below Casimir limit. The scale bars represent the phonon MFP in corrugated nanowire (blue), Casimir limit (red), and straight nanowire (yellow) [100]. (**c**) Si nanowire with serpentine structures can reduce the thermal conductance up to 40% [101]. (**d**) Dispersion relation of full simple membrane of silicon nitride (Blue lines) and silicon (Black lines) in comparison with the same membrane with periodic holes (**e**) [48].

1.8 Nanophononics

Nanophononics is a recent field of research that refers to engineering the properties of lattice vibrations sound or heat in all type of materials. By engineering we mean designing materials or structures in the aim of promoting the fundamental properties to control and manipulate elastic waves or acoustic phonons [87]. Phononic crystals (PnC) which is one of the branches of nanophononics contains a diverse spectrum of technology such as thermoelectric applications, thermal insulation, thermal diode, guiding elastic waves or acoustic phonons, energy harvesting, and even earthquake protection [88–91].

PnC can be achieved by periodically pattering inclusions in a matrix. The inclusions can be holes (see Fig. 1.19 **a**) [92, 93], implants [94] or pillars [95–97]. The PnC can exhibit absolute band gaps where the propagation of acoustic waves is prohibited for any polarization (see Fig. 1.19 **e**). The appearance of the band gap is due to the contrast between the elastic properties of the matrix and the inclusions. Differently said, it is the consequence of the coherent destruction of phonon modes by Bragg scattering [94, 98, 99].

PnC have been widely used at room temperature to engineer acoustic band gap [94]. However, at low temperatures in addition to the effects caused by modified dispersion relation, purely geometrical effect, and coherent effects can be seen as well. In our group, it was shown that corrugated silicon nanowires exhibit a thermal conductivity even below the Casimir limit due to emergence of phonon backscattering by surfaces (Fig. 1.19 **b**) [100]. Another work below 4 K on nanowires having S-shaped chicanes (Fig. 1.19 **c**) showed a reduction in the thermal conductance ranging between 20% and 40% in comparison with a straight nanowire [101]. This purely geometrical effect comes from the contribution of ballistic phonons to the thermal transport at low temperature [1].

All these possibilities of managing thermal transport via nano-engineering are feasible with regular nanofabrication. From suppression of thermal conductivity with PnC to phonon blocking and thermal diode devices are such a vast field of application that needs to be explored.

One of the most interesting concept of thermal management is the thermal diode; a device that can conduct heat only in one direction. This kind of device can be compared to their electronic counterparts. The condition of realization of the thermal rectification can be summarized in two basic assumptions: the device should be either geometrically asymmetric connecting to the two terminals, and the existence of non-linearity in system vibrational states.

The primary idea for the thermal rectification was based on nonlinear one dimensional lattice, connecting to two reservoirs at different temperatures [102–104]. Indeed, the nonlinearity of lattice will cause temperature dependence of the phonon band, and that makes the rectification effect possible.

The first microscopic solid-state thermal rectifier was built by Chang and coworkers [105]. By applying externally and inhomogeneously an assymetric mass-loaded of heavy molecules on carbon nanotubes or boron nitride nanotubes, they have observed a thermal rectification of 7%. This approach introduces assymetric boundary scattering of phonons. In an other work by Scheibner and coworkers [106] high effective thermal rectifier properties was observed with quantum dot semiconductors up to 10%. According to their analysis, the heat transfer is controlled by the electronic resonance inside the system.

Among all the achieved works, the thermal rectification by ballistics phonons in asymmetric nanostructures was proposed to have highest rectification [107]. The only feature to manipulate is the structural engineering in an asymmetric configuration. It is easy to fabricate, independent of electronic properties, and executable using the existing technologies. These kinds of thermal diodes have been analyzed theoretically [107], but not experimentally.

In general, thermal rectification would have deep implications in thermal circuits, thermal logic gate, and thermal transistors, and could be a new opening door to the quantum computers [103, 108].

1.9 Conclusion

In this chapter, the theoretical features of the thermal properties in two extreme situations of low temperature and low dimensions have been presented. The thermal properties are governed by both electrons and phonons. In semiconductors and dielectric insulators, the phonon contribution in the thermal properties dominates. The phonon characteristic lengths play an important role in both specific heat and thermal conductivity. These lengths are the phonon dominant wavelength and the phonon MFP, and they depend inversely on the temperature. Thus, by decreasing the temperature the phonon characteristic lengths will increase. For instance, below 1 K the phonon dominant wavelength λ_{dom} can reach several hundred nanometers, and the phonon MFP can reach several millimeter.

Low dimensions will have two major effects on the thermal properties. The first effect is an inherent low dimensional effect which is a new dispersion relation or energy states in comparison with bulk counterpart. The second one is the geometrical effect by the emergence of boundary scattering. When the dimension of the system is smaller than the phonon characteristic length, then the whole scattering of phonons are governed by the boundaries. Based on the way that phonons are scattered from the surfaces, there are coherent effects (elastic scattering) or incoherent effect (inelastic scattering). Phonon scattering varies from classical inelastic boundary scattering known as Casimir regime to completely elastic scattering of quantum limit. Indeed, when the phonon dominant wavelength becomes much bigger than the roughness of the surfaces, then the scattering of phonons will be specular by the edges. In this case, in a 1D channel for example, the heat current can be expressed by the probability of phonon transmission. So, when the whole phonon scattering are specular, and the transmission coefficient is equal to one, then the thermal conductance of 1D channel should tend to the universal value of thermal conductance. However, there are some fundamental physical features that dominates the transmission coefficient and cause a deviation of thermal conductance from universal value. The effect of low temperature and low dimension will cause a new set of fundamental properties in both phonon conduction and energy storage. The possibility of tailoring the thermal properties by confinement has created a new field of physical science that is known as *nanophononic*. One of the most interesting branch of nanophononics is the phononic crystal (PnC); which is engineering the geometry in the aim of controlling the properties of the system. The main advantage of working with PnC at low temperature is that the coherent effects and purely geometrical effect can be seen as well.

The key to understand the effects of low dimensionality and low temperature on thermal properties is the experimental measurements. Measuring such small systems at low temperatures requires highly developed and low noise measurement setups. The next chapter is focused on the experimental approaches for the measurement of thermal conductivity and specific heat in confined systems at very low temperature.

2 CHAPTER

Sample fabrication and experimental techniques for measurement of thermal conductance

2.1 Introduction

Measuring thermal properties of nanosize objects at low temperature is quite challenging. For instance, to evaluate the specific heat of 2D membrane with a mass less than 0.2 ng, or to measure the thermal conductance of 1D channel, where the expected value is the universal quantum of thermal conductance ($\cong 10^{-13}$ W/K), one needs to elaborate highly sensitive experiments. The basic principle of measuring the specific heat is first of all

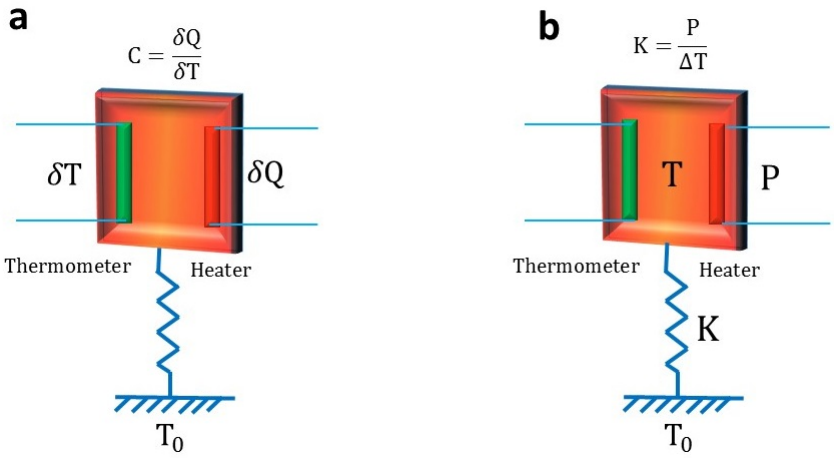

Figure 2.1: **The schematic configuration of the thermal properties measurement.** (**a**) Specific heat measurement and, (**b**) thermal conductance measurement.

isolating the system, then introducing a quantity of energy δQ into the system, and measure the temperature variation δT. The specific heat can be calculated as $C_p = \delta Q/\delta T$. For measuring the thermal conductance as $K = P/\Delta T$ (P is the dissipated power and ΔT is the temperature gradient), one needs to create a ΔT by supplying a heat power to one of the ends of the system and measuring the resulting temperature gradient. A schematic representation of the measurement of specific heat and thermal conductance is shown in Fig. 2.1. In order to measure a thermal conductance in the range of the universal value of the quantum of thermal conductance (10^{-13} W/K), one needs to apply very low temperature gradient in the order of 10 mK. Consequently, it leads to dissipated power P of 10^{-15} W. These small energies necessitate to use low noise and highly sensitive electronic setups at sub-kelvin temperature on nanosize samples. The considered experiments require a fully adapted system to the temperature range of experiment. In this chapter, first of all, we will explain the fabrication process of the suspended nanocalorimeters for measurement of specific heat of 2D membrane and the thermal conductance of 1D channel. Then, the different characteristics of the thermometer from the sensitivity and precision of measurement to the limitations of the measurement are explained. At the end, different possible techniques for measuring the thermal conductance are shown. We will also explain why some measurement techniques such as 3ω for thermal conductance measurement is not adapted to the limits of our experiments.

2.2 State of art of calorimetry

Nanocalorimetry is a powerful technique which is widely employed to reveal a great deal of information in various field of physics. It has been applied to study enthalpy of chemical reactions [109], absorption sensor [110], kinetics and glass transitions [111–114], biological analysis of DNA [115, 116]. Low-temperature nanocalorimetry is particularly suited for the investigation of superconductors [117], fundamental energy excitation, and other novel systems with anomalous electronic phase transitions.

2.3 Sample preparation

Generally, for measuring transport properties in any material, the sensing structure must be more insulated than the sample under test, which prevents the leakage of heat or current (this applies both to electrical and thermal measurements). However, the electrical conductivity of materials spans over 20 orders of magnitude, while the thermal conductivity of any solid lies within 4 orders of magnitude range (0.1 $\mathrm{Wm^{-1}K^{-1}}$ to 1000 $\mathrm{Wm^{-1}K^{-1}}$). This implies that the measurement of the thermal conductivity cannot be performed in the same conditions than the electrical conductivity. To thermally isolate a system, one should build the structures mechanically suspended. In the framework of this thesis, all samples have been synthesized at Institut Néel in the Nanofab clean room.

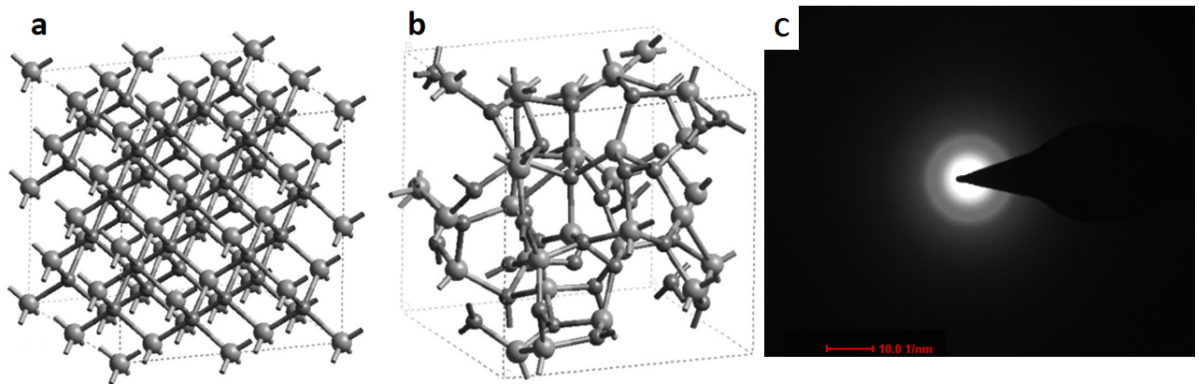

Figure 2.2: **Silicon nitride structure.** (**a**) Crystalline and (**b**) amorphous supercell of silicon nitirde. (**c**) TEM diffraction pattern of SiN_x (obtained by Martien Den Hertog at Institut Néel). The TEM diffraction pattern shows that the SiN used in our experiments has fully amorphous structure.

2.4 Fabrication of Si_3N_4 membrane-based nanocalorimeter

The samples are micro-fabricated from 100 mm^2 Si wafer having a 100 nm thick thermally grown silicon nitride layer on top, with an internal stress of 0.85 GPa. Amorphization of silicon nitride structure has been investigated theoretically by F. Alvarez *et al.* [118]. Through their analysis, the crystalline and amorphous phase of silicon nitride are compared (see Fig. 2.2 **a** and **b**). It can be seen that in amorphous state of SiN (Fig. 2.2 **b**) the low density regions (micro and nanovoids) are significantly enhanced in comparison to the crystalline one (Fig. 2.2 **a**). The TEM diffraction pattern of steochiometric SiN_x shows that it has a fully amorphous structure (see Fig. 2.2 **c**). The fabrication process contains several steps of laser and electronic lithography, thin film deposition and, chemical etching that will be explained in more details.

The elaborated nanocalorimeter is a membrane-based calorimeter suspended by eight supporting beams. On each membrane, there exists a resistive heater as a thin film of copper and gold (Cu/Au), and a resistive thermometer made of niobium nitride (NbN). The fabrication of each step is explained in the following sections.

2.4.1 Current leads

The current leads are made of 70 nm thick of niobium titanium/gold (NbTi/Au) deposited by homemade magnetron deposition. Niobium titanium with its critical temperature around 7 K is used to reduce significantly the thermal conductance of the electrical leads due to their low thermal conductance. Indeed, the thermal conductance of a super-

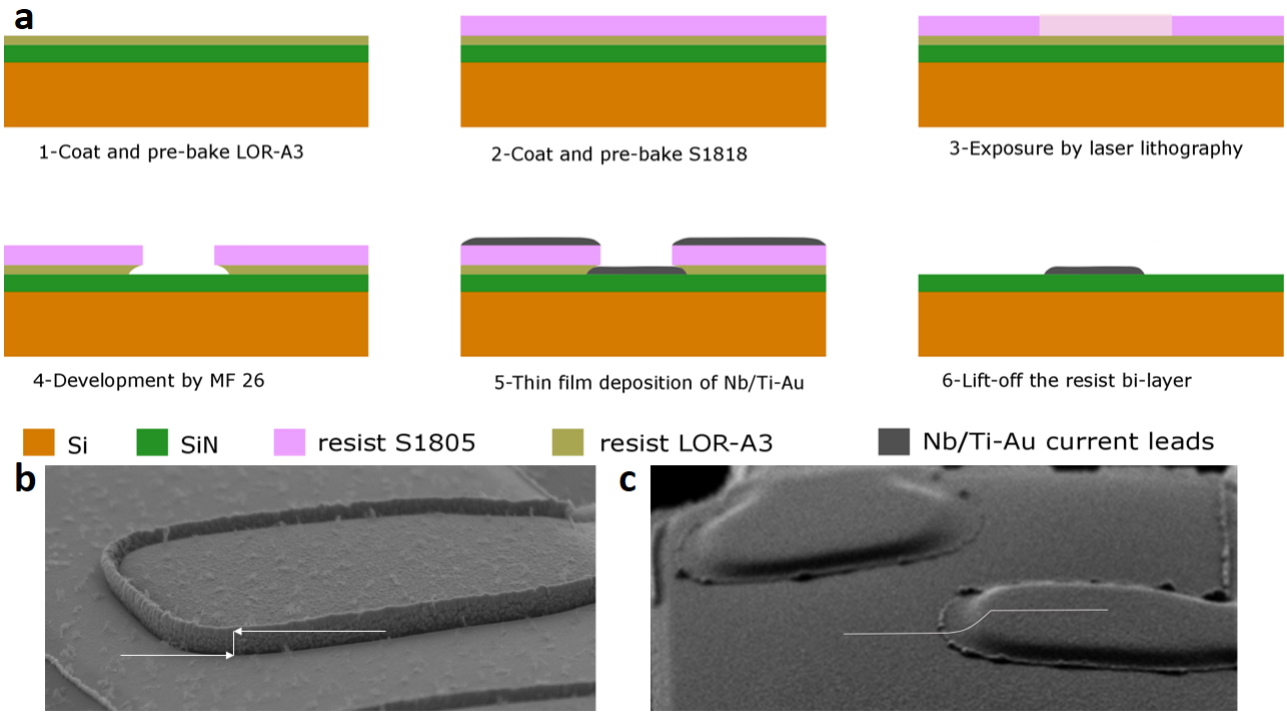

Figure 2.3: **Smooth integration of current leads to the contacts.** (**a**) The schematic configuration of each step of current leads deposition with bi-layer photo resist S1805 + LOR-3A. (**b**) The current leads with use of just the resist S1805. (**c**) The current leads with use of the bi-layer resist S1805 + LOR-3A.

conductor is much lower that the one of a normal metal, because part of the electrons at Fermi level are condensed in cooper pairs. As the temperature decreases less and less unpaired electron exist at the Fermi level to carry heat. In the temperature range of our experiments niobium titanium is superconductor, thus the only part that generates heating effect (Joule effect) is the heater and not the current leads.

30 nm of gold is deposited on the top of NbTi to ensure good electrical contacts within the interface of the thermometer. The quality of the contacts has a direct impact on the sensitivity of the measurement. Any kind of bad electrical contacts to the thermometer creates a capacitive impedance that gives rise to electronic noises. Moreover, to avoid these capacitive impedances, before deposition of current leads we used a bi-layer of photo-resist in order to have smooth connections. At the connection of current leads to heater or thermometer, the use of two different resists (Shipley 1805 and LOR-3A) creates a smooth step instead of an abrupt one (see Fig. 2.3).

2.4.2 Heater

The heater is a resistive element in which an ac or dc current passes to dissipate energy into the system by Joule effect. It should have several criteria to respect: the resistance should not depend on temperature, it should have very low specific heat, and the thermal contact with silicon nitride should be optimized. Copper deposited by Joule evaporation for 70 nm thickness fulfills these requirements. The average resistance is in order of 50 Ω. The heat capacity of the thin film of Cu is estimated in table 4.1.

2.4.3 Thermometer

The thermometer is the key element of the calorimeter. In our experiments either for specific heat or thermal conductance measurements, we need to have a very small temperature gradient. In this aim, there are various requirements which the thermometer has to fulfill:

- the thermometer should have a sensitivity of measurement about microkelvin.
- the functionality of the thermometer should be optimized in the operating temperature range (from 0.03 K to 6 K).
- the thermometer should be reproducible over several cycles of temperature.
- the integration of the thermometer into the nanocalorimeter should be optimum with good thermal couplings (Kapitza).

Based on these criteria, a resistive thermometer has been used. This kind of thermometry is based on the dependence of the electrical resistance of the material on temperature. Metal thermometers such as Pt have a resistance saturation around 20 K, and at lower temperature, their resistance becomes temperature independent. Thus, metals cannot be used as a thermometer at very low temperatures. The thermometer we used is based on niobium nitride ($Nb_1N_{1.6}$) which is known as Mott-Anderson insulators [119]. The NbN films are deposited by reactive sputtering using a pulsed power supply magnetron in a mixture of nitrogen and argon gases. Two mass flow debimeters control the composition of the gas mixture. The level of nitrogen in alloy thin film is adjusted by the proportion of nitrogen and argon gases. By controlling this level, one can adapt the performance of the thermometer in any willing temperature range [120]. This kind of resistive thermometry can rise to unprecedented sensitivity over a wide range of temperature. Moreover, the deposition process allows the integration of such thin films into any micro or nanofabricated devices. The mechanism of Mott-Anderson resistive thermometer is described in section 2.6.

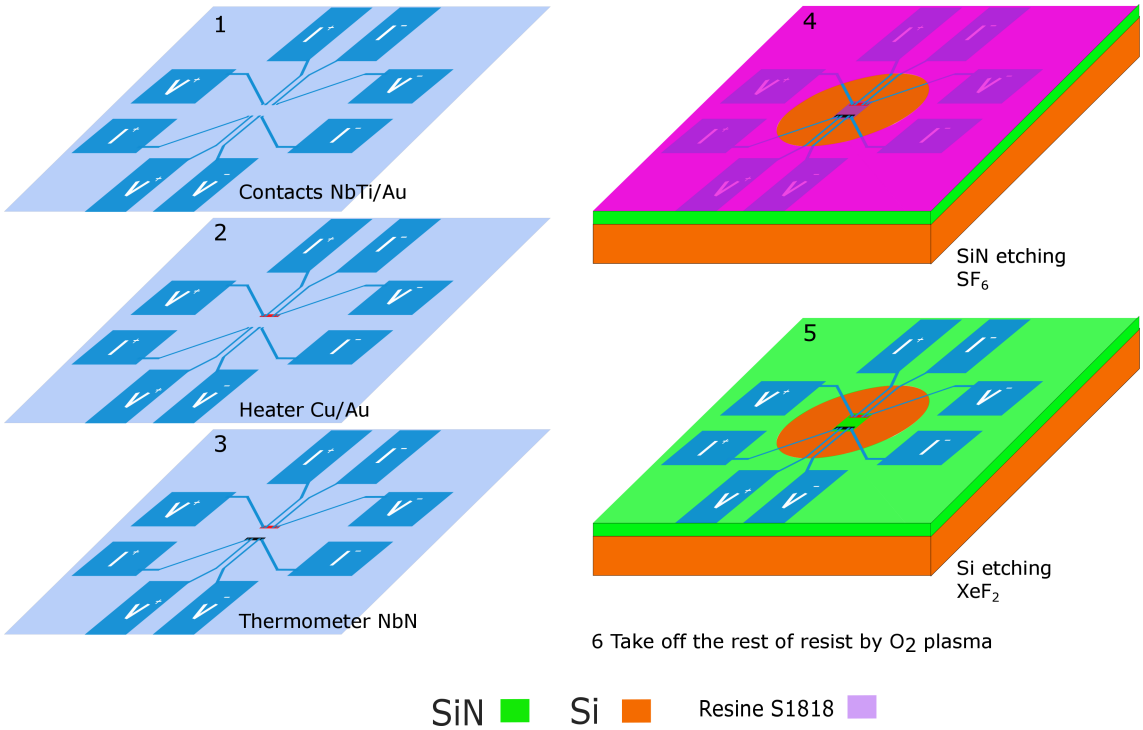

Figure 2.4: **The fabrication steps of membrane-based nanocalorimeter.** Schematic representation of the fabrication process for the membrane-based nanocalorimeter for the measurement of specific heat of 2D membrane. 1- Design and deposition of current leads (NbTi/Au). 2- Deposition of 70 nm thick of copper and 20 nm of Au as the heater. 3- Deposition of NbN sensors. 4- Etching SiN by SF_6 plasma. 5- Etching Si by XeF_2. 6- Take off the rest of resist by O_2 plasma.

2.4.4 Etching processes

After having done the three first steps of fabrication including, contacts (current leads), heater and thermometer, one need to make the structure suspended. Since the wafers in use consist in 100 nm of SiN and a bulk Si, the etching will be done in two parts. Etching SiN by SF_6 plasma, and etching Si by XeF_2.

1 - SiN etching with SF_6 plasma: by using laser lithography, the geometry of the membrane, and the structure which will be suspended, is determined. Then under SF_6 plasma, the unprotected area will be etched homogeneously with the rate of 40 nm/min for high-stress SiN. The time management in this step is quite crucial, especially in the case of a double platform with nanowires (it will be explained in the next section 2.5). If the etching time is not enough, then in the next etching process (Si etching), the structure will not be suspended. In contrast, if the etching time is too long, then the structure will be over-etched, and it will weaken the structure. In the case of the fabrication of nanocalorimeters with bridging nanowires, the smallest over-etching can break the nanowire easily. What should be also mentioned is that the etching rate will change

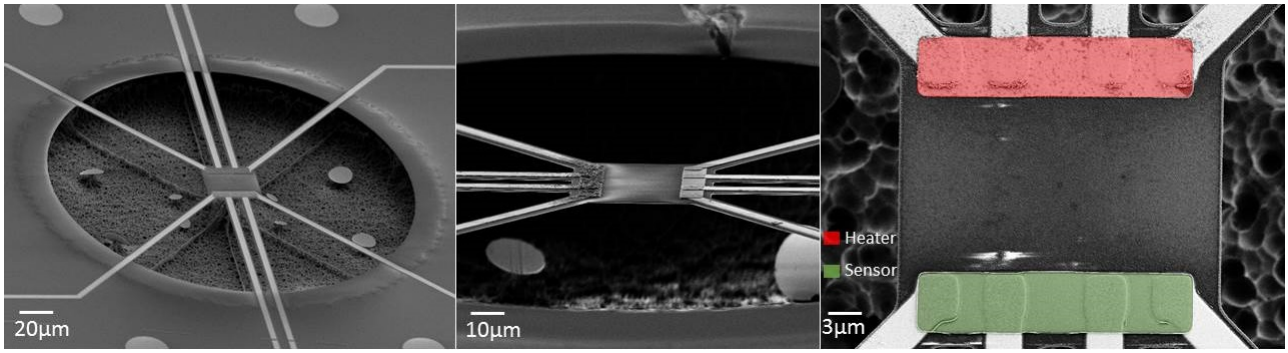

Figure 2.5: **SEM images of the membrane-based nanocalorimeter.** Nanocalorimeter is made of high-stress silicon nitride suspended by eight suspending beams. The membrane contains a heater (red rectangular), and a resistive thermometer of NbN (green rectangular). Each heater or thermometer is polarized or measured by four point measurement. This nanocalorimeter is elaborated for the measurement of specific heat of 2D phonon cavity or the thermal conductance of the supporting beams.

based on the internal constraint of material in use. In fact, the speed of etching for high-stress SiN, is faster than low-stress and super low-stress SiN.

2 - Si etching with XeF_2: when the SiN is fully etched, then by etching the Si bulk the whole structure will be mechanically suspended. To avoid the oxidation of silicon, SiN etching and Si etching processes should be done one after another with no waiting time. The xenon difluoride gas does not etch SiO_2, aluminum, nor resists, and it has a high selectivity between Si and SiN. This is very convenient as it allows the suspension of the SiN nanocalorimeter as the final step. The nanocalorimeter is protected by resist S1818 in order to avoid any chemical interaction of XeF_2 with the NbN thermometer. The chemical reaction is the following:

$$XeF_2\ (gas)\ +\ Si\ (solid) \Longrightarrow 2\ Xe\ (gas)\ +\ 4\ SiF_4\ (gas) \tag{2.1}$$

This etching process is based on cycles of 30 seconds, with a pressure 3 bar of XeF_2 gas. The number of cycles will be chosen based on the surface and the depth of etching. The Si etching is the final and the most delicate step of fabrication because the smallest mechanical constraint between a released part of nanocalorimeter and an unreleased part can break the supporting beams, and as a result, destroy the sample. When this step is done, the rest of resist will be taken off by O_2 plasma. A representative scheme of each step is presented in Fig. 2.4. A fabricated sample is shown in Fig. 2.5. This kind of nanocalorimeter can be used for the measurement of the heat capacity of the membrane, or the thermal conductance of the supporting beams.

After having explained the fabrication of membrane-based nanocalorimeter, now the fabrication of double suspended nanocalorimeter with bridged nanowires between the membranes will be explained. This system is designed for the measurement of the thermal

conductance of nanowires at very low temperatures.

2.5 Bridging Si_3N_4 nanowires between double suspended nanocalorimeter

Double suspended nanocalorimeter consist of two membrane-based nanocalorimeters (as it is explained in section 2.5) with nanowires connecting them monolithically. The nanowires are designed in a way of having a perfect coupling to the membranes without any contact resistance. In the fabrication process, we have identical steps as in a simple nanocalorimeter for current leads, heater, and thermometer.

2.5.1 E-beam lithography

The main objective of fabricating the double suspended nanocalorimeter with nanowire connecting between the two nanocalorimeters is to investigate the quantum limit of heat flow in a 1D channel. As explained in section 1.5.3, in order to attain the quantum limit of heat flow in a nanowire, the section of the nanowire d should be much smaller than the phonon dominant wavelength λ_{dom}. So having the nanowire with small section is a crucial criterion to reach to the quantum limit. In this objective, the nanowires are designed to have a diameter in the center of approximately 100 nm. Such small dimension can be elaborated only by e-beam lithography. The minimal area size of the beam is 4 nm. This allows us to create any wanted shape of nanowires. The connection parts of the nanowires to the membranes are patterned with the catenoidal shape (the choice of this shape is explained in section 1.5.3).

Al mask: in the thermal conductance measurement of 1D channel, the phonon scattering by the edges will affect the regime of the phonon transport (explained in section 1.5.2). To have a perfect specular reflection by the edges of the nanowire, one needs to have the minimum roughness on the surface. To do so, after electronic lithography, an aluminum thin layer (30 nm thick) is evaporated on the isolated area by e-beam (shape of nanowires). This evaporation is achieved by fixing the temperature of the sample at 100 K. This cold evaporation will cause the minimum roughness on the edges (roughness < 3 nm).

The silicon nitride layer is then structured by SF_6 reactive etching, using the aluminum as a mask. This step will determine the final geometry of the membranes, the nanowires, and the suspending beams. Then a basic solution (MF26) will remove the aluminum on the nanowires. Then the sample is ready for Si etching by XeF_2. After etching Si and full suspension of the membranes and nanowire, the rest of resist will be taken off using O_2 plasma. A schematic representation is shown in Fig. 2.6, and a finished nanocalorimeter

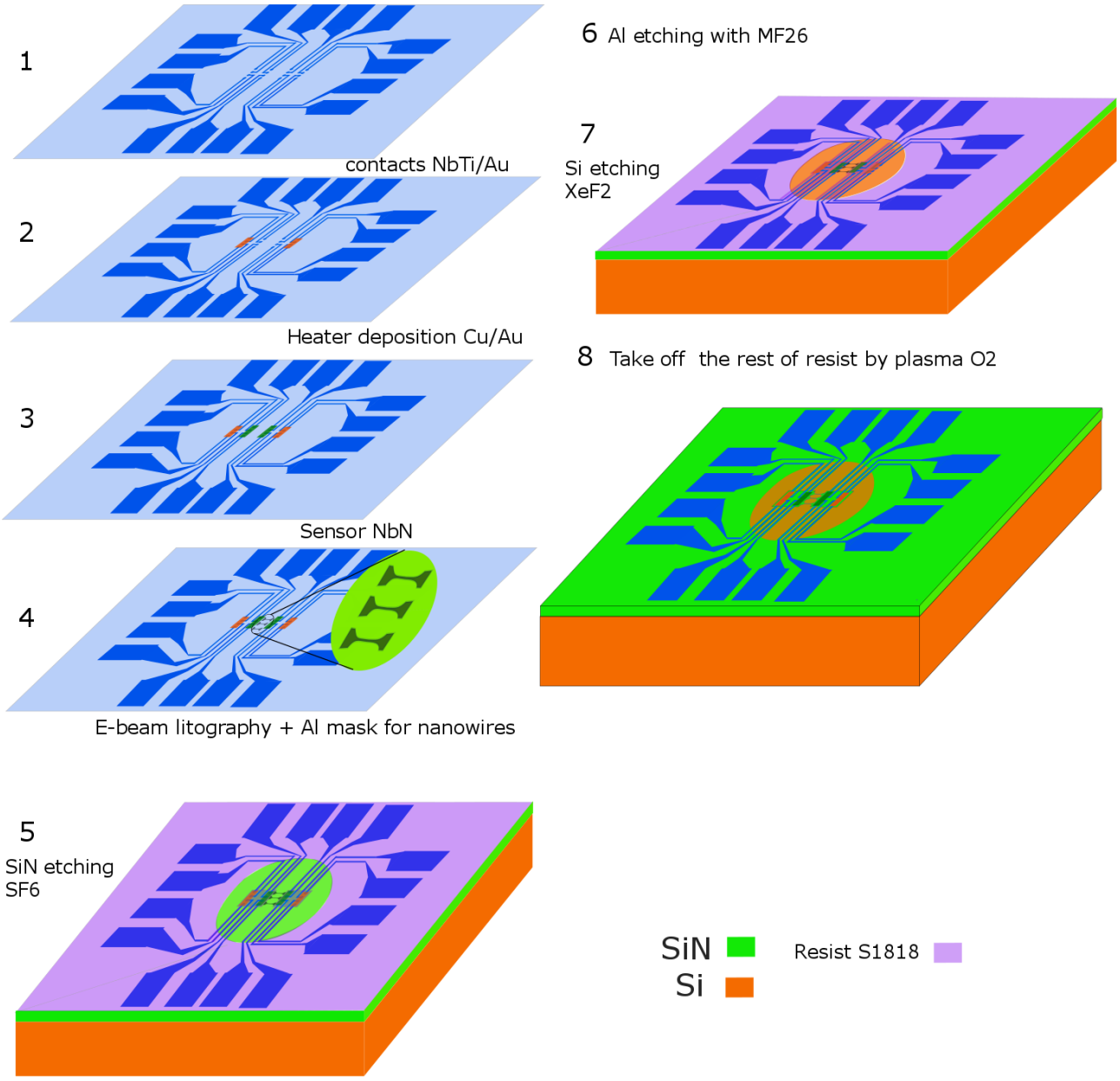

Figure 2.6: **The fabrication steps of double membrane-based nanocalorimeter with bridging nanowires.** The fabrication steps are the evaporation of 1- current leads NbTi/Au , 2- heater Cu/Au, 3- the NbN thermometer, 4- design of nanowire by e-beam with catenoidal shape of the contacts and Al evaporation on the nanowires, 5- SiN etching by SF_6 plamsa, 6- Al etching 7- Si etching by XeF_2, and 8- removing the rest of the resist with O_2 plasma.

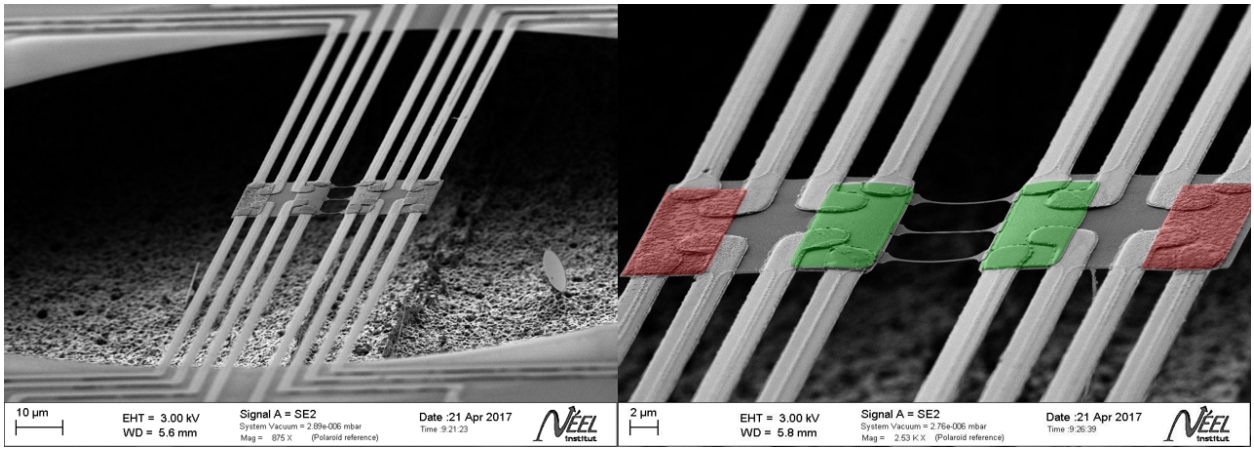

Figure 2.7: **SEM images of the double membrane-based nanocalorimeters with bridging nanowires**. Right image shows an angle view of the nanocalorimeter including nanowires between the membranes. Left image is a zoom on the membranes and nanowires. Red parts are the heaters, and green parts are the thermometers.

including nanowires are shown in Fig. 2.7.

2.6 Thermometer characterisation

Functionality of metal-insulator resistive thermometer: niobium nitride ($Nb_1N_{1.6}$) is a resistive thermometer which is known as metal-insulator (Mott-Anderson) materials. The niobium is a superconductor at low temperature. By alloying it with nitrogen, it becomes a metal-insulator material. In these materials, the electronic conduction happens in an intermediate regime between metal and insulator, within a process that is called *hopping*. At room temperature, thermal agitation leads to delocalize the electrons from one potential to another, so NbN remains a conducting material like a bad metal. At low temperature, the localized disorder introduced by the nitrogen dominates. The electrons are localized in the potentials energy well created by nitrogen deposition, inducing NbN to act as an insulator at T=0 K. Thus the resistance increases progressively as the temperature decreases (see Fig 2.9). In this regime of low temperature, the resistivity of the metal-insulator materials can be described by [121, 122]:

$$\rho(T) = \rho_0 \exp\left[\left(\frac{T_0}{T}\right)^{\frac{1}{4}}\right] \tag{2.2}$$

The other well-known methods for low temperature thermometry are, e.g., transition edge sensors (TES) [13, 123, 124], superconducting tunneling junctions (NIS/SINIS) [125–127], Coulomb blockade junctions [128]. They have a good integration into the systems of very small dimensions, but when it comes to sensitivity on the large range of temperature, the metal-insulator thermometry is a better option.

Thermometry measurement: the resistance of the thermometer is measured by the most commonly applied technique of four-wire setup (see Fig. 2.8). Four-wire setup configuration permits spatial separation of the current leads and the voltage measurement so that one can extract only the resistance of the thermometer, without including the contribution of the contact resistances and connecting wires to the final value of the resistance. **The sensitivity of the NbN thermometer**: the sensitivity of a resistive

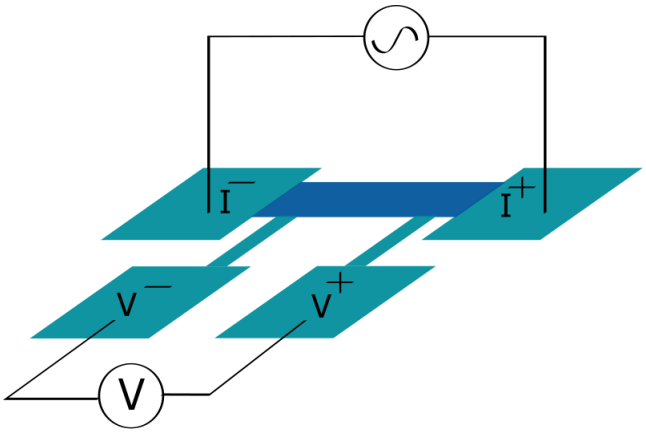

Figure 2.8: **Four-wire setup measurement.** The two external contacts (I+ and I-) are the brings of the current and two internal contacts to measure the voltage, (V+ and V-).

thermometer can be evaluated by the temperature coefficient of resistance α.

$$\alpha = \frac{1}{R}\frac{dR}{dT} \tag{2.3}$$

The higher this value, the better the thermometer will be. Among many thermometric materials, metals such as Pt, have been widely employed. For instance, in earlier calorimeters used for nanoscale thermal measurements [8, 129, 130] due to the ease of fabrication and well integration into various systems. Their main drawback is relatively low α ($10^{-3}K^{-1}$ at 300 K for Pt). NbN thermometer have $\alpha > 1$ K^{-1} below 1 K (see Fig. 2.9 **b**). This high value of α especially at very low temperature makes this kind of materials among the best for low temperature thermometry. In the following section, the specificity of these materials at low temperature is explained.

2.7 Specificity of NbN thermometry at low temperature

Until now, we explained the main advantages of using niobium nitride as a resistive thermometer at low temperature. Now, we will focus on the characteristics of metal-insulator materials at very low temperature. The first observation of the calibration

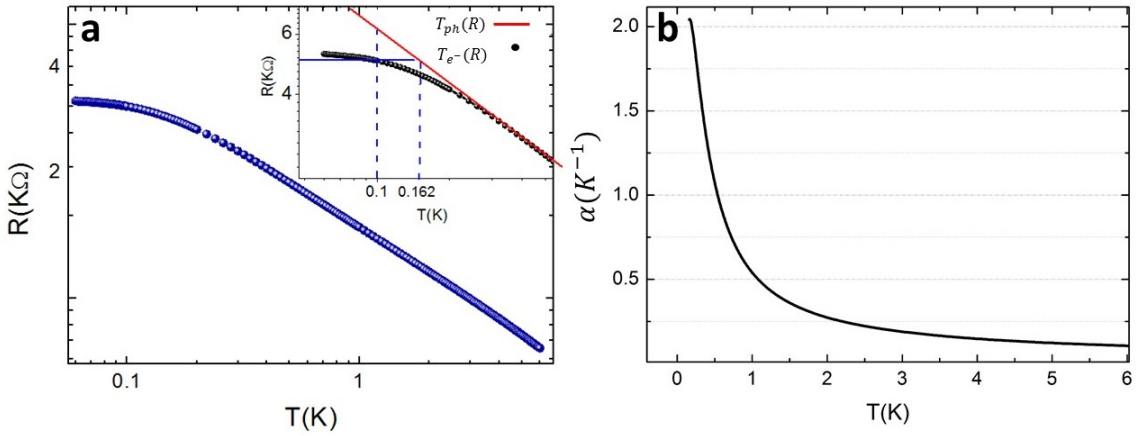

Figure 2.9: **The NbN thermometer calibration and its temperature coefficient of resistance.** (**a**) The NbN thermometer resistance over the temperature range of experiment traced in log-log (from 0.03 K to 6 K). Inset represents a zoom on the low temperature variation of thermometer, where the thermometer starts to saturate. Below 0.1 K the resistance deviates from the fit obtained by equation 2.2. If we consider this saturation as an over-heating, it shows a δT= 62 mK. (**b**) The temperature coefficient of resistance. As it is shown below 1 K $\alpha > 0.5$ and it reaches to 2 at very low temperature.

of NbN thermometer (see Fig. 2.9 **a**) shows a saturation of the thermometer resistance below 0.1 K. The inset of this graph shows a zoom on the resistance variation at very low temperature; the red line is the exponential theoretical fit for metal-insulator materials. A slight deviation of the thermometer resistance from the exponential fit is clearly observed. This saturation will limit the sensitivity of the thermal measurement, that's why it should be understood. This resistance saturation can be originated from either the intrinsic properties of metal-insulator materials, or it can be caused by some external features. The possible scenarios for the saturation of the NbN thermometer at low temperature are:

- decoupling of electron-phonon inside of the thermometer,
- the presence of thermal interface resistance known as *Kapitza* resistance between SiN and NbN,
- self-heating of the thermometer due to the bias current,
- radiative heating (thermal or electromagnetic radiations),
- or it may be related to the intrinsic properties of Mott-Anderson materials.

In the following discussion, each aspect is analyzed separately.

First of all, what we want to measure is the temperature of the phonons inside of the SiN membrane T_{ph-SiN}. What we really measure is the resistance of the NbN thermometer

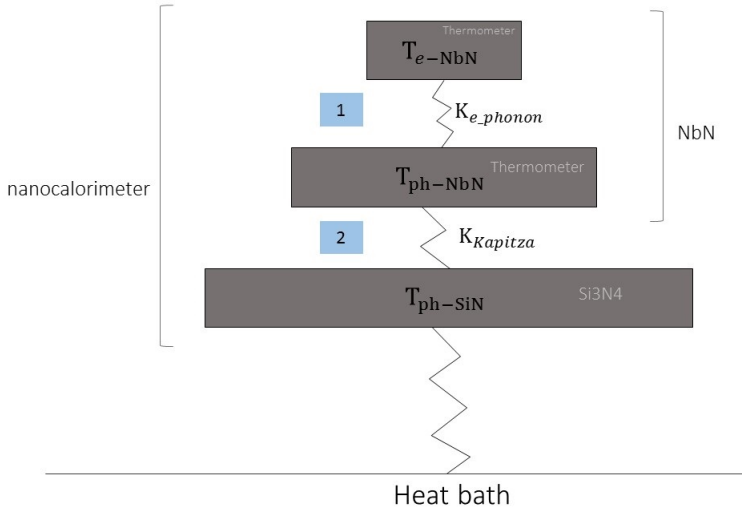

Figure 2.10: **Schematic representation of the interfacial resistances.** Part 1 is related to the coupling of electrons in NbN and the phonons in NbN. Part 2 is the Kapitza resistance which is related to the coupling of phonons in NbN to the phonons in SiN.

by using an electric current. The measured resistance will give a specific temperature which is the temperature of electrons inside of NbN T_{e-NbN}. If there is a good coupling between electrons and phonons of NbN, then their temperature will be equal $T_{ph-NbN} \cong T_{e-NbN}$. The part 1 in Fig. 2.10 shows this coupling process inside thermometer.

The phonons of SiN should be well coupled to the phonons of NbN through the interface between SiN and NbN to have $T_{ph-SiN} \cong T_{ph-NbN}$. The thermal interface resistance that rises due to the non-ideal coupling of the phonons of SiN to the phonons of NbN is the *Kapitza* resistance, and it is shown as part 2 in Fig. 2.10. In the following sections, the analysis on the coupling between electron-phonon and phonon-phonon are discussed.

Electron-phonon coupling: in this section, we will focus on part 1 of Fig. 2.10 that is related to the coupling of the electrons and the phonons inside of NbN. If this *e-ph* coupling is optimized, then $T_{e-NbN} \cong T_{ph-NbN}$. Reciprocally, if this coupling is not sufficient, it means that inelastic scattering of electrons with phonons may not be sufficient to thermalize them, so that $T_{e-NbN} \ncong T_{ph-NbN}$. This phenomenon is described by the following equation:

$$\frac{P}{V} = g_{e\text{-}ph}\left(T_{e-NbN}^5 - T_{ph-NbN}^5\right) \tag{2.4}$$

P is the generated Joule heating power in the thermometer, V is the volume of the NbN film, and $g_{e\text{-}ph}$ is the electron-phonon coupling coefficient. For the coupling coefficient $g_{e\text{-}ph}$ we use the measured value for thin film of $Nb_{1.35}Si_{86.5}$ which is in the order of $(1\pm0.25)\times 10^2$ W/K^{5}cm^3 [121]. If $g_{e\text{-}ph}$ is too low, or equivalently P is too high, we may observe a saturation of the resistance due to electron heating [121, 131, 132].

Let us consider that the resistance saturation is because of *e-ph* decoupling, so $T_{e-NbN} > T_{ph-NbN}$. In Fig. 2.9 **a** inset, the red line shows when *e-ph* are well coupled $T_{e-NbN} \cong T_{ph-NbN}$, and the black dots are measured values, so they represent T_{e-NbN}. The deviation of the black dots from the red line shows the starting point of the *e-ph* decoupling. It shows that when the red line is at 0.1 K (T_{ph-NbN}=0.1 K), the measured value (black dots) shows T_{e-NbN}= 0.162 K. By using these values in equation 2.4, one can calculate the dissipated power inside of thermometer to have this temperature gradient (δT_{e-ph}=0.062 K) between electron and phonon.

A numerical application for a typical measurement (V= 2.24× 10^{-11} cm^3), estimates a dissipated power in thermometer which is $P_{estimated}$ =1.84 × 10^{-13} W. This means if the saturation of the thermometer resistance is because of *e-ph* coupling, the generated power in the thermometer should be equal to $P_{estimated}$. But the real dissipated power in the thermometer (for the resistance of $R \cong 5$ kΩ and I_{th}=1 nA) is $P_{real} \cong 5 \times 10^{-15}$ W. The real dissipated power P_{real} is two orders of magnitude lower than the estimated one $P_{estimated}$. This simple calculation shows that the real generated power in the thermometer is not big enough to cause *e-ph* decoupling.

The difference in the calculation of estimated power and real dissipated power in thermometer proves that this resistance saturation cannot be due to the *e-ph* decoupling.

Self-heating of the thermometer: if the resistance saturation is caused by self-heating of the thermometer, by using a progressive current in the thermometer we promote self-heating. Consequently, the resistance of the thermometer should decrease as the current increases. Within an experimental verification, it was investigated whether the resistance saturation is caused by self-heating of the thermometer or not. The temperature of the heat bath is fixed at 0.03 K, then the current of the thermometer is increased from 20 pA to 4 nA, and its resistance is measured. The measurement is shown in Fig. 2.11. The inset shows the value of voltage with linear variation as a function of current. We see that the resistance of thermometer varies within a constant value without any overheating effect of the membrane.

The measurement with increasing current shows that the resistance saturation is not due to the self-heating of the thermometer.

Kapitza resistance: Kapitza resistance is an interfacial thermal resistance in the region separating any two materials. It will cause a discontinuity in temperature arising across an interface between two materials. This thermal boundary resistance or its inverse the thermal boundary conductance at the interface becomes particularly important at very low temperature [133, 134].

In our device, the membrane is connected to the heat bath by suspending beams. Then, NbN is sputtered on the top of SiN. Thus Kapitza resistance appears at the interface between SiN and NbN thermometer. This interfacial phenomenon is related to the coupling of phonons in the thermometer and the phonons in the SiN membrane (part 2

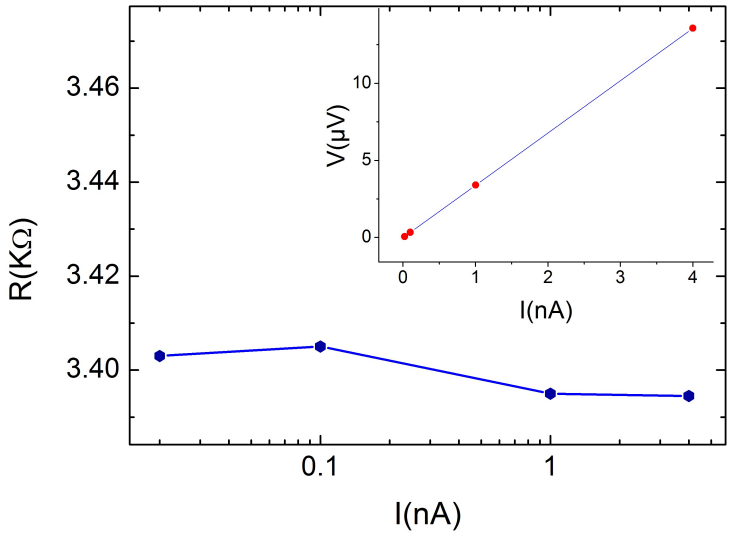

Figure 2.11: **The resistance of NbN thermometer as function of increasing current.** The temperature is fixed at T=30 mK. The current is increased from 20 pA to 4 nA, but the resistance is maintained within a constant value. Inset shows the voltage as a function of dissipated current.

Fig. 2.10).

There are two models for evaluating this resistance, describing the two limits of the heat exchange process between the media. The acoustic mismatch model (**AMM**), and the diffuse mismatch model (**DMM**).

In the AMM, it is considered that on each side of the interface there is a different crystalline material, with different phonon dispersion relation, phonon density of state and sound velocity. These different features of each material will limit the phonon exchange, giving rise to an interfacial thermal resistance. In this model, no scattering occurs at the interface.

In the DMM, at the interface of two mediums all the phonons are diffusely scattered. Below 60 K both models give the same formula: K=$(A/\ \beta)$T^3; where A is the exchange surface in cm^2 and β is a coefficient of Kapitza depending on the materials in contact [133]. In our case β is estimated to be 15 [133]. An optimized coupling between NbN and SiN is then required to ensure $T_{ph-SiN} \cong T_{ph-NbN}$. Hence, $K_{Kapitza} = 1/R_{Kapitza}$ should be optimal. As we see in this formula, the Kapitza thermal conductance depends directly on the exchange surface, so by increasing this surface, one can improve the thermal coupling and reduce the interfacial thermal resistance.

In our case, we have an exchange surface of $A = 7.2\times\ 10^{-4}\times\ 32.8\times10^{-4}$ cm^2. This will gives us $K_{Kapitza} \cong 1.4\ \times\ 10^{-10}$ W/K at T= 0.1 K.

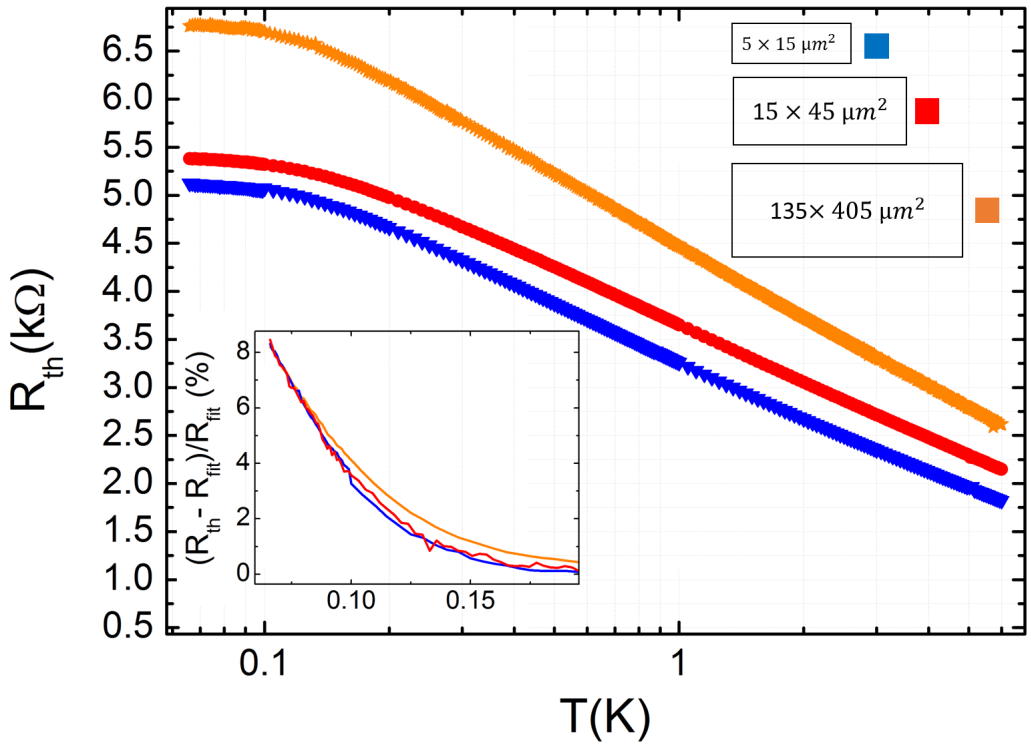

Figure 2.12: **The resistance profile of NbN thermometer with different exchange surfaces.** The resistance of all the NbN thermometers starts to saturate below 0.2 K. The inset shows the derivation of the resistances at very low temperature in percentage (R_{fit}-R_{th})/R_{fit}, R_{fit} is obtained from the equation 2.2.

To verify whether the Kapitza resistance causes the resistance saturation below 100 mK we have two approaches. The first approach is based on calculating the Kapitza thermal conductance between the two interfaces. This Kapitza thermal conductance is equivalent to $K_{Kapitza} = P_{th}/\Delta T$ (P_{th} is the dissipated power in the thermometer $P_{th} = 5 \times 10^{-15}$ W, and ΔT is the temperature gradient between the two interfaces). We know the exact dissipated power in the thermometer, so one can calculate the temperature gradient at the interface by $\Delta T = P_{th}/K_{Kapitza}$. This numerical application gives us a $\Delta T = 4 \times 10^{-5}$ K which is too low in comparison to the temperature gradient that will cause the resistance deviation.

The other approach is showing experimentally that Kapitza resistance does not contribute in the saturation of thermometer. As we see in the Kapitza thermal conductance formula, it depends directly on the exchange surface; so if the saturation of the resistance is due to the Kapitza resistance, by increasing the exchange surface, the temperature at which saturation starts (T_{sat}) should decrease.

In this regard, we have done an experiment based on calibration of various thermometers, fabricated by exactly the same method, but different exchange surfaces. As it is

illustrated in Fig. 2.12, the resistance saturation in all of the dimensions start below 0.2 K. All the calibration show almost the same T_{sat}, even though their exchange surfaces are completely different. The inset of Fig. 2.12 shows the percentage of deviation of the resistances at very low temperature from expected resistance obtained from the equation 2.2. This empirical result shows us that the saturation does not come from Kapitza resistance.

Parasitic radiation: In experiments at very low temperature, the parasitic radiations can have strong impacts on the measured signal. These electromagnetic (EM) radiations can be categorized in two forms:

- from room temperature outside of the cooling system through the cables,
- from low temperature from liquid helium to the sample.

From room temperature through the cables: as explained in previous sections, in order to insulate the systems under measurement, it is mechanically suspended. Thanks to the suspension of the structures, by injecting a small quantity of energy δQ, one can raise the temperature of the system as δT. Thus, even the low frequency electromagnetic waves coming through the cables can raise the temperature of the system, and could be the reason of the resistance saturation of the thermometer at the lowest temperatures. But if the thermometer is not suspended, and it is deposited on bulk Si substrate (it is well coupled to a large heat bath), to raise the temperature of the system as δT much more energy is needed. Generally in non-suspended systems, the low frequency waves can not raise its temperature.

In our experimental setup, all the electrical connections are equipped with a low-pass filter in order to filter the high-frequency waves coming from outside of the cooling system. In Fig. 2.13 **a** the calibration of a thermometer with two different passive filters with different cutoff frequencies (f_c=10 kHz and f_c=1 MHz) is shown. Below 1 K the filter with lower cutoff frequency (f_c=10 kHz) exhibits a sharper slope. This shows how EM waves can affect the sensitivity sharpness of the sensors.

Within an experimental achievement, the resistance profile of a thermometer with suspended structure (Fig. 2.13 **a** blue dots), and a thermometer with the same size with non-suspended structure (Fig. 2.12 blue dots) are compared. The saturation of the thermometer in both graphs starts almost at the same temperature (0.1 K). Whereas, if the thermometer saturation is because of low frequency EM waves, the saturation on suspended structure should occurs at higher temperature because it is more sensitive to the low energy EM waves.

We can conclude that the low frequency waves coming from outside of the cooling system can have an effect on the sharpness of the thermometers, but they are not the source of the resistance saturation of the thermometer.

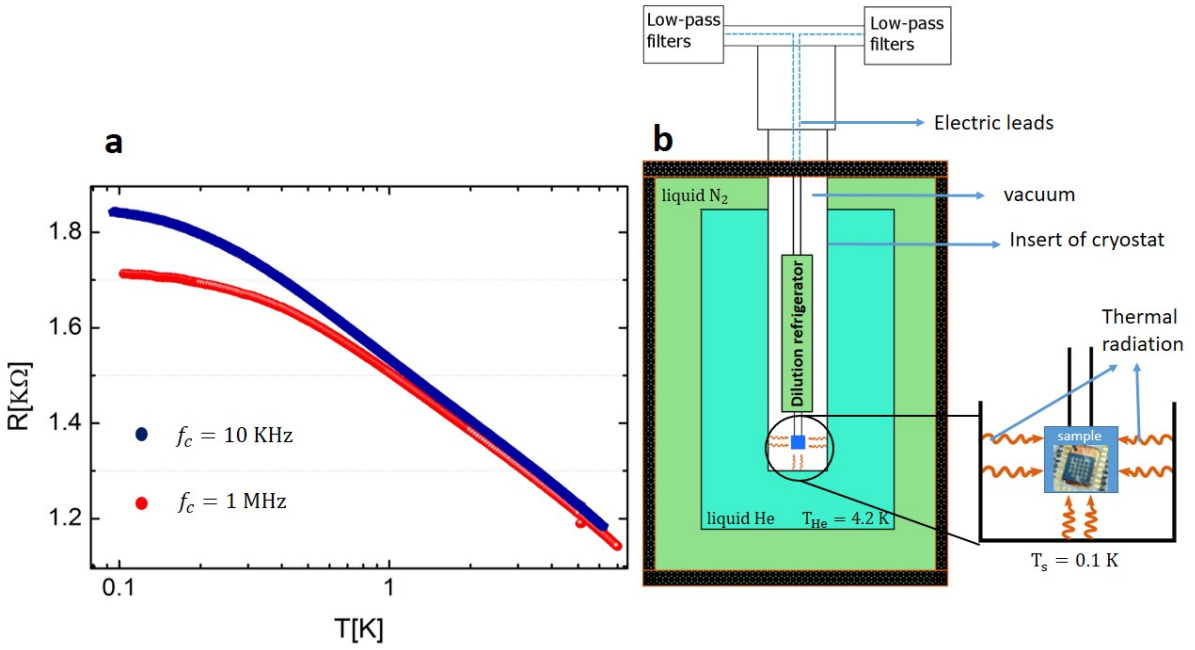

Figure 2.13: **The resistance profile of NbN thermometer of the same device with two different low pass filters, and schematic figure of the cooling system.** (**a**) Red dots represent the filter with the cutoff frequency of f_c=1 MHz, and blue dots with f_c=10 KHz. (**b**) The insert of the cooling system is surrounded by liquid helium at 4.2 K. The thermal radiation comes from the wall of the insert to the sample.

From low temperature from liquid helium to the sample: another radiative parasite is the thermal radiation, that is the emission of electromagnetic waves from all bodies that have non zero temperature. Based on the Stefan Boltzmann law, each body radiates energy in terms of its temperature. The radiative power output from a body with temperature of T_1 to another body with T_2 ($T_1 > T_2$) is given by this mathematical formula:

$$P = \epsilon\ \sigma\ A\ \left({T_1}^4 - {T_2}^4\right) \tag{2.5}$$

where ϵ is the emissivity factor for surfaces which are not black bodies, σ=5.67 $\times 10^{-8}$ (W/K^{4}m^2) is the Stefan-Boltzmann constant, A is the radiating surface area. In the extreme case we consider our sample as a black body of radiation which means ϵ =1. The surface of the nanowire is about A=1.68 $\times$ 10^{-12} m^2.

Fig. 2.13 **b** shows a schematic of our cooling system. The insert of cryostat contains the dilution refrigerator, the electric leads, and the sample. The insert is surrounded by liquid helium. So when the temperature of sample is at T_s=0.1 K, the wall of the insert is at T=4.2 K. Therefore, the radiative power from the structure of the insert to the sample

gives us a power of P=2.7×10^{-17} W. This power is already negligible in comparison with the power that is dissipated through the nanowire which is about ≅10^{-15} W. Even though this radiative parasite could be neglected at this temperature range of experiment, we installed a copper shield in front of the device under measurement. The temperature of the copper shield is regulated at the same temperature than the one of the sample. The copper shield will absorb the thermal radiations coming from the calorimeter walls and reduces significantly the radiative power below 10^{-21} Watt.

The calculated radiative power confirms that the thermal radiation coming from the heat bath cannot be responsible for the resistance saturation below 0.1 K. Another very likely possible reason of this saturation could be due to the intrinsic properties of Mott-Anderson materials.

Intrinsic properties of Mott-Anderson materials: among Mott-Anderson materials, NbSi has shown a similar resistance saturation in its resistance profile similar to what has been observed in the NbN thin film (see Fig. 2.14). A deep insight in the electronic transport of a metal-insulator medium at low temperature can explain this saturation in their nature of electronic transport. Indeed, the saturation originates from an inhomogeneous destruction of superconductivity, even if the material is morphologically homogeneous. The nature and origin of such inhomogeneous electronic transport in such system, whether of quantum metal or incoherent Cooper pairs, is still a subject of debate [121, 135].

All these analysis demonstrate that the resistance saturation of the NbN thermometer at very low temperature is not due to over-heating effect, and it could be originated from intrinsic characteristics of NbN or the EM radiations coming from outside of the cryostat.

2.8 Thermal conductance measurements on nanoscale systems

Measuring the thermal properties of nanoscale systems at low temperatures is a challenging project, because of the difficulties lying in the thermal connection of samples to the bath, and also the measurement itself.

The measurement method of thermal conductance on the systems with nanoscale dimensions can be divided into two groups:
-Dynamical method, in which the thermal gradient varies with time and which allows a frequency detection of the electrical signal.
-Steady-state method, in which the temperature gradient is continuous.

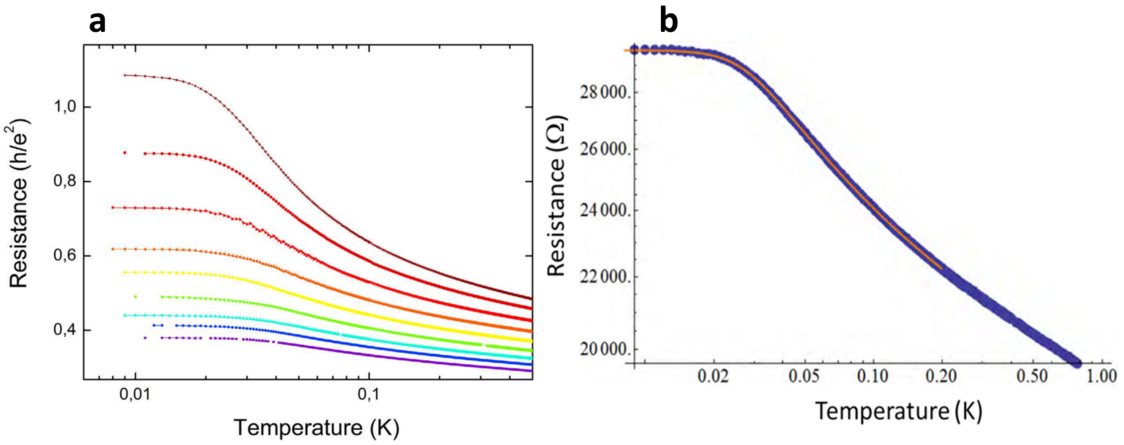

Figure 2.14: **The sheet resistance as a function of temperature for $Nb_{13.5}Si_{86.5}$ film.** (**a**) The disorder of NbSi is tuned through thermal treatment. Each color corresponds to a different annealing temperature for 5 nm thick film done by Couedo and coworkers [135]. (**b**) Resistance of 50 nm thick a-NbSi film [121].

2.8.1 Dynamical method

We can characterize the thermal properties of materials at the micro/nanoscale with the use of a temperature gradient modulated in time. In such methods the sensitivity is even improved. These methods are named as AC calorimetry or 3ω techniques.

3ω method: in the principles of the 3ω method, a transducer metal line is required to be deposited on the surface of the sample material, generally in a four point measurement geometry as shown in Fig. 2.8 **a**. It serves as both the heater and the thermometer, and it is polarized with an a.c current $I{=}I_0\cos(\omega t)$. Heat is then generated and dissipated via the transducer due to the Joule effect and will cause a temperature oscillation which varies like $\Delta T \sim \cos(2\omega t{+}\Phi)$. The measured voltage $V{=}RI$ (R resistance of transducer and I a.c current) includes a term at ω and a term at 3ω [136].

$$V = \frac{dR}{dT}\Delta T\cos(2\omega t{+}\Phi)I_0\cos(\omega t) = \frac{dR}{dT}\Delta T I_0(\cos(\omega t{+}\Phi){+}\cos(3\omega t{+}\Phi) = V_\omega{+}V_{3\omega} \quad (2.6)$$

So the measured voltage signal contains two terms in two harmonic components V_ω, $V_{3\omega}$. The third harmonic component $V_{3\omega}$ permits the extraction of the temperature oscillation:

$$V_{3\omega} = \frac{dR}{dT}\frac{I_0}{2}\Delta T_0\cos(3\omega t + \Phi) \quad (2.7)$$

To extract this $V_{3\omega}$ signal, highly developed electronic methods are indispensable. Then from the measured $V_{3\omega}$ signal, the temperature oscillation at the sample surface can be analyzed to study the thermal properties of the sample.

The main advantage of this technique is its relatively simple implementation and adaptability to different geometrical configurations. Recently, highly sensitive thermal

conductivity and specific heat measurement on 2D suspended SiN membranes [137–139], 1D SiN nanowire [11, 73, 140] are done using this technique.

The previous PhD works in our group focused on the measurement of thermal properties of 1D and 2D geometries using 3ω method [141–143]. The main limitation of this approach is that for the 3ω method to be properly implemented, a local temperature must be defined along the measured system (nanowire or membrane).

A local temperature connot be defined over a distance smaller than the phonon mean free path. When the phonons inside of the system under study have inelastic interaction (diffusely scattered), they thermalize and define a temperature along the system. If in the system all the phonons are transported ballistically (as we expect in the temperature limit of this work), they do not experience inelastic scattering, thus, they do not thermalize inside the systems (nanowire). In this case, there will be no thermalization along the system. As a consequence, this method is not trustworthy at very low temperature, where the phonon transport is expected to be completely ballistic.

2.8.2 Steady-state method

The problem of defining a local temperature along the nanowire can be overcome by the steady-state method. The steady state method has been extensively used in the measurement of the thermal conductance of nanoscale structures. This method is based on applying a steady temperature gradient between the two end of the structure under measurement (nanowire). The suitable configuration for steady-state method consists of two suspended membranes. This kind of structures allows an optimized thermal isolation for the measurement of the thermal conductance of suspended 1D nanowire, [8, 39, 129, 144–146], beams [54] or 2D systems [57]. Several elaborated devices in the aim of measuring the thermal conductance of 1D and 2D structures are shown in Fig. 2.15.

The arrangement used by Li shi [129] is shown in Fig. 2.16 **a**. Their device consists of two suspended membranes. Both of the membranes contain a Pt sensor, so the temperature of each membrane is measured. One of the membrane will act as the heating membrane by generating a power. The dissipated power will be relaxed through the sample and the suspending beams (see Fig. 2.16 **a**). By knowing the exact dissipated power to the heat bath through the suspending beams, and measured temperature gradients between the membranes and the heat bath, the thermal conductance of 1D carbon nanotube can be expressed as:

$$G_s = G_b \frac{\Delta T_S}{\Delta T_h - \Delta T_S} \tag{2.8}$$

where G_b is the thermal conductance of the suspending beams toward the heat bath, and ΔT_h and ΔT_S respectively are the thermal gradients between the heating membrane and the heat bath, and the sensing membrane and the heat bath. The measured thermal conductance and thermal conductivity of two different carbon nanotubes are presented in

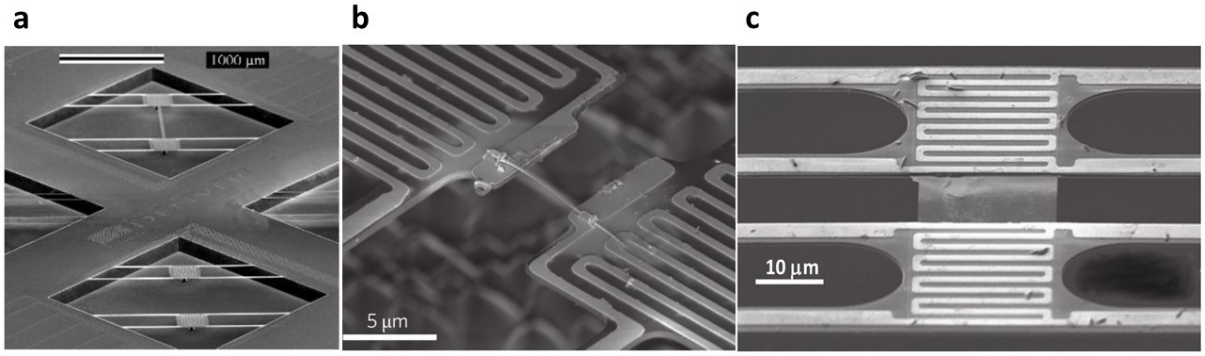

Figure 2.15: **The SEM images of three suspended microdevices for measuring the thermal conductance.** (**a**) Thermal conductivity test fixture of suspended beams made of low stress SiN done by Sultan and coworkers [54]. (**b**) 1D nanostructures based on suspended microdevices integrated into a Wheatstone bridge configuration done by Hsiao *et al.* [39]. (**c**) The suspended structure employed to measure the thermal conductivity of a 2D 17.5 nm thick monocrystalline layer [57].

Fig. 2.16 **b**.

The configuration of double suspended membranes with nanowires between the membranes is what has been used for the experimental measurement of the thermal conductance of nanowire during this PhD. This configuration is particularly adapted for thermal measurements in the ballistic limit at very low temperature where the local temperature cannot be defined along the nanowire. The membrane-based nanocalorimeters are the reservoirs in each side of the nanowire, and they are sufficiently large so that thermalization occurs within them. The details of the measurement setup are explained in the following sections.

2.8.3 Measurement setup

During this PhD all of the experiments have been done in a dilution refrigerator. The principle of such a cooling system is based on a mixture of stable isotopes of helium which are 3He/4He that provides continuous cooling to temperatures as low as 30 mK. At first, the refrigerator is pre-cooled down by liquid nitrogen and liquid helium. Then the mixture of 3He and 4He is injected to circulate part of the system. When the system is cooled below approximately 870 mK, the mixture undergoes spontaneous phase separation to form a 3He-rich phase (the concentrated phase) and a 3He-poor phase (the dilute phase). The evaporation of the 3He from the concentrated phase to the diluted phase is highly endothermic. This cools down diphasic mixture to several millikelvin.

The method we used for the measurement of thermal conductance of 1D profiled nanowire is the steady state method. There are three major differentiating points in this

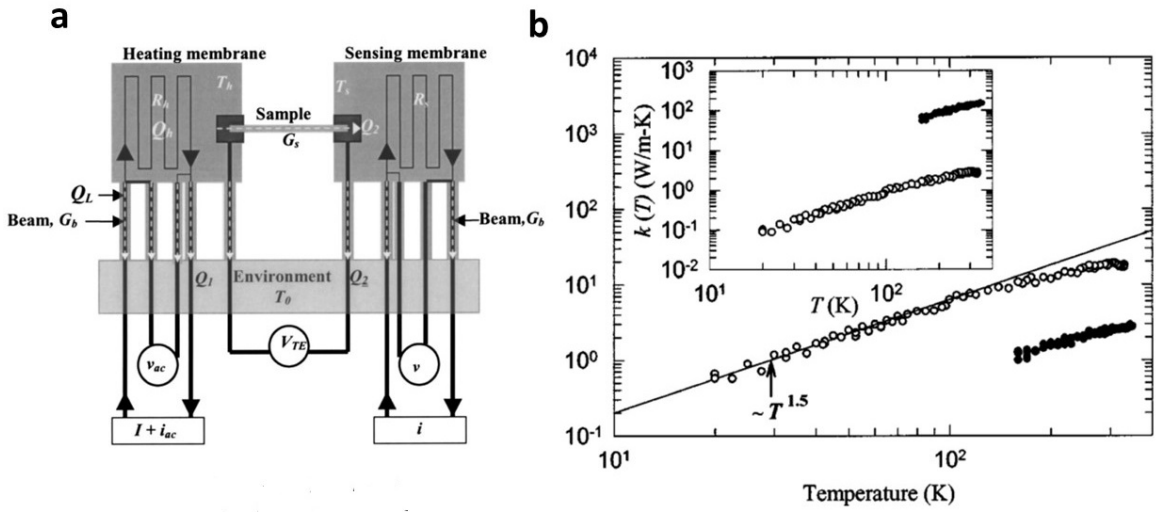

Figure 2.16: **The experimental setup used by Li shi, and their measurements**. (**a**) A thermal gradient is generated between the heating membrane and the sensing membrane. The sample connects the two membranes. (**b**) The measured thermal conductance and thermal conductivity (inset) for two different diameters of carbon nanotube [129].

experiment in comparison to the other achieved experiments: first, the nanowires and the membranes are elaborated monolithically. This aspect eliminates the contact resistance between the nanowires and its reservoirs. Second, there is no deposited material on top of the suspended nanowire (no parasitic thermal path). Third, each suspended membrane contains a heater and a thermometer. The temperature gradient can be reversed between the two membranes to probe the symmetry of the heat flux. In this case, if there is an anomaly in one of the measurements, it will be detected by the reverse measurement.

Experimental protocol: the protocols of the different thermal experiments are detailed in Fig. 2.18. In the first protocol (Fig. 2.18 **a**), a continuous power is dissipated in the heater of the membrane 1. A temperature gradient is then established between the two membranes, the heat flowing through the two nanowires. The direction of the heat flow is reversed in the second protocol where the membrane 2 has a higher temperature than membrane 1 (Fig. 2 2.18 **b**), the power being dissipated in the heater of membrane 2. These protocols are essential to probe the symmetry of the heat transport in order to prove the reliability of the measurements.

Fig. 2.18 **c** shows the same steps of Fig. 2.18 **a** and **b** after having cut one of the nanowire by focus ion beam (FIB). This is modifying the total number of conducting channel from potentially eight quantum channels to only four in the case of one 1D nanowire. Finally, Fig. 2.18 **d** shows the last protocol allowing the measurement of the thermal conductance of the suspending beams without any nanowire connecting the two membranes.

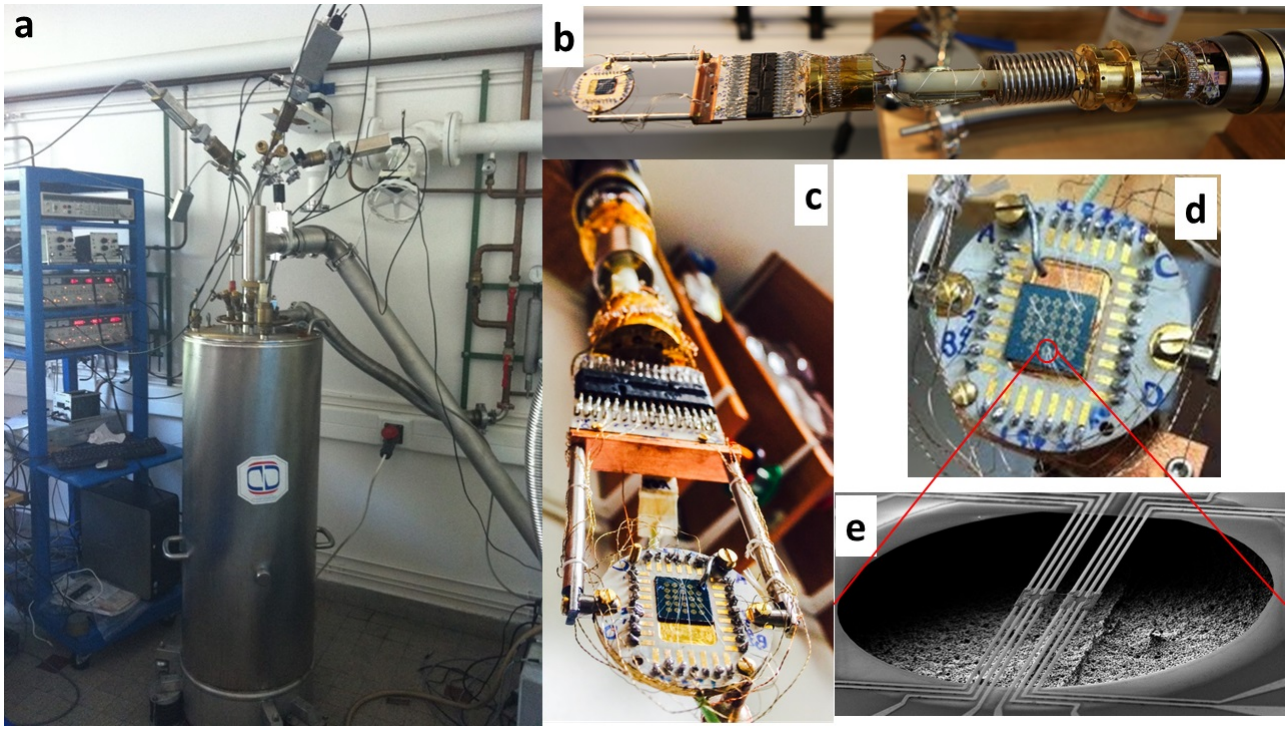

Figure 2.17: **The experimental setup.** (**a**) The dilution refrigerator containing the electronic measurement devices (pre-amplifiers, lock-in amplifiers, LC01 current sources, and LP electronic filters). (**b**) and (**c**) The cooling down part of the dilution refrigerator with the installed chip at the end. (**d**) Chip of 1 mm^2 wafer of Si_3N_4 installed on the sample holder and it is connected with micro-bonded wires to the electrical connections. Each chip contains 24 double membrane-based nanocalorimeter which is shown in (**e**).

The measurements are performed down to 50 mK. The dilution refrigerator with the electronic setup is shown in Fig. 2.17). The chip is installed on a copper based printed circuit board (PCB) that can be regulated in temperature up to 10 K. This experimental set-up is put under vacuum in the measurement chamber. The electronic setup of each membrane is shown in Fig. 2.19. All the electrical connections are equipped with a low-pass frequency filter (f_c = 50 kHz). The current source and the preamplifiers have very low drift (below 5 ppm per Celsius degree) and the input noise of 0.65 nV/$\sqrt{\text{Hz}}$ at a frequency lower than 1 kHz. The heaters have a resistance of approximately 50 Ω and the thermometers of few kilo ohm.

In order to explain the analysis technique to extract the thermal conductance of nanowire, one needs to describe the energy balance during experiment. In Fig. 2.20 a schematic representation of the measurement platform is illustrated. The measurement of the thermal conductance is performed by heating up one of the membrane using the Joule effect in the heater: $\dot{Q}_h = R_h I_h^2$. The heating current I_h is comprised between 10 nA and 10 μA depending on the temperature of the regulated stage of the PCB. During the measurements, the temperature of both membranes is continuously monitored with

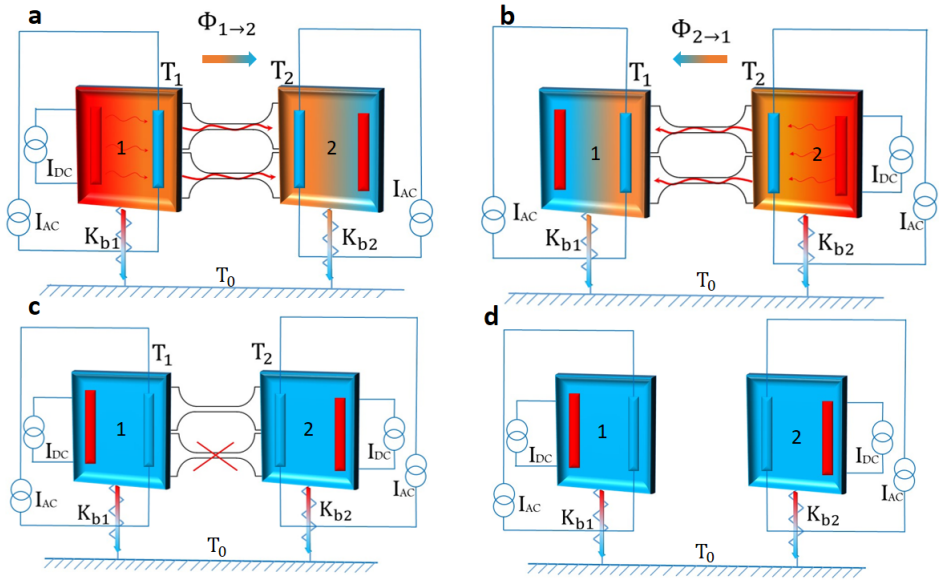

Figure 2.18: **The experimental protocols.** The membranes are schematized by a colored square containing a heater in red and a thermometer in blue. Several experimental protocols have been used, (**a**) where the temperature gradient is established through a DC current applied to the heater of membrane 1 creating a continuous heat flow to the membrane 2. The two temperatures T_1 and T_2 are measured with the two thermometers. (**b**) The DC current is supplied to the heater on the membrane 2, the heat flow is then reversed as compared to the case (**a**). The two first protocols (**a**) and (**b**) have been established to verify the symmetry of heat transport in the nanowires. In protocol (**c**) one of the nanowires has been cut by FIB, then the steps (**a**) and (**b**) are repeated to check the additivity of the heat flow and potentially the number of conducting channels in each nanowire. In (**d**) both nanowires have been cut to measure the thermal conductance of the suspending beams of a single membrane.

the NbN thermometers measured using an ac current of 5 nA at the frequency of $f_{th} \sim$ 157.7 Hz.

The power dissipated in the thermometers is much smaller than $\dot{Q}_h$. Regarding the performance of the measurements, the smallest variation in temperature that the thermometers can capture is $\delta T \cong 50\ \mu$K, and in the terms of power, the absolute error is below the 10^{-18} W.

When one membrane is heated up by $\dot{Q}_h$, a first part of the heat is relaxed to the heat bath by the supporting beams of the first membrane (part 1 in Fig. 2.20). Then, the thermalization of the second membrane appears thanks to a heat flow through the nanowires (part 2 in Fig. 2.20). The equilibrium in temperature of both membranes is obtained when the power is balanced between the heat that flows through the nanowire and through the suspending beams of the second membrane part 3 in Fig. 2.20.

If T_0, T_1 and T_2 are respectively the temperatures of the heat bath, the membrane 1 and the membrane 2, then the two flows of heat from each membrane to the heat bath

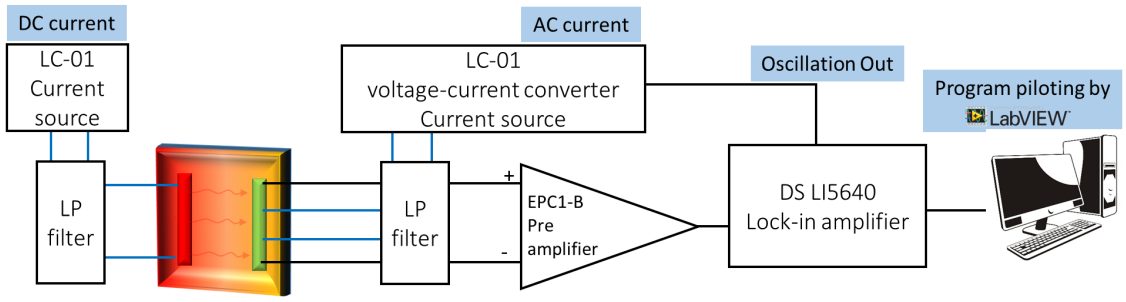

Figure 2.19: **The electronic setup.** This electronic setup is for each membrane in double suspended nanocalorimeter for the measurement of the thermal conductance of nanowires. The experimental setup consists low pass filters (LP filter) at the connections, LC01 current source, EPC1-B pre-amplifiers, and DC LI5640 lock-in amplifier.

can be defined as:

$$\dot{Q}_1 = K_{b1}(T_1 - T_0) \tag{2.9}$$

$$\dot{Q}_3 = K_{b2}(T_2 - T_0) \tag{2.10}$$

and the heat through the nanowires between the two membranes will be equal to:

$$\dot{Q}_2 = K_{NW}(T_1 - T_2) \tag{2.11}$$

K_{bi} being respectively the thermal conductance between the membrane i and the heat bath, and K_{NW} is the thermal conductance of nanowires. By knowing the exact temperature of each membrane along with the power dissipated, we have access to the full balance of the transported flow of energy through the nanowires and membranes, so to the thermal conductance of the nanowires. By changing the heating membrane, one can reverse the heat flowing through the nanowires.

This measurement method based on two membranes having different temperatures permits accessing to the thermal properties in the ballistic limit of a 1D nanowire. In this limit, local temperature is not anymore a relevant physical concept. Here, the temperature will be defined only by the membrane that is considered as a sufficiently large reservoirs to allow inelastic phonon diffusion.

Here we derive the basic equations ruling the heat balance of the systems constituted by the two membranes, the nanowires, and the suspending beams. This will permit the determination of the thermal conductance of the nanowires. We can write down the energy balance by starting from the heating power dissipated by the heater:

$$\dot{Q}_h = R_h I_h^2 = \dot{Q}_1 + \dot{Q}_2 \tag{2.12}$$

where $\dot{Q}_2$ is the power flow through the nanowires defined in equation 2.11. At the thermal equilibrium, the system can be considered as a stationary regime so the heat flux between

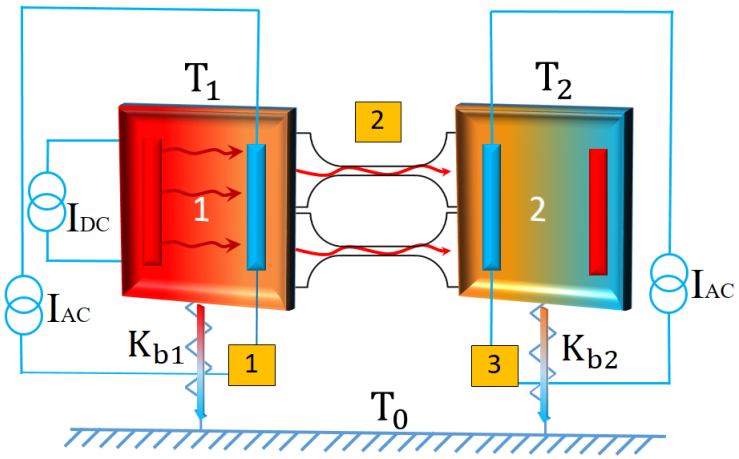

Figure 2.20: **The representative platform of the thermal conductance measurement.** The power is generated by membrane 1. Firstly, the major part of power will be relaxed to the heat bath by beams of the first membrane (part 1). Then the minor part of heat will be transported to the second membrane through the nanowires (part 2). Since the condition of experiment is in stationary regime, the transported heat through the nanowire will be relaxed to heat bath by the beams of the second membrane as well (part 3).

the membrane and the heat flowing from the second membrane to the heat bath can be equaled: $\dot{Q}_2 = \dot{Q}_3$. Using this equation, the thermal conductance of the nanowires can be expressed by:

$$K_{NW} = K_{b2} \left(\frac{T_2 - T_0}{T_1 - T_2} \right) \tag{2.13}$$

if the conditions $T_1 - T_2 << T_0$ and T_2 close to T_0 are fulfilled. By monitoring T_0, T_1 and T_2 (only T_0 is regulated) and having calibrated K_{b2} as a function of temperature, K_{NW} will be obtained as a function of T_0. K_{b2} is a key element for the measurement of the thermal conductance of the nanowire. Thus, K_{b2} has been qualitatively and quantitatively measured by AC calorimetry (explained in section 4.3.1) method on similar membrane without the presence of nanowires (see Fig. 2.21). The measurement of T_1-T_2, T_2-T_0 are also presented in Fig. 2.22.

2.8.4 Noise characterisation

To demonstrate highly sensitive measurement, an important step consists in evaluating the real noise in comparison with the expected noise at the working temperature, and to figure out what phenomena dominate the noise of the measurements.

In a calorimeter with a resistive thermometer, two fundamental noise sources are identified: the electronic noise, and the thermal noise. The electronic noise is generated by

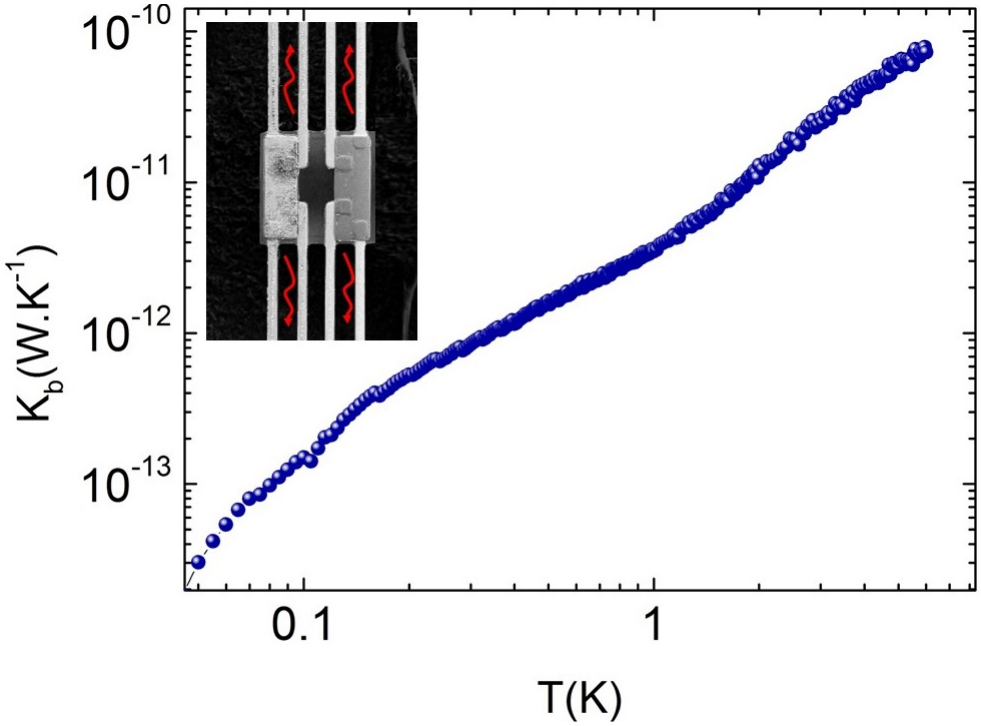

Figure 2.21: **Measurement of the thermal conductance of the supporting beams.** The measurement has been done without nanowires bridging between the membranes; by AC calorimetry method from 0.03 K to 6 K (the technique of measurement is explained in section 4.3.1).

the thermal agitation of the electrons inside an electrical conductor at equilibrium and it is knwon as the Johnson-Nyquist noise. The thermal noise is the thermal fluctuations between the sensor (membrane) and the heat sink, called phonon noise (or thermal fluctuations noise).

In this section, all the noise analysis are related to the measurement of thermal conductance of nanowires bridging suspended nanocalorimeter (see Fig.2.7). Before describing the mathematical formulae, a schematic figure of the measurement of the thermal conductance of nanowires is shown in Fig. 2.23. Fig. 2.23 **a** shows an overview of the whole system under study, Fig. 2.23 **b** presents the part that is related to the phonon conduction through the nanowires, and 2.23 **c** presents the phonon conduction from the membranes to the heat bath. All of the calculation and the measurement of the noise characterisation is done at 0.1 K.

Johnson-Nyquist noise: the electronic noise that is generated by the thermal agitation of the electrons inside of the thermometer is expressed as noise equivalent voltage (NEV) [147]. This noise can be calculated from the equation:

$$NEV_{Johnson} = \sqrt{4\ k_B\ T\ R} \tag{2.14}$$

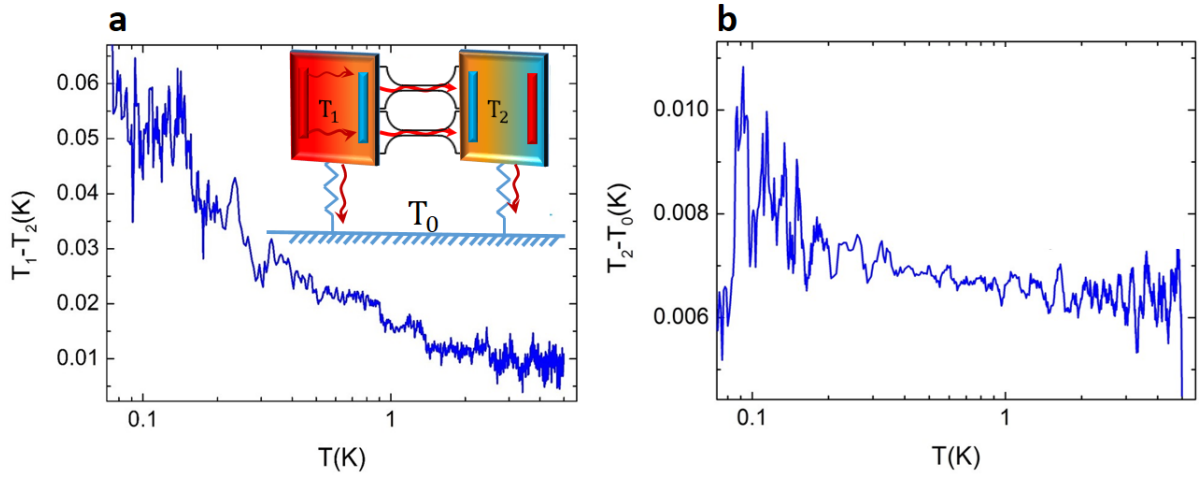

Figure 2.22: **Typical temperature gradient profile of the experimental setup.** (**a**) The temperature gradient measured between the two membranes during an experiment of thermal conductance as a function of temperature. This temperature gradient is mostly of the order of 20/40 mK. (**b**) Typical temperature gradient measured between the second membrane and the thermal bath (baseline). The temperature gradient is smaller than 10 mK. The inset represents the schematic of the measurement configuration.

where k_B is the Boltzmann constant, T the temperature, R the resistance of thermometer as a function of temperature, and Δf is the bandwidth of frequency over which the measurement has been achieved. The expected Johnson noise (for $R \cong 2$ kΩ, at $T = 0.1$ K) obtained from the equation 2.14 is about $NEV = 0.16$ nV/$\sqrt{\text{Hz}}$. Now in order to compare this noise to the phonon noise, one should extract the phonon noise in the form of NEV.

Phonon noise: the thermal fluctuation noise (phonon noise) is linked to the measurement of thermal conductance, and it can be described as the noise equivalent power (NEP). The mathematical formula of the phonon noise is [148, 149]:

$$NEP_{ph,j} = \sqrt{4\ k_B\ T^2\ K_j} \tag{2.15}$$

where K_j is an index that represents the thermal conductance of either nanowires, or the beams K_{bi}. Therefore, in our device, there exist two sources of the thermal fluctuation noise by phonons. The numerical calculation gives $NEP_{phonon-NW} = 9.18 \times 10^{-20}$ W/$\sqrt{\text{Hz}}$, and $NEP_{phonon-beam} = 2.73 \times 10^{-19}$ W/$\sqrt{\text{Hz}}$. The total NEP_{ph} is equal to:

$$NEP_{ph,total} = \sqrt{\sum_j NEP^2_{ph,j}} \tag{2.16}$$

$$= \sqrt{NEP^2_{ph,K_b} + NEP^2_{ph,K_{NW}}} \tag{2.17}$$

The numerical application gives $NEP_{ph,total} = 2.88 \times 10^{-19}$ W/$\sqrt{\text{Hz}}$. Since the whole system is in quasi-static limits, the noise equivalent temperature can be expressed as

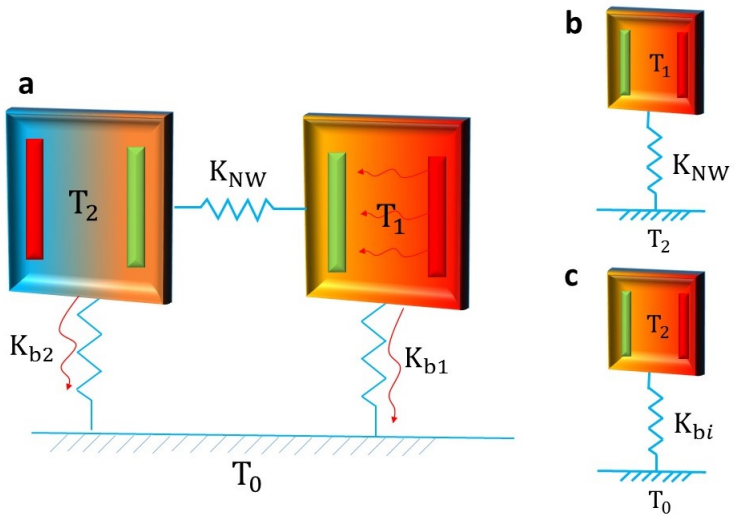

Figure 2.23: **A schematic overview of the whole system unders study**. (**a**) The system under study is composed of two membrane-based nanocalorimeters, the nanowires, and the beams of each nanocalorimeter K_{bi}. **b** and **c** present respectively a schematic of thermal conductance of the suspended nanowires and the suspending beams.

(NET):

$$NET = NEP_{ph,total}/K_j = \sqrt{\frac{4k_B T^2}{K_j}} \tag{2.18}$$

The total NET_{total} can be calculated in the same way as the equation 2.17. The numerical calculation gives $NET_{total} = 6\ \mu\text{K}/\sqrt{\text{Hz}}$. This value represents the noise equivalent of temperature that rises from thermal fluctuation. In order to compare this noise to the Johnson noise, one ought to convert it to a noise equivalent voltage NEV appearing across the NbN thermometer. Thus, the NEV is given by:

$$NEV_{ph} = NET \times I_s\ R\ \alpha_s \tag{2.19}$$

where I_s is the current used to polarize the thermometer, α_s is temperature coefficient of resistance TCR. The estimated NEV_{ph} (for I_s= 1 nA, α= 1, and R≅2 kΩ) is about $0.012\ \text{nV}/\sqrt{\text{Hz}}$. By comparing NEV_{ph} and $NEV_{Johnson}$, it is clear that the dominant noise in our setup is the Johnson noise.

2.8.5 Measurement of noise

The calculated noise should be compared to the real noise. For measuring the noise, the temperature has been fixed at 0.1 K, and each 1 second the voltage of thermometer has been measured. A statistical analysis on measured value demonstrates the signal distribution plotted as histogram which fits correctly by a Gaussian function. The noise measurement on a membrane-base SiN nanocalorimeter is presented in Fig. 2.24.

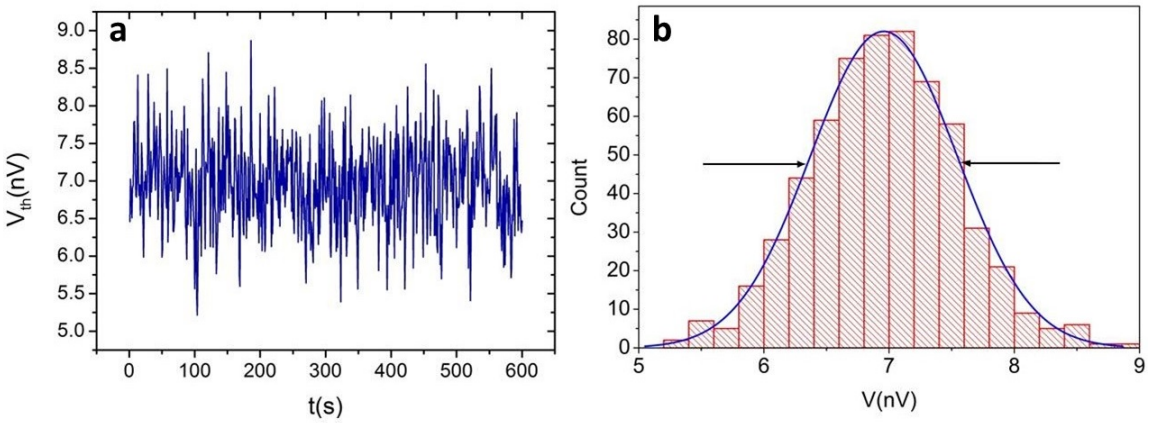

Figure 2.24: **Measurement of the noise.** (**a**) Measured noise on a membrane-base SiN nanocalorimeter at 0.1 K as a function of time. (**b**) The signal distribution plotted as a histogram. The full width at half maximum corresponds to the noise of the measurement. In this case, the noise is evaluated to be around 0.7 nV/$\sqrt{\text{Hz}}$.

Table 2.1: Noise calculation for the measurement of the thermal conductance of the nanowires between the two nanocalorimeters.

$NEV_{Johnson}$(nV/$\sqrt{\text{Hz}}$)	NEV_{phonon} (nV/$\sqrt{\text{Hz}}$)	NEV_{total}(nV/$\sqrt{\text{Hz}}$)	$NEV_{measured}$(nV/$\sqrt{\text{Hz}}$)
0.16	0.012	0.162	0.7

The measured noise equivalent voltage is about $NEV_{measured} \cong 0.7$ nV/$\sqrt{\text{Hz}}$. The noise calculations and the noise measurement are presented in Table 2.1. Since the input noise of the pre-amplifier EPC1B is about 0.65 nV/$\sqrt{\text{Hz}}$, from this table we understand that the dominant noise is the pre-amplifier noise. On the other hand, there is a factor of 3 between the measured noise and the total calculated noise. Indeed, the measured noise is constrained by both intrinsic and extrinsic noises of the thermometer, including all the noises that are coming from the electronic devices. We believe that the noise coming from the electrical contacts resistances is the reason of this factor 3 between measured noise and the calculated noise. The measured power sensitivity is equal to $\delta P = 4\times 10^{-18}$ W. The resolution of the signal which is defined as noise/average signal ratio is about $\Delta K/K = 7$ %.

2.9 Conclusion

In this chapter, the technical aspect of the fabrication of confined suspended systems, and the techniques of the measurement of thermal properties at low temperature (from 0.05 K to 5 K) are presented. The fabricated systems are in two different configurations:

membrane-based suspended nanocalorimeter made of high-stress silicon nitride (for the measurement of the specific heat of 2D membrane), and double suspended membrane-based nanocalorimeters with bridging nanowires (for the measurement of the thermal conductance of the nanowires). Both configurations are monolithically fabricated and contain a very sensitive resistive thermometer based on metal-insulator material NbN. In this kind of material the resistance is very sensitive to the temperature, and it gives a temperature coefficient of resistance $\alpha > 1$ at very low temperature. All of the electronic setups are equipped with low noise devices such as low noise current sources, pre-amplifier, and lock-in amplifiers. The electronic connections are also equipped with low pass filters in order to filter high frequency electromagnetic waves. All these technical facilities exhibits a total voltage noise which is dominated by pre-amplifier noise and it is about $NEV < 0.7\ \mathrm{nV}/\sqrt{\mathrm{Hz}}$, and the power sensitivity goes down to several attoWatt.

The design of the double suspended nanocalorimeters with nanowires in the gap, is thoughtfully elaborated in the aim of the investigation of heat conduction in the quantum limit. Each membrane act as sufficiently large reservoir so that the thermalization will certainly occur. Thus, if there is a ballistic phonon transport along the nanowire between two reservoirs, with such configuration it can be detected. In the next chapter the experimental results of the thermal conductance of the nanowire in ballistic regime will be presented.

3 CHAPTER

Phonon heat transport in 1D quantum channel

3.1 Introduction

The study of the phonon thermal transport in extreme conditions (low dimensions and low temperature) holds the key to many fundamental questions, concerning the heat transport in the quantum limit. Decreasing the temperature causes the increase of the phonon characteristic lengths (the phonon dominant wavelength λ_{dom} and the phonon MFP). This will change the regime of heat conduction for phonons in a reduced dimension system. The increase of the phonon dominant wavelength will impact the phonon scattering processes and the phonon transport. First of all, when the phonon dominant wavelength becomes much bigger than the roughness of the surfaces ($\lambda_{dom} \gg \eta$), most of the phonon boundary scatterings become specular (see Fig. 1.8 **b**). Moreover, when the phonon dominant wavelength becomes bigger than the section of the channel $\lambda_{dom} > d$, there exist only four populated vibrational modes that will propagate along the nanowire axis. In this condition, a transition from 3D (diffusive) to 1D (ballistic) is expected in the regime of heat transport as function of temperature.

When the phonon scatterings on the edges are specular, and the phonon MFP exceeds the length of the nanowire, then the phonon transport through the nanowire is expected to be ballistic. In this regime, the phonons travel along the channel without any inelastic interaction or thermalization, and they will conserve their energy. In such a 1D channel, the heat current can be expressed in the framework of the Landauer theory [150]. The heat current is then given by:

$$\dot{Q}_x = N_\alpha G_q (T_H - T_C)\mathcal{T} \tag{3.1}$$

where N_α is the number of populated vibrational modes (conducting channels), G_q is the quantum of thermal conductance $G_q = \pi^2 k_B^2 T/3h$ (shown in section 1.5.3), T_H and T_C are the temperature of hot and cold reservoir, and $\mathcal{T}$ is the transmission coefficient from

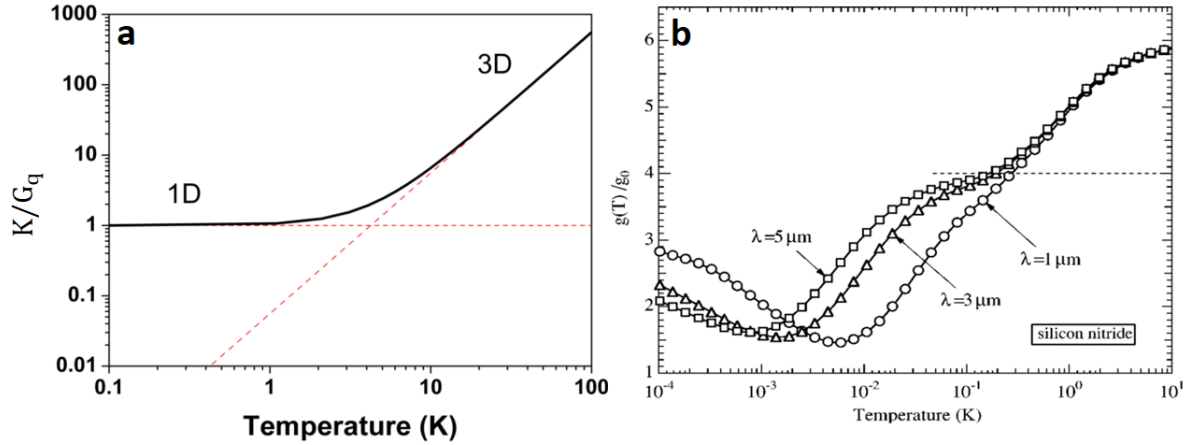

Figure 3.1: **Numerical calucations of the transmission coefficient**. The thermal conductance normalized by the quantum of thermal conductance for each vibrational mode. (**a**) In a perfect case of phonon ballistic transport in a single nanowire with four populated modes of vibration. Below 1 K the transmission coefficient becomes equal to unity $\mathcal{T} = 1$ and the crossover shows the transition from 3D to 1D. (**b**) Calculated transmission coefficient for silicon nitride catenoidal nanowire for different characteristic lengths of the catenoïd (λ corresponds to the one used in equation 1.46) [41].

the reservoir through the 1D waveguide. The thermal conductance of the channel is then written as:

$$K = N_\alpha G_q \mathcal{T} \tag{3.2}$$

In this mathematical description, the phonon transport is expressed through the probability of a phonon to be transmitted from one heat bath to the other one when they are kept at different temperatures. Thus, in a fully ballistic phonon waveguide, the transmission coefficient will set the actual value of the thermal conductance.

We assume that the phonon transport is ballistic, and the transmission coefficient is equal to unity $\mathcal{T} = 1$. By normalizing the thermal conductance of the phonon waveguide to the quantum of thermal conductance for each vibrational mode ($K/N_\alpha G_q$), and by plotting this value as a function of temperature, a plateau should appear. This plateau (as it is shown in Fig. 3.1 **a**) shows the transition of phonon conduction to the quantum limit, in other words, it shows the transition from 3D to 1D. Now the principal question is that whether is it possible to obtain a optimal transmission coefficient $\mathcal{T} = 1$? According to the noticeable number of theoretical works, the transmission coefficient contains resonances and cutoff frequencies at very low energy vibrational modes. For instance, the calculation of the transmission coefficient for a silicon nitride nanowire done by Tanaka *et al.* [41] is shown in Fig. 3.1 **b**. The graphs are plotted for the nanowires with catenoïd shapes, with different characteristic lengths of the catenoïd λ (see equation 1.46). It is clearly shown that the transmission coefficients keep decreasing as the temperature decreases. This fact comes from the dependence of transmission coefficients on the frequency and phonon modes, or lattice vibrations. Consequently, according to these more realistic calculations,

the plateau caused by the normalization of the thermal conductance to the quantum of thermal conductance cannot be easily observed [41].

Having an experimental access to this quantum regime is highly challenging because, in addition to the ballistic transport of phonon, a optimal transmission coefficient is required. Measuring the phonons thermal conductance in the quantum limit is of great importance in understanding several features:

- what are the dominant parameters of transmission coefficient (shape of reservoirs, length of nanowires, roughness of the edges, etc) ?
- where is located the temperature drop ?
- where appears the thermal resistance ?
- where do the phonons scatter and thermalize ?

In this chapter, we present a highly sensitive experimental study of phonon thermal transport from 0.05 K to 5 K between two large reservoirs through a 1D phonon waveguide. The temperature range of measurement and the dimension of the system under study are designed to favor the access to the quantum limit of phonon conduction. In this case, the dominant factor in the measurement of the thermal conductance will be the transmission coefficient. Then, the dependence of transmission coefficient on the shape of the junctions, length of nanowire and roughness of the surfaces will be discussed.

3.2 Experimental achievements

Before describing the experimental achievements, it is worth reminding the particularity of our samples and experiments. All of the experiments have been done on samples made of high stress silicon nitride (SiN) as shown in Fig. 2.7. The experimental platform contains two membrane-based nanocalorimeters and the nanowires (without any material deposition on the top) are connected monolithically to the two membranes. The nanocalorimeters are the thermal reservoirs (heat bath) on each side of the nanowires. The shape of the junctions of the nanowires is designed in the form of a catenoïd to exhibit an optimized transmission coefficient (close to unity), as it is explained in 1.13. The parameters of nanowire junctions based on equation 1.46 are $A_0 = 2.3 \times 10^{-8}$ and $\lambda = 0.86 \times 10^{-6}$. During the experiment, the temperature of each reservoir and the heat bath are continuously measured. This gives us the ability to measure the smallest heat exchange through the nanowires. The experimental protocol is as described in section 2.8.3 with two major objectives:

- verification of the symmetric aspect of heat transport by reversing the heat flow,

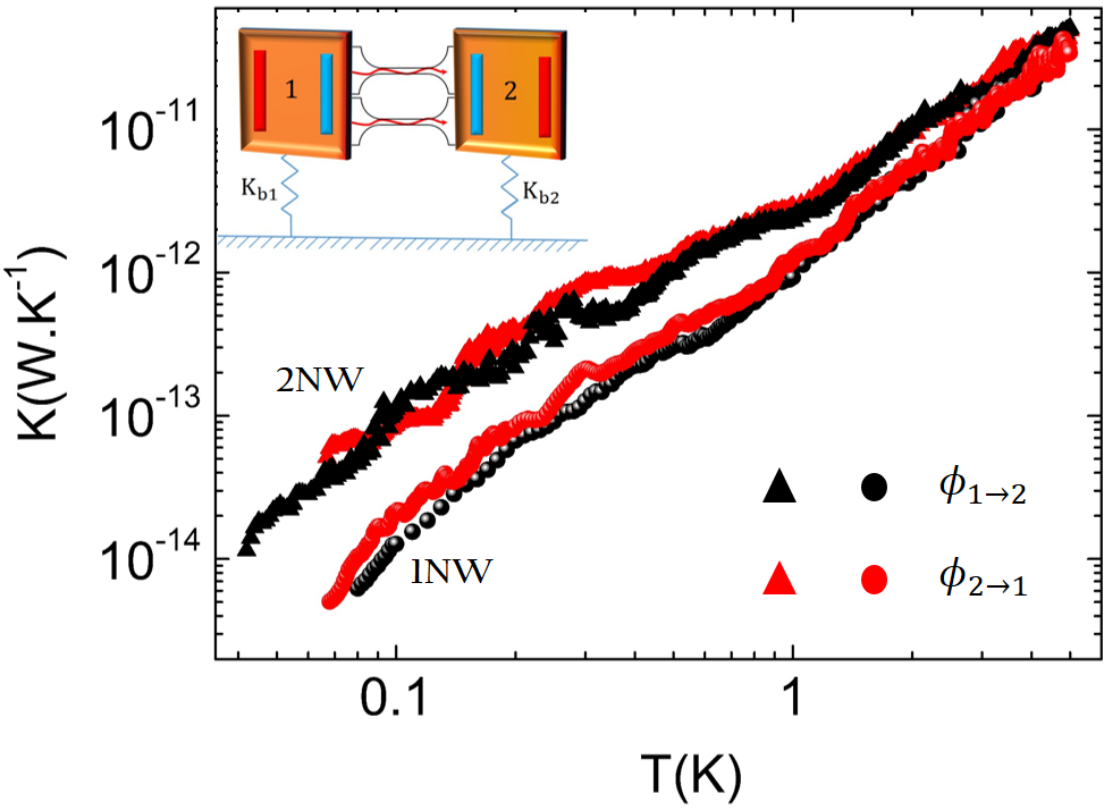

Figure 3.2: **The experimental results of the thermal conductance of nanowires.** Triangles are the thermal conductance of two nanowires, and circles are that of one nanowire versus the temperature in log-log. These results have been measured in two different heating configurations. Red symbols refer to the thermal conductance when the heating is done from membrane 1 to membrane 2, and black symbols correspond to the thermal conductance when the heat flow is reversed.

- evaluation of the number of conducting channels by cutting one of the nanowires.

The thermal conductance measurements versus temperature are presented in Fig. 3.2 for one (1NW) and two nanowires (2NW). The variation of thermal conductance covers more than three orders of magnitude as the temperature is lowered down to 50 mK. The superposition of the two measurements (red and black dots) that have been acquired using different directions of temperature polarization clearly demonstrates the symmetry of the heat transport. If we compare the thermal conductance of one or two nanowires, it appears that at temperatures T>1 K the heat flow for two nanowires is indeed two times that of one nanowire. As the temperature is lowered, the difference becomes larger than a factor of two; this is attributed to different transmission coefficient between the two nanowires.

In order to distinguish the different regimes of phonon heat transfer, it is essential to compare the dependence of the thermal conductance on temperature to theoretical

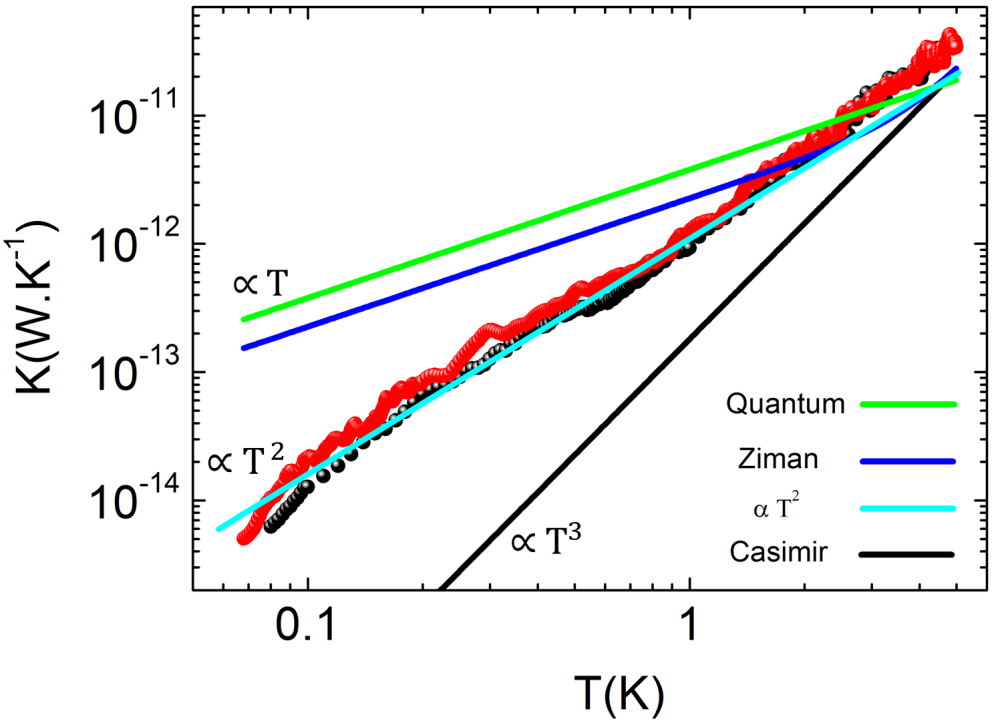

Figure 3.3: **The thermal conductance of one nanowire in comparison to the theoretical models.** The black line corresponds to the boundary limited regime (Casimir regime). The clear blue is a simple quadratic fit likely to describe thermal transport in amorphous materials when the phonons are scattered by Two-Level Systems (TLSs). The deep blue line is the diffusive-ballistic regime (Ziman regime), and the green line is the universal value of the quantum of thermal conductance. It corresponds to the thermal conductance of a 1D channel for four populated vibrational modes with the assumption that the transmission coefficient is equal to unity $\mathcal{T} = 1$.

models.

3.3 Comparison with theoretical models

The dependence of the thermal conductance on temperature unveils the various mechanisms of phonon transport at low temperatures. Here we compare the different regimes of phonon transfer at low dimension and low temperature with the experimental data. Fig. 3.3 represents the thermal conductance of one nanowire with two different heating directions in comparison with theoretical fits.

The black line shows the cubic behavior of thermal conductance in the boundary limited regime of phonon transport (Casimir regime). This regime is expected in a 3D

system where the phonon MFP is only limited by inelastic boundary scattering. The intermediate regime between partly diffusive and partly ballistic (Ziman regime) is shown by the deep blue line. In this regime with the increase of phonon dominant wavelength and phonon MFP, gradually the boundary scattering will change from inelastic boundary scattering to elastic. The fully ballistic regime known as the quantum limit of thermal conductance corresponds to the green line. It is characterized by a linear dependence on the temperature where $\mathcal{T}$ the transmission coefficient is assumed to be equal to one (optimal transmission). The clear blue line is a simple quadratic fit likely to describe thermal transport in bulk amorphous materials when the phonons are predominantly scattered by Two-Level Systems (TLSs).

As it is shown in Fig. 3.3, the dependence of the measured thermal conductance on temperature is indeed mostly quadratic, a variation in temperature departing strongly from the expected universal value of thermal conductance. In order to understand the true regime of phonon exchange between the two membranes and the possible presence of ballistic transport, we need to evaluate the phonon MFP and compare it to the dimension of the nanowires (diameter and length).

3.3.1 Mean free path analysis

In Fig. 3.3, the experimental thermal conductances fall between boundary limited regime (Casimir regime) and fully ballistic regime (quantum regime). This demonstrates that within the nanowires and the reservoirs, there exists both elastic and inelastic phonon scatterings.

To calculate the MFP from the measurement of thermal conductance, we suppose that the experimental data of thermal conductance can be modelled by the Ziman thermal conductance $K_{exp} = K_{Ziman}$ (refer to section 1.5.2), and it can be expressed by:

$$K_{Ziman} = \beta_{cas}\ \Lambda_{cas} \times \left(\frac{1+p}{1-p}\right)\ T^{\,3} \tag{3.3}$$

where β_{cas} is the constant from the equation of Casimir (see equation 1.37). $\Lambda_{cas} = 1.12\sqrt{e \times w}$ is the Casimir MFP (e is the thickness, and w is the width of nanowire), and p is the probability of phonon specular reflexion by the surfaces that is explained in equation 1.40. Therefore, the experimental MFP can be written as:

$$\Lambda_{exp} = \Lambda_{Ziman} = \left(\frac{1+p}{1-p}\right)\ \Lambda_{cas} \tag{3.4}$$

$$= \frac{K_{exp}}{\beta_{Cas} T^{\,3}} \tag{3.5}$$

The calculated MFP is obtained by the equation 3.5, and it is presented in Fig. 3.4. The blue solid line represents the estimation of the theoretical MFP based on the prediction

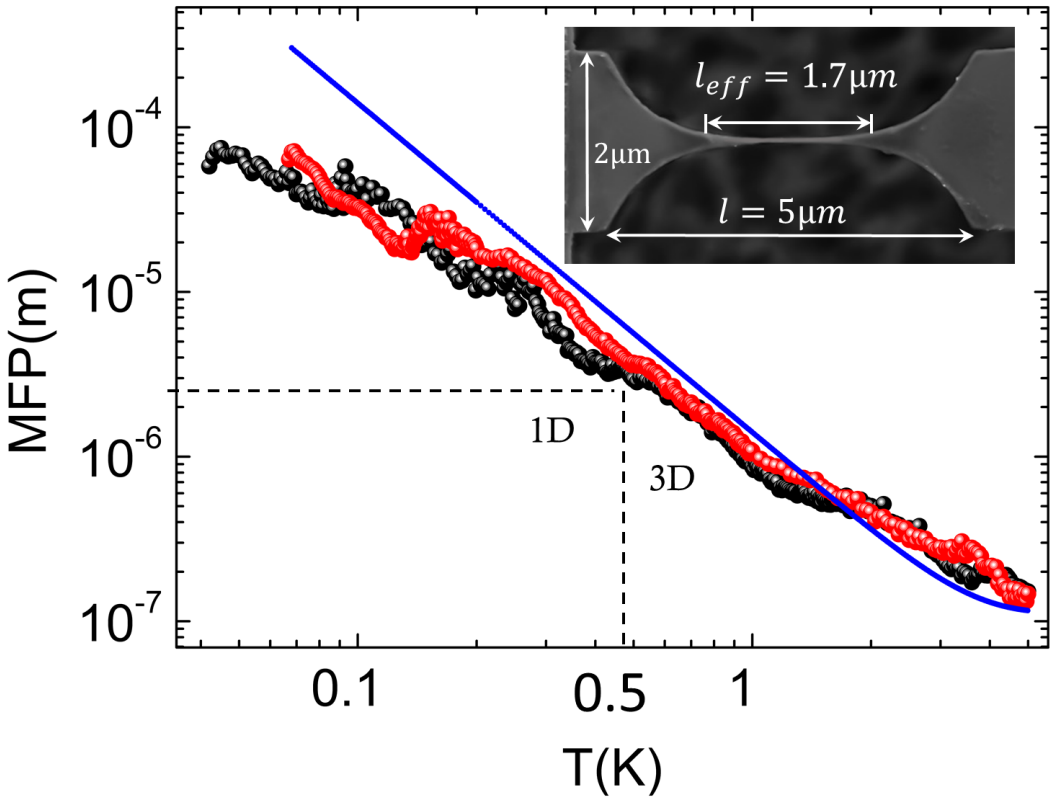

Figure 3.4: **The extracted phonon MFP from the experimental results.** The black and red dots are obtained from the equation 3.5 for one nanowire. The blue line is the expected MFP calculated from the Ziman model with an estimated roughness of $\eta = 3$ nm. Dashed line shows the temperature at which the phonon MFP exceeds the effective length ($l_{eff} = 1.7$ μm) of the nanowire. The inset shows the top view of the nanowire illustrating the various dimensions of the nanowire. Below 0.5 K the phonon MFP exceeds the effective length of the nanowire (MFP$> l_{eff}$).

of the Ziman model adapted to the dimension of the channel with a mean roughness of $\eta = 3$ nm. The inset of Fig. 3.4 shows top view of the nanowire. Since the nanowires do not have a constant diameter, one needs to find a way estimating an effective length for these nanowire. We use the definition given by Tanaka *et al.* to calculate the effective length. The effective length of the nanowire l_{eff} is obtained from $l_{eff} = 2\lambda$, where λ is the characteristic length of the catenoïd in equation 1.46 [41]. By comparing the experimental MFP to the l_{eff}, we can conclude that below 0.5 K, the MFP becomes larger than the effective length of the nanowire. This means that phonons travel without any inelastic collision through the 1D channel. This is demonstrating that the transport of phonons is ballistic at low temperatures (T$<$ 0.5 K), temperatures at which the nanowire can be considered as a 1D phonon waveguide. Indeed, the transition from 3D to 1D should occurs when $\lambda_{dom} > d$ (d is the diameter of the nanowire). With the use of the equation 1.11,

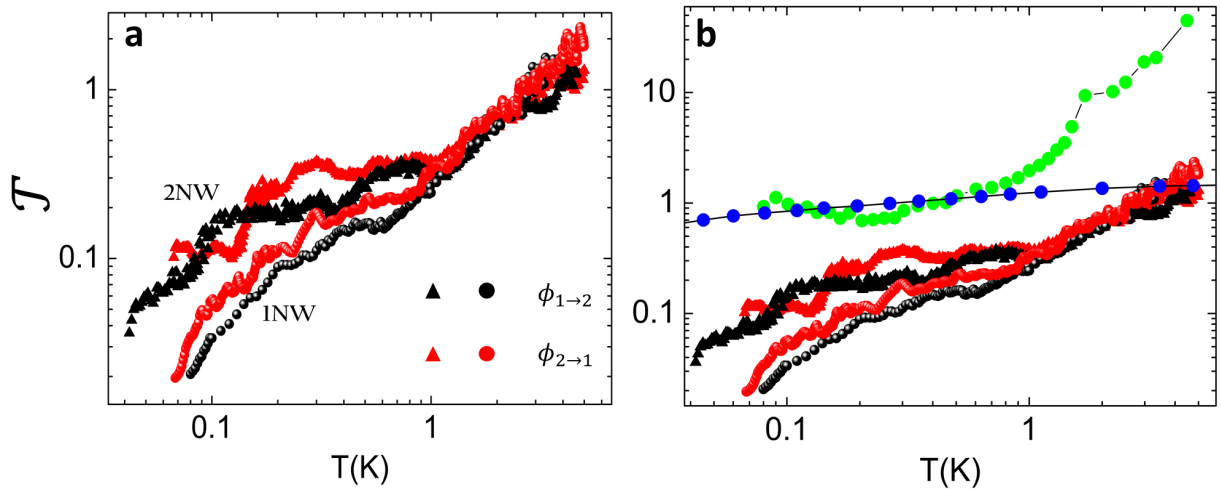

Figure 3.5: **Landauer transmission coefficient.** (**a**) Black and red dots are the transmission coefficient extracted from the experimental results for both one and two nanowires for both heating directions. This value is obtained by normalizing the thermal conductance of the nanowires to the universal value of quantum of thermal conductance for four channels for each 1D phonon waveguide. (**b**) The comparison of the experimental transmission coefficient with that of Schwab *et al.* [37] (green dots), and the calculation of Tanaka *et al.* on SiN nanowire (blue dots) [41].

the temperature of crossover can be estimated as:

$$T_{cross} = \frac{h\nu_s}{2.82k_B d} \tag{3.6}$$

where h is the Planck constant, k_B the Boltzmann constant and ν_s is the speed of sound. The predicted T_{cross} for SiN is about $T_{cross} = 1.6$ K, then below that temperature we can expect to see 1D behavior in the thermal properties. As shown previously from the calculated MFP, below T=0.5 K, the thermal transport is most probably ballistic (MFP$> l_{eff}$). Since at 0.5 K the phonon dominant wavelength is even larger than at 1.6 K ($\lambda_{dom-SiN} = 335$ nm, more than three times bigger than the section of the nanowire). This shows that the phonon conduction in nanowires can be considered as ballistic in this 1D phonon waveguide. The ballistic transport in a 1D channel is a prerequisite to enter into the quantum limit of heat conduction.

In this quantum regime of phonon transport, a linear dependence of thermal conductance on temperature is expected (quantum of thermal conductance). Based on our analysis of the phonon MFP, we have demonstrated that below 0.5 K the phonon MFP becomes bigger than the effective length of the nanowire showing that indeed the phonon transport is ballistic in the nanowire at low enough temperature. However, it is clearly observed that the thermal conductance exhibits a quadratic power law in the overall temperature range, a result departing from the linear regime. This analysis shows that temperature dependence of the thermal conductance may find its origin in the transmission coefficients.

3.4 Transmission coefficient

Since we demonstrated that the thermal transport is in the quantum regime below 1 K, it is appropriate to analyze the data using Landauer model and calculate the transmission coefficient with the equation:

$$\mathcal{T} = \frac{K_{exp}}{N_\alpha G_q} \tag{3.7}$$

The extracted transmission coefficients are presented in Fig. 3.5 **a**. From the first observation it can be seen that at high temperature (T>1 K), the transmission coefficients of two nanowires are perfectly superposed to that of one nanowire. The second part, the transmission coefficients keep decreasing as the temperature decreases, and it does not reach the unity value. This shows that different mechanisms are preventing a perfect transmission of phonons through the phonon waveguide between the reservoirs. In Fig. 3.5 **b** transmission coefficients of our experiments are compared to extracted transmission coefficients from K. Schwab *et al.* works [37] (green dots) on silicon nitride nanowire. The blue dots represent the calculated transmission coefficient for SiN nanowire by Y. Tanaka *et al.* [41]. Since our results depart significantly from the calculated transmission coefficient by Tanaka *et al.* [41], it shows that the intrinsic quantum value of thermal conductance of the 1D nanowire has to be seen as in series with the thermal resistance of the contacts. To find out the source of the thermal contact resistance, one ought to discuss each possible scenarios.

3.5 Possible scenarios for the non-perfect transmission coefficient

In general, the possible scenarios that could explain the origin of the contact resistance at the reservoirs are:

- the shape of the junctions between nanowire and the reservoirs which is related to the acoustic impedence between nanowire and the reservoir [17, 41, 42]
- the non-perfect coupling between 1D nanowire and 2D reservoirs (this effect comes from the difference of phonon states between a 1D and 2D systems) [44, 151]
- the presence of the cutoff frequencies and oscillating behavior of transmission coefficient at low energies [41, 152]
- the details of the structure such as defects, roughness, length of the nanowire [47, 153–155]
- the nature of the material in use.

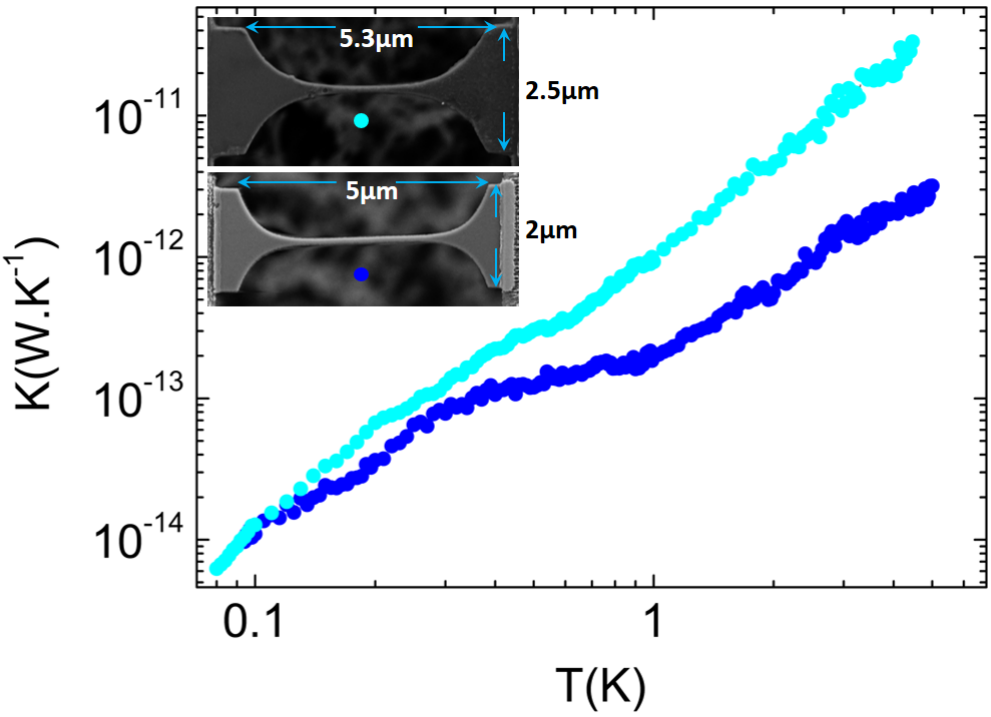

Figure 3.6: **Thermal conductances with different shapes of the junctions.** Thermal conductances of two different nanowires with almost the same length, but different characteristic lengths of the catenoïd. Clear blue dots represent the thermal conductance of the nanowires with the characteristic length of the catenoïd of λ_1=0.86 $\times 10^{-6}$ m, and dark blue λ_2=0.95 $\times 10^{-6}$ m. Below 0.1 K the two measurements exhibit the same value.

We will investigate each of the possible scenarios and their potential applicability to our measurements in the following sections.

3.5.1 Dependence of the transmission coefficient on the shape of the junctions

In our study, the shape of the junctions is designed with catenoïd shape based on the numerical calculation to exhibit the maximum value of transmission coefficient ($\mathcal{T} = 1$). In a specific experiment, the importance of the geometry of the junctions of the nanowire to the reservoirs has been probed. In Fig. 3.6 the thermal conductance of two nanowires with almost the same length, but different parameters for the catenoidal junctions are compared. It is found that the more the contact is abrupt, the smaller the transmission coefficient will be. These experimental results show that the contacts with smaller curvature exhibit higher thermal conductance, in good agreement with recent theoretical work [42].

The interesting point of Fig. 3.6 is that at T<0.1 K the two graphs reach to the same value. This may show that at very low temperature, the dominant factor that governs the thermal conductance of the nanowires becomes independent of the shape of the junctions, and the effects of the geometry of the contacts are mostly pronounced at T>1 K.

The shape of the junctions has a noticeable effect on the transmission coefficient and it can be optimized by patterning the connecting part of the junctions to the reservoirs to a larger value by using a slighter curvature from reservoirs to the nanowire.

3.5.2 Thermal contact resistance between 1D nanowire to 2D reservoirs

The 1D-2D coupling of nanowires to the reservoirs could indeed have dramatic consequences on the phonon transport as demonstrated by Chalopin *et al.* [151]. In their study they use the diffusive limit approximation for the calculation of transmission coefficient, which is:

$$\mathcal{T}_{wire \to bath} = \frac{C_b \nu_b}{C_b \nu_b + C_w \nu_w} \tag{3.8}$$

The indexes of b and w refers respectively the heat bath and the wire, and C is the heat capacity and ν is the group velocity. The total thermal conductance is expressed as:

$$\frac{1}{K} = \frac{1}{C_w \nu_w} + \frac{1}{C_b \nu_b} \tag{3.9}$$

This equation shows that the contact conductance appears as the combination of two conductances (from bath to nanowire and from nanowire to bath) [44]. Based on their calculations, they found that the thermal contact conductance is smaller than the thermal conductance of the nanowire. This means that even if in the nanowire the thermal conductance is equal to the quantum of thermal conductance, the contact conductance dominates the heat exchange. In Fig. 3.7 the calculation of the thermal conductance of nanowires with square section from 1 nm to 10 nm, are compared separately with the thermal conductance of the contact. It is clear that below 1 K the contact thermal conductance is more than 4 orders of magnitude smaller than the quantum of thermal conductance in the nanowire. This high thermal resistance arises from a smaller number of excited modes per volume in the membrane reservoir than in the nanowire. According to the theoretical investigation by Chalopin *et al.* [151], when the heating is introduced through reservoirs into the nanowire, heat transfer along the nanowire is driven by the contacts, and the measurement of the quantum of conductance in nanowires may not even be feasible.

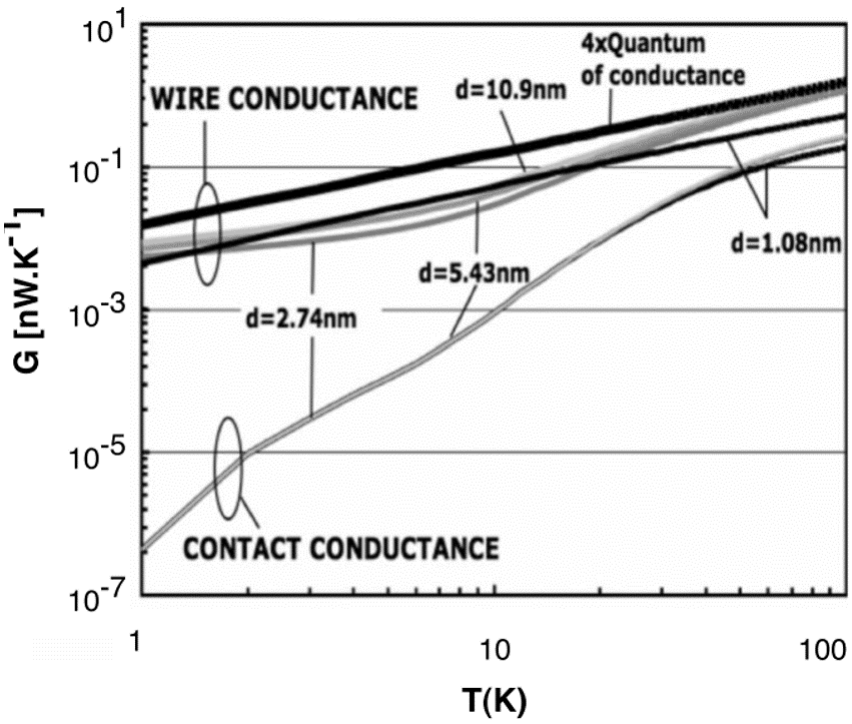

Figure 3.7: **Contact thermal conductance.** Thermal conductance of contact between wires and bath compared to conductance of the nanowires with different sections [45].

3.5.3 The cutoff frequencies of transmission coefficient

According to numerical calculations, the cutoff frequency of transmission rate at low energies for different modes of vibrations happens below 2 GHz [17, 41]. This cutoff frequency depends on the intrinsic properties of material, and the geometrical parameters of sample. The efficiency of transmission coefficient is limited by reflections that happen on passing between the straight region and the curved one. The minimum frequency that we reach at the lowest temperature of the experiment (T_{min}=0.05 K) is f_{min}=2.93 GHz. In Fig. 3.8 the transmission coefficient of different modes with their cutoff frequencies are presented. These calculations are obtained for GaAs nanowire. Moreover, it is evident that except shear mode, for the other modes the cutoff frequency occurs below 1 GHz. It can be also mentioned that only three modes are contributing to the transmission coefficient in 1D channel. The calculations of the cutoff frequencies and the minimum frequency that we attain during our experiment (f_{min}=2.93 GHz) mean that the low transmission rate appears at low enough frequency and should not impact our results.

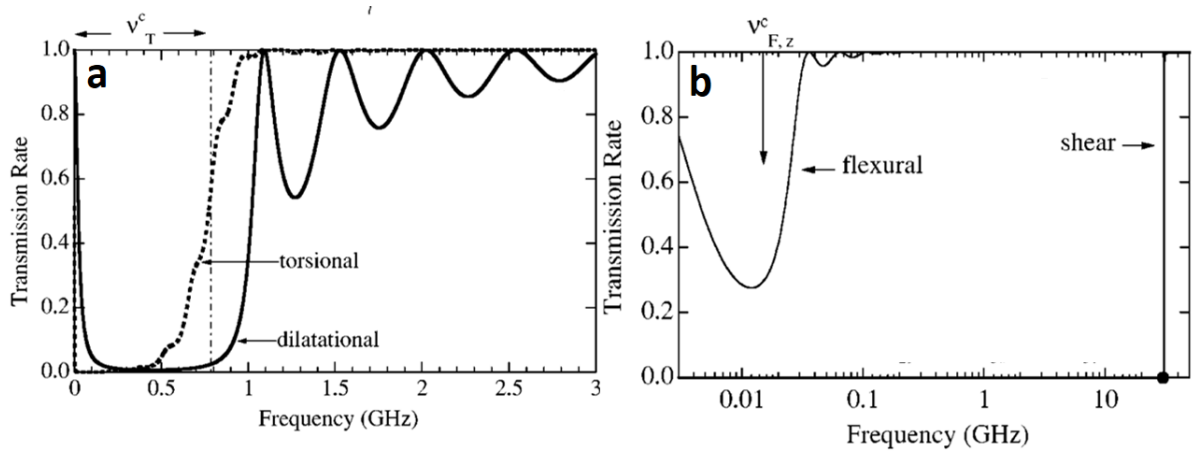

Figure 3.8: **Cutoff frequencies in transmission coefficient.** The calculated transmission rates of GaAs nanowire. (**a**) The transmission rates for the dilatational mode (solid line) and torsional mode (dotted line). (**b**) The coupled flexural (thin line) and shear (bold line) mode perpendicular to the plane. The term ν_i^c denotes the cutoff frequencies of each mode [41].

3.5.4 Dependence of the transmission coefficient on the length of nanowire

Some theoretical studies have reported a quadratic dependence of the thermal conductance of a nanowire on the details of the structure of the nanowire (roughness, dislocations, voids, defects, etc). Several theoretical works have reported the dependence of thermal conductance in ballistic regime on the roughness of the surfaces K$\propto \eta^2$ (η as the roughness) [154, 155]. Other works have reported the dependence of the transmission coefficient on the length of nanowire at low energy vibrations [47, 156]. It was also mentioned that the transmission coefficient depends on the regime of phonon scattering [43, 47, 156]. For the ballistic regime of heat transport the transmission coefficient is expressed to have a form of:

$$\mathcal{T} = \frac{1}{1 + L/\Lambda_{ph}} \tag{3.10}$$

where L is the length of nanowire and Λ_{ph} is the phonon MFP [47]. Measuring the thermal conductance with different lengths is one of the most straightforward approach to detect the presence of ballistic heat transport, and verifying whether the transmission coefficient depends on the length or not. Indeed, in the ballistic regime, the thermal conductance is independent of the length, the surface roughness or any internal processes introducing additional thermal resistance [12, 150].

Recently, an experimental achievement has reported the ballistic phonon transport in silicon nanowires with different length at low temperature. The ballistic phonon transport was estimated for the nanowires having the lengths smaller than 4μm [40]. Another experimental measurement on CNTs has reported the dependence of thermal conduction on the length of the sample as $\kappa \propto L^{\alpha}$ ($\alpha > 0$) [157]. The CNTs do not have an outer

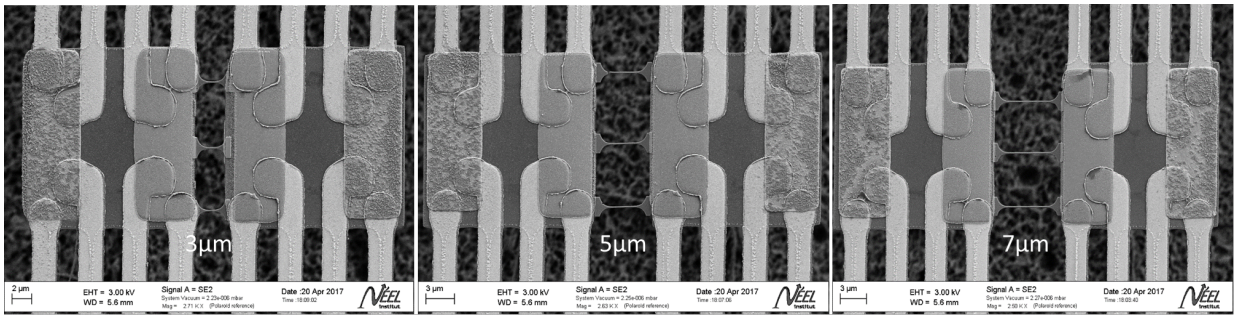

Figure 3.9: **SEM images of nanocalorimeters with different gaps.** The nanocalorimeters have identical contacts geometry but different lengths of the nanowires. The lengths of the nanowires are 3 μm, 5 μm, and 7 μm.

surface to provide boundary scattering. So, even at low temperature the only scattering mechanisms are lattice anharmonicity, and 3-phonon processes [158–160].

In our case, in order to ensure the existence of ballistic transport, and verify the dependence of transmission coefficient on the details of the structure, an experiment has been carried out measuring the thermal conductance of nanowires with different lengths. The samples have been fabricated with exactly the same shape of the junctions, but different lengths of the nanowires. The SEM images of the samples are presented in Fig. 3.10 with three different lengths 3, 5 and 7 μm. The experimental results are presented in Fig. 3.10. As it can be seen, the thermal conductances of the three different lengths are mostly superposed over all the temperature range. This justifies that the phonon conduction is in the ballistic regime, independent of the length conserving energy during their propagation.

These measurements prove two major aspects in our experiments. First of all, there exist purely ballistic transport within the nanowires. On the other hand, since all the different lengths exhibited the same thermal conductance, so the transmission coefficient does not depend on the nanowire itself but rather on the precise details of the contacts.

3.5.5 Role of Two-Level Systems on the transmission coefficient

In the experimental results, the thermal conductances exhibited a quadratic dependence on the temperature in the overall temperature range. This dependence is hardly explained by different models of thermal transport at very low temperature (elastic continuum model, thermal contact, Ziman regime, etc.). However, it could be in relative agreement with expected thermal transport in a bulk amorphous solids (a-solids) at low temperature.

Here, two fundamental phenomena are happening. On one hand, we have the evidence of ballistic transport by the proof of long phonon MFP, and comparable thermal conduc-

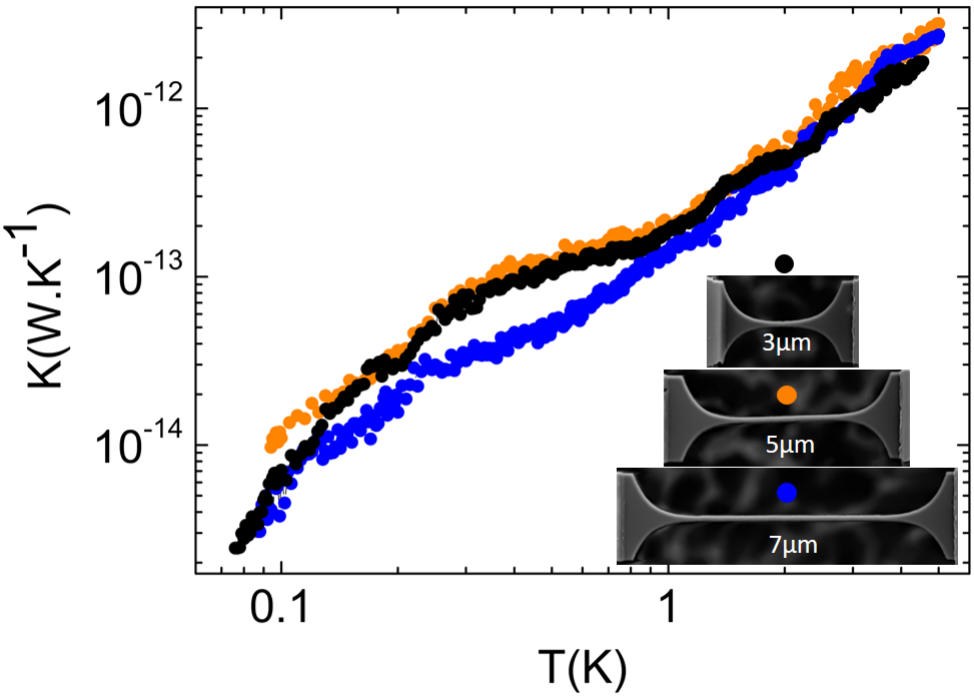

Figure 3.10: **The thermal conductance measurements for different lengths of nanowires.** The experimental thermal conductance based on different length of the nanowires versus temperature plotted in a log-log plot. The lengths of nanowires are 3 μm, 5 μm, and 7 μm, and the top views of the nanowires are shown in the inset.

tances of nanowires with different lengths. On the other hand, the quadraticity of the temperature variation of the thermal conductance reminds the low temperature thermal characteristics of bulk a-solids. As explained in section 1.7, this quadratic behavior may come from the presence of the localized TLSs in amorphous silicon nitride; the thermal transport being set by the scattering of phonons on these TLSs. The controversial point is that basically in a nanostructured system (made by either crystalline or amorhous network), the phonon transport is governed by boundaries and not the internal process of the material in use.

In order to understand the robustness of the universal behavior of a-solids in systems having a restricted geometry, we have investigated a new set of experiments [73]. This experimental achievement is done by 3ω method by measuring the thermal conductance of various nanoscale systems (membrane, large microwire, narrow microwire, and nanowire). The details of the dimension of the different kinds of samples are presented in table 3.1. Schematic representation of the membrane and the nanowire used for the measurement are shown in Fig. 3.11 **a-c**. The measurements have been done down to 0.3 K, and it should be mentioned that the thermal conductances measured below T<0.5 K are not reliable because of the significant presence of ballistic phonons (where the temperature is not defined along the systems).

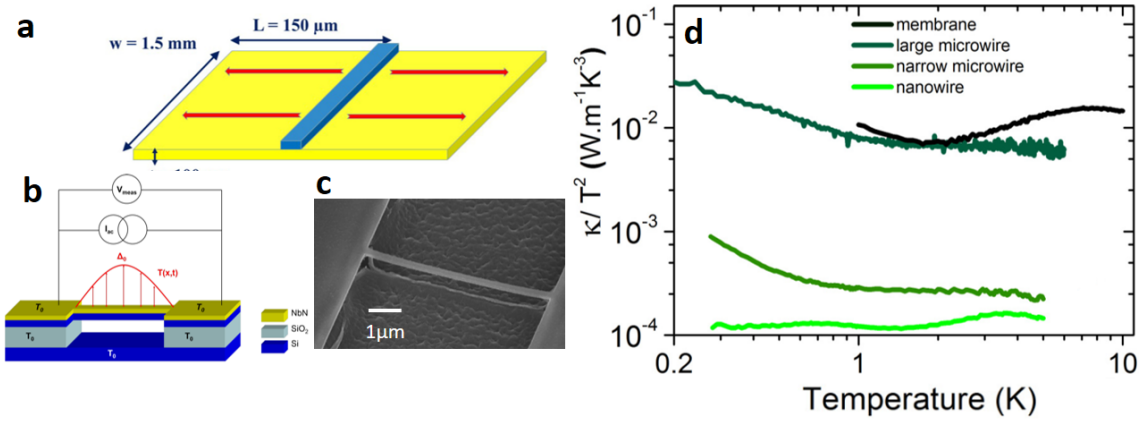

Figure 3.11: **The thermal conductivities normalized to the square of the temperature (κ/T^2).** (**a**) Schematic representation of the silicon nitride membrane. The red arrows represent the heat flux, and the blue layer represents the niobium nitride (NbN) that is the thin film transducer used for the thermal measurements. (**b**) Schematic principle of the 3ω method on a suspended nanowire. In black, the electronic circuit; in red, the temperature profile, and (**c**) shows the suspended silicon nitride nanowire used for the measurement. (**d**) The thermal conductivity of nanoscale systems (membrane, large microwire, narrow microwire, and nanowire) normalized to the square of the temperature, plotted in log-log. Almost all the strcutures exhibit a thermal conductivity that has a quadratic dependence on the temperature as published in [73].

In a dielectric single crystal, at low temperature and low dimension, when the phonon MFP is only set by boundary scattering, the regime of thermal transport is well described by the Casimir model (refer to section 1.5.1). In this regime, it is expected that the thermal conductance varies with a cubic power law in temperature. On the other hand, in amorphous solids the phonon-TLSs interactions limit the phonon MFP (Λ^{bluk}_{ph-TLS}) and give a quadratic variation of thermal conductance in temperature [64, 65]. For instance, the bulk phonon MFP which is set by the phonon-TLSs interactions, lies in the range of 20 μm $< \Lambda^{bulk}_{ph-TLS} <$ 200 μm [63]. In our analysis, the dimension of the systems are designed purposely below the characteristic length set by the bulk phonon-TLS MFP in amorphous materials Λ^{bulk}_{ph-TLS} (below a few tenth of micron). Thus, it is expected that only the boundary scattering set the phonon MFP, the thermal conductance varies with

Sample type	$\mathcal{W}$	**L (μm)**	**t (nm)**
membrane	1.5 mm	150	100
large microwire	7 μm	50	100
narrow microwire	1 μm	10	100
nanowire	200 nm	2.5	100

Table 3.1: Details of the dimensions of the four different kinds of samples made out of Si_3N_4 thin films: sample types and their width $\mathcal{W}$ and length L and thickness t.

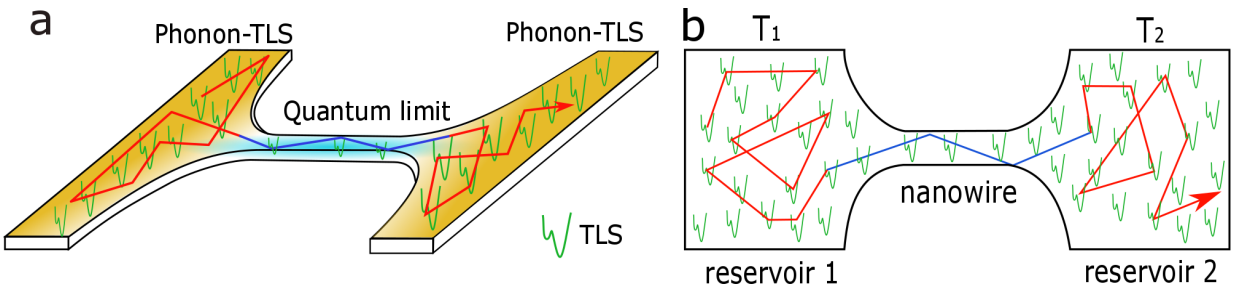

Figure 3.12: **The scheme of the TLSs distribution in the nanowire and the reservoirs.** Both schemes show the distribution of TLSs in the nanowire and the reservoirs. The phonon trajectory is shown by the red line (where the scattering is inelastic by phonon-TLS interactions in the reservoirs), and the blue line (the scattering is elastic along the nanowire). (**a**) Angled view and (**b**) top view of schematic of the nanowire and the reservoirs with the distribution of TLSs (the green sign) are shown. TLSs are distributed in the volume and notably on the surfaces of the system. Since the surfaces of the reservoirs are much larger than that of nanowire, the interaction of phonon-TLS is more probable in the reservoir. Thus along the nanowire the phonon transport is ballistic, whilst the inelastic interactions of phonon-TLS occurring in the reservoirs (shown by orange color) cause the thermalization of the phonons.

a cubic power law (Casimir regime).

In Fig. 3.11 **d** the thermal conductance of silicon nitride nanostructures (membrane, large microwire, narrow microwire, and nanowire) are normalized by T^2. It is demonstrated that even though the dimension of the systems are smaller than Λ^{bulk}_{ph-TLS}, the temperature dependence of the thermal conductance remains mostly quadratic independent of the system section. It does not follow the cubic power law in temperature as expected in a Casimir regime of boundary-limited thermal transport. This has been ascribed to an unexpectedly high density of TLSs on the surfaces which still dominates the phonon scattering processes at low temperatures [73].

In the actual case with the nanowire between the two reservoirs, TLSs could be notably distributed on the surfaces. A schematic representation of the distribution of the TLSs in the reservoirs and the nanowire is shown in Fig 3.12 **a** and **b**. What should be understood is that phonons interact less with TLSs in nanowire than in the membranes. Since the TLSs are highly located on the surface, the strong interaction of phonon-TLS are more probable in the reservoirs than in the nanowire due to their respective size. Thus along the nanowire the phonon transport is ballistic and due to the interaction of phonon-TLS, thermalization then occurring in the reservoirs (shown by orange color Fig. 3.12 **a** and **b**). We believe that is the reason why the power law of the experimental thermal conductances remains quadratic over all the temperature range. This analysis gives us a conceptual insight that the ballistic transport of phonons is enclosed between two diffusive reservoirs.

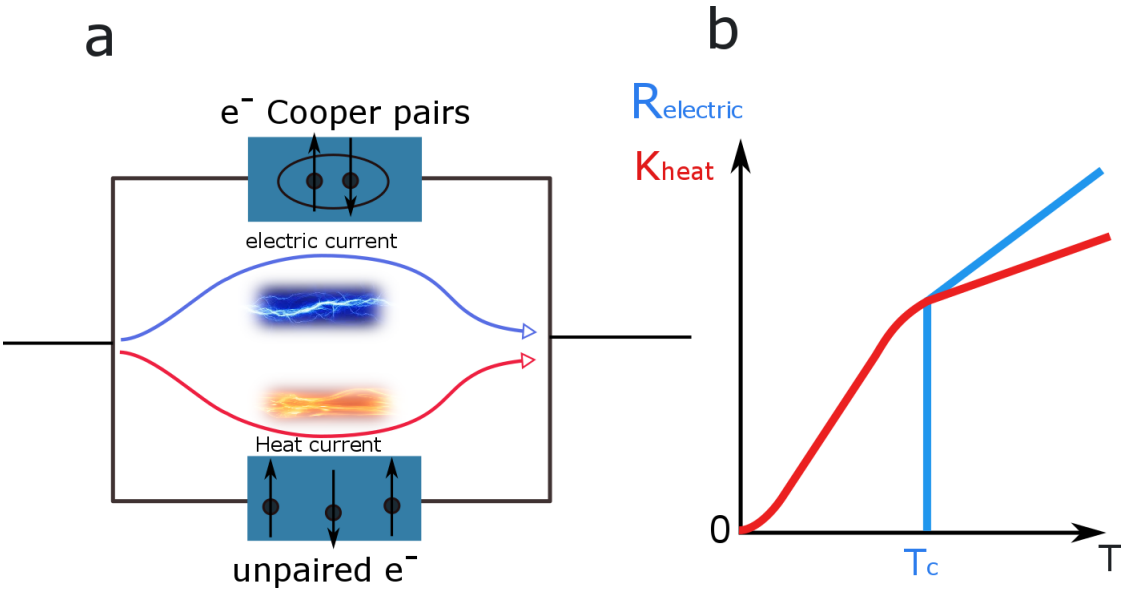

Figure 3.13: **Two fluid scheme.** (**a**) A scheme of two channels of electric and heat conduction are presented. At the temperature T<T_c, the channel with cooper pairs electrons serves as short circuit for electronic transport, and the channel with unpaired electrons conduct heat even if they are not conducting electricity anymore. (**b**) The schematic graph shows the contribution of electrons in electric resistance (the blue line), and thermal conductance (the red line) before and after the critical temperature T_c. At T<T_c the electric resistance drops instantly to zero, while the thermal conductance gradually tends to zero.

3.6 Comparison of the present results to anterior experiment by K. Schwab *et al.*

Until now, we have made a deep analysis of our experiments. These measurements have been proved to be reproducible even though many parameters where changed. We have demonstrated a purely ballistic phonon transport along the 1D phonon waveguide, with a thermalization most probably occurring in the two reservoirs. Our data analysis based on the Landauer model shows transmission coefficients much lower than the ideal value ($\mathcal{T} = 1$); the possible scenarios of the low value of $\mathcal{T}$ have been discussed.

It is now of crucial importance to compare our experimental data to the only similar measurement done by K.Schwab *et al.* in 2000 in the group of Mickael Roukes [37]. Their measurement, shown in Fig. 1.12, has been done on a similar material and geometry, amorphous SiN nanowires, between 0.05 K and 5 K. However, there are two major differences between our devices and their. In our experiments, both reservoirs are isolated from the heat bath, and more importantly there is no materials evaporated on the nanowires. In the case of K. Schwab experiment, the current leads (thin-film of superconducting Nb) evaporated on the top of the nanowires will act as parasitic thermal path, in contradiction

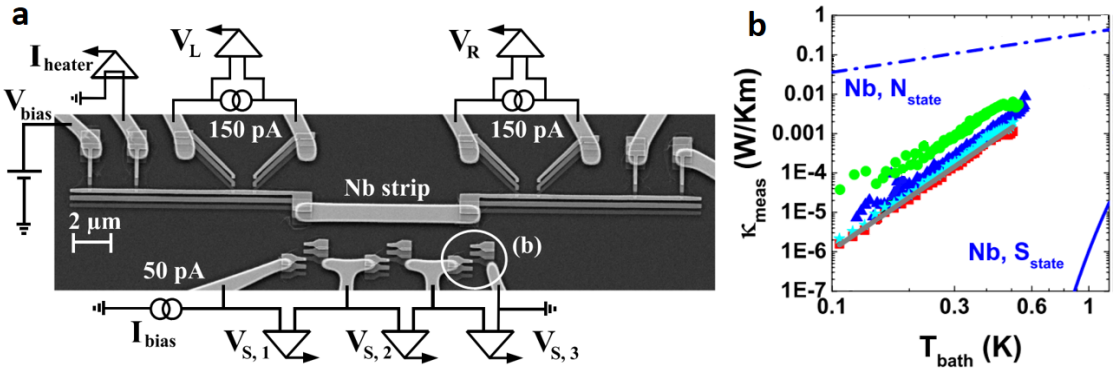

Figure 3.14: **Thermal conductivity of Nb thin-films.** (**a**) SEM image with a schematic of the experimental setup of the device used for the measurement of the thermal conductivity of Nb thin-film. (**b**) The experimental thermal conductivity of Nb for 1μm wide and 200 nm thick Nb are presented. Red filled squares, blue triangles, and green circles, respectively relate to 5, 10 and 20 μm long Nb strips. Bulk thermal conductivities of Nb in the normal (dashed-dotted line) and superconducting (solid line) states are shown in blue [161].

to what has been mentioned in the original paper: "By virtue of their superconductivity, these leads do not provide a parasitic thermal path" see ref [37]. This is obviously wrong, and we will show why. In a regular superconductor, just below the critical temperature T_c, part of the electrons close to the Fermi energy start to condensate in Cooper pairs. These electrons indeed do not contribute any more to the thermal transport since their energy cannot change. On the other hand all the unpaired electrons still conduct heat even if they are not conducting electricity anymore. This can be seen through a two fluid picture (see Fig. 3.13 **a**), two channels of conduction are present, if one of the channel serves as short circuit for electronic transport, this is not true for thermal transport. It is only at very low temperature when $T << T_c$ that most of the electrons close to the Fermi level are paired and then, the thermal conductivity of the superconductor tends to zero. It is shown in Fig. 3.13 **b** that at the temperature below T_c, the electric resistance drops instantly to zero, while the thermal conductance gradually tends to zero. In order to have a better comprehension of the experimental data provided in the seminal work of K. Schwab *et al.*, one needs to extract the thermal conductance of the thin-film of Nb used on top of the SiN nanowires in their experiment. This analysis can be done with the use of the measurement of thermal conductivity of thin-film of Nb done recently by Feshchenko *et al.* [161]. Fig. 3.14 **a** shows the SEM image of the device used by Feshchenko *et al.* with a schematic of the experimental setup. In this experiment, the temperature of the electronic bath is measured using the SINIS junction technique. The thin-film of Nb is shown as Nb strip. In Fig. 3.14 **b** the measurement of the thermal conductivity of 5, 10 and 20 μm long Nb strips, with 1 μm width and the thickness of 200 nm are shown by colored symbols. With the use of a fit from these measurements, one can extrapolate the thermal conductivity of thin-film of Nb up to 5 K. By normalizing the thermal conductivity of Nb to the dimension of the nanowire used by K. Schwab *et al.* (thickness of 25 nm, width of 200 nm and effective length of 2 μm), one can extract the expected

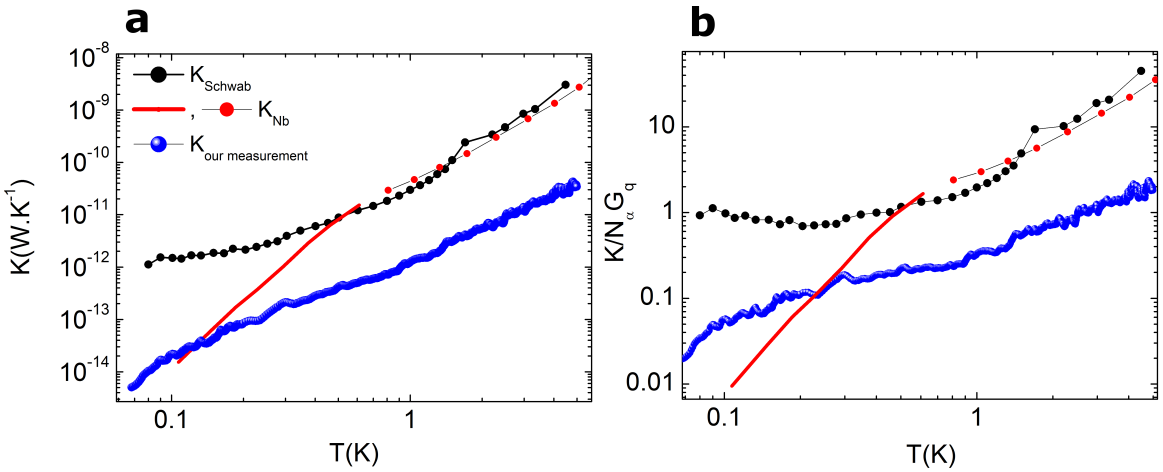

Figure 3.15: **Thermal conductance of Nb thin-film and SiN nanowire.** (**a**) The comparison of the measured thermal conductance of SiN nanowire (black dots) done K. Schwab *et al.* [37], with the thermal conductance of Nb normalized to the geometry of their experiment (red line/dots), and our experimental measurement on SiN nanowires (blue dots). (**b**) Thermal conductances of SiN nanowire from K. Schwab *et al.* our measurement, and Nb thin-film normalized to the quantum of thermal conductance.

thermal conductance of Nb in that original experiment.

In Fig. 3.15 **a** the measured thermal conductance of SiN nanowire by K. Schwab *et al.* (black dots), a fit of the thermal conductance of Nb on the top of their nanowires below 1 K (red line), and the thermal conductance of our experiment on SiN nanowires (blue dots) are shown. The red dots are the estimated thermal conductance of Nb for K. Schwab *et al.* sample at T< 1 K. The agreement between the predicted thermal conductance of Nb and the Schwab measurement is impressive, no adjustment have been made. It is clear that at T >1 K what they are measuring is essentially the thermal conductance of the current leads (Nb) and not the SiN nanowires. When we actually compare to our experimental results, there is a noticable difference between our measurements, close to one order of magnitude. Fig. 3.15 **b** illustrates the normalized thermal conductance of SiN and Nb of Schwab experiment to the quantum of thermal conductance. As a concluding remark to this section, we can say that the measurement of thermal transport in the quantum regime is still a quite open issue. Our measurements are very well controlled in terms of transport regime (ballistic and 1D limit). However, it is elusive to find a clear evidence of the quantum of thermal conductance in our measurements. Most probably, the contribution to the thermal transport of the contact profile is certainly essential as shown using the Landauer model.

3.7 Conclusion

In this chapter, the experimental measurements of the thermal conductance of the nanowires have been reported. The conditions of the experiments, from the temperature range of measurement to the design of the nanowires junction has been designed to be in the quantum regime of 1D heat transport. In such conditions, the transport of heat can be expressed by Landauer formalism, where the probability of transmission between two reservoirs is the crucial parameter.

The experimental results of thermal conductance of nanowires between 0.05 K and 5 K show a clear deviation from the quantum of thermal conductance. The analysis of the experimental phonon MFP shows that the phonon transport is indeed ballistic. Thus, the deviation from the quantum of thermal conductance comes from some dominant features in the contact to the reservoirs limiting the transmission coefficient.

In order to figure out the dominant factor in the transmission coefficient, several scenarios had been investigated: the dependence of transmission coefficient on the shape of the junctions, the coupling between 1D nanowire and 2D reservoirs, the dependence of the transmission coefficient on the length of nanowires and roughness of the surfaces, and the fundamental characteristics of amorphous solids at very low temperature. The measurement on nanowires having different lengths shows that the transmission coefficient does not depend on the length or roughness. However, it was shown that the transmission coefficient depends strongly on the shape of the junction of the nanowire to the reservoirs.

Another very important issue in limiting the transmission coefficient is the integration of 2D reservoirs into a 1D nanowire. Even though the thermal conductance inside of the nanowire may be equal to the quantum of thermal conductance, the contact thermal conductance is much lower than the quantum value and dominates the heat transport.

Our experimental measurements of thermal conductance show a uniform quadratic dependence on the temperature. This quadraticity could come from the fact that our device is made of an amorphous solid (silicon nitride Si_3N_4). Quasi-quadratic thermal conductivity and quasi-linear specific heat may be attributed to the existence of two-level systems inside of amorphous solids at very low temperature. We believe that the dominant factor for the transmission coefficient could find its origin in the existence of TLSs in silicon nitride. According to our recent research, the TLSs are highly distributed on the surfaces [73]. Since, the heat transport is mostly ballistic inside of the nanowire, then the thermalization occurs in the reservoirs. The interaction of phonon-TLSs on the surfaces of the reservoirs could be the reason of low transmission coefficient. One way of testing this scenario is to perform specific heat measurement. In fact, it has been noticed in the past that TLSs have also a strong signature on specific heat at very low temperature. Therefore, the measurement of specific heat on thin membrane of SiN may carry new insight in the TLS physics.

4 CHAPTER

Heat capacity of 2D phonon cavities

4.1 Introduction

This chapter of the thesis is about the effects of confinement and stress on the heat capacity of 2D membranes at low temperature. On one hand, low temperature measurement of specific heat is an important issue for revealing a great deal of information about the fundamental excitations in a system [162]. The temperature dependence of the specific heat may, for instance, reveal the electronic nature of the system, including energetic contributions of material, anisotropy, and possible signatures of quantum phase transitions [117, 163]. On the other hand, the study of specific heat at low dimensions unveils a new set of properties that differ significantly from their bulk counterparts. When the microstructural length scales of a system become comparable to the phonon MFP, surfaces start to influence the overall thermal properties (including specific heat). The phonons with different polarizations are absorbed to the surface, couple together, and form the standing waves with a new set of vibrational modes, and new dispersion relations. The new dispersion relations exhibit a different specific heat. Broadly speaking, the confinement effects become a new variable to tailor the properties of material in many exciting ways that are simply not possible in bulk 3D systems.

Beside the effects of confinement and low temperature, what should not be underestimated is the nature of the system under study. The material used in this work is amorphous silicon nitride (SiN_x). At very low temperatures amorphous solids (a-solids) have physical features that are markedly different than crystals. Almost all a-solids exhibit a nearly linear specific heat, and a thermal conductivity roughly proportional to T^2. The low temperature behavior of a-solids is attributed to TLSs (refer to section 1.7).

Measuring the specific heat of nanoscale systems made of a-solids at very low temperature will encounter two different effects: the phonon confinement effect on specific heat, and the low temperature behavior of a-solids known as TLS. In this chapter, at first, the technique used for the measurement of specific heat at low temperature is explained.

Then two fundamental aspects have been investigated: the effect of confinement, and internal stress of the medium on the specific heat.

4.2 Theoretical prediction for specific heat of 2D phonon cavity

The specific heat of 2D phonon cavity can be explained either by the dynamical lattice theory, or the elastic continuum model. As explained in section 1.6, for a 2D system (the dimensionality of d=2), the lattice theory predicts that at low temperature the specific heat should be proportional to T^2 [49]. More realistic theoretical calculations on the specific heat of 2D phonon cavity have been done based on the elastic continuum model.

4.2.1 Elastic continuum model

According to the elastic continuum theory, with the presence of the boundary conditions, different polarizations will couple together at the surfaces, and generate new set of vibrational modes: dilatational waves (DW), flexural waves (FW) and shear waves (SW) (refer to section 1.6). The qualitative difference between the dispersion relations of these modes have important consequences on the low temperature specific heat. By integrating over the wave vector parallel to the membrane surface $q_{||}$, the total specific heat can be written as:

$$C_V = \frac{A}{k_B T^2 2\pi} \sum_{\sigma} \sum_{m=0}^{\infty} \int_0^{\infty} dq_{||} \frac{q_{||} (\hbar\omega_{m,\sigma})^2 exp(\beta\hbar\omega_{m,\sigma})}{\left[exp(\beta\hbar\omega_{m,\sigma}) - 1\right]^2} \tag{4.1}$$

where σ represents the DW, FW and SW modes, $\sum_m$ is the summation over the branches, $\hbar$ is the Planck constant, $\beta = (k_B T)^{-1}$ and k_B is the Boltzmann constant. According to the calculations at sub-Kelvin temperature the contribution of the flexural waves (FW) become dominant. The overwhelming of FW modes with quadratic dispersion relation leads the heat capacity of 2D phonon cavities to a linear dependence on temperature below 1 K [50, 51, 53]. In Fig. 4.1 **a** the specific heat of thin membrane and bulk a-SiC are presented. As calculated by Gusso and Rego [50], the transition from 3D to 2D occurs at the crossover of the solid black line (the specific heat of 2D phonon cavity) with dashed dot line (fully 3D limit). The temperature of the transition is shown by the green dashed line in Fig 4.1 **a**. The temperature exponents of the calculated specific heats are presented in Fig. 4.1 **b**. In contrast to the dynamical lattice model, the elastic continuum theory predicts that in a 2D limit, a linear variation of specific heat (not quadratic) as a function of temperature is expected.

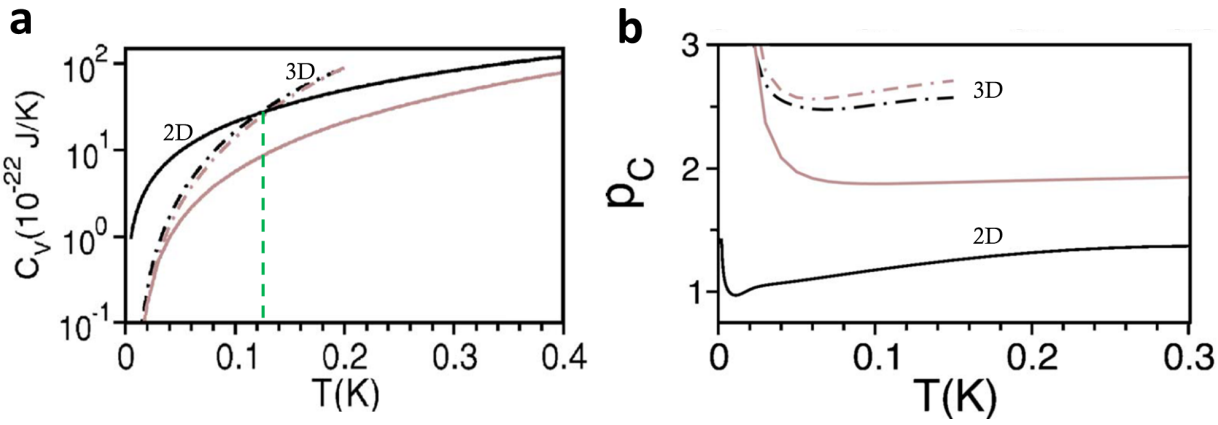

Figure 4.1: **The specific heat calculation of free standing a-SiC thin membrane.** (**a**) The black solid line represents the heat capacity of realistic 2D phonon cavity, and the dashed dot line shows that of fully 3D bulk. The gray curves are predictions from the bounded plane wave model (BPWM). (**b**) The temperature exponents of the calculated specific heats that are presented in part (**a**) [50].

4.2.2 Low temperature specific heat of amorphous solids

Our samples are made of a-SiN, and as it has been explained before (section 1.7), the thermal properties of a-solids have unique characteristics at low temperatures. In the typical amorphous solids, the total specific heat at low temperature can be written as:

$$C_{tot}(T) = C_D(T) + C_{TLS} + C_{ex}(T) \tag{4.2}$$

$C_D(T)$ is the Debye specific heat, C_{TLS} is the contribution of TLSs in low temperature specific heat of a-solids, and C_{ex} is attributed to the non-propagating harmonic modes (soft potential modes) with cubic dependence on temperature, and it is estimated for most disordered materials to be in the order of $C_{ex} \cong (1-10)\times 10^{-7}$ T^3 (J/gK) [62]. The TLSs and Debye specific heat can be written as:

$$C_D = \frac{4\pi^3 k_B^4}{15\hbar^3\rho}\left(\frac{2}{\nu_t^3}+\frac{1}{\nu_l^3}\right)T^3 \tag{4.3}$$

$$C_{TLS} = \frac{\pi^2}{6}k_B^2\frac{n_0}{\rho}T^{\alpha}\times\frac{1}{T^{*\alpha-1}} \tag{4.4}$$

where ρ (g/m^3) is the density of the sample, ν_t and ν_l respectively are transversal and longitudinal speed of sound, n_0 is the density of TLSs, and α is the power law of TLS specific heat and it is estimated to be in the order of $\alpha = 1.3 \pm 0.03$ [164]. The term $1/T^{*\alpha-1}$ is written to equilibrate the unity of specific heat. Basically, in a-solids below 1 K, C_{TLS} becomes dominant and the specific heat will exhibit a linear variation as a function of temperature. It should be mentioned that this linear dependence is not due to the geometrical effects, and it is related to the disordered nature of the system.

In confinement point of view, there are two major theoretical predictions for the heat capacity of 2D a-SiN membrane at very low temperature. Either the temperature dependence of the specific heat is quadratic (2D limit of dynamical lattice theory), or it varies linearly based on the prediction of the elastic continuum theory. Concerning the nature of material in use (disordered SiN), the low temperature fundamental vibrational modes of amorphous SiN should dominate the specific heat of 2D phonon cavity and exhibit a linear dependence.

In the following sections the experimental techniques of the measurement of the heat capacity at very low temperature are explained.

4.3 Low temperature measurement of specific heat

There exists plenty of calorimetric methods for the measurements of the heat capacity. We can name as adiabatic method, ac calorimetry, relaxation calorimetry, heat pulse calorimetry, dual slope calorimetry or differential scanning calorimetry. The specific heat measurement that is commonly used for low temperature measurements is known as adiabatic techniques that is considered as the most accurate way to estimate the absolute value of the specific heat [165, 166]. However, it requires samples masses of several grams and the subtraction of the addenda. Since we want to measure the specific heat of very small samples with masses less than one nanogram (0.5 ng to be exact), the adiabatic technique is not the suitable method for small samples measurement.

The quasi-adiabatic techniques (known as ac calorimetry) are the techniques developed for the thermal measurement of very small systems. These techniques are often preferred at low temperatures, because it allows good thermal isolation of the system with small masses. In addition, it allows the use of signal averaging techniques to improve the resolution (noise/average signal ratio) of the measurement. By ac calorimetry the specific heat can be measured with very high sensitivity, despite the small masses. In this section, we will basically focus on ac calorimetry.

4.3.1 ac calorimetry

The basic principle of measuring the heat capacity C_p consists in isolating the system and introducing a quantity of energy δQ into the system with the use of a resistive heater (see Fig. 4.2). The implied power will raise the temperature of the system δT, so by measuring the variation of temperature by a thermometer, we can obtain the heat capacity using the relation $C = \delta Q/\delta T$.

ac calorimetry also known as modulated temperature calorimetry is the method used for the heat capacity measurements of 2D suspended membranes. This method consists

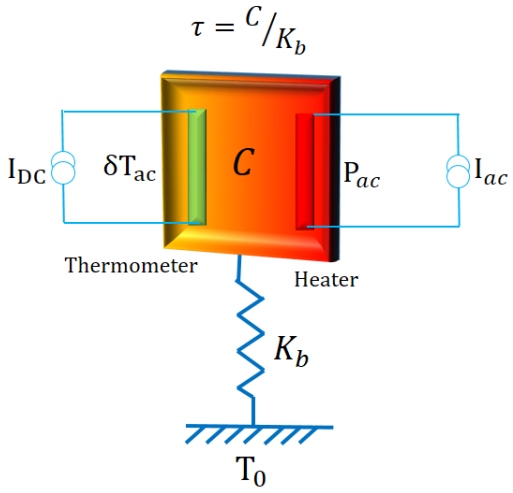

Figure 4.2: **The schematic configuration of the heat capacity measurement.** C is the heat capacity of the membrane, K_b is the thermal conductance of the thermal leak to the heat bath, T_0 is the temperature of the heat bath. The heater is polarized by ac current, and by thermometer the oscillation of the temperature are measured. the relaxation time is equal to $\tau = C/K_b$.

of polarizing the heater by a periodic oscillating current with the frequency of ω. The generated current cause an oscillating power $P(t)=R_H I_H^2$ at the frequency of 2ω. The alternating power will produce an oscillation of the temperature, and by measuring the oscillating part of temperature, one can measure the heat capacity of the membrane. A representative scheme is shown in Fig. 4.2 with the oscillating power δQ that cause an oscillating temperature δT_{ac}. The basic relations for a modulated temperature calorimeter result from the following common equations that describes, in its simplest form, any calorimetric system. The thermal power balance gives:

$$P(t) = C(T)\left(\frac{dT}{dt}\right) + K_b(T_s - T_0) \tag{4.5}$$

where $P(t)$ is the generated power, $C(T)$ is the heat capacity of membrane, and K_b is the thermal conductance of the supporting beams. T_s and T_0 respectively are the measured temperatures by the thermometer and the heat bath. The heater is polarized with a current I_H, with the amplitude of I_0, and frequency of $\omega/2$.

$$I_H(t) = I_0 \ \cos(\omega/2t) \tag{4.6}$$

With the use of equation 4.5, we have:

$$P(t) = R_H I_H^2 = P_0\,(1 + \cos(\omega t)) = C(T)\left(\frac{dT}{dt}\right) + K_b(T_s - T_0) \tag{4.7}$$

Now, one should solve the differential equation of 4.7 by considering the characteristics time in the calorimeter. The internal diffusion time is defined as $\tau_{int} = C/K_{int}$, where

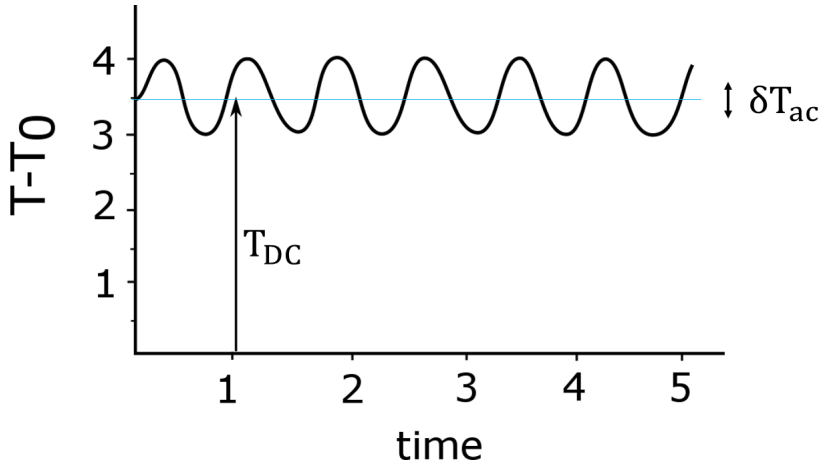

Figure 4.3: **The temperature as a function of time in an ac calorimetric measurement.** A continuous temperature gradient T_{DC} is superposed on a temperature oscillation δT_{ac} with amplitude inversely proportional to the heat capacity C of the cell.

K_{int} is the thermal conductance of the membrane. The relaxation time of the energy from the membrane to the heat bath is $\tau = C/K_b$. So the solution of equation 4.7 in stationary regime is:

$$T = T_0 + \frac{P_0}{K_b} + \frac{P_0}{\omega C\sqrt{1 + \frac{1}{(\omega\tau)^2} + (\omega\tau_{int})^2 + \frac{2K_b}{3K_{int}}}}\cos(\omega t - \phi) \tag{4.8}$$

where

$$T_{DC} = T_0 + \frac{P_0}{K_b}\ , \qquad \delta T_{ac} = \frac{P_0}{\omega C\sqrt{1 + \frac{1}{(\omega\tau)^2} + (\omega\tau_{int})^2 + \frac{2K_b}{3K_{int}}}}\cos(\omega t - \phi) \tag{4.9}$$

The temperature *T(t)* is thus a superposition of a continuous term T_{DC}, and an alternating term δT_{ac} (see Fig. 4.3)

Simplifying the equation 4.8 requires a good understanding of internal diffusion and relaxation processes. Since a perfect isolation for small systems is difficult to obtain, so the isolation of the calorimeter is carried out by the correct choice of frequency. First criterion is that the frequency of temperature modulation (f_{mes}) should be fast enough so that the generated power has not time to relax to the heat bath $f_{mes} \gg 1/\tau$. However, if the chosen frequency is even higher than τ_{int}, the system is not heated isothermally. Thus the second criteria is to have $f_{mes} \ll 1/\tau_{int}$. In order to get $K_b \ll K_{int}$ the membrane

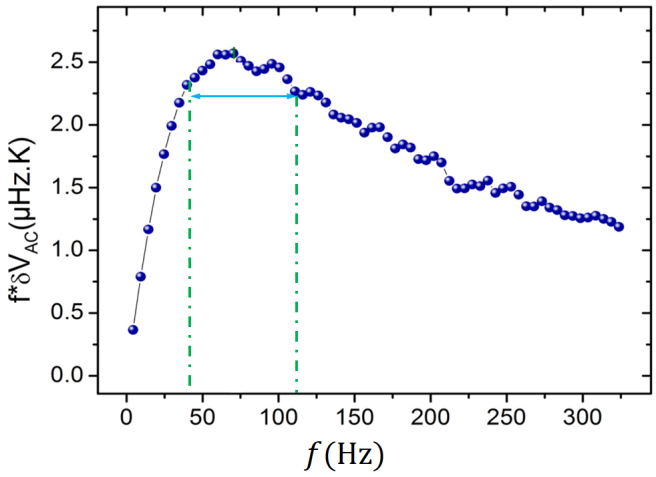

Figure 4.4: $f \times \delta V_{ac}$ **plotted as the function of the frequency of the heater**. When $f \times \delta V_{ac}$ does not depend on the frequency, this means that the system is in the adiabatic regime. In this measurement has been done at fixed temperature of 100 mK, and the adiabatic regime occurs between the frequencies of 40 Hz $< f <$ 120 Hz.

is fabricated within a suspended structure by suspending beams. The beams are made of the same material as the membrane, and they have thinned width in comparison to the membrane, and very long length. In this configuration, the thermal leakage from the membrane to the heat bath is much less than the thermal conductance of the membrane itself $K_b \ll K_{int}$. So the suitable frequency which verifies the conditions is:

$$1/\tau \ll \omega \ll 1/\tau_{int} \tag{4.10}$$

Under these conditions, the system can be considered to be quasi-adiabatic, or differently said effectively isolated from the thermal reservoirs. Now the equation 4.8 becomes:

$$T = T_0 + \frac{P_0}{K_b} + \frac{P_0}{2\omega C}\cos(\omega t - \phi) \tag{4.11}$$

We can write it as:

$$T = T_0 + \frac{P_0}{K_b} + \delta T_{ac} \tag{4.12}$$

The component δT_{ac} carries the information about the heat capacity. The thermometer is polarized with a DC current, and the RMS value of temperature modulation δT_{ac} at the frequency of 2ω is obtained by measuring the second harmonic voltage of the thermometer δV_{ac} by standard lock-in amplifiers.

$$\delta T_{ac} = \frac{\delta V_{ac}}{I_{th}\ \alpha\ R_{th}(T)} \tag{4.13}$$

Here I_{th} is the DC current used to bias the thermometer. $R_{th}(T)$ and α respectively are the resistance of the thermometer and the temperature coefficient of the resistance. By measuring δV_{ac} we will have δT_{ac}, then one can obtain the heat capacity by:

$$C = \frac{P_0}{\omega\ \delta T_{ac}} = \frac{R_H\ I_H^2}{4\pi f_{mes}\ \delta T_{ac}} \tag{4.14}$$

By this formula we can calculate the heat capacity of the membrane from the measured signal. The choice of frequency of the measurement is within the adiabatic range. If the heater is polarized by a current at very low frequency, then the whole dissipated power will be relaxed to the heat bath by supporting beams. By simplifying equation 4.8 with the estimation of $\omega \to 0$, one can find the thermal conductance of the beams by:

$$K_b = \frac{P_0}{2\delta T_{ac}} = \frac{R_H\ {I_0}^2}{4\delta T_{ac}} \tag{4.15}$$

The measurement of the thermal conductance of the supporting beams is shown in Fig. 2.21. As a conclusion, ac calorimetry method, can measure either the heat capacity of suspended membrane, or the heat loss by conduction to the thermal bath through the suspending beams [167, 168].

Choice of working frequency

For the measurement of heat capacity, the working frequency should be within quasi-adiabatic range. This range is defined as the frequency window where the response of transducer ($f \times \delta V_{ac}$) is almost independent of frequency. To find out this acceptable range one need to measure V_{ac} as the function of frequency f, then we trace $f \times \delta V_{ac}$. The Fig. 4.4 presents the evolution adiabatic regime over the frequency at a fixed temperature (100 mK). In this figure, we can see that the adiabatic regime (low variation of $f \times \delta V_{ac}$) corresponds to frequencies between 40 and 120 Hz.

4.3.2 Measurement setup

All the measurements of heat capacity have been carried out in a dilution refrigerator equipped with the electronic measurement devices (shown in Fig. 2.17). The electronic setup of our experiment is shown in Fig. 4.5. All the electrical signals are filtered at the connection by a low pass filters (shown as LP filter). The current is generated by an

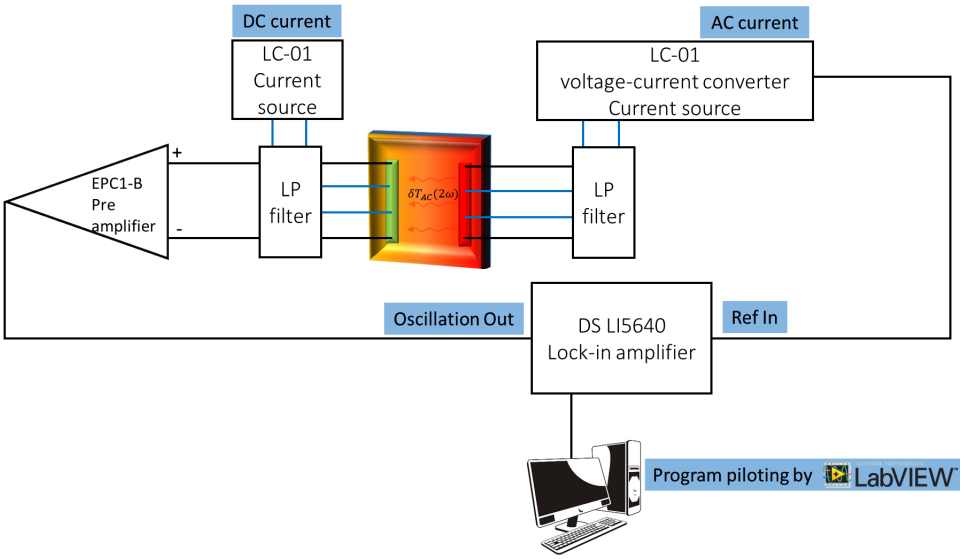

Figure 4.5: **The electronic setup for the measurement of heat capacity.** The heater is polarized by an ac current and the thermometer measures the second harmonic of the signal by a DC current. All the electronic measurement are connected to the low pass filter, very low-noise preamplifier, and low-noise current sources. The signals are monitored and treated by computer.

ultra-low drift generator (less than 5 ppm/°C) LC01 developed at the Institut Néel, which permits to deliver a very low current (down to 0.1 nA). The signal is preamplified by a very low noise (0.65 nV/$\sqrt{\text{Hz}}$) amplifier (EPC1-B). Then the voltage is measured with a lock-in amplifier LI 5640. The low noise electronic allows a highly sensitive measurement of the second harmonic of the signal, and consequently, allowing a sensitive measurement of the heat capacity of suspended membrane.

Noise characterization for ac calorimetry

The noise for the measurement of heat capacity using ac calorimetry has been studied. To measure the total noise of the experiment, the temperature has been fixed on 0.1 K, and each 1 second the ac voltage of thermometer (δV_{ac}) have been measured during 600 s. The measurement of δV_{ac} as a function of time is shown in Fig. 4.6 **a**, and Fig. 4.6 **b** shows a statistical analysis on the measured value. It is demonstrated that the signal distribution plotted as a histogram correctly fits by a gaussian function. The measured noise equivalent voltage is about $NEV_{ac} \cong 0.7$ nV/$\sqrt{\text{Hz}}$. By knowning the noise equivalent voltage we can extract the noise equivalent heat capacity (NEHC) by:

$$\frac{NEV_{ac}}{V_{ac}} = \frac{NEHC}{C_p} \tag{4.16}$$

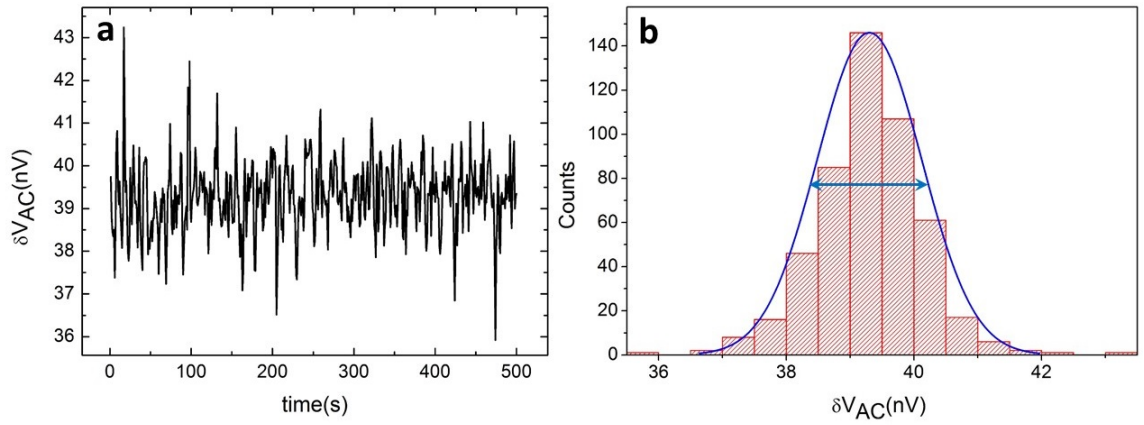

Figure 4.6: **Noise measurement with ac calorimetry.** (**a**) Measured δV_{ac} signal of the membrane-based nanocalorimeter at 0.1 K with ac calorimetry method. (**b**) The signal distribution is plotted as a histogram. The full width at half maximum corresponds to the noise of the measurement. In this measurement noise equivalent voltage is about $NEV_{ac} \cong 0.7$ nV/$\sqrt{\text{Hz}}$.

$$NEHC = C_p \frac{NEV_{ac}}{V_{ac}} \tag{4.17}$$

This measurement demonstrates a sensitivity of heat capacity $\Delta C \cong 2.3 \times 10^{-16}$ J/K. The noise equivalent energy ΔE can be calculated by the equation $\Delta E = NEHC \times NET \times \Delta f$ (NET is the noise equivalent temperature, and Δf is the bandwidth of frequency over which the measurement has been achieved). We have $\Delta E \cong 2.3 \times 10^{-20}$ J which is an unprecedented zeptoJoule sensitivity obtained thanks to highly developed low noise electronic devices and very sensitive NbN thermometers.

4.4 The measurement of low temperature heat capacity

In order to investigate the effect of confinement on heat capacity, an experiment had been set up measuring the heat capacity of 2D suspended membranes with two different thicknesses (100 nm and 300 nm). The samples under study are the suspended membrane-based nanocalorimeters (as shown in Fig. 4.7). Both samples are microfabricated from high-stress (HS) silicon nitride. The quantitative measurements of heat capacity versus temperature with double Y axis are presented in Fig. 4.8 **a** in J.K^{-1} left axis, and J.K^{-1}.m^{-2} right axis, and **b** J.g^{-1}.K^{-1} left axis, and J.K^{-1}.m^{-3} right axis. The right axis of Fig. 4.8 **a** and **b** are presented in order to highlight either volumetric or surface effect.

In Fig. 4.8 **a** right axis the heat capacities are normalized to the surfaces of the membranes. It can be seen that at $T < 0.5$ K the heat capacity of Si_3N_4 membranes with

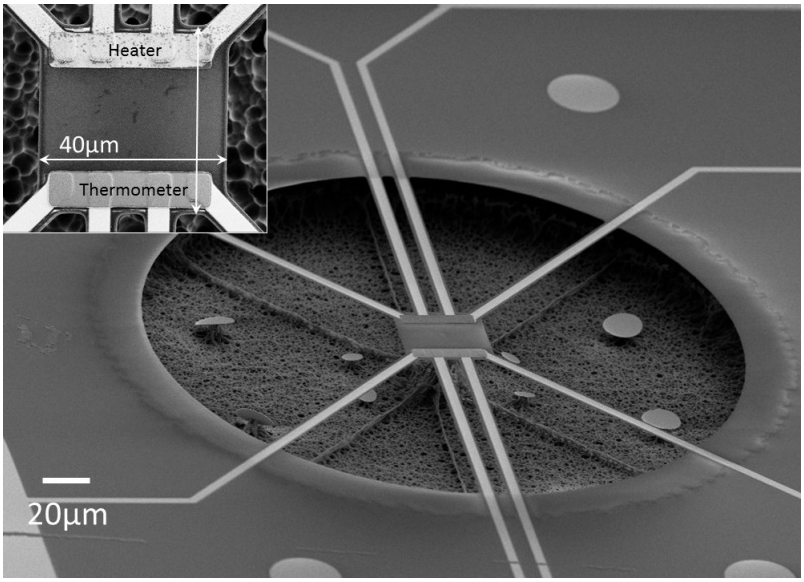

Figure 4.7: **Suspended membrane-based nanocalorimeter.** The 2D suspended platform made of a-SiN contains a heater and a thermometer, and it is suspended by eight suspending beams. The inset shows a top side view of the membrane.

the same surfaces and different thicknesses of 100 nm and 300 nm exhibit almost the same value. This superposition of the heat capacity at sub-Kelvin temperature shows that even though the two samples have a different volume, their heat capacity is in the same range. Somehow, the volume of the membranes does not contribute to the heat capacity, showing that below 0.5 K heat capacity seems to be governed by the surfaces. On the other hand, in Fig. 4.8 **b** right axis, when the heat capacities are normalized to the volume, at high temperature (T> 1 K) the specific heat of both membranes are nearly superposed. This shows at T> 1 K, the specific heat is governed by volumetric effect.

Through these measurements, we can clearly say that from 6 K to almost 1 K the heat capacities are volume-dominated, then between 1 K and 0.7 K the transition from the volume-dominated to the surface-dominated occurs, and below 0.5 K the heat capacity is totally set by surfaces of the systems. The interesting point is that at this temperature (T=0.5 K) the phonon wavelength ($\lambda_{ph} = 337$ nm) is much bigger than the thickness of both membranes. At the temperature where $\lambda_{ph} > t$ (t the thickness of the membranes), it is possible that 2D confinement effect will be seen in the phonon heat capacity. This will be discussed in the next paragraph.

4.4.1 Data treatment

First of all, we should prove what has been measured is the heat capacity of SiN_x membrane and this value is not dominates by other materials (Cu or NbN) on the nanocalorime-

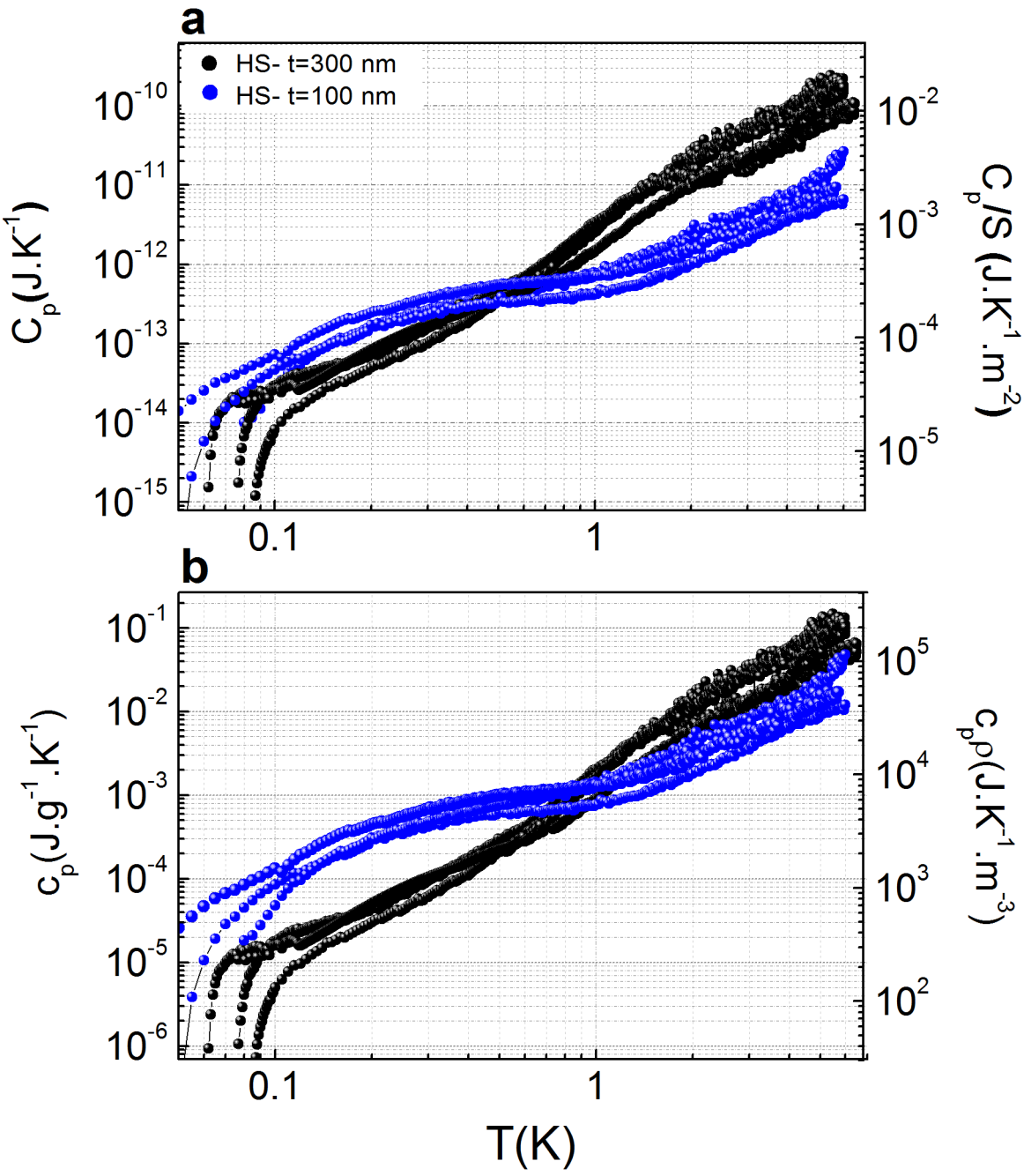

Figure 4.8: **Confinement effect on the heat capacity of high-stress Si_3N_4.** The heat capacity of 2D suspended membranes made of HS a-SiN versus temperature plotted in double Y axis. The blue dots are the measurements of several membranes with the thickness of 100 nm, and the black dots are that of 300 nm thickness. (**a**) The heat capacity plotted in log-log in J.K^{-1} (left axis), and J.K^{-1}.m^{-2} normalized to the surfaces of the membranes (right axis). (**b**) Left axis shows the specific heat J.g^{-1}.K^{-1} of both dimensions, and in the right axis the heat capacity is normalized to the volumes of the membranes J.K^{-1}.m^{-3}. ρ is the density of the the SiN_x membranes.

	ρ (g/cm^3)	V (cm^3)	m (g)	c_p (J/gK)	C_p (J/K)
Cu	9	1.6×10^{-11}	1.44×10^{-10}	10^{-5}	1.44×10^{-15}
NbN	5	1.6×10^{-11}	7.5×10^{-11}	2×10^{-4}	3×10^{-14}
SiN$_x$ (measured)	3.2	1.6×10^{-10}	4.8×10^{-10}	10^{-3}	10^{-12}

Table 4.1: The calculation of the heat capacity of the heater and the thermometer on the nanocalorimeter. The heat capacities and the specific heats are calculated for T=1 K.

ter. To do so, in Table. 4.1 a numerical calculation of the heat capacities of Cu and NbN are compared to that of SiN_x membrane at T=1 K. It can be seen that the contribution of the Cu and NbN in total heat capacity is negligible. In order to analyze the experimental results more precisely, two important aspects should be verified: the temperature dependence of the heat capacity, and comparison of the experimental data to the corresponding theoretical fits. If the heat capacity varies as $C_p \propto T^{p_c}$ (p_c is the temperature exponent of the heat capacity), the quantity of p_c can be calculated as:

$$p_c(T) = T\frac{\delta[lnC_p(T)]}{\delta T} \tag{4.18}$$

The temperature exponents of the heat capacity of the membranes with the thicknesses of 100 and 300 nm are presented in Fig. 4.9. The temperature exponent of the thick membrane (black dots) has almost a temperature dependence that varies between quadratic and cubic, and below 0.3 K it approaches to linear behavior. Meanwhile, the temperature exponent of the thinner membrane (blue dots) exhibits almost a quadratic dependence on temperature from 6 to 2 K. Then, the temperature exponent varies from quadratic to linear/sub-linear dependence at sub-Kelvin temperature.

The linear dependence of the specific heat in the thin membrane is in good qualitative agreement with the prediction of the elastic continuum theory on the specific heat of 2D membrane (see Fig. 4.1 **b**). But, in the terms of quantitative analysis, our measurements exhibit a value that differs for more than three orders of magnitude in comparison to what has been predicted by 2D Debye model and the elastic continuum theory (see Fig. 4.10 **a**). In Fig. 4.10 **b** the experimental specific heats (in J.g^{-1}.K^{-1}) are compared with theoretical models and the similar experiments performed by the other group [139]. The clear blue line is C_{ex}, the dashed green line is the specific heat of TLSs C_{TLS} and the red line is the total specific heat from equation 4.2. The green and the orange dots are the measurements of specific heat on a-SiN membranes with the thicknesses of 50 and 200 nm respectively, done by D. R. Queen and F. Hellman [139]. The triangle symbols show the specific heat of bulk vitreous silica taken from Zeller [61].

As one can see in Fig. 4.10 **a**, the order of magnitude of our measurements have surprisingly large value in comparison with the theoretical models (including the elastic continuum theory). Even when we compare to a typical bulk a-solids (a-SiO_2 for example) or the measurement on a-SiN membranes, it has more than two orders of magnitude of

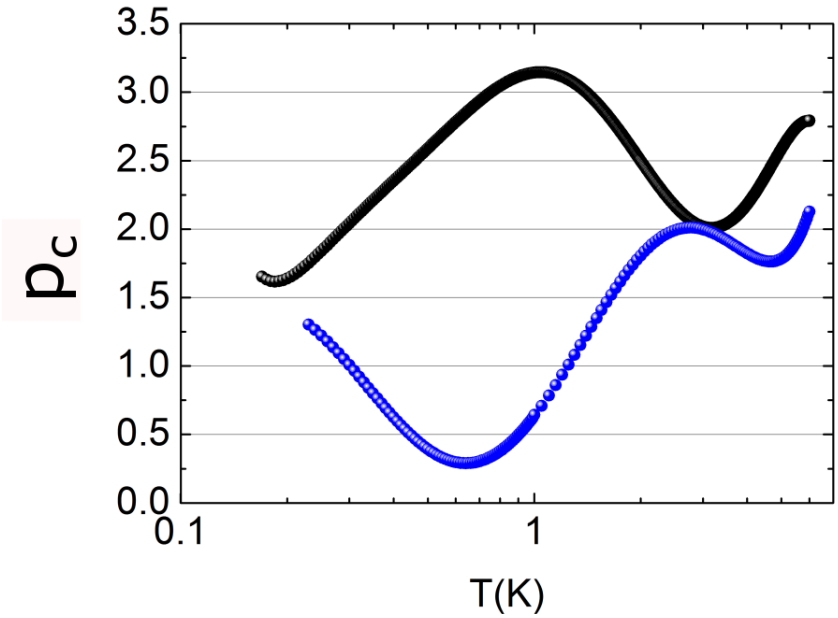

Figure 4.9: **The temperature exponent of the heat capacity.** The temperature exponent of the membranes with thicknesses of 300 nm (black dots) and 100 nm (blue dots) are presented. The black dots show that from 6 K to 0.3 K the temperature dependence of the heat capacity varies between quadratic and cubic variation, and at very low temperature it goes toward the linear behavior. The blue dots show that from 6 K to 2 K the heat capacity of thinner membrane is quasi-quadratic. However, below 2 K it drops to linear, even sub-linear behavior.

difference. This excess of specific heat can be attributed to low vibrational modes that exist in a-solids. For low temperatures $T < 1$ K, the specific heat is dominated by the standard tunneling model (TLS), and it exhibits a quasi-linear variation on temperature. At higher temperature, $T > 1$ K the localized soft modes in glasses that are described by the soft potential model (SPM) become dominant [169]. The contribution of localized soft modes in high temperature specific heat C_{ex} ($T > 1$ K) explains the deviation of specific heat from the standard tunneling model.

We have estimated that in our experiment the TLSs density of states in HS a-SiN is about $n_0 \cong 9 \times 10^{48}$ ($J^{-1}m^{-3}$) and the $C_{ex} \cong 5.3 \times 10^{-5}\ T^3$ ($J.g^{-1}.K^{-1}$). A feedback to the Fig.4.8 **a** and **b** with the transition from volumetric to surface effect, and high value of specific heat show that two fundamental features are happening:

- the emergence of surface effect on specific heat at sub-Kelvin temperature (confinement effect),
- the dominancy of the low vibrational modes in a-Si_3N_4 (TLS and localized soft modes) over all the temperature range of the measurement.

The coexistence of these two effects gives us a novel insight about restricted geometry

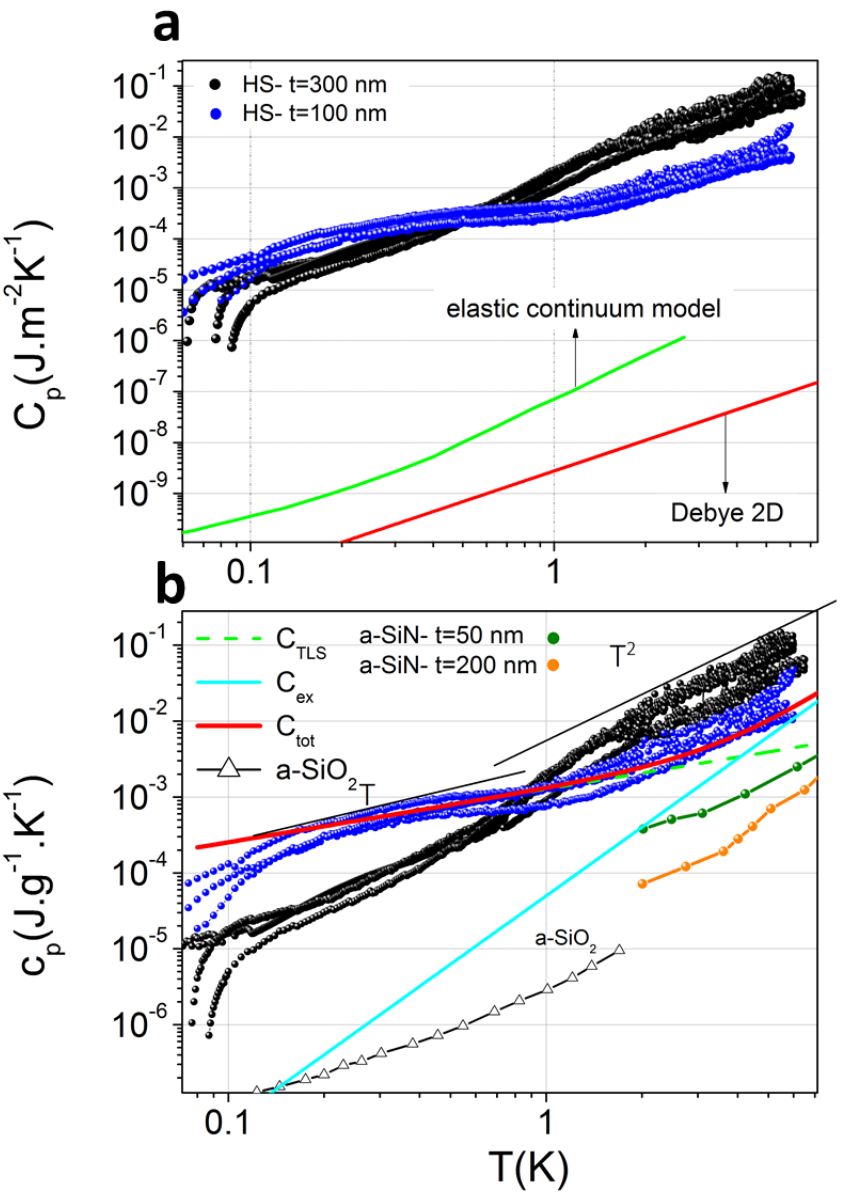

Figure 4.10: **The specific heat of thin membranes made of high-stress Si_3N_4.** (**a**) The heat capacity normalized by the surfaces of the membranes, in comparison to the predicted heat capacity for 2D phonon cavity. The green line is the prediction of elastic continuum theory, and the red line is 2D Debye model [170]. (**b**) The clear blue line is the excess of specific heat C_{ex} in the equation 4.2, the green dashed line is the specific heat of TLSs C_{TLS}, and the red line is the total estimated specific heat from equation 4.2 for a-solids. The green and orange dots are the specific heat of a-SiN with the thickness of 50 nm and 200 nm respectively measured by Queen *et al* [139]. The triangle symbols are the specific heat of a-SiO_2 taken from measurements of Zeller and Pohl [61].

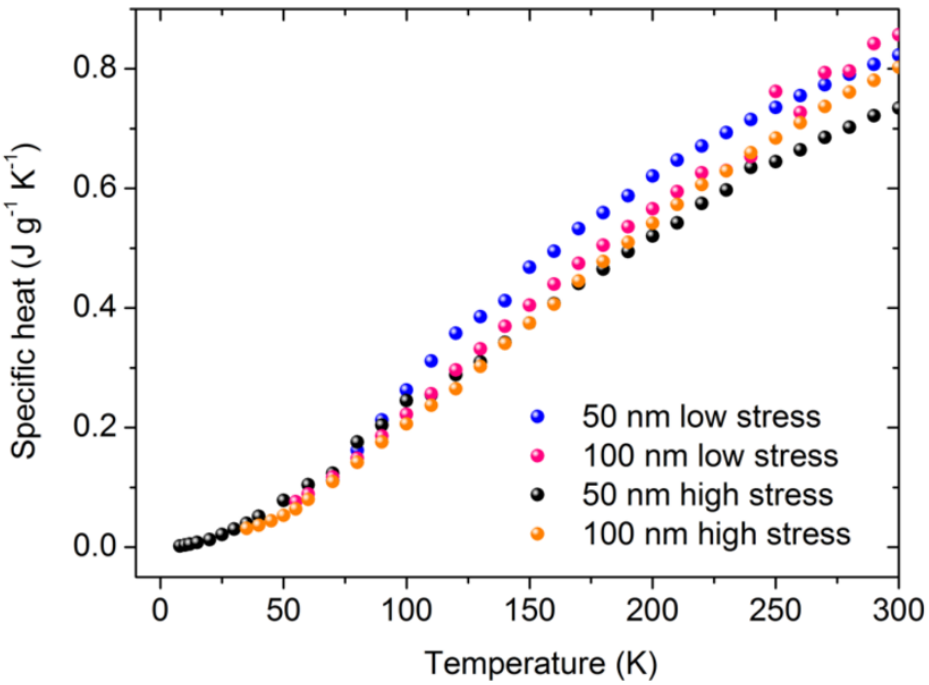

Figure 4.11: **High temperature dependence of specific heat on internal stress.** The specific heat measurements of 50 and 100 nm thick amorphous silicon nitride for LS and HS, from 10 K to room temperature [171].

made of a-solids. Indeed, the TLSs are not only distributed in the volume of the system, but could also have a high concentration on the surfaces of the system. In the next section we investigate the formation of TLSs based on internal stress.

4.5 Effect of stress on heat capacity

Understanding the effect of stress on the properties of a-solids can help us to unveil the microscopic nature of TLSs in disordered materials. Recently, the dependence of thermal properties on stress in a-silicon nitride was investigated by our group from 300 K down to 20 K [171]. The measurements of heat capacity on HS and LS silicon nitride with two different thicknesses (50 and 100 nm) showed that the thermal properties are not significantly affected by the presence of internal stress (see Fig. 4.11). This experimental study was in the limit where the heat capacity is still dominated by Debye phonons. Meanwhile, if the temperature is low enough (T$<$ 1 K), the low energy vibrational modes in a-solids will dominate the thermal properties [61]. So if these low vibrational modes depend on stress, with the change of internal stress, the thermal properties (in our case the heat capacity) should be affected. In a theoretical work by Wu and Yu [172] it was considered that the stress (bond constraints, impurities, local defaults, or even external strain) can

SiN_x	HS	LS	SLS
ρ (g/m^3)	3.2	2.9	2.4±0.2
n_0 (1/Jm^3)	9×10^{48}	2.2×10^{49}	2×10^{50}
stress (GPa)	0.85	0.2	<0.1
p_c	0.7	0.4	0.25

Table 4.2: Parameters for high-stress (HS), low-stress (LS), and super low-stress (SLS) SiN_x. ρ is the density of material, n_0 is the TLS density of states, and P_c is the temperature exponent of the measured heat capacity below 1 K.

modify either the TLS barrier height or the coupling between TLS and phonons. However, it has never been proved experimentally.

In order to understand the dependence of TLSs on the internal stress, we have measured the heat capacity of 2D suspended membranes made of high-stress (HS), low-stress (LS), and super low-stress (SLS) amorphous silicon nitride. The experimental measurements are shown in Fig. 4.12. The measurements show that all of the samples with different stresses exhibit almost the same power law as the function of temperature. At T> 1 K it is mostly a quadratic dependence of heat capacity on temperature, and at T< 1 K a sub-linear behavior appears. Moreover, by decreasing the stress, the heat capacity is increased up to even two orders of magnitude. These values are surprisingly high in comparison to what has been measured until now. We suppose that this high value of heat capacity is attributed to physics of TLSs and localized modes in a-SiN_x.

Through a phenomenological analysis (by adjusting the TLS density of states and the value of C_{ex} in order to get good fit of the experimental data with the equation 4.2), the SiN_x parameters are extracted and noted in Table. 4.2. In this Table, there are two interesting phenomena: the extracted TLS density of states from the measurement shows a factor of 20 between HS and SLS a-SiN_x. This noticeable difference shows that TLS distribution has a direct relation with the internal stress, and the internal stress is set by the preparation techniques as the TLS density of states. It has to be noticed that the sub-Kelvin temperature exponent is also stress dependent. By decreasing the stress, the temperature exponent decreases. Between HS and SLS there is more than a factor of two in p_c. This sub-linear behavior has never been reported in a-solids, and its physical nature is not yet clear. In order to understand the source of the high value of heat capacity in a SiN membranes, one needs to analyze the structural details of silicon nitride.

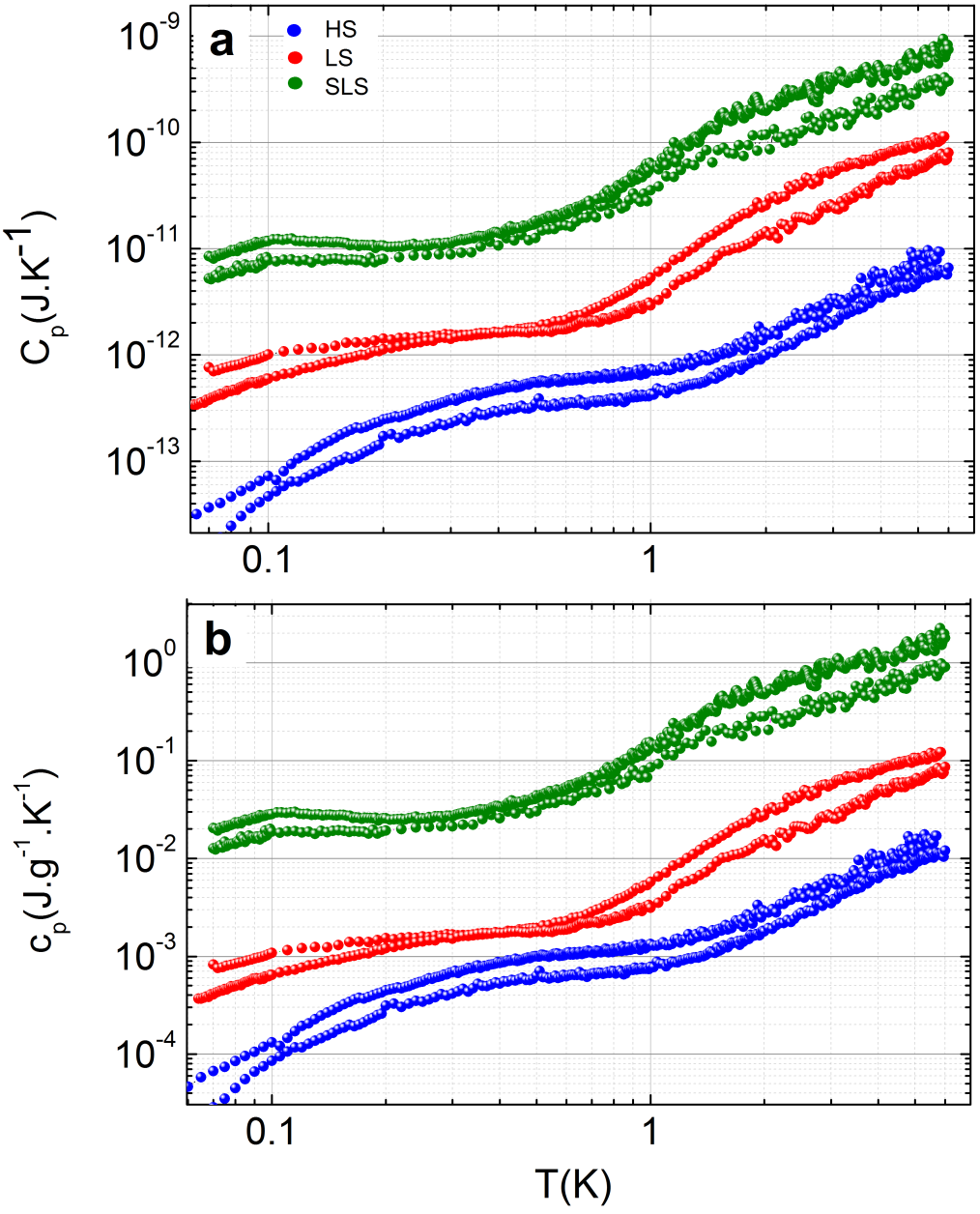

Figure 4.12: **The dependence of heat capacity on the internal stress of a-SiN$_x$.** The samples have the same geometry with a thickness of 100 nm. The blue, red and green dots are respectively the heat capacity of HS, LS and SLS a-SiN$_x$. (**a**) The heat capacity plotted in J.K^{-1}, and (**b**) is the specific heat J.g^{-1}.K^{-1}.

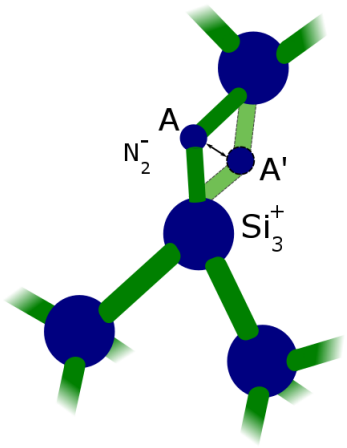

Figure 4.13: **Silicon nitride structure analysis.** In SiN_x atomic structure, the nitrogen atoms can have two potential minima A and A'. The tunneling motion between these two potentials could form the TLS.

4.6 Tunneling states in tetrahedrally bonded materials

According to Phillips, the formation of TLS is possible in materials having open structure with low coordination sites, and in tetrahedrally bonded materials like a-SiN_x, a-Si or a-Ge TLS should not occur [64]. There are conflicting results reporting the TLSs in these systems are the same as those found in other glasses [74, 164]. Indeed, TLS density of states in tetrahedrally bonded materials depends strongly on preparation techniques (temperature of growth) [72, 74, 75]. This dependence is due to the fact that TLSs occur in microstructural detail of the material such as nanovoids. These nanovoids or structural inhomogenities are created in low density regions, and the formation of these regions is directly related to preparation techniques.

By decreasing the stress, these low density regions increase, and consequently it give rise to more tunneling states (TLS). This could be the reason that HS SiN_x with a denser structure has a density of TLS more than one order of magnitude lower than that of SLS SiN_x. Thus indirectly, the density of TLS is related to the atomic density of the material [72, 77].

A mechanism that can be responsible for the high value of heat capacity in SiN_x can be originated from the possible local atomic motion in SiN_x. In the analysis of ac transport in a-SiN_x at low temeprature by Shimakawa and coworker, it was suggested that the nitrogen atoms in SiN_x structure could be stabilized in two potential minima (shown as A and A' in Fig. 4.13). According to their analysis, the local atomic motion of twofold coordinated N_2^- bonds is likely to be responsible for the TLS [173, 174]. If each nitrogen

atom contributes in formation of TLS, it can give rise to very high TLS density of states in systems made of SiN_x.

We can conclude that the stress along with the different fabrication processes may strongly impact the presence and the density of TLS. Then the significant difference in the heat capacity of HS, LS, and SLS could find its origin in varying TLS density of state as a function of stress. It should be mentioned that all these interpretations remain controversial, and a deep theoretical development using the concept of localized excitations in a-solids as a function of stress and confinement is needed.

4.7 Conclusion

This chapter was focused on the measurement of the heat capacity of 2D suspended phonon cavity at very low temperature. ac calorimetry is the technique used for the measurement of low temperature heat capacity. The sensitivity at which the measurements have been achieved is about $\Delta E = 2.3 \times 10^{-20}$J. All of the samples are microfabricated from various kinds of amorphous SiN_x: high-stress (HS), low-stress (LS), and super low-stress (SLS).

Two important aspects have been investigated within our measurements: the effect of confinement and the effect of internal stress on the heat capacity. The consequences of confinement have been investigated by measuring the heat capacity of membranes made of HS a-SiN_x with two different thicknesses (100 nm and 300 nm). The measurements show that at $T > 1$ K, the heat capacity is governed by volumetric effect of system, while at $T < 1$ K, the surfaces will set the value of heat capacity. Indeed, the surface becomes the predominant factor when the phonon wavelength exceeds the thickness of both systems.

The quantitative comparison of our experimental measurements with theoretical models shows that the dominant physical feature in what we have measured may be due to the low vibrational modes that exist in a-solids. Indeed, we believe that the transition from volumetric to surface effect that appears in our measurements is not because of the formation of a new set of phonon modes, and new dispersion relation (as explained by elastic continuum theory). But, in fact it could be related to the high concentration of localized modes such as TLSs and soft potentials modes on the surfaces of the membrane.

Concerning the effect of stress, the heat capacity of membranes with the same configuration but different internal stresses (high-stress HS, low-stress LS and super low-stress SLS) at low temperature have been measured. The measurements show a strong dependence of heat capacity on the internal stress with surprisingly large value. In this case, we also assume that the absolute value of heat capacity could be affected by low energy vibrational modes (TLSs) that exist in a-solids at low temperature. It was shown that the TLSs density of state between HS and SLS systems varies nearly by a factor of twenty.

This observation can be a robust signature that in tetrahedrally bonded material such as SiN_x, the TLSs parameters depend strongly on the preparation techniques. It can be also concluded that the formation of TLSs in a-solids may have a noticeable concentration on the surfaces as well as the volume of the material. These measurements are the very first observations on the effect of confinement and internal stress in a-SiN, and a deeper theoretical works are needed to confirm these observations.

5 CHAPTER

Thermal rectification

5.1 Introduction

Until now all the experimental achievements and the scientific prospections were in the aim of probing the fundamental thermal properties within nanoscale systems. But in this chapter of thesis, we will focus on the possible application of thermal management by ballistic phonons.

While electronics has been able to control the flow of charges in solid state devices for many years, the control of heat flow still seems out of reach. The objective of controlling heat flow has become one the most interesting topic in field of nanophononics, and it can be a promising step forward to the futural practical application. For instance, a thermal diode by controllability of the heat current can be applied as thermal transistor [108], thermal logic gates [175], and thermal memory [176]. The concept of the thermal diode is similar to electronic one; a device that lets heat flow more easily in one way than in the other.

One of the simplest and effective idea to build a solid-state thermal diode was proposed by Peyrard [177] which is based on two-segment systems. It requires to connect two nonidentical materials with thermal conductivities $\kappa_A(\mathrm{T})$ and $\kappa_B(\mathrm{T})$ that varies very differently as a function of temperature. Indeed, in this method the choice of materials is the key point. The materials should have opposite behaviors in their thermal conductivities. The thermal conductivity of first material $\kappa_A(\mathrm{T})$ should decrease around some temperature T_c, while κ_B rises significantly around the same temperature. The experimental point of view of this idea has been investigated by Kobayashi *et al.* [178] in bonded perovskite cobalt oxides $LaCoO_3$ and $La_{0.7}Sr_{0.3}CoO_3$. The dependence of thermal conductivity of each material on temperature and a schematic figure of their device are presented in Fig. 5.1 (**a**) and (**b**).

The two-segment systems works verly well in bulk materials at high temperature

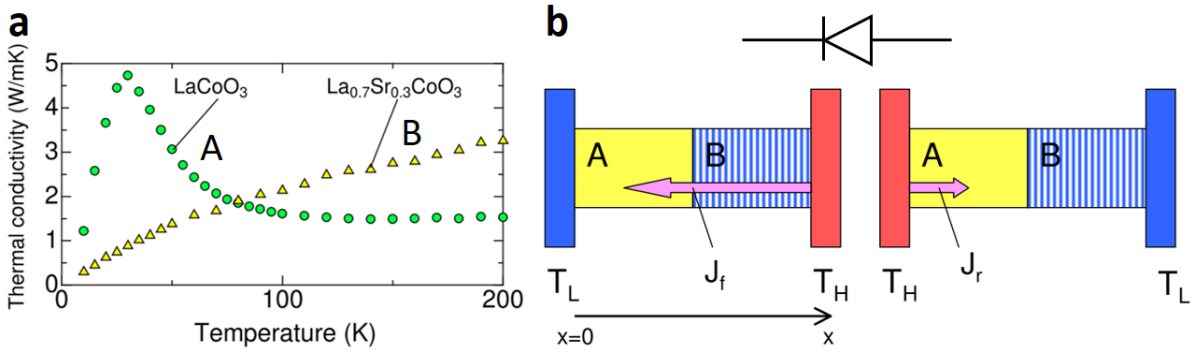

Figure 5.1: **Two-segment thermal diode.** (**a**) The temperature dependence of the thermal conductivity $LaCoO_3$ and $La_{0.7}Sr_{0.3}CoO_3$ used by by Kobayashi *et al.* [178]. (**b**) conceptual diagrams of the thermal rectification in bonded materials for two-segment thermal diode.

gradient leading to a large rectifying coefficient ($R = (|J_+|/|J_-|)$ of 1.43. However, for nanoscale systems with very small temperature gradient, thermal rectification can be achieved differently. In this work, among various possible nanoscale thermal rectification mechanisms, we focus on two approaches: thermal rectification by (**1**) asymmetric mass gradient, and (**2**) asymmetric nanostructured geometry.

5.2 Thermal rectification by asymmetric mass gradient

The thermal rectification in one dimensional anharmonic lattices with a mass gradient has been investigated theoretically by Yang *et al.* [179]. According to their calculations, the thermal conductivity diverges with the system size linearly, $\kappa \propto L$. In asymmetric mass anharmonic lattices, the thermal conductivity diverges with system size as $\kappa \propto L^{\alpha}$ (α is a phenomenological parameter that seems to be independent of temperature and boundary conditions) [179]. The context of thermal rectification by asymmetric mass gradient has been verified experimentally by Chang *et al.* [105]. In their experiments boron nitride nanotubes (BNNTs) and carbon nanotube (CNTs) were inhomogeneously mass loaded by macromolecules of $C_6H_{16}Pt$. In Fig. 5.2 the sample used by Chang *et al.* and their measurement are presented. The thermal rectification ratios, *i.e.*, $(J_+ - J_-)/J_-$ were measured 2% for CNTs and 7% for BNNTs. These values are very small and have to be taken with precaution. The difference of thermal rectification ratio between BNNTs and CNTs is because electrons do not contribute to the thermal transport for BNNTs, and the observed rectification effects can be attributed to phonons. This means that in systems made of semiconductors or insulating materials, where the heat transport is dominated by phonons, the rectification effect may be more effective.

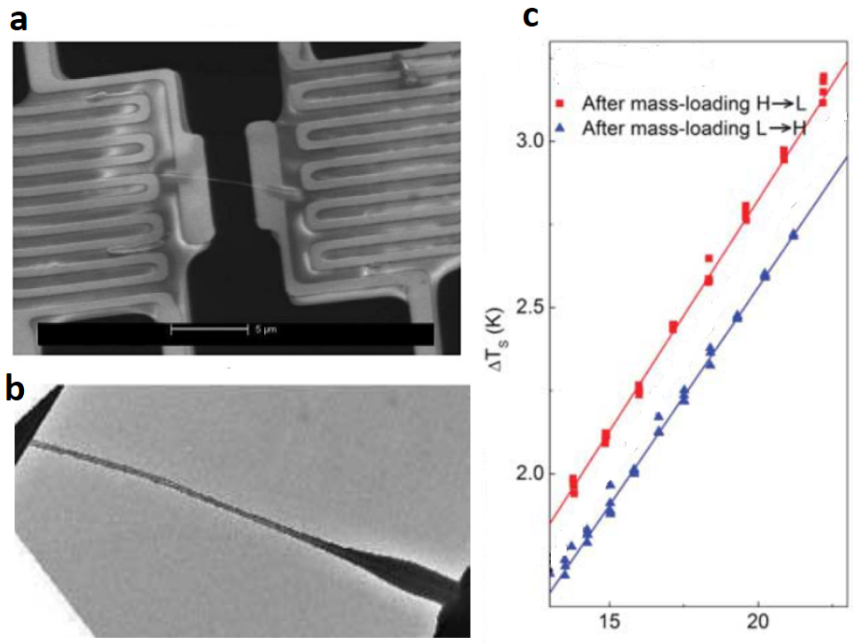

Figure 5.2: **Solids state thermal rectifier.** (**a**) SEM image of the device used by Chang *et al.* [105] as Solid-State Thermal Rectifier. It contains two suspended membranes, one acts as heating membrane and other as sensing membrane; the nanowire is placed between the two membranes. (**b**) A zoom on the carbon nanotubes with inhomogeneously mass loaded by macromolecules of $C_6H_{16}Pt$. (**c**) The temperature changes of the sensor membrane (ΔT_s), and the heater membrane (ΔT_s) after deposition of $C_6H_{16}Pt$.

5.2.1 Experimental achievement

In the perspective of developing an efficient thermal rectifier based on asymmetric mass gradient, in collaboration with G. Benenti, D. Donadio and G. Casati, we have developed a new experiment. The principle idea is to connect two non-linear systems with different masses and coupled to different on-site potentials by a ballistic thermal conductor (see Fig. 5.3 **a**). The ballistic channel can be described by the Landauer formalism. The ballistic aspect of the channel removes the size dependence of the rectification factor, leading to higher rectification. In order to obtain a gradient of mass along the nanowire, we decided to deposit Pt/C by FIB (50% platinum and 50% carbon with the density of $\rho = 11.5\ g/m^3$). The deposited masses have square shapes with different sizes. The actual sample is shown in Fig. 5.3 **b** and **c**. The sizes of the deposited Pt/C increase from left reservoir to the right one. The dimensions and the masses of deposited materials are presented in Table. 5.1. The mass gradient between the two reservoirs is about $\Delta m = 0.48$ pg.

In chapter 3 the symmetric aspect of heat transport in a simple nanowire was verified by reversing the heat flow (see Fig.3.2), and the heat transport in both direction was equal.

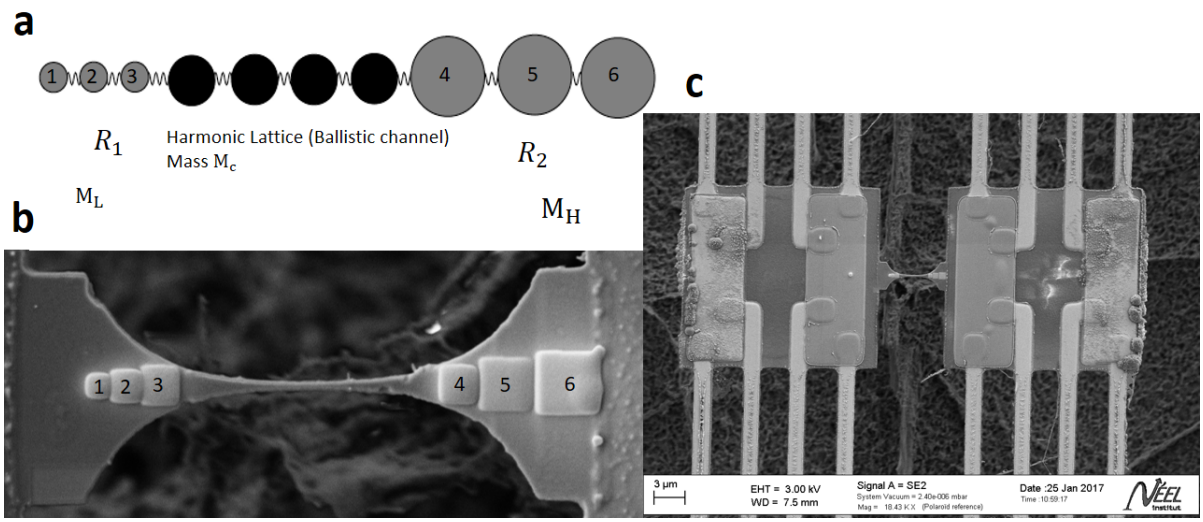

Figure 5.3: **Asymmetric mass gradient nanowire.** (**a**) Schematic plot of the statistical model, in which two diffusive R_1 and R_2 reservoirs are coupled by a harmonic ballistic channel. (**b**) SEM image of the elaborated nanowire with asymmetric mass segments loaded. (**c**) The SEM image of sample with two suspended membrane-based nanocalorimeters, and the nanowire with asymmetric mass is placed between the membranes.

	1	2	3	4	5	6
S(nm^2)	270× 270	350 ×330	400× 400	385× 400	550× 550	680× 680
m(pg)	0.07	0.1	0.15	0.14	0.27	0.4

Table 5.1: The dimensions and the masses of deposited material on each side of nanowire. The thickness of deposition is estimated $t = 70 \pm 30$ nm.

Now, on the same nanowire the asymmetric mass (Pt) was loaded to verify whether the thermal rectification occurs or not. The idea is that the asymmetric mass-loaded will cause phonon interacts differently with each reservoirs. We expect to measure a higher value of thermal conductance when the heat flow comes from the reservoirs with higher deposited mass (right reservoir in Fig. 5.3 **b**), than the opposite. The experimental data is shown in Fig. 5.4. Surprisingly, there is no signature of thermal rectification in our measurement, and the measurements on each direction of heat flow are perfectly superposed.

In a theoretical work done by Hopkins *at al.* [180], the thermal rectification in asymmetric harmonic 1D chain using nonequilibrium Green's function formalism was studied. According to their investigation, the rectification is extremely sensitive to impurity position with a large asymmetry in the mass loading. The possibility to imply the thermal rectification by asymmetric mass gradient in ballistic regime is still an open question. Maybe in our case the asymmetric aspect of mass gradient was simply not enough, or the mass gradient should be basically implanted in the reservoirs rather than to be deposited

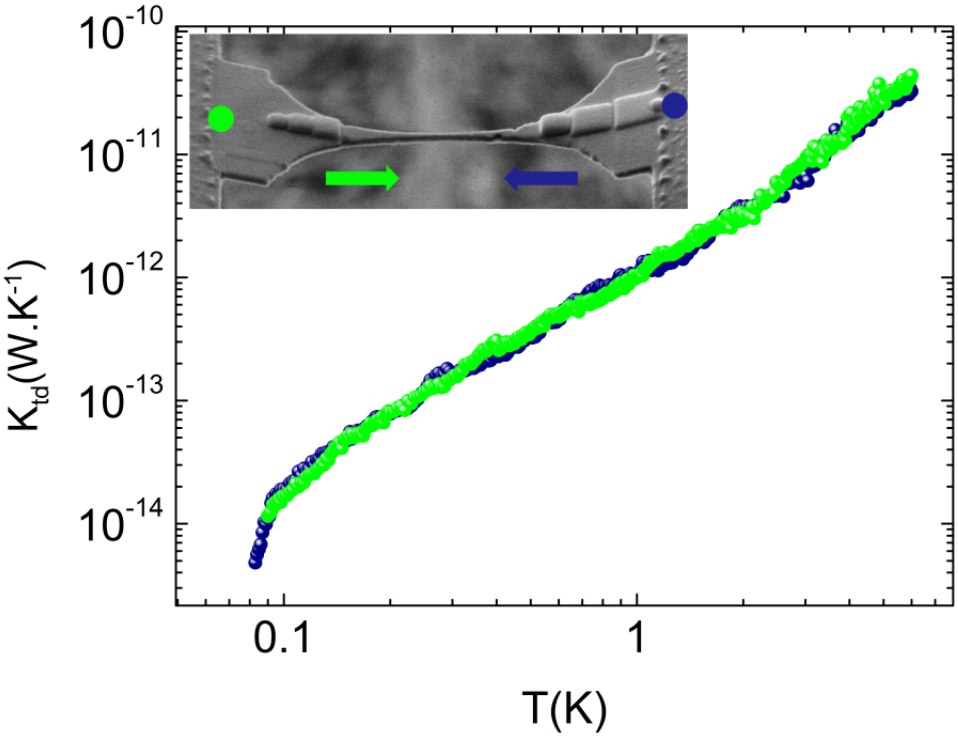

Figure 5.4: **Thermal conductance of asymmetric mass gradient nanowire.** The thermal conductance measurement of 1D channel by asymmetric mass gradient on each reservoir. The green and blue dots show two different heating directions. No thermal rectification was observed and the thermal conductance of both direction are superposed. The inset shows the nanowire of the experiment with deposited mass on each reservoir.

on the top of them. Another possible reason of not seeing rectification is that maybe our range of experiment is within a limit that is too ballistic, and to observe this kind of rectification the regime of heat transport should be mostly oriented in the intermediate regime between ballistic and diffusive regime of heat transport (Ziman regime).

The context of building a thermal rectification device in ballistic regime of phonon transport gives the ability to use purely geometrical effect and not specially intrinsic properties of the material. In the next section thermal rectification by ballistic phonons in asymmetric nanostructures is discussed.

5.3 Thermal rectification by asymmetric nanostructured geometry

The principle concept of asymmetric geometrical shape can, in principle, introduce asymmetric boundary scattering of phonons, where the thermal conductance would be controlled by the design of the structures. In a theoretical work, the effect of surface roughness on phonon transport in a nanowire was investigated by Monte Carlo simulations. It was found that sawtooth roughness on a nanowire can cause phonon backscattering and suppress the thermal conductivity below the diffuse surface limit. This fact was also proved experimentally [100, 181]. Miller *et al.* have investigated in a theoretical work the thermal rectification in devices with nanostructured asymmetric inclusions and voids. A rectification ratio of 43% was calculated for voids in the form of pyramid. Recently, in an experimental work by Anufriev *et al.* [182], on phononic crystals with asymmetric design, the controllability of ballistic phonon transport using Si membranes with arrays of holes, or thermal lens (see Fig. 5.5 **a**) nanostructures have been investigated. Other geometries with potential rectification effect proposed by Miller *et al.* [107] are shown in Fig 5.5 **b** and **c**. In the aim of building a thermal diode, asymmetric sawtooth nanowires have been elaborated by our group (Fig 5.5 **d**). The effect of directional roughness in this kind of geometry has been numerically calculated by ray tracing analysis. The thermal rectification ratio is calculated for two heating direction (from part 1 in Fig. 5.5 (**d**) to the part 2, and the reverse). It was found when the heat is generated from 1→2 the thermal rectification ratio is 83%, while in the reserve case (2→ 1) it is 73%. The heat transport is optimized from 2 to 1. In addition of directional sawtooth nanowire, the fabrication process of various asymmetric engineered phononic crystals is in progress, and all these asymmetric engineered structures will be placed between the two suspended membranes.

In order to go further in such geometries, a primary experimental achievement at low temperature needs to be done, and based on the observation the design of the geometries, the temperature range of experiment, and other potential way of thermal rectification can be improved.

5.4 Conclusion

This chapter is dedicated on a tentative experimental realization of thermal rectification. Thermal rectification by asymmetric mass gradient in one dimensional channel in ballistic limit of phonon conduction has been investigated. No thermal rectification was observed. We believe in order to see rectification effect, the phonon transport should be within Ziman regime (with both elastic and diffusive scattering). This measurement is our primarily experienced on nano-engineered systems, and it need to be explored in more details. In addition, the fabrication of various asymmetric structures with potential possibility of thermal rectification are in progress. The art of thermal management by design of the

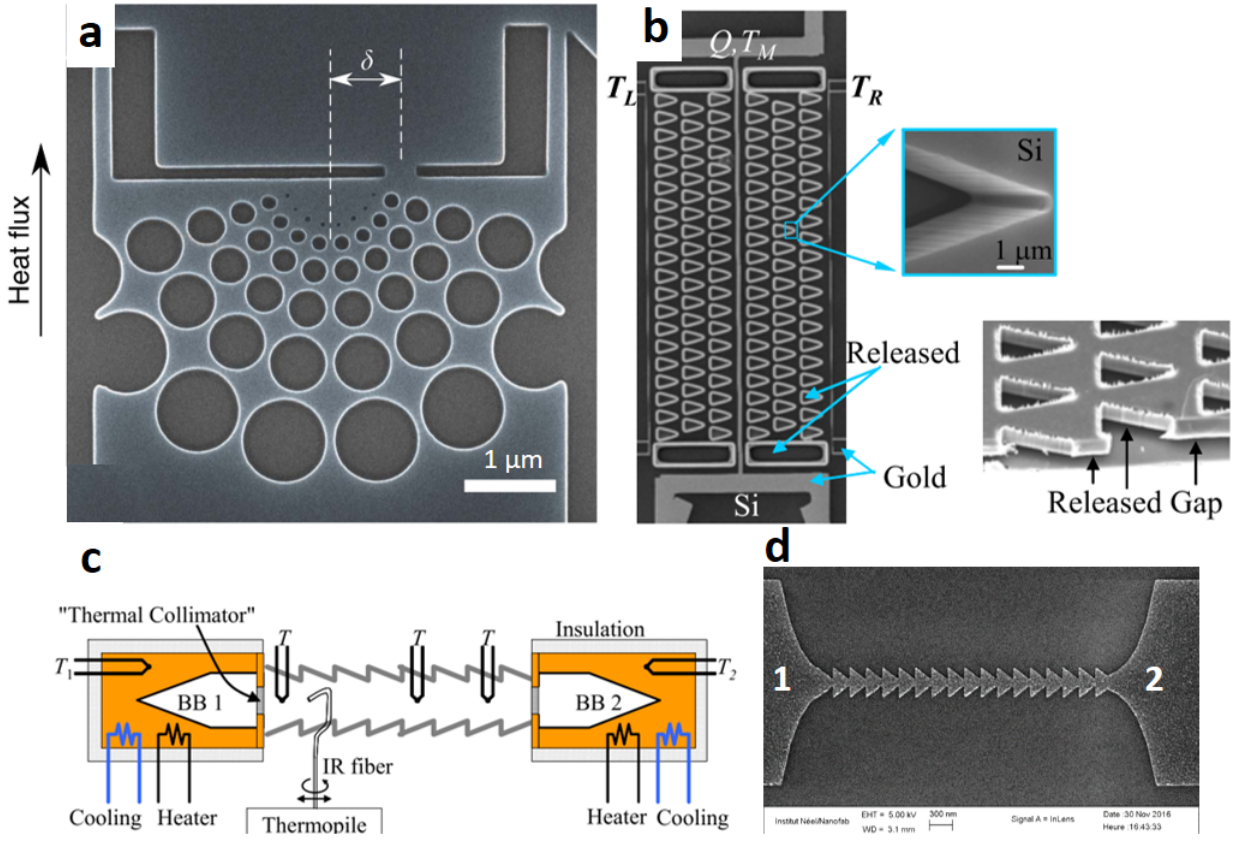

Figure 5.5: **Thermal management by engineered nanostructures.** (**a**) SEM image of converging thermal lens [182]. (**b**) Rectification of phonons by asymmetric microfabricated pores. (**c**) Asymmetric sawtooth nanowire between two blackbodies along a thermal rectification test section with [107]. (**d**) Asymmetric sawtooth nanowire elaborated by our group as thermal diode (the fabrication in progress).

structures can be notable step forward into the future applications.

Conclusion

The work of this PhD has been dedicated to qualitative and quantitative experimental realizations of the thermal properties measurements of confined structures in the quantum limit (very low temperature). Two principle configurations have been studied: the phonon transport in 1D quantum channel, and the specific heat of 2D suspended phonon cavities. To do such experimental investigations multiple steps have been realized: fabrication of the systems geometrically adapted to the thermal properties measurement at low temperature range, and measurement via high sensitive electronic setup.

All of the samples are made of amorphous silicon nitride elaborated with suspended structures. For the measurement of specific heat of 2D phonon cavity, the sample is a membrane-based suspended nanocalorimeter with supporting beams. For the measurement of the thermal conductance of a 1D channel, the platform of the measurement is composed of double suspended membrane-based nanocalorimeters with nanowires connecting the two membranes. The thickness of membrane-based nanocalorimeter, and the size of the section of the nanowires have been chosen purposely to be below the phonon characteristic length scales in the temperature range of the experiment.

The measurement chain used during this thesis contains very low noise electronics devices like pre-amplifiers, lock-in amplifiers, LC01 current sources, and LP electronic filters. Moreover, the niobium nitride sensor that is used on the samples is purposefully designed to have the highest sensitivity at low temperature. Low noise technical facilities, and highly sensitive NbN sensor give a voltage noise of 0.7 $\mathrm{nV}/\sqrt{\mathrm{HZ}}$ which is dominated by pre-amplifier noise. The power sensitivity in the measurement of thermal conductance is in the order of several attoWatt (10^{-18} W), and the energy sensitivity in heat capacity measurement is down to zeptoJoule (10^{-20} J). Thanks to low noise measurement techniques qualitative measurements with unprecedented sensitivities at the lowest temperature are achieved.

The measurements of the thermal conductance of 1D channel reveals several fundamental physical features. Through these measurements, ballistic phonon transport is successfully proved by two different ways. First, the calculation of the phonon mean free path extracted from experimental data shows that at very low temperature the phonon conduction enters into the quantum limit. The transition into this limit occurs when the phonon wavelength becomes much bigger than the section of the nanowire (1D limit) and the phonon mean free path becomes bigger than the length of the channel (ballistic limit). Second, in another experimental attempt the thermal conductance of nanowires

with exactly the same shape of the reservoirs but different lengths have been measured and compared. The results shows that the thermal conductances of the three different lengths (3, 5, and 7 μm) are mostly superposed over all the temperature range. This superposition confirms the ballistic aspect of heat conduction.

The thermal conductance measured at very low temperature departs significantly from the expected universal value of quantum of thermal conductance. Analysing this experimental data within the framework of the Landauer formalism shows that our measurements exhibit very low transmission coefficient. Somehow, the intrinsic quantum value of thermal conductance of the 1D channel has to be seen as in series with some thermal resistances. The possible source of these thermal resistances are identified as: non-perfect coupling between 1D channel and 2D reservoirs, the shape of the junctions between nanowire and the reservoirs, and the nature of the material in use. Over all the temperature range, the thermal conductance exhibits a quadratic behavior as function of temperature. We believe that the high concentration of two-level systems (TLS) (which are the unique characteristics of amorphous solids at very low temperature) on the surfaces of the reservoirs might be the major reason of low transmission rate. This fact was also investigated by heat capacity measurements.

The heat capacity measurement of 2D phonon cavities unveils the effect of spatial confinement, and internal stress on low temperature heat capacity. The measurement of heat capacity on membranes having two thicknesses (100 and 300 nm) but the same surfaces, shows a clear transition in behavior of the specific heat from volumetric-dominated to surface-dominated. It is shown that below 1 K the heat capacity of both geometries is mostly superposed. The superposition occurs within the temperature range where the phonon dominant wavelength becomes bigger than the thickness of the membranes (2D limit).

There exist two theoretical predictions for specific heat of 2D limit: the lattice dynamical theory, or the elastic continuum model. The lattice theory predicts that at low temperature the specific heat should be proportional to T^d (d is the dimension of the system). So in a 2D membrane it is expected to see a quadratic behavior of specific heat as a function of temperature. On the other hand, the elastic continuum model describes the 2D heat capacity as contribution of new vibrational modes created by boundaries (dilatational waves DW, flexural waves FW, and shear waves SW). These new modes have different dispersion relations, consequently different contribution to the absolute value of specific heat. According to the model, the quadratic dispersion proper to FW modes overwhelms the heat capacity of 2D phonon cavities leading to a linear dependence on temperature below 1 K. The prediction of linear behavior of specific heat is in good agreement with our experimental results. If we compare the absolute value of specific heat predicted with elastic continuum model and our results, there is more than two orders of magnitude difference.

In order to have a better understanding of this high value of specific heat an experiment has been carried out measuring the heat capacity of membranes made of high-stress (HS),

low-stress (LS), and super low-stress (SLS) amorphous SiN_x. The results show that the heat capacity of the membranes highly depend on internal stress. The measured heat capacities are inversely dependent on the stress; decreasing the stress by a factor of eight has caused an increase of specific heat more than two orders of magnitude. We believe this noticeable excess of heat capacity is attributed to the TLSs. With a conceptual analysis it can be said that the formation of TLSs in amorphous structures depends strongly on the preparation techniques, and their notable concentration on the surfaces dominates the thermal properties of confined systems.

The last part of this work was dedicated to the potential applications of nanoscale devices in the objective of thermal management. Thermal conductance measurements have been performed on a nanowire fractionalized with a gradient of mass. This gradient of mass is expected to create a dissymmetric thermal transport; but no rectification was observed. We can say that in order to observe rectification effects in such system, the regime of heat transport should be in the intermediate regime of phonon conduction, where the phonons are partly diffusively scattered and partly ballistic.

As a perspective of this work, the fabrication of asymmetric geometries are in progress in the aim of thermal rectification in ballistic regime. Since ballistic limit is more sensitive to the geometry of the system, controllability of heat transport in this limit by engineered structure will be more feasible. In a futuristic point of view, the intention of thermal management within intrinsic properties of material and nano-engineered structures can be real step forward in fabrication of thermal diode, thermal transistor or thermal memory. These potential devices can bring the technology into the point that heat dissipation is no more a wasted energy. In contrast, it becomes a facility to improve the performance of computer processors, or any kind of electronic devices which generates heat.

Bibliography

[1] O. Bourgeois, D. Tainoff, A. Tavakoli, Y. Liu, C. Blanc, M. Boukhari, A. Barski, and E. Hadji. Reduction of phonon mean free path: From low-temperature physics to room temperature applications in thermoelectricity. *Comptes Rendus Physique*, 1:1–7, 2016.

[2] N.W Ashcroft and N. D Mermin. *Solids State physics*. Harcourt Brace College Publishers, 1976.

[3] G.P SRIVASTAVA. *The Physics of Phonons*. Springer, 1990.

[4] S Fisher Timothy. *Thermal energy at the nanoscale*, volume 3. World scientific, 1969.

[5] Sebastian Vloz. *Thermal Nanosystems and Nanomaterials*. Springer, 2009.

[6] L. Shinde Subhash and P. Sirivastava Gyaneshwar. *Length-Scale Dependent Phonon Interactions*, volume 128. Springer, Topics in Applied Physics, 2014.

[7] A. Khitun, A. Balandin, and K.L. Wang. Modification of the lattice thermal conductivity in silicon quantum wires due to spatial confinement of acoustic phonons. *Superlattices and Microstructures*, 26:181–193, 1999.

[8] D. Li, Y. Wu, P. Kim, L. Shi, Pe. Yang, and A. Majumdar. Thermal conductivity of individual silicon nanowires. *Applied Physics Letters*, 83:2934–2936, 2003.

[9] H. B. G Casimir. Note on the conduction of heat in crystals. *Physica*, 5:595, March 1939.

[10] W. Fon, K. C. Schwab, J. M. Worlock, and M. L. Roukes. Phonon scattering mechanisms in suspended nanostructures from 4 to 40 K. *Physical Review B*, 66:045302, 2002.

[11] J. S. Heron, T. Fournier, N. Mingo, and O. Bourgeois. Mesoscopic size effects on the thermal conductance of silicon nanowire. *Nano Letters*, 9:1861–1865, 2009.

[12] J.M. Ziman. *Electrons and Phonons*. CLARENDON PRESS. OXFORD, 1960.

[13] K. Rostem, D. J. Goldie, S. Withington, D. M. Glowacka, V. N. Tsaneva, and M. D. Audley. On-chip characterization of low-noise microstrip-coupled transition edge sensors. *Journal of Applied Physics*, 105:1–9, 2009.

[14] J. Carrete, L. J. Gallego, L. M. Varela, and N. Mingo. Surface roughness and thermal conductivity of semiconductor nanowires: Going below the Casimir limit. *Physical Review B*, 84:1–4, 2011.

[15] T. S. Tighe, J. M. Worlock, and M. L. Roukes. Direct thermal conductance measurements on suspended monocrystalline nanostructures. *Applied Physics Letters*, 70(20):2687–2689, 1997.

[16] K. Rostem, D. T. Chuss, F. A. Colazo, E. J. Crowe, K. L. Denis, N. P. Lourie, S. H. Moseley, T. R. Stevenson, and E. J. Wollack. Precision control of thermal transport in cryogenic single-crystal silicon devices. *Journal of Applied Physics*, 115:0–10, 2014.

[17] L. G. C. Rego and G. Kirczenow. Quantized Thermal Conductance of Dielectric Quantum Wires. *Physical Review Letters*, 81:232, 1998.

[18] N. Nishiguchi, Y. Ando, and M. N. Wybourne. Acoustic phonon modes of rectangular quantum wires. *Journal of Physics*, 9:5751–5764, 1999.

[19] D. V. Anghel. Universality of heat and entropy transport in 1D channels at arbitrary temperatures. *Europhysics Letters*, 94(6):60004, 2011.

[20] M. P. Blencowe and V. Vitelli. Universal quantum limits on single-channel information, entropy, and heat flow. *Physical Review A*, 62(5):052104–052101, 2000.

[21] J. B. Pendry. Quantum limits to the flow of information and entropy. *Journal of Physics A: Mathematical and General*, 16:2161–2171, 1983.

[22] C. L. Kane and Matthew P. a. Fisher. Quantized Thermal Transport in the Fractional Quantum Hall Effect. *Physical Review B*, 55:6, 1996.

[23] I. V. Krive, E. N. Bogachek, A. G. Scherbakov, and U. Landman. Heat current fluctuations in quantum wires. *Physical Review B*, 64(23):233304, 2001.

[24] I.V. Krive and E.R. Mucciolo. Transport properties of quasiparticles with fractional exclusion statistics. *Physical Review B*, 60(3):1429–1432, 1999.

[25] J. Ordonez-Miranda, L. Tranchant, B. Kim, Y. Chalopin, T. Antoni, and S. Volz. Quantized thermal conductance of nanowires at room temperature due to Zenneck surface-phonon polaritons. *Physical Review Letters*, 112(5):1–5, 2014.

[26] M. Käso and U. Wulf. Quantized thermal conductance via phononic heat transport in nanoscale devices at low temperatures. *Physical Review B*, 89:134309, 2014.

[27] X. F. Peng, K. Q. Chen, Q. Wan, Z., and W. Duan. Quantized thermal conductance at low temperatures in quantum wire with catenoidal contacts. *Physical Review B*, 81:1–6, 2010.

[28] F. Vázquez, F. Márkus, and K. Gambár. Quantized heat transport in small systems: A phenomenological approach. *Physical Review E*, 79(3):1–7, 2009.

[29] Y. Zhang, Z. X. Xie, X. Yu, H. B. Wang, and K. M. Li. Ballistic thermal transport in a cylindrical semiconductor nanowire modulated with bridge contacts. *Journal of Applied Physics*, 116:144304, 2014.

[30] W. Wang and X. X. Yi. Quantized phononic thermal conductance for one-dimensional ballistic transport. *Chinese Journal of Physics*, 41:92–100, 2003.

[31] O. Chiatti, J. T. Nicholls, Y. Y. Proskuryakov, N. Lumpkin, I. Farrer, and D. A. Ritchie. Quantum thermal conductance of electrons in a one-dimensional wire. *Physical Review Letters*, 97(5):11–14, 2006.

[32] S. Jezouin, F. D. Parmentier, A. Anthore, A. Gennser, Y. Cavanna, and F. Pierre. Quantum limit of heat ïňĆow across a single electronic channel. *Science*, 342:601–604, 2013.

[33] N. Mosso, U. Drechsler, F. Menges, P. Nirmalraj, S. Karg, H. Riel, and G Gotsmann. Heat transport through atomic contact. *Nature Nanotech*, 12:430–433, 2017.

[34] M. Meschke, W. Guichard, and J. P. Pekola. Single-mode heat conduction by photons. *Nature*, 444:187–190, 2006.

[35] M. Partanen, K.Y. Tan, J. Govenius, R.E. Lake, M.K. Makela, T. Tanttu, and M. Mottonen. Quantum-limited heat conduction over macroscopic distances. *Nature Physics*, 12:460–464, 2016.

[36] M. Banerjee, M. Heiblum, A. Rosenblatt, Y. Oreg, D. E. Feldman, and V. Stern, A.and Umansky. Observed quantization of anyonic heat flow. *Nature*, 545:75–79, 2017.

[37] K. Schwab, E. A. Henriksen, J. M. Worlock, and M. L. Roukes. Measurement of the quantum of thermal conductance. *Nature*, 404:974–977, 2000.

[38] K. Schwab, J. L. Arlett, J. M. Worlock, and M. L. Roukes. Thermal conductance through discrete quantum channels. *Physica E*, 9:60–68, 2001.

[39] T. Hsiao, H.i Chang, S. Liou, M. Chu, S. Lee, and C. Chang. Observation of room-temperature ballistic thermal conduction persisting over 8.3 μm in SiGe nanowires. *Nature nanotechnology*, 8:534–8, 2013.

[40] J. Maire, R. Anufriev, and M. Nomura. Ballistic thermal transport in silicon nanowires. *Scientific Reports*, 7, 2017.

[41] Y. Tanaka, F. Yoshida, and S. Tamura. Lattice thermal conductance in nanowires at low temperatures: Breakdown and recovery of quantization. *Physical Review B*, 71(20):205308, 2005.

[42] J. J. Yao, W. Q. Huang, G. F. Huang, Y. Chen, L. L. Wang, W. Hu, and A. Pan. Effects of contact shape on ballistic phonon transport in semiconductor nanowires. *Current Applied Physics*, 12:437–442, 2012.

[43] M.C. Cross and R. Lifshitz. Elastic wave transmission at an abrupt junction in a thin plate with application to heat transport and vibrations in mesoscopic systems. *Physical Review B*, 64:085324, 2001.

[44] R. Venkatesh, Y. Amrit, J.and Chalopin, and S. Volz. Thermal resistance of metal nanowire junctions in the ballistic regime. *Physical Review B*, 83:1–5, 2011.

[45] Y. Chalopin and S. Volz. A microscopic formulation of the phonon transmission at the nanoscale. *Applied Physics Letters*, 103:1–5, 2013.

[46] Ch. Jeong, R. Kim, M. Luisier, S. Datta, and M. Lundstrom. On Landauer versus Boltzmann and full band versus effective mass evaluation of thermoelectric transport coefficients. *Journal of Applied Physics*, 107:1–7, 2010.

[47] J. Hyun Oh, M. Shin, and M. Jang. Phonon thermal conductivity in silicon nanowires: The effects of surface roughness at low temperatures. *Journal of Applied Physics*, 111:044304, 2012.

[48] T. A. Puurtinen and I. J. Maasilta. Low temperature heat capacity of phononic crystal membranes. *AIP Advances*, 6:121902, 2016.

[49] D. V. Anghel and M. Manninen. Behavior of the phonon gas in restricted geometries at low temperatures. *Physical Review B*, 59:9854–9857, 1999.

[50] A. Gusso and Luis G. C. Rego. Heat capacity of suspended phonon cavities. *Physical Review B*, 75(4):1–6, 2007.

[51] T. Kühn, V. Anghel, J. P. Pekola, M. Manninen, and Y. M. Galperin. Heat transport in ultrathin dielectric membranes and bridges. *Physical Review B*, 70:1–6, 2004.

[52] F. Graff Karl. *Waves Motions in Elastic Solids*. OXFORD universitu press, 1975.

[53] E. Chávez, J. Cuffe, F. Alzina, and C. M. Sotomayor Torres. Calculation of the specific heat in ultra-thin free-standing silicon membranes. *Journal of Physics: Conference Series*, 395:012105, 2012.

[54] R. Sultan, A. D. Avery, G. Stiehl, and B. L. Zink. Thermal conductivity of micromachined low-stress silicon-nitride beams from 77 to 325 K. *Journal of Applied Physics*, 105:1–7, 2009.

[55] B. Revaz, B. L. Zink, and F. Hellman. Si-N membrane-based microcalorimetry: Heat capacity and thermal conductivity of thin films. *Thermochimica Acta*, 432:158–168, 2005.

[56] J. M. Fink, M. Kalaee, A. Pitanti, Richard Norte, Lukas H., Marcelo D., Kartik S., and O. Painter. Quantum Electromechanics on Silicon Nitride Nanomembranes. *Nature Communications*, pages 1–10, 2015.

[57] P. Ferrando-Villalba, a F. Lopeandia, L.l. Abad, J. Llobet, M. Molina-Ruiz, G. Garcia, M. Gerbolès, F. X. Alvarez, a. R. Goñi, F. J. Muñoz-Pascual, and J. Rodríguez-Viejo. In-plane thermal conductivity of sub-20 nm thick suspended mono-crystalline Si layers. *Nanotechnology*, 25:185402, 2014.

[58] Binder Kurt and Kob Walter. *Glassy Materials and Disordered Solids*. World Scientific Publishing, 2005.

[59] Gang Chen. *Nanoscale Energy Transport and Conversion*. OXFORD, 2005.

[60] E. Courtens, M. Foret, B. Hehlen, and R. Vacher. Vibrational modes of glasses. *Solid State Communications*, 117:187–200, 2001.

[61] R. C Zeller and Pohl R. O. Thermal conductivity and specific heat of noncrystalline solids. *Physical Review B*, (6):2030, 1970.

[62] Richard B Stephens. intrinsic low-temperature thermal properties of glasses. *Physical Review B*, 13(2):852–865, 1975.

[63] R. O. Pohl, X. Liu, and E. Thompson. Low-temperature thermal conductivity and acoustic attenuation in amorphous solids. *Reviews of Modern Physics*, 74:991–1013, 2002.

[64] W. A. Phillips. Tunneling states in amorphous materials. *Journal of Non-Crystalline Solids*, 78:1329–1338, 1972.

[65] P. W. Anderson, B. I. Halperin, and C. M. Varma. Tunneling states in amorphous semiconductors. *Philosophical Magazine*, 25:1, 1972.

[66] S. Ashtekar, G. Scott, J. Lyding, and M. Gruebele. Direct imaging of two-state dynamics on the amorphous silicon surface. *Physical Review Letters*, 106:2–5, 2011.

[67] V. Lubchenko and P. G. Wolynes. The origin of the boson peak and thermal conductivity plateau in low-temperature glasses. *Proceedings of the National Academy of Sciences of the United States of America*, 100(9):1515–1518, 2003.

[68] D. A. Parshin. Soft potential model and universal properties of glasses. *Physica Scripta*, 1993(T49A):180, 1993.

[69] E. Thompson, G. Lawes, J. Parpia, and R.O. Pohl. Low temperature acoustic properties of amorphous silica and the tunneling model. *Physical Review Letters*, 84(20):4601–4, 2000.

[70] A. D. Fefferman, R. O. Pohl, A. T. Zehnder, and J. M. Parpia. Acoustic Properties of Amorphous Silica between 1 and 500 mK. *Physical Review Letters*, 100(19):195501, 2008.

[71] R. Jankowiak and G. J. Small. Thermal conductivity in amorphous solids at temperatures below 1 K. *Physical Review B*, 37(14):8407–8411, 1988.

[72] D. R. Queen, X. Liu, J. Karel, T. H. Metcalf, and F. Hellman. Excess specific heat in evaporated amorphous silicon. *Physical Review Letters*, 110(13):1–5, 2013.

[73] A. Tavakoli, C. Blanc, H. Ftouni, K. J. Lulla, A. D. Fefferman, and O. Collin, E.and Bourgeois. Universality of thermal transport in amorphous nanowires at low temperatures. *Physical Review B*, 95:165411, 2017.

[74] D. R. Queen, X. Liu, J. Karel, H. C. Jacks, T. H. Metcalf, and F. Hellman. Two-level systems in evaporated amorphous silicon. *Journal of Non-Crystalline Solids*, 426:19–24, 2015.

[75] Xiao Liu and R. Pohl. Low-energy excitations in amorphous films of silicon and germanium. *Physical Review B*, 58:9067–9081, 1998.

[76] X. Liu, B.E. White, and R.O. Pohl. Amorphous Solid without Low Energy Excitations. *Physical Review Letters*, 78:4418–4421, 1997.

[77] Xiao Liu, Daniel R. Queen, Thomas H. Metcalf, Julie E. Karel, and F. Hellman. Hydrogen-free amorphous silicon with no tunneling states. *Physical Review Letters*, 113(2):1–5, 2014.

[78] J. L. Black. Relationship between the time-dependent specificc heat and the ultrasonic properties of glasses at low temperatures. *Physical Review B*, 17(14):2740–2761, 1977.

[79] Clare C. Yu. Thermal conductivity and specific heat of glasses. *Physical Review B*, 36(14):7620–7624, 1987.

[80] J.C. Lasjaunias and a. Ravex. The density of low energy states in vitreous silica: Specific heat and thermal conductivity down to 25 mK. *Solid State Communications*, 17:1045–1049, 1975.

[81] S. T. Skacel, C. Kaiser, S. Wuensch, H. Rotziger, A. Lukashenko, M. Jerger, G. Weiss, M. Siegel, and A. V. Ustinov. Probing the TLS Density of States in SiO Films using Superconducting Lumped Element Resonators. *Arxiv*, pages 3–6, 2014.

[82] J. Gao, J. Zmuidzinas, B. A. Mazin, H. G. Leduc, and P. K. Day. Noise properties of superconducting coplanar waveguide microwave resonators. *Applied Physics Letters*, 90:102507, 2007.

[83] R. W. Simmonds, K. M. Lang, D. A. Hite, S. Nam, D. P. Pappas, and John M. Martinis. Decoherence in josephson phase qubits from junction resonators. *Physical Review Letters*, 93:1–4, 2004.

[84] Li Chung Ku and Clare C. Yu. Decoherence of a Josephson qubit due to coupling to two-level systems. *Physical Review B*, 72:024526, 2005.

[85] J. Lisenfeld, A. Bilmes, S. Matityahu, S. Zanker, M. Marthaler, M. Schechter, G. Schön, A. Shnirman, and G. Weiss. Decoherence spectroscopy with individual two-level tunneling defects. *Scientific Reports*, pages 1–8, 2016.

[86] J. M. Martinis, K. B. Cooper, R. McDermott, M. Steffen, M. Ansmann, K. D. Osborn, K. Cicak, S. Oh, D. P. Pappas, R. W. Simmonds, and C. C. Yu. Decoherence in Josephson qubits from dielectric Loss. *Physical Review Letters*, 95:1–4, 2005.

[87] C. Sotomayor Torres and J. Ahopelto. Position Paper on Nanophotonics and Nanophononics. *NanoICT*, page 43, 2011.

[88] H.J. Xiang, Z. F. Shi, S. J. Wang, and Y. L. Mo. *Smart Materials and Structures*, 21:1–10, 2012.

[89] H.J. Xiang, Z. F. Shi, D. Yu, H. Zhao, and Y. Liu. *Computers and Structures*, 87:1559âĂŞ1566, 2009.

[90] J. Wen, G. Wang, D. Yu, H. Zhao, and Y. Liu. *Journal of Applied Physics*, 97:114907, 2005.

[91] J. Christensen and F. J. Garcia de Abajo. Anisotropic Metamaterials for Full Control of Acoustic Waves. *Physical Review Letters*, 108:124301, 2012.

[92] N. Zen, T. Puurtinen, T. J. Isotalo, S. Chaudhuri, and I. J. Maasilta. Engineering thermal conductance using a two-dimensional phononic crystal. *Nature communications*, 5:3435, 2014.

[93] M. R. Wagner, B. Graczykowski, J. S. Reparaz, A. El Sachat, M. Sledzinska, F. Alzina, and C. M. Sotomayor Torres. Two-Dimensional Phononic Crystals: Disorder Matters. *Nano Letters*, 16:5661–5668, 2016.

[94] Y. Pennec, J. O. Vasseur, B. Djafari-Rouhani, L. Dobrzyński, and P. A. Deymier. Two-dimensional phononic crystals: Examples and applications. *Surface Science Reports*, 65(8):229–291, 2010.

[95] H. Honarvar, L. Yang, and M. I. Hussein. Exploring interface morphology of a deeply buried layer in periodic multilaye. *Applied Physics Letters*, 108:263101, 2016.

[96] H. Honarvar and M. I. Hussein. Spectral energy analysis of locally resonant nanophononic metamaterials by molecular simulations. *Physical Review B*, 93:081412, 2016.

[97] B. L. Davis and M. I. Hussein. Nanophononic Metamaterial: Thermal Conductivity Reduction by Local Resonance. *Physical Review Letters*, 112:055505, 2014.

[98] Y. Pennec, B. D. Rouhani, H. Larabi, A. Akjouj, A. Khelif, J. Gillet, J. Vasseur, and G. Thabet. Phonon transport and waveguiding in a phononic crystal made up of cylindrical dots on a thin homogeneous plate. *Physical Review B*, 80:144302, 2009.

[99] M. Maldovan. Phonon wave interference and thermal bandgap materials. *Nature Materials*, 14:667–674, 2015.

[100] C. Blanc, A. Rajabpour, S. Volz, T. Fournier, and O. Bourgeois. Phonon heat conduction in corrugated silicon nanowires below the Casimir limit. *Applied Physics Letters*, 103, 2013.

[101] J. S. Heron, C. Bera, T. Fournier, N. Mingo, and O. Bourgeois. Blocking phonons via nanoscale geometrical design. *Physical Review B*, 82:1–5, 2010.

[102] M Terraneo, M Peyrard, and G Casati. Controlling the energy flow in nonlinear lattices: a model for a thermal rectifier. pages 11–14, 2008.

[103] B. Li, L. Wang, and G. Casati. Thermal diode: Rectification of heat flux. *Physical Review Letters*, 93:1–4, 2004.

[104] D. Segal. Single mode heat rectifier: Controlling energy flow between electronic conductors. *Physical Review Letters*, 100:1–4, 2008.

[105] C. W. KChang, D. Okawa, A. Majumdar, and A. Zettl. Co-evolutionary algorithm for structural damage identification using minimal physical testing. *Science*, 314(5):1121–1123, 2006.

[106] R. Scheibner. Thermoelectric Properties of Few-Electron Quantum Dots. page 147, 2007.

[107] J. Miller, W. Jang, and C. Dames. Thermal rectification by ballistic phonons in asymmetric. *Proceedings of HT2009 2009 ASME Summer Heat Transfer Conference*, pages 1–10, 2009.

[108] B. Li, L. Wang, and G. Casati. Negative differential thermal resistance and thermal transistor. *Applied Physics Letters*, 88:2006–2008, 2006.

[109] Y. Nakagawa, R. Schäfer, and H. J. Güntherodt. Picojoule and submillisecond calorimetry with micromechanical probes. *Applied Physics Letters*, 73:2296–2298, 1998.

[110] D. Caspary, M. Schröpfer, J. Lerchner, and G. Wolf. A high resolution IC-calorimeter for the determination of heats of absorption onto thin coatings. *Thermochimica Acta*, 337:19–26, 1999.

[111] J.-L. Garden, A. Tavakoli, T. Nguyen-Duc, A. Frydman, M. Laarraj, J. Richard, and O. Bourgeois. Very sensitive nanocalorimetry of small mass systems and glassy materials. *NATO Science for Peace and Security Series A: Chemistry and Biology*, 2016.

[112] M. Laarraj, R. Adhiri, S. Ouaskit, M. Moussetad, C. Guttin, J. Richard, and J.-L. Garden. Highly sensitive pseudo-differential ac-nanocalorimeter for the study of the glass transition. *Review of Scientific Instruments*, 86:115110, 2015.

[113] A. A. Minakov and C. Schick. Ultrafast thermal processing and nanocalorimetry at heating and cooling rates up to 1 MK/s. *Review of Scientific Instruments*, 78:073902, 2007.

[114] A. A. Minakov, S. A. Adamovsky, and C. Schick. Non-adiabatic thin-film (chip) nanocalorimetry. *Thermochimica Acta*, 432:177–185, 2005.

[115] J. Valle-Orero, J.-L. Garden, J. Richard, A. Wildes, and M. Peyrard. Calorimetric study of melted DNA glass. *AIP Conference Proceedings*, 1518:766–771, 2013.

[116] J. L. Garden, H. Guillou, A. F. Lopeandia, J. Richard, J. S. Heron, G. M. Souche, F. R. Ong, B. Vianay, and O. Bourgeois. Thermodynamics of small systems by nanocalorimetry: From physical to biological nano-objects. *Thermochimica Acta*, 492:16–28, 2009.

[117] S. Poran, T. Nguyen-Duc, A. Auerbach, N. Dupuis, A. Frydman, and O. Bourgeois. Quantum criticality at the superconductor-insulator transition revealed by specific heat measurements. *Nature Communications*, 8:14464, 2017.

[118] F. Alvarez and A. A. Valladares. The atomic and electronic structure of amorphous silicon nitride. *Revista Mexicana de Fisica*, 48:528–533, 2002.

[119] E. Bourgeois, O.and André, C. MacOvei, and J. Chaussy. Liquid nitrogen to room-temperature thermometry using niobium nitride thin films. *Review of Scientific Instruments*, 77:1–3, 2006.

[120] A. Tavakoli and e*t al.* paper in preparation. *Journal of Low Temperature Physics*.

[121] Vincent Humbert. *Etude des etats fondamentaux dans des systemes supraconducteurs desordonnes de dimension 2*. PhD thesis, Universite Paris-Sud, 2016.

[122] Stefanos Marnioros. *Couches minces d'isolant d'Anderson. Application à la bolométrie à tres basse température*. PhD thesis, Universite de Paris Sud U.F.R. Scientifique d'Orsay, 1998.

[123] V. Yefremenko, G. Wang, V. Novosad, A. Datesman, J. Pearson, R. Divan, C. L. Chang, T. P. Downes, J. J. McMahon, L. E. Bleem, A. T. Crites, S. S. Meyer, and J. E. Carlstrom. Low temperature thermal transport in partially perforated silicon nitride membranes. *Applied Physics Letters*, 94:5–7, 2009.

[124] D. J. Goldie, A. V. Velichko, D. M. Glowacka, and S. Withington. Ultra-low-noise MoCu transition edge sensors for space applications. *Journal of Applied Physics*, 109:1–9, 2011.

[125] F. Giazotto, T. T. Heikkila, A. Luukanen, A. M. Savin, and J. P. Pekola. Opportunities for mesoscopics in thermometry and refrigeration: Physics and applications. *Reviews of Modern Physics*, 78:217–274, 2006.

[126] Z. Geng, K. K. Kinnunen, and I. J. Maasilta. Development of an Inductive SINIS Thermometer. *Journal of Physics: Conference Series*, 400:052005, 2005.

[127] M. M. Leivo and J. P. Pekola. Thermal characteristics of silicon nitride membranes at sub-Kelvin temperatures. *Applied Physics Letters*, 72:1305–1307, 1998.

[128] L. N. Maurer. Developing a low temperature Coulomb Blockade Thermometer. Master's thesis, Dartmouth College, 2008.

[129] L. Shi, D. Li, C. Yu, W. Jang, Z.and Kim P. Kim, D.and Yao, and A. Majumdar. Measuring Thermal and Thermoelectric Properties of One-Dimensional Nanostructures Using a Microfabricated Device. *October*, 125:881–888, 2003.

[130] E. Dechaumphai and R. Chen. Sub-picowatt resolution calorimetry with niobium nitride thin-film thermometer. *Review of Scientific Instruments*, 85:094903, 2014.

[131] M. L. Roukes, M. R. Freeman, R. S. Germain, R. C. Richardson, and M. B. Ketchen. Hot electrons and energy transport in metals at millikelvin temperatures. *Physical Review Letters*, 55:422–425, 1985.

[132] Altshuler .B and Aronov A. Zero bias anomaly in tunnel resistance and electron-electron interaction. *Solid State Communications*, 30:115–117, 1979.

[133] E.T. Swartz and R.O. Pohl. Thermal boundary resistance. *Reviews of Modern Physics*, 61:605, 1989.

[134] E. Gmelin, M. Asen-Palmer, M. Reuther, and R. Villar. Thermal boundary resistance of mechanical contacts between solids at sub-ambient temperatures. *Journal of Physics D: Applied Physics*, 32:R19–R43, 1999.

[135] F. Couëdo, O. Crauste, A. A. Drillien, V. Humbert, L. Bergé, C. A. Marrache-Kikuchi, and L. Dumoulin. Dissipative phases across the superconductor-to-insulator transition. *Scientific Reports*, 6:35834, 2016.

[136] David G. Cahill. Thermal conductivity measurement from 30 to 750 K: The 3ω method. *Review of Scientific Instruments*, 61:802–808, 1990.

[137] H. Ftouni, D. Tainoff, J. Richard, K. Lulla, J. Guidi, E. Collin, and O. Bourgeois. Specific heat measurement of thin suspended SiN membrane from 8 K to 300 K using the 3ω-Völklein method. *Review of Scientific Instruments*, 84:8094902, 2013.

[138] A. Sikora, H. Ftouni, J. Richard, C. Hébert, D. Eon, F. Omnès, and O. Bourgeois. Highly sensitive thermal conductivity measurements of suspended membranes (SiN and diamond) using a 3ω-Völklein method. *Review of Scientific Instruments*, 83:054902, 2012.

[139] D. R. Queen and F. Hellman. Thin film nanocalorimeter for heat capacity measurements of 30 nm films. *Review of Scientific Instruments*, 80:063901, 2009.

[140] C. Blanc, J. S. Heron, T. Fournier, and O. Bourgeois. Heat transmission between a profiled nanowire and a thermal bath. *Applied Physics Letters*, 105:2–6, 2014.

[141] Christophe Blanc. *Nanoscale structuration effects on phonon transport at low temperatures*. PhD thesis, Ecole doctorale de Physique de Grenoble, 2013.

[142] Hossein Ftouni. *Thermal transport in very thin amorphous SiN membranes*. PhD thesis, Ecole doctorale de Physique de Grenoble, 2013.

[143] Yanqing LIU. *Thermal engineering in an epitaxial nanostructured germanium semiconductor*. PhD thesis, 2015.

[144] E. Pop, D. Mann, Q. Wang, K. Goodson, and H. Dai. Thermal Conductance of an Individual Single-Wall Carbon Nanotube above Room Temperature. *Nano Letters*, 6:96–100, 2005.

[145] A. I. Hochbaum, R. K. Chen, R. D. Delgado, W. J. Liang, E. C. Garnett, M. Najarian, A. Majumdar, and P. D. Yang. Enhanced thermoelectric performance of rough silicon nanowires. *Nature*, 451:163–U5, 2008.

[146] P. Kim, L. Shi, A. Majumdar, and P. L. McEuen. Thermal transport measurements of individual multiwalled nanotubes. *Physical Review Letters*, 87:19–22, 2001.

[147] J.B Johnson. On the shot-noise limit of a thermal current. *Physical Review*, 32:97, 1928.

[148] K. R. Patton. On the shot-noise limit of a thermal current. *Journal of Physics*, 20:1–4, 2008.

[149] M. Galeazzi. Fundamental Noise Processes in TES Devices. *Applied Superconductivity*, 21:267–271, 2011.

[150] Supriyo Datta. *Electronic Transport in Mesoscopic Systems*. CAMBRIDGE university press, 1997.

[151] Y. Chalopin, J. N. Gillet, and S. Volz. Predominance of thermal contact resistance in a silicon nanowire on a planar substrate. *Physical Review B*, 77:233309, 2008.

[152] D. H. Santamore and M. C. Cross. Effect of surface roughness on the universal thermal conductance. *Physical Review B*, 63:184306, 2001.

[153] D. H. Santamore and M. C. Cross. Surface scattering analysis of phonon transport in the quantum limit using an elastic model. *Physical Review B*, 66:27, 2002.

[154] P. Martin, Z. Aksamija, E. Pop, and U. Ravaioli. Impact of phonon-surface roughness scattering on thermal conductivity of thin Si nanowires. *Physical Review Letters*, 102:1–4, 2009.

[155] D. H. Santamore and M. C. Cross. Effect of surface roughness on the universal thermal conductance. *Physical Review B*, 63(18):184306, 2001.

[156] P. G. Murphy and J. E. Moore. Coherent phonon scattering effects on thermal transport in thin semiconductor nanowires. *Physical Review B*, 76:155313, 2007.

[157] V. Lee, C. H. Wu, Z. X. Lou, W. L. Lee, and C. W. Chang. Divergent and Ultrahigh Thermal Conductivity in Millimeter-Long Nanotubes. *Physical Review Letters*, 118:1–5, 2017.

[158] N. Mingo and D. A. Broido. *Nano Letters*, pages 1221–1225.

[159] N. Mingo and D. A. Broido. Carbon nanotube ballistic thermal conductance and its limits. *Physical Review Letters*, 95:26–29, 2005.

[160] A. Dhar. Heat transport in low-dimensional systems. *Advances in Physics*, 57:457–537, 2008.

[161] A. V. Feshchenko, O. P. Saira, and J. P. Pekola. Thermal conductance of Nb thin films at sub-kelvin temperatures. *Scientific Reports*, 7:1–16, 2016.

[162] G. R. Stewart. Measurement of low-temperature specific heat. *Review of Scientific Instruments*, 54:1–11, 1983.

[163] S. Poran, M. Molina-Ruiz, A. Gérardin, A. Frydman, and O. Bourgeois. Specific heat measurement set-up for quench condensed thin superconducting films. *Review of Scientific Instruments*, 85:83–86, 2014.

[164] J.E. Graebner and L.C. Allen. Thermal conductivity of amorphous germanium at low temperatures. *Physical Review B*, 29:5626–5633, 1984.

[165] M. Bretz. Specific Heat of Para-Hydrogen Monolayers on Graphite. *Journal of Low Temperature Physics*, 17:479–488, 1974.

[166] M. T. Alkhafaji and A. D. Migone. Heat-capacity study of butane on graphite. *Physical Review B*, 53(16):152–158, 1996.

[167] E. Gmelin. Classica1 temperature-modulated calorimetry: A review. *Thermochimica Acts*, 305:1–26, 1997.

[168] *Thermal Properties of Solids at Room and Cryogenic Temperatures*. Spiringer, 2014.

[169] U. Buchenau, U. Galperin, Parchin D.A. Gurevich, V.L. and, M.A. Ramos, and H.R. Schober. Interaction of soft modes and sound waves in glasses. *Physical Review B*, 46:2798–2808, 1992.

[170] In collaboration with Tuomas Puurtinen and Ilari Maasilta.

[171] H. Ftouni, C. Blanc, D. Tainoff, A. D. Fefferman, M. Defoort, K. J. Lulla, J. Richard, E. Collin, and O. Bourgeois. Thermal conductivity of silicon nitride membranes is not sensitive to stress. *Physical Review B*, 92:1–7, 2015.

[172] J. Wu and Clare C. Yu. How stress can reduce dissipation in glasses. *Physical Review B*, 84:1–9, 2011.

[173] K. Shimakawa, S. Wakamatsu, M. Kojima, H. Kato, and A. Imai. Ac Transport in Amorphous Silicon-Nitrogen Alloys. *Journal of Applied Physics*, 72:2889, 1992.

[174] K. Shimakawa and S. Wakamatsu. A model for ac conduction in amorphous silicon nitrides. *Journal of Applied Physics*, 68:371–374, 1990.

[175] L. Wang and B. Li. Thermal logic gates: Computation with phonons. *Physical Review Letters*, 99:1–4, 2007.

[176] L. Wang and B. Li. Thermal memory: A storage of phononic information. *Physical Review Letters*, 101:1–4, 2008.

[177] M. Peyrard. The design of a thermal rectifier. *Europhysics Letters (EPL)*, 76:49–55, 2006.

[178] W. Kobayashi, Y. Teraoka, and I. Terasaki. An oxide thermal rectifier. *Applied Physics Letters*, 95:93–96, 2009.

[179] N. Yang, N.and Li, L. Wang, and B. Li. Thermal rectification and negative differential thermal resistance in lattices with mass gradient. *Physical Review B*, 76:1–4, 2007.

[180] P.E. Hopkins and J. R. Serrano. Phonon localization and thermal rectification in asymmetric harmonic chains using a nonequilibrium Green's function formalism. *Physical Review B*, 80:1–4, 2009.

[181] Vl. Poborchii, Y. Morita, T. Hattori, J.and Tada, and P. I. Geshev. Corrugated Si nanowires with reduced thermal conductivity for wide-temperature-range thermoelectricity. *Journal of Applied Physics*, 120:154304, 2016.

[182] A. Ramiere, J. Maire, R. Anufriev, and M. Nomura. Heat guiding and focusing using ballistic phonon transport in phononic nanostructures. *Nature Communications*, 8(May):1–8, 2017.

Heat conduction in a ballistic 1D phonon waveguide: breakdown of the thermal conductance quantization

Adib Tavakoli,[1,2] Kunal Lulla,[1,2] Thierry Crozes,[1,2] Eddy Collin,[1,2] and Olivier Bourgeois[1,2]

[1] *Institut NÉEL, CNRS, 25 avenue des Martyrs, F-38042 Grenoble, France*

[2] *Univ. Grenoble Alpes, Inst NEEL, F-38042 Grenoble, France*

(Dated: today)

Abstract

Emerging quantum technologies require mastering thermal management, especially at the nanoscale. It is now accepted that thermal metamaterials (phononic diodes, thermocrystals) based on phonon manipulation are made possible especially at sub-Kelvin temperatures [1–3]. In these extreme limits of low temperature and low dimension, heat conduction enters into a quantum regime where the phonon exchange obeys the Landauer formalism [4–8]. In this regime, phonon transport is governed by the value of the transmission coefficients between the ballistic conductor and the thermal reservoirs [10–13]. Here, we report an ultra-sensitive thermal experiments made on a ballistic 1D phonon conductor using a micro-platform suspended sensor. We achieved the measurement of thermal conductance with a resolution of $\Delta K/K$ of 1.5% and a power sensitivity down to attoWatts at 70 mK. The ballistic thermal transport is dominated by non-ideal transmission coefficients and not by the quantized thermal conductance of the nanowire itself. The measurements reveal scattering mechanisms dominated by phonon diffusion in the reservoirs. This limitation of heat transport in the quantum regime will have significant impacts on the design of modern thermal circuits and nanoelectronics (Josephson junction, quantum solid state devices) [14, 15]. This high resolution experimental achievement gives new insight of heat transport in the quantum regime, a scientific goal that has remained uncertain till now.

In a one dimensional (1D) quantum channel connecting two reservoirs, the heat current can be expressed through the probability of a phonon to be transmitted from one heat bath to the other one when they are kept at different temperatures. This is well described by the Landauer formalism viewing thermal conductance as transmission between reservoirs; the heat transport being expressed through the transmission coefficient of plane waves in a ballistic thermal conductor between two contacts [6, 12, 13]. As many experiments have been done for electrons [16–18] or photon [19, 20], very few experimental attempts have been made to probe this limit for phonons [9, 21]. This leaves open crucial questions like: where is located the temperature drop, where appears the thermal resistance and consequently where do the phonons scatter and thermalize ? This should be clearly expressed through the transmission coefficient that quantifies the connection between the 1D conductor and the reservoir, the mismatch of phonon eigenmodes, and the potential thermal resistance at the contact.

The Landauer expression for the heat flux in a ballistic 1D nanowire between two reservoirs is given by [6–8, 22]:

$$\dot{Q} = \sum_{\alpha} \int_0^{\infty} \frac{dk}{2\pi} \, \hbar\omega_\alpha(k)\nu_\alpha(k)[\eta_h - \eta_c]\mathcal{T}_\alpha(k), \tag{1}$$

where α is the mode index, $\omega_\alpha(k)$ is the dispersion relation for the phonon with wave vector k, $\nu_\alpha(k)$ is the group velocity, $\eta_i(\omega) = 1/(e^{\hbar\omega/k_B T} - 1)$ represents the thermal distribution of phonons in the reservoirs, k_B the Boltzmann constant, and $\mathcal{T}_\alpha(k)$ is the transmission coefficient between the two reservoirs.

At low enough temperature, when only fundamental acoustic modes are occupied in the 1D quantum channel connecting the two reservoirs, the heat flux given by Eq. 1 can be expressed through the following approximation:

$$\dot{Q} = N\mathcal{T}G_q(T_2 - T_1) \tag{2}$$

valid only when $T_2 - T_1 << \frac{T_2+T_1}{2}$, and where N is the number of conducting channels, $\mathcal{T}$ is the transmission coefficient integrated over all the wave-vector, $G_q = \pi^2 k_B^2 T/3h$ is the universal upper limit of phonon heat transport known as the quantum of thermal conductance for one channel; T_1 and T_2 being the reservoir's temperature [4–9].

Having an experimental access to this quantum regime is highly challenging since ballistic transport of phonon and optimized coupling of the quantum channels to the two reservoirs

are required. This can be obtained at very low temperatures where the phonon mean free path (MFP) can be longer than the length of the heat conductor and the dominant phonon wavelength much bigger than the nanowire diameter. In this extreme limit, we expect phonons to have ballistic travel between the two reservoirs through the 1D waveguide; the thermal transport being dominated by the wave aspect of phonons and then by the transmission coefficient $\mathcal{T}$. To the best of our knowledge, this has never been addressed in previous experiments with such a control on all the thermal flows and characteristic lengths involved.

Here we report a highly sensitive experimental study of thermal transport between two large reservoirs through a 1D nanowire. The experimental platform constituted by two membranes (thermal reservoirs) and the nanowires are micro and nano-engineered from stoichiometric silicon nitride (SiN), the most used material for low temperature thermal and mechanical measurements that behaves like an ideal elastic continuum medium [2, 6, 23]. Indeed, the dominant phonon wavelength given by:

$$\lambda_{dom} = \frac{h\nu_s}{2.82k_BT} \tag{3}$$

is reaching 200 nm at 1 K in SiN and still increases as the temperature decreases up to 2 μm at 0.1 K [24–26]; h and ν_s, being respectively the Planck constant and the phonon group velocity. We can then assume that a nanowire of diameter d below 100 nm will enter the 1D regime below 1 K (when $\lambda_{dom} >> d$). The second characteristic length for heat transport is the phonon mean free path Λ_{ph} that has to be longer than the length in order to have ballistic transport. This ballistic limit will be probed experimentally by measuring nanowires having different lengths.

The thermal conductance and hence the transmission coefficient are then measured as a function of temperature in the ballistic regime. This is done on 1D heat conductors suspended between two 2D membrane reservoirs both controlled in temperature. Importantly, the temperature gradient can be reversed to measure the thermal flow in both directions.

As it is shown in Fig. 1 the measurement platform consists of two adjacent membranes suspended by eight supporting beams and thermally connected to each other by one or two nanowires, the 1D phonon waveguides. Each 1D nanowire has four quantum channels of heat conduction corresponding to the four different acoustic phonon polarizations (one longitudinal, two transverse and one shear modes) [7]. To reduce any kind of thermal

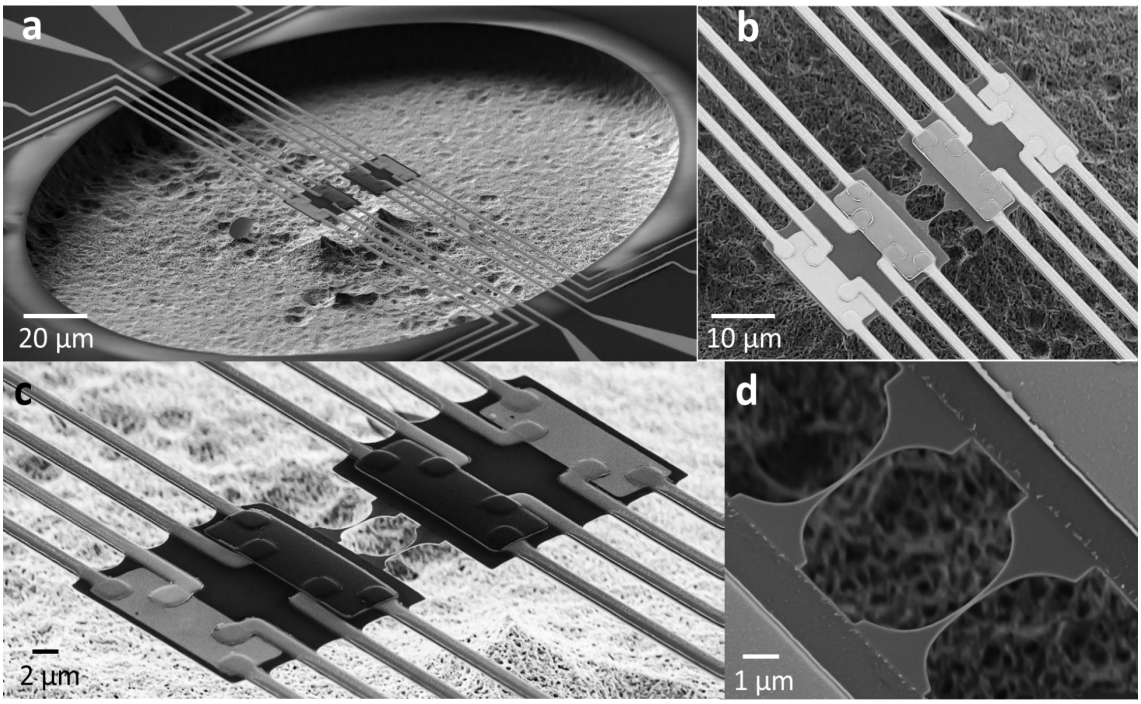

FIG. 1. **Suspended silicon nitride measurement platform**. **a** Scanning Electron Microscopy (SEM) images of the fully suspended silicon nitride membrane-based nanocalorimeters designed for very low temperature measurements. **b** and **c** Ensemble view of the nanocalorimeters with, for each membrane, a copper heater (in red) and a NbN thermometer (in blue). The thermometers have been purposely installed to probe the temperature very close to the 1D nanowires. A four contact geometry on the heaters and thermometers allows the high sensitive electrical measurements of the thermal properties. The two membranes are thermally connected through the 1D nanowires. **d** Up-side view of the nanowires obtained by e-beam lithography. The connection of the 1D nanowires to the reservoirs has a catenoidal shape to optimize the value of the transmission coefficient [7].

contact resistance due to acoustic mismatch between the nanowire and the membrane, the whole system has been microfabricated with the same material (SiN) with thickness of 100 nm. The thermal link between the 1D phonon waveguide and the reservoirs is patterned with a catenoidal shape to optimize the transmission of the phonon modes [7]. Based on numerical calculations, this geometrical design was found to represent the ideal case for maximizing the transmission coefficient [7, 12]. Each membrane-based calorimeter contains a copper heater and a niobium nitride (NbN) resistive thermometer [27]. For this work, this kind of sensitive thermometry has been adapted to get the best performances at very

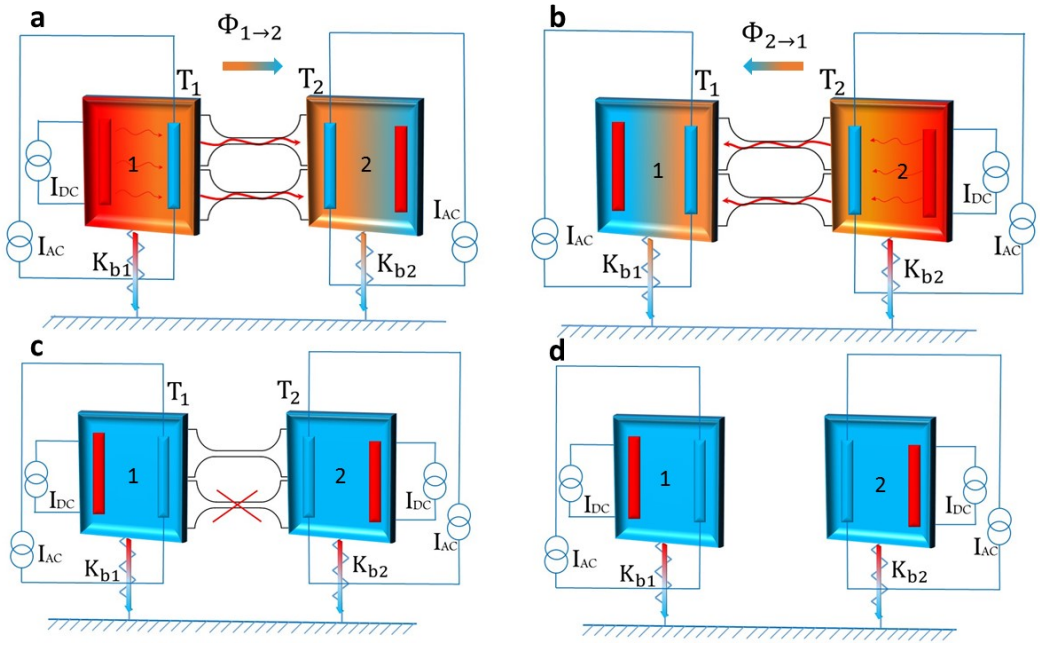

FIG. 2. **Sample design and experimental protocols.** The membranes are schematized by a colored square containing a heater in red and a thermometer in blue. Several experimental protocols have been used, **a** where the temperature gradient is established through a DC current applied to the heater on the right membrane creating a continuous heat flow to the left membrane through the 1D phonon waveguide. The two temperatures T_1 and T_2 are measured with the two thermometers and **b**) the DC current is supplied to the heater on the left membrane, the heat flow is then reversed as compared to the case **a**. The two first protocols **a** and **b** have been established to verify the symmetry of heat transport in the nanowires. In protocol **c**, one of the nanowires has been cut by FIB, then the steps **a** and **b** are repeated to check the additivity of the heat flow and potentially to probe the number of conducting channels in each nanowire. In **d** both nanowires have been cut to measure the thermal conductance $K_{b1,2}$ of the suspending beams of a single membrane.

low temperature, from 30 mK to 10 K. The resistance of the heater is precisely measured allowing the exact estimation of the dissipated power. Thanks to a low noise measurement technique, the double membrane nanocalorimeter has state of the art power sensitivity of below the attoWatt at 0.1 K, allowing the measurement of thermal conductance variation below 10^{-16} W/K (0.1 femtoWatt/K) [28]. This measurement configuration based on a continuous heat flow between two reservoirs has been used in the past to probe the thermal

properties of suspended nanostructures at room temperature [29–32]. This configuration is particularly adapted for thermal measurements in the ballistic limit at very low temperature where the local temperature cannot be defined along the nanowire; temperature can only be set on large thermodynamic reservoirs like the membranes. There is two major differentiating points in this experiment: first, there is no deposited material on top of the suspended nanowire (no parasitic thermal path) and second, the temperature gradient can be reversed between the two membrane sensors to probe the symmetry of the heat flux.

The protocols of the different thermal experiments are detailed in Fig. 2. In the first protocol (Fig. 2 a), a continuous power is dissipated in the heater of the membrane 1. A temperature gradient is then established between the two membranes, the heat flowing through the two nanowires (the two heat waveguides). The direction of the heat flow is reversed in the second protocol where the membrane 2 has a higher temperature than membrane 1 (Fig. 2 b), the power being dissipated in the heater of membrane 2. These protocols are essential to probe the symmetry of the heat transport in order to proof the reliability of the measurements.

Fig. 2 c shows the same steps of Fig. 2 a and b after having cut one of the nanowire by focused ion beam (FIB). This is modifying the total number of conducting channels from potentially height quantum channels to only four in the case of one 1D nanowire. Finally, Fig. 2 d shows the last protocol allowing the measurement of the thermal conductance of the suspending beams without any nanowire connecting the two membranes. The temperature T corresponds to the average temperature at the two extremities of the nanowires $T = \frac{T_1+T_2}{2}$, with the condition $|T_1 - T_2| << T$ enforced in all the experiments (see Methods). The thermal conductance of the nanowire is obtained by using the equation:

$$K_{NW} = K_{b2} \left(\frac{T_2 - T_0}{T_1 - T_2} \right) \tag{4}$$

where T_0 is the temperature of the bath, K_{b2} is the thermal conductance of the suspending beams of each membrane at the temperature T_2, $T_1 - T_2$ is of the order of 20 mK and $T_2 - T_0$ of 10 mK. The details of the power balance, calibration and sensitivity are presented in the Methods section.

The thermal conductance measurements versus temperature along with the data interpretation are presented in Fig. 3 for one and two nanowires. The variation of thermal conductance covers more than three decades as the temperature is lowered down to 50 mK.

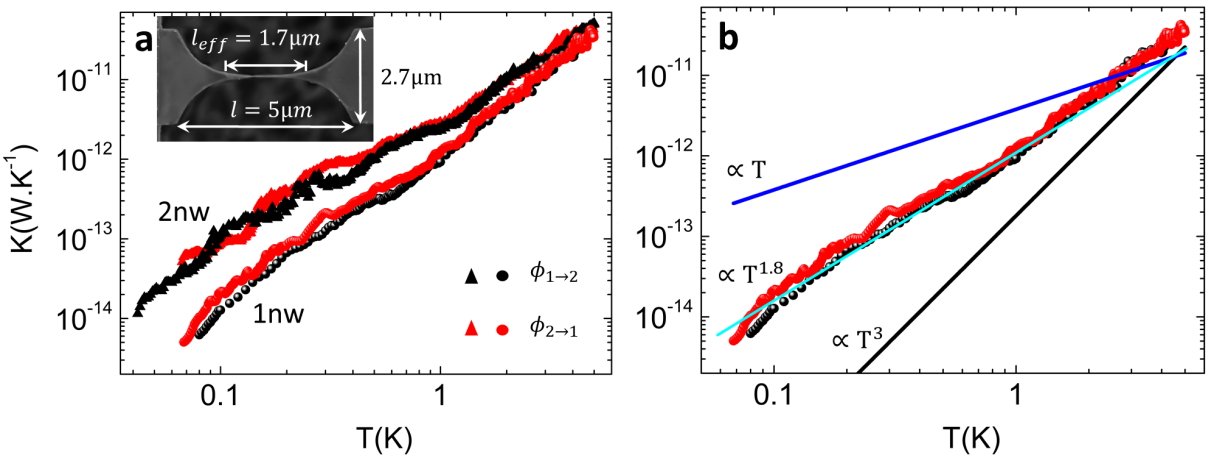

FIG. 3. **Thermal measurements of nanowires as a function of temperature. a** Thermal conductances of two nanowires (2 NWs) and one nanowire (1 NW) versus temperature. These have been measured in two different heating configurations; red symbols refer to the heating from right to left, and black symbols from left to right. The inset shows the top view of the nanowire illustrating the various dimensions of the nanowire and especially the full length.**b** The thermal conductance of one nanowire is compared to the theoretical fits. The black line corresponds to the boundary limited regime in T^3 (Casimir regime), the dark blue line is the universal quantum value of thermal conductance and the light blue line represents the best adjustment obtained with a power law in temperature of 1.8.

The superposition of the two measurements (red and black dots) that have been acquired using different directions of the heat flow clearly demonstrates the symmetry of the heat transport. If we compare now the thermal conductance of one or two nanowires, it appears that at high temperature the heat flow for two nanowires is indeed two times the heat flow in one nanowire. As the temperature is lowered, the difference is larger than a factor of two; this is attributed to different transmission coefficients between the two nanowires; a discussion that will be more detailed below.

In order to distinguish the different regimes of phonon heat transfer, it is essential to compare the dependence in temperature of the thermal conductance to theoretical models. Indeed, $K(T)$ generally reveals the various mechanisms of phonon transport at low temperatures. This is illustrated in Fig. 3 b where the measurements are compared to the different expected regimes of heat conduction at low temperature: boundary limited heat transport

(the Casimir regime) characterized by a cubic behavior in temperature (black line), and the quantum limit of fully ballistic transport characterized by a linear regime (dark blue line) only when the transmission coefficients are equal to one; the light blue line is a simple quadratic fit likely to describe thermal transport in amorphous materials like SiN when phonons are predominantly scattered by two level systems (TLS) [33–37]; in amorphous materials atoms or group of atoms may tunnel between two different equilibrium positions creating what is called a TLS. As it is shown in Fig. 3 b, the dependency of thermal conductance on temperature is indeed mostly quadratic; a variation in temperature departing strongly from the universal value of thermal conductance [4–9].

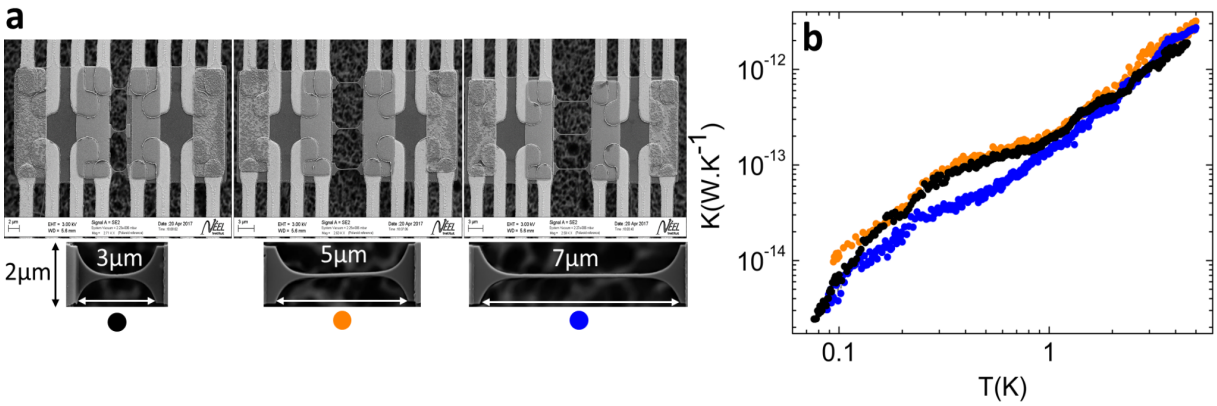

FIG. 4. **Thermal conductance measurements of nanowires having three different lengths as a function of temperature.** **a** SEM images of the three different nanowires suspended between the membranes having a length of 3 μm (black dots), 5 μm (orange dots) and 7 μm (blue dots). **b** Thermal conductances of the three nanowires as a function of temperature. The measurements are mostly superposed showing that the mean free path is at least greater than 7 μm whatever the temperature.

We now investigate the true regime of phonon exchange between the two membranes. To probe if the thermal transport is ballistic we performed thermal conductance measurement as a function of the length of nanowires. This is probing experimentally if the phonon mean free path is longer than the nanowire length. The different geometries are presented in Fig. 4 a; the samples are constituted by three nanowires connecting th two membranes; nanowires of length ranging from 3 μm to 7 μm have been measured. As shown in Fig. 4 b, the thermal conductances of these nanowires are largely superposed, showing no major difference in

phonon heat transport between them. This shows that the phonon MFP is much larger than the effective length of the nanowires at all temperatures of the experiment. This means that phonons travel without any collision through the phonon waveguide. This is a crucial experimental result demonstrating that the transport of phonons is ballistic at low temperatures. Since the nanowire can be considered as a 1D phonon waveguide when $\lambda_{dom} >> d$ (see Eq. 3), this implies that, at least below few Kelvin, the heat transport is in the quantum limit (ballistic and 1D).

It is however clear from Fig. 3 b and Fig. 4 b that the thermal conductance departs significantly from the expected universal value G_q. This is striking since we demonstrated above a phonon transport that is ballistic in a 1D phonon waveguide. This observation can be ascribed to transmission coefficients that are far from being close to unity. Consequently it is proposed to interpret these data in the light of the Landauer formalism. The transmission coefficients of the nanowire can be calculated from the measured thermal conductance presented in Fig. 3 a, using Eq. 2 since $T_1 - T_2 < T$. The transmission coefficients shown in Fig. 5 keep decreasing as the temperature decreases, showing that thermal conductance does not reach the expected universal value, a clear illustration of the breakdown of thermal conductance quantization.

This suggests that different mechanisms are at stake that prevent a perfect transmission of phonon between the reservoirs. The intrinsic quantum value of thermal conductance of the 1D nanowire has to be seen as in series with the thermal resistances of the contacts. Above 4 K, $\mathcal{T}$ is bigger than one, because more phonon modes than the minimum four modes are excited, leading to a thermal conductance bigger than the universal value. The transmission coefficients are identical for both 1 NW and 2 NWs from 5 K to 1 K, and starts to be different at lower temperature. This suggests that this could be the signature of a transition from 3D to 1D physics below 1 K; the dissimilarity being attributed to different couplings and hence different thermal resistances between the nanowire(s) and the heat bath in the quantum regime.

The source of the observed thermal resistance between the nanowires and the membrane reservoirs may have different origins. It could come either from the non-perfect coupling between 1D nanowire and 2D reservoirs [38], or from specific phonon scattering arising in the reservoirs. Calculation of the expected transmission coefficient in the catenoidal shape for the four different phonon polarizations have been done by Tanaka et al. especially for

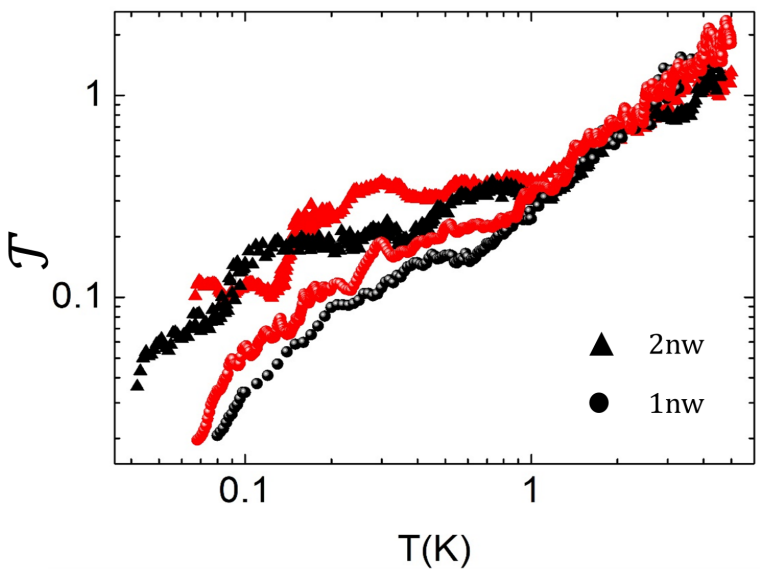

FIG. 5. **Landauer transmission coefficients.** The Landauer transmission coefficients $\mathcal{T}$ are extracted from the experimental results (see Eqs. 1 and 2). This value is obtained by normalizing the thermal conductance of the one and two nanowires shown in Fig. 3 a to the universal quantum of thermal conductance corresponding to four (1 NW) or eight channels (2 NWs).

SiN [39]. This numerical simulations show a thermal conductance very close to the universal value at 1 K for a wire similar to the one of this study. However, these calculations have been made for a transmission between a 1D system and an ideal 3D reservoir which is clearly not the case in most experiments (see this work and Schwab *et al.* [9]). Here, the 1D-2D coupling could indeed have dramatic consequences on the phonon transport as demonstrated by Chalopin *et al.* where the numerical simulations clearly show a thermal transport dominated by the contact resistances arising from a smaller number of excited modes in the membrane reservoir than in the nanowire [38]. A thermal resistance similar to Kapitza resistance is expected, as it is well known at low temperature, reducing the transmission coefficient below one. However, this is not the only possible origin for this thermal resistance. It has been shown recently that, in amorphous nanostructures, the phonon-TLS scattering is the limiting mechanism of the phonon transport in the diffusive regime [37]. As it has been shown in Fig. 3 b, the overall temperature variation of the thermal conductance approaches $T^{1.8}$, a quadraticity in good agreement with the expected thermal properties in amorphous structures at low temperature. It is commonly accepted

that this characteristic behavior can be ascribed to the scattering of phonons on TLS. This scattering mechanism, mostly arising in the reservoir, is another possible explanation for very low transmission coefficient between the ballistic nanowire and the membrane.

To summarize, these highly sensitive thermal measurements allow probing thermal conductance of 1D phonon waveguides down to very low temperature. At these temperatures, it is shown that phonon exchange is ballistic between the two reservoirs. In this quantum regime, the experimental data can be understood in the framework of the Landauer model through the calculation of the transmission coefficient. Even in the ballistic regime, the thermal transport is driven by reduced transmission coefficient far below the unity. Kapitza like thermal resistance [38, 39], boundary conditions [8] or phonon scattering [40] in the reservoirs creates a breakdown of the thermal conductance quantization. This is severely impeding the observation of the regime of maximum exchange of heat or information (the quantum of thermal conductance) in a one dimensional phonon waveguide as proposed by Pendry [4]. Whilst we expected to observe a linear thermal conductance in temperature close to the quantum universal value, a quadratic temperature dependence is dominant below few Kelvins. This low exchange of heat even in the quantum regime will have major consequences in the thermalization of lots of nanophononic or nanoelectronic systems at low temperatures. Finally, this measurement platform having an attoWatt sensitivity opens up tremendous possibilities for the next generation of thermal measurements at the nanoscale and low temperature. Maximizing transmission coefficients will be the next challenge if one wants to address exciting issues like phonon thermal rectification or phonon coherent effects.

We thank the micro and nanofabrication facilities of Institut Néel CNRS: the Pôle Capteurs Thermométriques et Calorimétrie (E. André, G. Moiroux, P. Lachkar and J.-L. Garden) and Nanofab (S. Dufresnes, B. Fernandez, T. Fournier, G. Julié and J.-F. Motte) for their advices in the preparation of the samples. We have also benefited from the support of the Pole Cryogenie and Electronique. OB and EC acknowledges the financial support from the ANR project QNM Grant No. 040401, the European projects MicroKelvin EUFRP7 Grant No. 228464 and MERGING Grant No. 309150.

METHODS

Sample fabrication. The samples are microfabricated from 100 mm Si wafer having a 100 nm thick thermally grown stoichiometric silicon nitride layer on top. The electrical superconducting leads that connect the transducers (heaters and thermometers) are in niobium titanium (100nm) and gold (20 nm), they are made by laser lithography and deposited by sputtering. This NbTi/Au layer ensures very good electrical contact between the electrical leads and the transducers (heater and thermometer). Superconducting materials are used to reduce significantly the thermal conductance of the suspending beams far below the critical temperature T_c; T_c is in most of the case above 7 K. This limits the thermal measurements below that temperature. After a laser lithography step, the copper heaters are deposited by e-gun evaporation and the niobium nitride (NbN) thermometers by sputtering using argon nitrogen plasma. All transducers are connected in a four-wire arrangement.

The nanowires linking the two membranes are nanofabricated using e-beam lithography. This allows a better definition of the shape and the boundary of the nanowires than laser lithography. The nanowire has a diameter in the center smaller than 100 nm; the catenoidal shape has been designed using the formula $A(x) = A_0 cosh^2(x/\lambda)$, where $A_0 = \times 10^{-7}$ m is the size of the thinnest part of the nanowire and $\lambda = 1.2\mu$m is the characteristic length of the catenoide. An aluminum mask is deposited by e-gun evaporation at low temperature (100 K) to reduce the size of the grains. The silicon nitride layer is then structured by SF_6 reactive etching using the aluminum and photoresist as a mask; this step will determine the final geometry of the membrane, the nanowire and the suspending beams. After removing the aluminum layer by chemical etching, the whole measurement platform composed of the membrane, the nanowires and suspending beams are released by a gaseous chemical etching of the underlying silicon using an XeF_2 etching process [42]. The full platform is consequently mechanically suspended and partly thermally isolated from the surrounding thermal bath. The chip is installed on a copper based printed circuit board (PCB) regulated in temperature. This experimental set-up is installed under vacuum in the measurement chamber.

Experimental set-up. The measurements are performed down to 50 mK in a dilution refrigerator; the PCB can be regulated in temperature up to 10 K. All the electrical connections are equipped with a low pass frequency filter ($f_c = 50$ kHz). The current source and the preamplifier are very low drift (below 5 ppm per Celsius degree) and very low noise

(below 1 nV/$\sqrt{\text{Hz}}$) at frequency lower than 1 kHz. The heaters have a resistance of approximately 50 Ω and the thermometers of few kilo Ω. The measurement of the thermal conductance is performed by heating up one membrane using the Joule effect of one of the heater: $\dot{Q}_h = R_h I_h^2$. The heating current I_h is comprised between 10 nA and 10μA depending on the temperature of the regulated stage of the PCB. During the measurements, the temperature of both membranes is continuously monitored with the NbN thermometers measured using an AC current of 5 nA at 27 Hz. The power dissipated in the thermometers is much smaller than $\dot{Q}_h$. Regarding the performance of the measurements, the smallest variation in temperature that the thermometers can capture is $\delta T \simeq 50$ µK giving an absolute error below the attoWatt in power (see below the section on sensitivity for more details).

When one membrane is heated up, the temperature of the second membrane raised due to the circulating heat flow through the nanowires. The stabilization of the temperature of both membranes in that steady state is obtained when the powers are balanced between the heat that flows through the nanowire and through the suspending beams. If T_0, T_1 and T_2 are the temperatures of respectively the heat bath, the membrane 1 and the membrane 2 then we can defined the two flows of heat from each membrane to the heat bath:

$$\dot{Q}_1 = K_{b1}(T_1 - T_0) \tag{5}$$

$$\dot{Q}_2 = K_{b2}(T_2 - T_0), \tag{6}$$

K_{b_i} being respectively the thermal conductance between the membrane i and the heat bath. By knowing the exact temperature of each membrane along with the power dissipated, we have access to the full balance of the transported flow of energy through the nanowires and membranes, and hence to the thermal conductance of the nanowires. By changing which platform is heated, one can reverse the heat flowing through the nanowires and then probe the symmetry of the heat transport in the nanowires.

This measurement method based on two membranes having different temperatures permits accessing the thermal properties in the ballistic limit of a 1D phonon waveguide. In this limit, local temperature along the nanowire is not any more a relevant physical concept. At these very low temperatures (100 mK) competing methods like the 3ω cannot be used

because the temperature has to be known all along the suspended nanostructures. Here, the temperature will be well defined only on the membrane considered as a sufficiently large thermodynamic reservoir.

Thermal model of the measurement platform. Here we derive the basic equations ruling the heat balance of the platform constituted by the two membranes, the nanowires and the suspending beams. This will permit the determination of the thermal conductance of the nanowires. We can write down the thermal balance by starting from the heating power dissipated by the heater:

$$\dot{Q}_h = R_h I_h^2 = \dot{Q}_1 + \dot{Q}_{NW} \tag{7}$$

where $\dot{Q}_{NW}$ is the heat flow through the nanowires. Similarly, this heat flow is related to the thermal conductance of the nanowires through:

$$\dot{Q}_{NW} = K_{NW}(T_1 - T_2), \tag{8}$$

in which K_{NW} is the thermal conductance of the nanowires. In the steady state configuration, the system can be considered to be in a stationary regime so the heat flux between the membrane and the heat flowing from the second membrane to the heat bath can be equaled : $\dot{Q}_{NW} = \dot{Q}_2$. Using this equation, the thermal conductance of the nanowires can be expressed by:

$$K_{NW} = K_{b2} \left(\frac{T_2 - T_0}{T_1 - T_2} \right) \tag{9}$$

if the conditions $T_1 - T_2 << T_0$ and T_2 close to T_0 are fulfilled. By monitoring T_0, T_1 and T_2 (only T_0 is regulated) and having calibrated K_{b2} as a function of temperature, K_{NW} will be obtained as a function of T_0. K_{b2} is measured on a similar sensor without the presence of nanowires (see Fig. 2 d). The measurement of $T_1 - T_2$, $T_2 - T_0$ and the calibration of K_{b2} are presented in the following figures: Fig. 6, Fig. 7 and Fig. 8.

Signal to noise ratio, attoWatt sensitivity. One can estimate the expected signal to noise ratio of the thermal conductance measurement the using the law of propagation of uncertainty from Eq. 9:

$$\left(\frac{\delta K_{NW}}{K_{NW}} \right)_{Theor} = \sqrt{\left(\frac{\delta T_2}{T_2} \right)^2 + \left(\frac{\delta T_0}{T_0} \right)^2 + 2 \left(\frac{\delta (T_1 - T_2)}{T_1 - T_2} \right)^2} \tag{10}$$

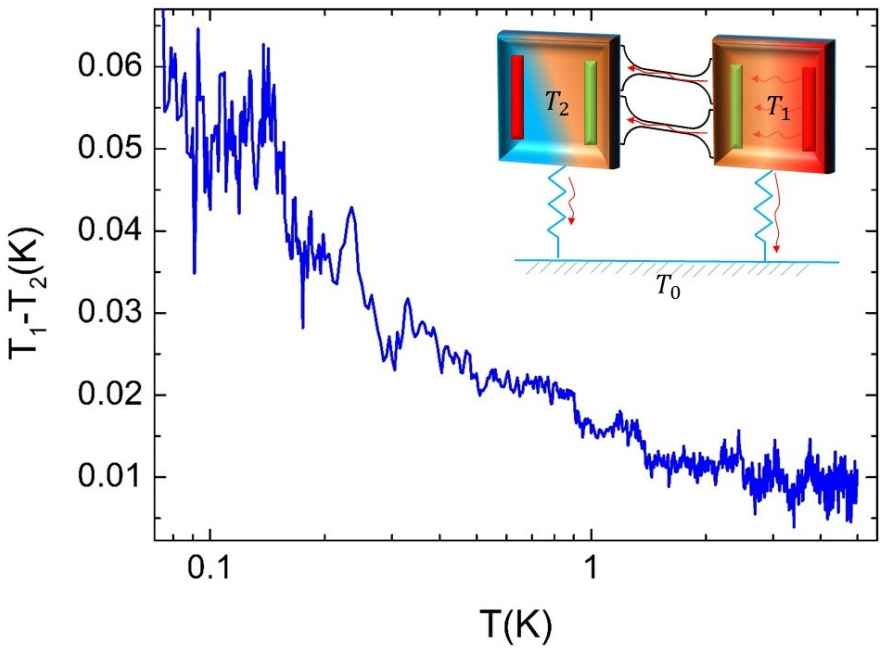

FIG. 6. Typical temperature gradient measured between the two membranes during an experiment of thermal conductance as a function of temperature. This temperature gradient is smaller than 30 mK above 200 mK. In inset, the schematic of the experimental set-up.

There is no added noise from K_b since the input value comes from the fit of the measurement shown in Fig. 8. If the only limit is the Johnson-Nyquist noise of the thermometer, the theoretical error in the temperature measurement is given by $\left(\frac{\delta T}{T}\right) = \left(\frac{\delta V}{V}\right)$. The Johnson voltage noise is calculated using the Nyquist relation $\delta V = \sqrt{4k_B T R_{Th}}$ in Volt/$\sqrt{\text{Hz}}$, where R_{Th} is the resistance of the thermometer. Then from Eq. 10, one can estimate the theoretical uncertainty on the thermal conductance: $\left(\frac{\delta K_{NW}}{K_{NW}}\right)_{Theor} = 4 \times 10^{-3}$; indeed the noise corresponding to a 4 kOhm thermometer resistance at 0.1 K is $\delta V = \sqrt{4k_B T R_{Th}} = 0.16$ Volt/$\sqrt{\text{Hz}}$ for a voltage of $V = 40$ nVolt.

This theoretical value has to be compared to the experimental one extracted from the noise measurement: $\left(\frac{\delta K_{NW}}{K_{NW}}\right)_{Exp} = 1.5 \times 10^{-2}$, knowing that $K_{NW} = 10^{-14}$ W/K, then variation of thermal conductance of the order of $\Delta K_{NW} \approx 10^{-16}$ W/K. This shows that the experimental error is only three times bigger than the expected theoretical one, attesting the low noise experiment. This also indicates the presence of other origin of noise like the preamp noise (1 nVolt/$\sqrt{\text{Hz}}$), the thermal drift of the equipments, etc... In any case, this helps to give a good estimate of the overall sensitivity of the experiment in terms of measurable

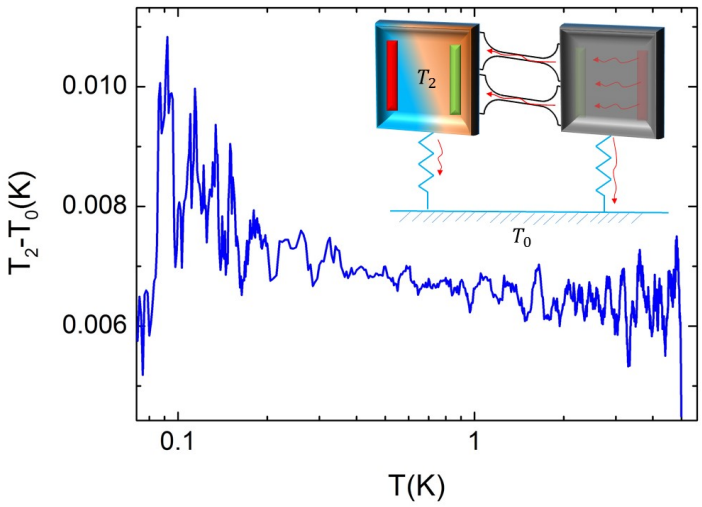

FIG. 7. Typical temperature gradient measured between the second membrane and the thermal bath (baseline) during an experiment of thermal conductance as a function of temperature. The temperature gradient is smaller than 10 mK. In inset, the schematic of the measurement configuration.

power: $\delta P = \delta K_{NW}(T_2 - T_0)$, since $(T_2 - T_0)$ is of the order of 10 mK, the sensitivity in power is of the order of $\times 10^{-18}$ Watt (one attoWatt). This sensitivity correspond to an averaging over one minute.

Phonon noise. The thermal fluctuation noise (phonon noise) is linked to the existence of thermal conductance connecting two heat baths. It can be described through a noise equivalent power (written down *NEP*) exchanged between these baths. The mathematical formula giving the phonon noise power is [43]:

$$NEP_{ph,j,bi} = \sqrt{4\ k_B\ T^2\ K_{j,bi}} \tag{11}$$

where $K_{j,bi}$ represents the thermal conductance of either nanowires (j) or the suspending beams bi. Therefore, in our measurement platform, there exist two sources of thermal fluctuation noise coming from the exchange of phonons between the membranes and the heat sink, and between the membranes themselves. The numerical calculation using the measured values of thermal conductances gives $NEP_{phonon-j}$= 9.18$\times$ 10^{-20} W/$\sqrt{\text{Hz}}$, and

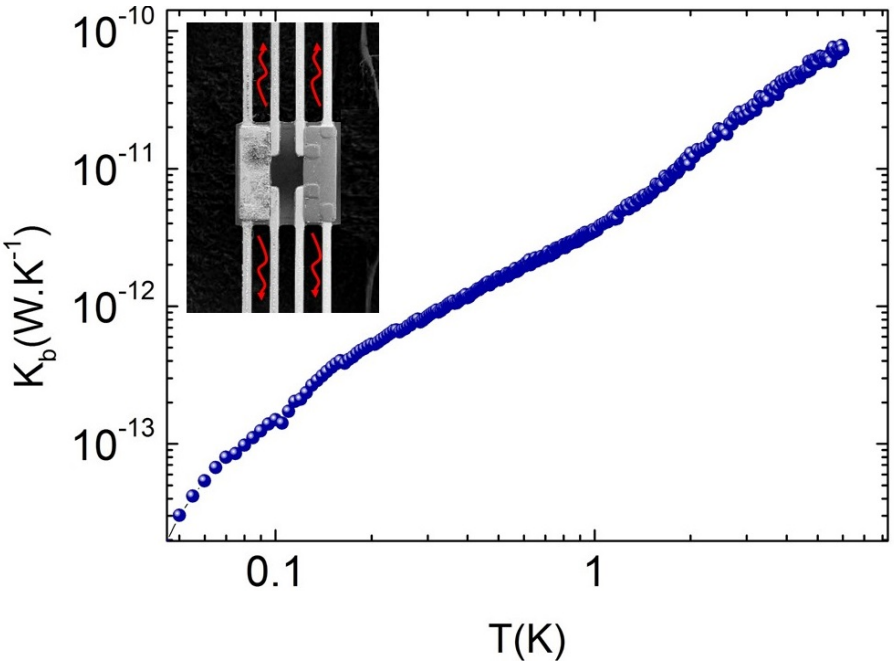

FIG. 8. Measurement of the thermal conductance of the suspending beams K_{b2} of one isolated membrane. In inset, the schematic of the measurement configuration.

$NEP_{phonon-bi}$= 2.73× 10^{-19} W/$\sqrt{\text{Hz}}$. The total NEP_{ph} is equal to:

$$NEP_{ph,total} = \sqrt{\sum_j NEP^2_{ph,j,bi}} \tag{12}$$

$$= \sqrt{NEP^2_{ph,j} + NEP^2_{ph,bi}} \tag{13}$$

The numerical computations give $NEP_{ph,total}$= 0.3 ×10^{-18} W/$\sqrt{\text{Hz}}$. A power smaller than the power sensitivity of the experiment (as shown above). Consequently, the temperature fluctuations created by the exchange of phonons are much smaller than what can be measured in that experiment, then the impact of the phonon noise on the results of the present work can be neglected.

Negligible heat loss by radiation. Experiment at low temperature has a significant difference with room temperature one: the contribution of radiation to the thermal balance becomes progressively negligible as the temperature is lowered. In order to show this, we can estimate the thermal power exchanged between the nanowire and the calorimeter walls:

$$P = \varepsilon\sigma S(T_1^4 - T_0^4) \tag{14}$$

where ε is the emissivity (taken at 1 here), σ is the Stefan-Boltzmann constant and S the surface of exchange between the membrane at temperature T_1 and the calorimeter wall at the temperature T_0. Using Eq. 14, P is estimated to be on the order of 10^{-16} Watt for a temperature gradient of 4 Kelvin, a very small power as compared to the thermal conductance to the heat bath. However, for more secure measurements, a screen has been installed between the sample and the calorimeter walls thermally coupled to the temperature of the baseline. This is reducing significantly the temperature gradient resulting in a power exchange through radiation smaller than 10^{-21} Watt. As a consequence, any parasitic thermal path through radiation heat loss can be excluded in this experiment.

[1] Maldovan, M. Phonon wave interference and thermal bandgap materials. *Nature Mater.* **14**, 667-674 (2014).

[2] Zen, N., Puurtinen, T.A., Isotalo, T.J., Chaudhuri, S., and Maasilta I.J. Engineering thermal conductance using a two-dimensional phononic crystal. *Nature Commun.* **5**, 3435 (2014).

[3] Lee, J. *et al.* Investigation of phonon coherence and backscattering using silicon nanomeshes. *Nature Commun.* **8**, 14054 (2017).

[4] Pendry, J.B. Quantum limits to flow of information and entropy. *J. Phys. A* **16**, 2161-2171 (1983).

[5] Maynard, R. and Akkermans E. Thermal conductance and giant fluctuations in one-dimensional disordered-systems. *Phys. Rev. B* **32**, 5440-5442 (1985).

[6] Angelescu, D.E., Cross, M.C., Roukes, M.L. Heat transport in mesoscopic systems. *Superlatt. Microstruct.* **23**, 673-689 (1998).

[7] Rego, L.G.C. and Kirczenow, G. Quantized thermal conductance of dielectric quantum wires. *Phys. Rev. Lett.* **81**, 232-235 (1998).

[8] Dhar, A, Heat Transport in low-dimensional systems, *Advances in Physics* **57**, 457-537 (2008).

[9] Schwab, K., Henriksen, E. A., Worlock, J. M. and Roukes, M. L. Measurement of the quantum of thermal conductance. *Nature* **404**, 974-977 (2000).

[10] Anghel, D.V. Universality of heat and entropy transport in 1D channels at arbitrary temperature. *Europhys. Lett.* **94**, 60004 (2011).

[11] Das, S.G. and Dhar, A. Landauer formula for phonon heat conduction: relation between

energy transmittance and transmission coefficient. *Eur. Phys. J. B***85**, 372 (2012).

[12] Oh, J.H., Shin, M., and Jang, M.G. Phonon thermal conductivity in silicon nanowires: the effects of the surface roughness at low temperatures. *J. Appl. Phys.* **111**, 044304 (2012).

[13] Käso, M., and Wulf, U. Quantized thermal conductance via phononic heat transport in nanoscale devices at low temperature. *Phys. Rev. B* **89**, 134309 (2014).

[14] Steffen, M., Ansmann, M., McDermott, R., Katz, N., Bialczak, R.C., Lucero, E., Neeley, M., Weig, E.M., Cleland, A.N., and Martinis J.M. State tomography of capacitively shunted phase qubits with high fidelity. *Phys. Rev. Lett.* **97**, 050502 (2006).

[15] Makhlin, Y., Schon, G., Shnirman, A. Quantum-state engineering with Josephson-junction devices. *Rev. Mod. Phys.* **73**, 357-400 (2001).

[16] Jezouin, S. *et al.* Quantum limit of heat flow across a single electronic channel. *Science* **342**, 601-604 (2013).

[17] Mosso, N., Drechsler, U., Menges, F., Nirmalraj, P., Karg, S., Riel, H., and Gotsmann, G. Heat transport through atomic contact. *Nature Nanotech.* **12**, 430-433 (2017).

[18] Cui, L. *et al.* Quantized thermal transport in single-atom junctions. *Science* **335**, 1192-1195 (2017).

[19] Meschke, M., Guichard, W., and Pekola, J.P. Single-mode heat conduction by photons. *Nature* **444**, 187-190 (2006).

[20] Partanen, M., Tan, K.Y., Govenius, J., Lake, R.E., Makela, M.K., Tanttu, T., and Mottonen, M. Quantum-limited heat conduction over macroscopic distances. *Nature Phys.* 12, 460-464 (2016).

[21] Kim, P., Shi, L., Majumdar, A., and McEuen, P.L. Thermal transport measurements of individual multiwalled nanotubes. *Phys. Rev. Lett.* **87**, 215502 (2001).

[22] Landauer, R., *IBM J. Res. Dev.***1**, 223-231 (1957).

[23] Anghel, D.V., Pekola, J.P., Leivo, M.M., Suoknuuti, J.K. and Manninen, M. Properties of the phonon gas in ultrathin membranes at low temperature. *Phys. Rev. Lett.* **81**, 2958-2011 (1998).

[24] Ziman, J.M. *Electrons and Phonons* (Clarendon Press, Oxford, 2001).

[25] Berman, R., Foster, E.L., and Ziman, J.M. Thermal conduction in artificial sapphire crystals at low temperatures. 1. Nearly perfect crystals. *Proc. R. Soc. London, Ser. A* **231**, 130-144 (1955).

[26] Bourgeois, O., *et al.* Reduction of phonon mean free path: From low-temperature physics to room temperature applications in thermoelectricity. *Comptes Rendus Physique* **17**, 1154-1160 (2016).

[27] Bourgeois, O., André, E., Macovei, C., and Chaussy, J. Liquid nitrogen to room-temperature thermometry using niobium nitride thin films. *Rev. Sci. Instrum.* **77**, 126108 (2006).

[28] Wei, J., Olaya, D., Karasik, B.S., Pereverzev, S.V., Sergeev, A.V., Gershenson, M.E. Ultrasensitive hot-electron nanobolometers for terahertz astrophysics, *Nature Nanotech.* **3**, 496â€“500 (2008)

[29] Shi, L., Li, D., Yu, C., Jang, W., Yao, Z., Kim, P., and Majumdar, A. Measuring thermal and thermoelectric properties of one-dimensional nanostructures using a microfabricated device. *J. Heat Transfer* **125**, 881-888 (2003).

[30] Wingert, M.C., Chen, Z.C.Y., Kwon, S., Xiang, J., Chen, R.K. Ultra-sensitive thermal conductance measurement of one-dimensional nanostructures enhanced by differential bridge. *Rev. Sci. Instrum.* **83**, 024901 (2012).

[31] Weathers, A., Bi, K., Pettes, M.T., and Shi, L. Reexamination of thermal transport measurements of a low-thermal conductance nanowire with a suspended micro-device. *Rev. Sci. Instrum.* **84**, 084903 (2013).

[32] Dechaumphai, E., and Chen, R.K. Sub-picowatt resolution calorimetry with niobium nitride thin-film thermometer. *Rev. Sci. Instrum.* **85**, 094903 (2014).

[33] Pohl, R.O., Liu, X., and Thompson, E. Low-temperature thermal conductivity and acoustic attenuation in amorphous solids. *Rev. Mod. Phys.* **74**, 991-1013 (2002).

[34] Zeller, R.C., and Pohl, R.O. Thermal conductivity and specific heat of noncrystallin solids. *Phys. Rev. B* **4**, 2029-2041 (1971).

[35] Phillips, W.A., Tunneling states in amorphous solids. *J. Low Temp. Phys.* **7**, 351-360 (1972).

[36] Anderson, P.W., Halperin, B.I., and Varma, C.M. Anomalous low-temperature thermal properties of glasses and spin glasses. *The Phil. Mag.* **25**, 1-9 (1972).

[37] Tavakoli, A., Blanc, C., Ftouni, H., Lulla, K.J., Fefferman, A.D., Collin, E. and Bourgeois O. Universality of thermal transport in amorphous nanowires at low temperatures. *Phys. Rev. B* **95**, 165411 (2017).

[38] Chalopin, Y., Gillet, J.N., and Volz, S. Predominance of thermal contact resistance in a silicon nanowire on a planar substrate. *Phys. Rev. B* **77**, 233309 (2008).

[39] Tanaka, Y., Yoshida, F., and Tamura, S. Lattice thermal conductance in nanowires at low temperatures: Breakdown and recovery of quantization. *Phys. Rev. B* **71**, 205308 (2005).

[40] Anghel, D.V., Kuhn, T., Galperin, Y.M., Manninen, M., Interaction of two-level systems in amorphous materials with arbitrary phonon fields. *Phys. Rev. B* **75**, 064202 (2007).

[41] Garden, J.-L., *et al.* Thermodynamics of small systems by nanocalorimetry: From physical to biological nano-objects. *Thermochimica Acta* **492**, 16-28 (2009)

[42] We used the Xetch e1 Series from XACTIX technology to process the double membrane measurement platform.

[43] Patton, K.R. On the shot-noise limit of a thermal current. *J. Phys.: Condens. Matter* **20**, 285213(2008).

Universality of thermal transport in amorphous nanowires at low temperatures

Adib Tavakoli, Christophe Blanc, Hossein Ftouni, Kunal J. Lulla, Andrew D. Fefferman, Eddy Collin, and Olivier Bourgeois
Institut NÉEL, CNRS, 25 avenue des Martyrs, F-38042 Grenoble, France
and Université Grenoble Alpes, Institut NÉEL, F-38042 Grenoble, France
(Received 22 November 2016; revised manuscript received 3 March 2017; published 10 April 2017)

Thermal transport properties of amorphous materials at low temperatures are governed by the interaction between phonons and localized excitations referred to as tunneling two-level systems (TLSs). The temperature variation of the thermal conductivity of these amorphous materials is considered as universal and is characterized by a quadratic power law. This is well described by the phenomenological TLS model even though its microscopic explanation is still elusive. Here, by scaling down to the nanometer-scale amorphous systems much below the bulk phonon-TLS mean free path, we probe the robustness of that model in restricted geometry systems. Using very sensitive thermal conductance measurements, we demonstrate that the temperature dependence of the thermal conductance of silicon nitride nanostructures remains mostly quadratic independently of the nanowire section. It does not follow the cubic power law in temperature as expected in a Casimir-Ziman regime of boundary-limited thermal transport. This shows a thermal transport counterintuitively dominated by phonon-TLS interactions and not by phonon boundary scattering in the nanowires. This could be ascribed to an unexpected high density of TLSs on the surfaces which still dominates the phonon diffusion processes at low temperatures and explains why the universal quadratic temperature dependence of thermal conductance still holds for amorphous nanowires.

DOI: 10.1103/PhysRevB.95.165411

Amorphous materials may have significant dispersion in their chemical compositions or their physical structures at the microscopic level. However, at low temperatures, the behavior of the thermal properties of almost all amorphous materials is thought to be universal [1]. These common features include a nearly linear specific heat and a nearly quadratic thermal conductivity in temperature below a few kelvins. As thermal transport is concerned, this universality is not only qualitative but also quantitative; indeed the thermal conductivity of all amorphous materials lies within a factor of twenty in the same order of magnitude called the *glassy range* [2,3]. Despite much theoretical effort, this universality remains poorly understood and its true microscopic origin is still elusive. Nowadays, the most accepted model is based on the presence of tunneling two-level systems (TLSs) involving tunneling between different equilibrium positions of an atom or group of atoms [4–6]. The scatterings of the phonons on these tunneling sites is assumed to be at the origin of the quadratic variation of thermal conductance in temperature. The phonon heat transport is then characterized by the phonon-TLS mean free path (MFP; the distance between two inelastic collisions), which is on the order of a few hundred micrometers.

Phillips suggested that TLSs are likely to form in materials with an open structure and low-coordination regions, and are unlikely in highly dense amorphous systems [4]. Recent experiments give indication of the correlation between the low-density regions, the presence of nanovoids, and the presence of TLSs [7,8]. In the opposite case the different experiments based on hydrogenated Si [9] and ultrastable glasses [10,11] have shown a significant reduction of the TLS density and a tendency to be more crystal-like [10–12]. These results support Phillips' original suggestion. Understanding the origin of these localized excitations (or TLSs) is one of the most challenging problems of modern condensed matter physics at low temperature. Indeed, many questions have been raised concerning their existence [13], their fundamental origins [14], their possible role in the decoherence of quantum entangled states in Josephson quantum bits [15,16], or their noise-producing aspects in superconducting resonators [17]. Probing the phonon-TLS scattering through the measurement of the phonon-TLS MFP in low-dimensional samples (membranes, nanowires) can bring significant insights into the understanding of thermal transport in amorphous materials at the nanoscale.

On another hand, in a dielectric single crystal far below the Debye temperature, the phonon mean free path is set by the phonon-phonon interaction leading to the well known cubic power law in temperature of the thermal conductivity [$\kappa(T) \propto T^3$]. This MFP can be very long at low temperature because the phonon-phonon interactions become less probable. This leads to boundary scattering limited transport called the Casimir-Ziman regime where phonon scattering only appears on the edges of the materials [18–20]. It has been shown recently that, at the nanoscale, the thermal transport in single-crystal silicon nanowires belongs to this regime. Thermal conductance having variation in temperature very close to the expected cubic power law has been found [21–24].

Then, the low-temperature thermal transport in amorphous materials (bulk or very thick film) departs strongly from its single-crystal counterparts by its universal quadratic thermal conductivity [1]. This quadratic variation is the distinctive picture of glassy materials, the bulk phonon MFP being limited by the phonon-TLS inelastic interactions which lie in the range of 20 μm $< \Lambda^{bulk}_{ph-TLS} <$ 200 μm, at 1 K [1,4–6,25]. The present experiments, done on glassy systems of restricted geometries, put into competition the Casimir-Ziman regime where phonons are essentially scattered by the boundaries (characterized by a thermal conductance cubic in temperature) and the amorphous regime where phonons are scattered by TLSs. The main objective of this work is then to probe phonon transport in spatially confined systems at the nanoscale, i.e., below the characteristic length set by the bulk phonon-TLS

MFP in amorphous materials Λ_{ph-TLS}^{bulk}. This should yield crucial insights on the location and maybe on the origin of the TLS in glasses.

Here, we carried out very sensitive thermal conductance measurements on silicon nitride nanostructures at low temperatures. The samples have various dimensions from millimeter membrane to micro- and nanowires, where the sizes are purposely much smaller than the bulk phonon MFP in amorphous materials (set by the phonon-TLS interactions). As silicon nitride is known to be a fully amorphous material, widely used for its exceptional mechanical and thermal properties [26–32], it is one of the best materials to study the competition between phonon boundary scattering and phonon-TLS interactions playing a significant role in the thermal transport.

The low-temperature thermal properties of Si_3N_4 have been already studied by different groups without considering the possible contribution of TLSs to the phonon scattering [30,33–35]; however, a little later the problem was raised by two theoretical works [36–39]. The present experiments will allow the probing of (1) the phonon-TLS interaction down to the nanometer scale and (2) its effect on the power law of the variation of thermal conductance versus temperature. Unexpectedly, as the Casimir-Ziman regime should be observed in nanowires through the T^3 behavior of $\kappa(T)$, a robust T^2 is observed, showing that even in restricted geometry, the phonon-TLS scattering is still governing the heat transport.

The thermal conductance measurements have been performed on 100 nm thick mechanically suspended stoichiometric Si_3N_4 structures from the millimeter scale (membrane) to the nanometer scale (nanowire) in order to cross the characteristic length given by Λ_{ph-TLS}^{bulk} (see Fig. 1). Various 3ω methods adapted to each geometry have been used; these different techniques have been already explained elsewhere [40–42]. All thermal measurements are done using a niobium nitride (NbN) thermometry very sensitive over a broad temperature range (from 0.1 K to 330 K) [43]. The thermal conductance of the micro- and nanowires is measured using the longitudinal 3ω technique where the heat flow is along the NbN transducer [see Fig. 1(a)]. Concerning the membrane, 3ω-Volklein geometry is used; in this technique the heat flow is perpendicular to the transducer since this one is deposited in the center of the membrane [along the long side; see Fig. 1(b)]. Four geometries of suspended structures have been used for that purpose; all the dimensions of samples are summarized in Table I.

In Fig. 2(a) the thermal conductance of the nanowire, the microwires, and the membrane is shown in a log-log plot. The first point that needs to be highlighted is the similar quadratic temperature behavior for all the different samples with a thermal conductance proportional to $T^{1.5}$ to T^2. It is in agreement with the universal behavior of glasses $T^{1.8}$, but far from the cubic behavior expected for the Casimir-Ziman regime [1,2]. Quantitatively, the conductance of the nanowire is almost two orders of magnitude below the conductance of the narrow microwire, and six orders of magnitude below the conductance of the membrane. This is the consequence of several concomitant effects: the reduction of the geometry (boundary scattering) and the reduction of the phonon MFP due to phonon-TLS interaction that both limit the heat transport.

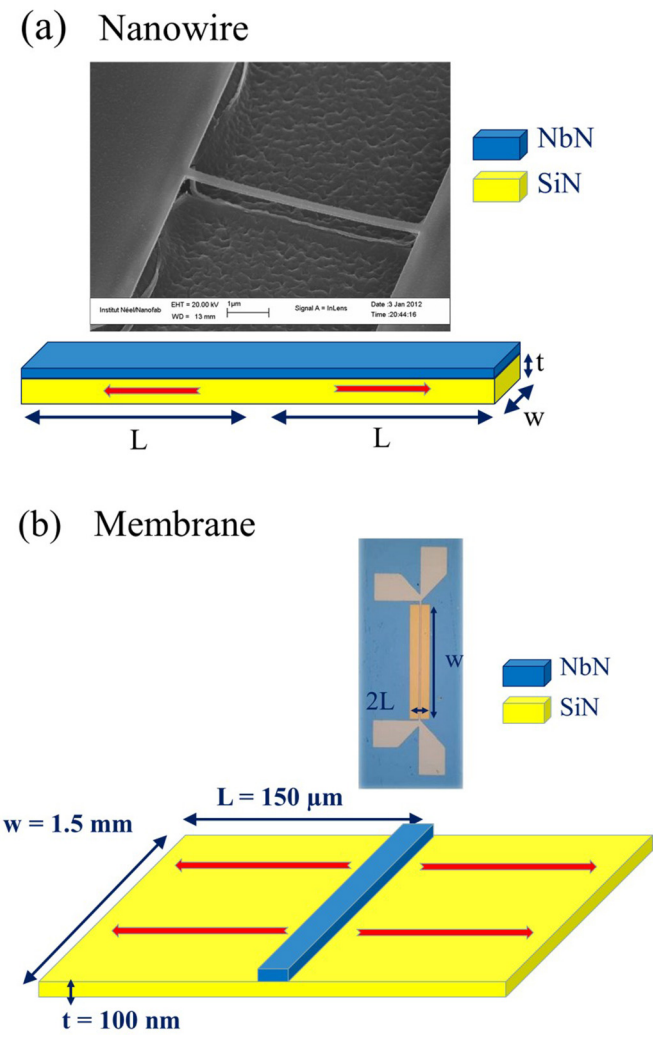

FIG. 1. Pictures and schematic representations of the various Si_3N_4 suspended structures. The red arrows represent the heat flux, the blue arrows, the dimensions of these samples. (a) Suspended silicon nitride nanowire measured with the longitudinal 3ω method [40] (the microwires are not shown) and (b) experimental configuration of the silicon nitride membrane measured using the planar 3ω-Volklein method [41,42]. The blue layer represents the niobium nitride (NbN), the thin film transducer used for the thermal measurements.

TABLE I. Details of the dimensions of the four different kinds of samples made out of Si_3N_4 thin films: sample types and their width and length (all samples are 100 nm thick). The NbN thermometer is 70 nm thick. The membrane is considered as a semi-infinite sample (very large aspect ratio), and three samples are reduced in dimensions: large and narrow microwires and nanowires. More than three orders of magnitude in sizes are covered by these four samples. The coefficients ζ_0 and Λ_{ph}^{1K}, extracted from the thermal conductivity measurements at 1 K, are necessary for the interpretation of the results.

Sample type	w	L (μm)	ζ_0 (W K^{-3} m^{-1})	Λ_{ph}^{1K} (μm)
membrane	1.5 mm	150	1.2×10^{-2}	31
large microwire	7 μm	50	9×10^{-3}	27
narrow microwire	1 μm	10	3×10^{-4}	0.9
nanowire	200 nm	2.5	1.2×10^{-4}	0.36

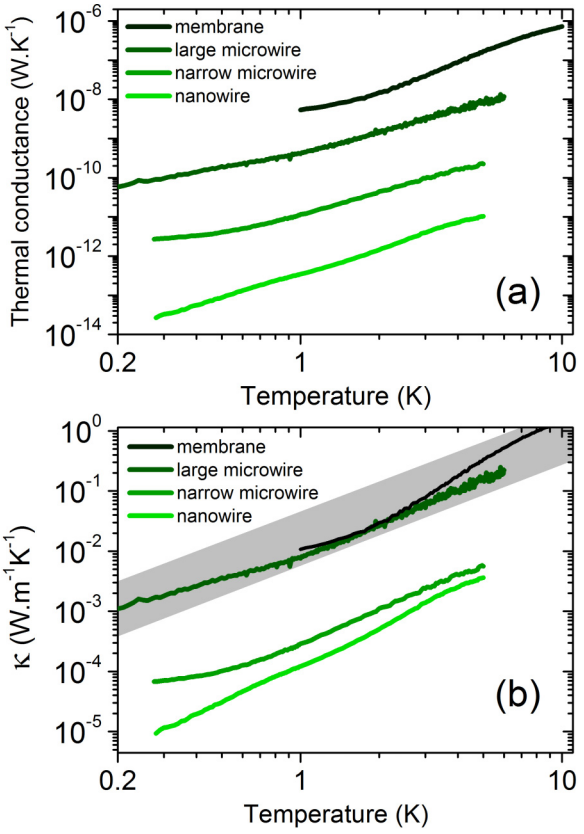

FIG. 2. (a) The thermal conductance of the membrane (black), the large microwire (dark green), the narrow microwire (green), and the nanowire (light green) is shown in a log-log plot. The overall temperature behavior of the thermal conductance of all these samples is quite similar. (b) Effective thermal conductivities calculated as a base for comparison of phonon thermal transport between the different geometries. As the dimensions are reduced, the thermal conductivities decrease. The glassy range is represented by the gray area in the plot.

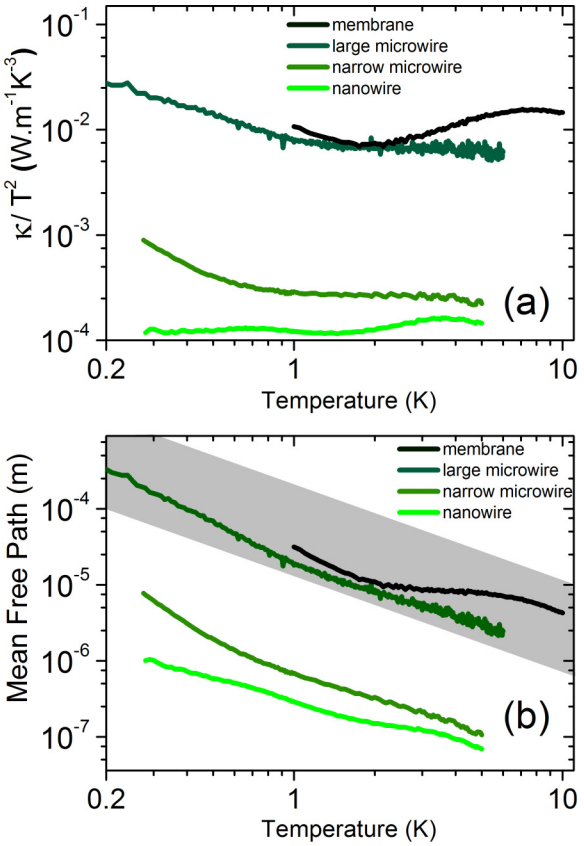

FIG. 3. (a) The thermal conductivity normalized to the square of the temperature (κ/T^2) in a log-log scale. (b) The phonon mean free path of the nanowire extracted from Eq. (3). The mean free paths decrease significantly as the size of the conductor is decreased, a clear signature of the impact of the low dimensions of the samples on the heat transport. The glassy range delimited by the gray area represents the maximum or minimum of the mean free path measured in bulk amorphous materials (see Ref. [1]).

In order to go deeper in the discussion and compare the dimensional reduction and TLS effects on phonon scattering on the thermal transport, one needs to report on thermal conductance normalized to length and widths [44]. This is done by calculating the thermal conductivity κ through the regular expression $\kappa = \frac{KL}{tw}$, where K is the measured thermal conductance, t the thickness of the materials, and w the width. This is shown in Fig. 2(b) where, for the same amorphous materials Si_3N_4, the thermal conductivities vary significantly from one geometry to the other, decreasing when the section of the heat conductor decreases. This illustrates the fact that the phonon transport is limited by boundary scatterings at low temperature, the so-called Casimir-Ziman regime of heat transport [18,19].

Deciphering the intrinsic mechanisms responsible for the heat transport implies obtaining the most relevant parameter: the phonon mean free path. In order to extract that crucial physical parameter from our measurements, one uses the phenomenological approach developed by Pohl, Liu, and Thompson [1] to interpret the thermal conductivity data obtained on bulk amorphous materials. The authors combine the well known kinetic relation $\kappa = \frac{1}{3} c_D v_s \Lambda_{ph}$ perfectly valid at low temperature (as long as ballistic transport is not involved) with the fact that the thermal conductivity κ is proportional to the square of the temperature as illustrated in Fig. 3(a):

$$\kappa(T) = \zeta_0 T^2 = \tfrac{1}{3} c_D v_s \Lambda_{ph}, \qquad (1)$$

where ζ_0 is a phenomenological proportionality factor equal to the thermal conductivity κ at 1 K; c_D is the volumetric specific heat of the phonons carrying heat; v_s is the average speed of sound, which is 9900 m/s in silicon nitride; and Λ_{ph} is the phonon MFP independent of dimensions. ζ_0 can be estimated through the TLS model; however this is not required for the determination of the phonon MFP. Indeed $\zeta_0 = \kappa_{T=1\mathrm{K}}$, then directly extracted from the experiments.

One important fact should be clarified in this approach: one needs to know the specific heat c_D related to phonons that are carrying heat. This should not be mixed up with the experimental specific heat of amorphous materials mostly dominated by the tunneling states [1]. By using the Debye model for estimating c_D, very good agreement is obtained between experiments and calculations for temperatures down

to 1 K as demonstrated by Pohl *et al.* [2,45]. Similarly here we use the regular Debye expression at low temperature as the input for the specific heat:

$$c_D = \frac{2}{5}\frac{k_B^4}{\hbar^3}\frac{\pi^2}{v_s^3}T^3. \tag{2}$$

When combining Eq. (1) and Eq. (2) the phonon MFP can then be expressed by

$$\Lambda_{ph} = \frac{15\hbar^3 v_s^2}{2\pi^2 k_B^4}\frac{\kappa(T)}{T^3}. \tag{3}$$

One can see in Eq. (3) that the MFP is given, not only by the temperature and the speed of sound, but also by the thermal conductivity as function of temperature. So, by measuring thermal conductivity one can have a direct experimental determination of the MFP as a function of the different sections of heat conductors. In our analysis, as shown in Fig. 3(a), we have first checked that the proportionality $\kappa \propto T^2$ is still valid even at the nanometer scale. Then, we have extracted the phonon MFP using Eq. (3); the results are presented in Fig. 3(b).

Two different limits are observed for the phonon MFP depending on the size of the samples. The first concerns the large systems (membrane and large microwire) for which the MFP lies in the glassy limit given by the gray area in Fig. 3(b). This glassy range is defined as the minimum or maximum MFP experimentally obtained on bulk amorphous materials. So concerning the large samples, we can conclude that the thermal transport is similar to what happens in bulk materials. On the other hand, for the small section samples, smaller phonon MFPs are clearly observed as if they were set by the interaction with the surfaces as expected in the Casimir-Ziman regime. The increase of MFP in narrow microwire and nanowire at low temperature is interpreted as the signature of specular reflections of phonons on the wire boundaries. When specular reflections are involved in the thermal transport, the temperature variation of the MFP is generally well described in the framework of the Berman-Foster-Ziman (BFZ) model of phonon boundary scattering using the sole physical roughness of the surfaces as a fitting parameter [20].

The phonon scattering on the boundaries may have two possible origins, either from the actual asperity (physical roughness) of the nanowires or due to the presence of TLSs on the surface. We will then calculate an *effective roughness* η_{eff} of the nanowire from the experimental phonon MFP variation with temperature and compare it to the roughness estimated from the scanning electron microscopy image (SEM). That effective roughness will be representative of all the phonon scattering processes: scattering on boundaries characterized by the actual physical roughness (asperity) and the scattering of phonons on TLSs.

To obtain the effective roughness for the nanostructures, we first extract the probability of specular reflection $p(\lambda,\eta) = \exp(-16\pi^3\eta^2/\lambda^2)$ where η is the roughness of the nanowire's edges, and λ is the dominant phonon wavelength. To do that, we equal the experimental MFP to the MFP calculated from the BFZ model [20]:

$$\Lambda_{ph} = \frac{1 + p_{exp}(\lambda,\eta)}{1 - p_{exp}(\lambda,\eta)}\Lambda_{Cas}. \tag{4}$$

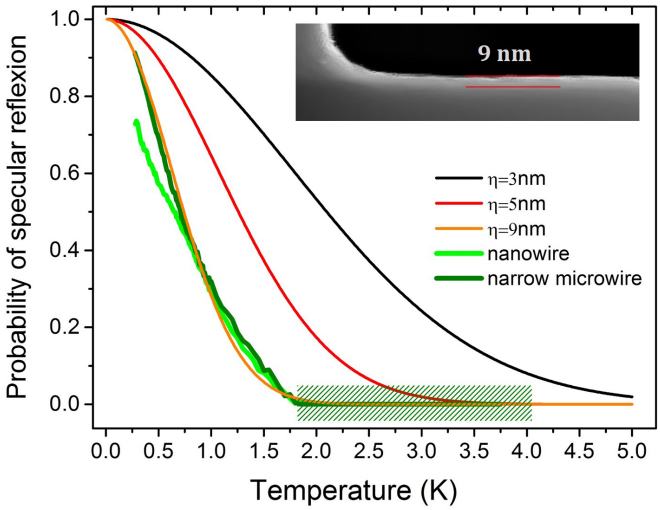

FIG. 4. Extracted probability of specular reflection for the nanowire (light green) and the narrow microwire (dark green) in comparison to the theoretical fit from the Ziman approach using Eq. (5) with different roughness. The hatched area shows a purely diffusive regime known as the Casimir regime where the MFP becomes equal to the diameter of the nanostructure. In the inset, an SEM picture of the SiN nanowire edge is shown. The actual roughness is much smaller than 9 nm.

$\Lambda_{Cas} = 1.12\sqrt{w \times t}$ is the Casimir MFP, where $w \times t$ is the section of the nanosystems. So the experimental probability of specular reflection can be obtained from Eq. (4) through

$$p_{exp} = \frac{\Lambda_{ph} - \Lambda_{Cas}}{\Lambda_{ph} + \Lambda_{Cas}}. \tag{5}$$

Λ_{ph} is the experimental MFP as calculated through Eq. (3) from the thermal conductance.

The experimental probability of specular reflection for narrow microwires and nanowires is illustrated in Fig. 4 as extracted from Eq. (5), in comparison with theoretical fits for different roughness. The fits help us to estimate this *effective roughness* η_{eff} that can be compared to the mean roughness obtained from the SEM characterization of the nanowire. The roughness that fits the experimental probability of specular reflection is of the order of $\eta_{eff} \cong 9$ nm three times bigger than the one evaluated by SEM observation which is about $\eta \cong 3 \pm 1$ nm (see inset of Fig. 4). This excess of roughness is attributed to TLSs that act on the surfaces as an artificial roughness, meaning that phonon-surface TLS scattering dominates the heat transport. This is indeed fully consistent with the quadratic temperature variation of the thermal conductance [46].

To conclude, we show that for amorphous nanowires the temperature variation of the thermal conductance is still quadratic, even if it would have been expected that in restricted geometry the behavior of thermal conductance would be cubic-like in the Casimir-Ziman regime (boundary scattering limit). This is ascribed to the presence of a strong density of phonon scattering centers located on the surface as seen in the study of the effective roughness obtained from the phonon mean free path. A possible high density of TLSs can explain this observation which is in good agreement

with the quadratic variation of $\kappa(T)$. Actually, the TLSs are expected to form in nanovoids or low-density regions which are sensitive to preparation methods (temperature growth and thickness) of the materials [7–10]. This means that, especially for thin films, the presence of voids in volume is less probable than on the surfaces. Consequently, the TLSs may indeed be concentrated on the surfaces in agreement with our experimental observations [8].

Both results (quadraticity and phonon MFP) show the robustness of the universality of thermal transport in amorphous materials even down to the nanometer scale. The high density of TLSs may have significant consequences for dissipation processes and decoherence phenomena in quantum nano-electromechanical systems made out of amorphous SiN [26,47,48]. Further experimental proofs of the high density of TLSs on the surface could be obtained by specific heat measurements on low-dimensional amorphous systems such as very thin membranes at very low temperature or by nano-electromechanical measurement at very low temperature (below 10 mK). An abnormally high TLS density would be revealed by an anomalously high surface specific heat.

ACKNOWLEDGMENTS

We thank the micro- and nanofabrication facilities of Institut Néel CNRS—the Pole Capteurs Thermométriques et Calorimétrie (E. André, P. Lachkar, G. Moiroux, and J.-L. Garden) and Nanofab (T. Crozes, S. Dufresnes, B. Fernandez, T. Fournier, G. Julié, and J.-F. Motte)—for their advice in the preparation of the samples. O.B. and E.C. acknowledge financial support from the ANR project QNM Grant No. 040401 and the European projects MicroKelvin EUFRP7 Grant No. 228464 and (O.B.) MERGING Grant No. 309150.

[1] R. O. Pohl, X. Liu, and E. Thompson, Rev. Mod. Phys. **74**, 991 (2002).
[2] R. C. Zeller and R. O. Pohl, Phys. Rev. B **4**, 2029 (1971).
[3] R. B. Stephens, Phys. Rev. B **8**, 2896 (1973).
[4] W. A. Phillips, J. Low Temp. Phys. **7**, 351 (1972).
[5] P. W. Anderson, B. I. Halperin, and C. M. Varma, Philos. Mag. **25**, 1 (1972).
[6] M. P. Zaitlin and P. W. Anderson, Phys. Rev. B **12**, 4475 (1975).
[7] D. R. Queen, X. Liu, J. Karel, T. H. Metcalf, and F. Hellman, Phys. Rev. Lett. **110**, 135901 (2013).
[8] D. R. Queen, X. Liu, J. Karel, T. H. Metcalf, and F. Hellman, J. Non-Cryst. Solids **426**, 19 (2015).
[9] X. Liu, B. E. White Jr., R. O. Pohl, E. Iwanizcko, K. M. Jones, A. H. Mahan, B. N. Nelson, R. S. Crandall, and S. Veprek, Phys. Rev. Lett. **78**, 4418 (1997).
[10] X. Liu, D. R. Queen, T. H. Metcalf, J. E. Karel, and F. Hellman, Phys. Rev. Lett. **113**, 025503 (2014).
[11] T. Perez-Castaneda, C. Rodriguez-Tinoco, J. Rodriguez-Viejo, and M. A. Ramos, Proc. Natl. Acad. Sci. U.S.A. **111**, 11275 (2014).
[12] X. Liu, D. R. Queen, T. H. Metcalf, J. E. Karel, and F. Hellman, Arch. Metall. Mater. **60**, 359 (2015).
[13] A. J. Leggett, Physica B **169**, 322 (1991).
[14] A. J. Leggett and D. C. Vural, J. Phys. Chem. B **117**, 12966 (2013).
[15] L. C. Ku and C. C. Yu, Phys. Rev. B **72**, 024526 (2005).
[16] R. W. Simmonds, K. M. Lang, D. A. Hite, S. Nam, D. P. Pappas, and J. M. Martinis, Phys. Rev. Lett. **93**, 077003 (2004).
[17] J. Gao, J. Zmuidzinas, B. A. Mazin, H. G. LeDuc, and P. K. Day, Appl. Phys. Lett. **90**, 102507 (2007).
[18] H. B. G. Casimir, Physica (Amsterdam) **5**, 495 (1938).
[19] J. M. Ziman, *Electrons and Phonons* (Clarendon Press, Oxford, 2001).
[20] R. Berman, E. L. Foster, and J. M. Ziman, Proc. R. Soc. London, Ser. A **231**, 130 (1955).
[21] J. S. Heron, T. Fournier, N. Mingo, and O. Bourgeois, Nano Lett. **9**, 1861 (2009).
[22] J. S. Heron, T. Fournier, N. Mingo, and O. Bourgeois, Nano Lett. **10**, 2288 (2010).
[23] J. S. Heron, C. Bera, T. Fournier, N. Mingo, and O. Bourgeois, Phys. Rev. B **82**, 155458 (2010).
[24] C. Blanc, J.-S. Heron, T. Fournier, and O. Bourgeois, Appl. Phys. Lett. **105**, 043106 (2014).
[25] C. C. Yu and J. J. Freeman, Phys. Rev. B **36**, 7620 (1987).
[26] D. R. Southworth, R. A. Barton, S. S. Verbridge, B. Ilic, A. D. Fefferman, H. G. Craighead, and J. M. Parpia, Phys. Rev. Lett. **102**, 225503 (2009).
[27] Q. P. Unterreithmeier, T. Faust, and J. P. Kotthaus, Phys. Rev. Lett. **105**, 027205 (2010).
[28] B. L. Zink and F. Hellman, Solid State Commun. **129**, 199 (2004).
[29] D. R. Queen and F. Hellman, Rev. Sci. Instrum. **80**, 063901 (2009).
[30] M. M. Leivo and J. P. Pekola, Appl. Phys. Lett. **72**, 1305 (1998).
[31] D. J. Goldie, A. V. Velichko, D. M. Glowacka, and S. Withington, J. Appl. Phys. **109**, 084507 (2011).
[32] N. Zen, T. A. Puurtinen, T. J. Isotalo, S. Chaudhuri, and I. J. Maasilta, Nat. Commun. **5**, 3435 (2014).
[33] D. V. Anghel, J. P. Pekola, M. M. Leivo, J. K. Suoknuuti, and M. Manninen, Phys. Rev. Lett. **81**, 2958 (1998).
[34] W. Holmes, J. M. Gildemeister, and P. L. Richards, Appl. Phys. Lett. **72**, 2250 (1998).
[35] H. F. C. Hoevers, M. L. Ridder, A. Germeau, M. P. Bruijn, P. A. J. de Korte, and R. J. Wiegerink, Appl. Phys. Lett. **86**, 251903 (2005).
[36] D. V. Anghel, T. Kühn, Y. M. Galperin, and M. Manninen, Phys. Rev. B **75**, 064202 (2007).
[37] T. Kühn, D. V. Anghel, Y. M. Galperin, and M. Manninen, Phys. Rev. B **76**, 165425 (2007).
[38] S. Withington, D. J. Goldie, and A. V. Velichko, Phys. Rev. B **83**, 195418 (2011).
[39] S. Withington and D. J. Goldie, Phys. Rev. B **87**, 205442 (2013).
[40] O. Bourgeois, T. Fournier, and J. Chaussy, J. Appl. Phys. **101**, 016104 (2007).
[41] A. Sikora, H. Ftouni, J. Richard, C. Hébert, D. Eon, F. Omnès, and O. Bourgeois, Rev. Sci. Instrum. **83**, 054902 (2012).

[42] A. Sikora, H. Ftouni, J. Richard, C. Hébert, D. Eon, F. Omnès, and O. Bourgeois, Rev. Sci. Instrum. **84**, 029901 (2013).

[43] O. Bourgeois, E. André, C. Macovei, and J. Chaussy, Rev. Sci. Instrum. **77**, 126108 (2006).

[44] In the Casimir regime of heat transport, the calculated thermal conductivity κ is meaningful only when comparing thermal transport between different sizes of samples of the same materials. Indeed, since the phonon MFP changes with the reduction of size in the case of nanostructured samples, the absolute value of thermal conductivity is not a relevant parameter.

[45] P. D. Vu, J. R. Olson, and R. O. Pohl, J. Low Temp. Phys. **113**, 123 (1998).

[46] We did not do the same data treatment to the two largest samples (microwire and membrane) because they belong to the quasi-bulk-limit for which the Berman-Foster-Ziman model may not fully apply.

[47] M. Defoort, K. J. Lulla, C. Blanc, H. Ftouni, O. Bourgeois, and E. Collin, J. Low Temp. Phys. **171**, 731 (2013).

[48] O. Maillet, F. Vavrek, A. D. Fefferman, O. Bourgeois, and E. Collin, New J. Phys. **18**, 073022 (2016).

C. R. Physique ••• (••••) •••–•••

Contents lists available at ScienceDirect

Comptes Rendus Physique

www.sciencedirect.com

Thermoelectric mesoscopic phenomena / Phénomènes thermoélectriques mésoscopiques

Reduction of phonon mean free path: From low-temperature physics to room temperature applications in thermoelectricity

Reduction du libre parcours moyen des phonons : de la physique des basses températures aux applications en thermoélectricité à l'ambiante

Olivier Bourgeois [a,b,*], Dimitri Tainoff [a,b], Adib Tavakoli [a,b], Yanqing Liu [a,b], Christophe Blanc [a,b], Mustapha Boukhari [c], André Barski [c], Emmanuel Hadji [c]

[a] *Institut Néel, CNRS, 25, avenue des Martyrs, 38042 Grenoble, France*
[b] *Université Grenoble Alpes, Inst Néel, 38042 Grenoble, France*
[c] *Institut Nanosciences et Cryogénie, SP2M, CEA-UJF, 17, rue des Martyrs, 38054 Grenoble, France*

ARTICLE INFO

Article history:
Available online xxxx

Keywords:
Phonon
Thermal transport
Thermoelectricity
Semiconductor
Nanowire
Inclusions

Mots-clés :
Phonon
Transport thermique
Thermoélectricité
Semiconducteur
Nanofil
Inclusions

ABSTRACT

It has been proposed for a long time now that the reduction of the thermal conductivity by reducing the phonon mean free path is one of the best way to improve the current performance of thermoelectrics. By measuring the thermal conductance and thermal conductivity of nanowires and thin films, we show different ways of increasing the phonon scattering from low-temperature up to room-temperature experiments. It is shown that playing with the geometry (constriction, periodic structures, nano-inclusions), from the ballistic to the diffusive limit, the phonon thermal transport can be severely altered in single crystalline semiconducting structures; the phonon mean free path is in consequence reduced. The diverse implications on thermoelectric properties will be eventually discussed.

RÉSUMÉ

Il a été proposé depuis longtemps maintenant que diminuer la conductivité thermique en réduisant le libre parcours moyen des phonons est une des meilleures façons d'améliorer les performances actuelles des matériaux thermoélectriques. En mesurant la conductance thermique et la conductivité thermique de nanofils et de couches minces, nous montrons différentes manières d'augmenter la diffusion des phonons des basses températures jusqu'à la température ambiante. Il est montré qu'en jouant sur la géométrie (constriction, structures périodiques, nano-inclusions), à partir de la limite balistique jusqu'à la limite diffusive, le transport thermique phononique peut être altéré de façon significative dans des structures monocristallines semiconductrices, le libre parcours moyen

* Corresponding author.
E-mail address: olivier.bourgeois@neel.cnrs.fr (O. Bourgeois).

http://dx.doi.org/10.1016/j.crhy.2016.08.008

Please cite this article in press as: O. Bourgeois et al., Reduction of phonon mean free path: From low-temperature physics to room temperature applications in thermoelectricity, C. R. Physique (2016), http://dx.doi.org/10.1016/j.crhy.2016.08.008

des phonons étant réduit en conséquence. Enfin, les diverses implications sur les propriétés thermoélectriques seront discutées.

1. Introduction

In the two last decades, materials structured at the nanoscale to have low thermal conductivity have attracted a lot of attention, due to their high-potential thermoelectric applications [1–4]. Indeed, as proposed by Dresselhaus et al. in 1993, nanostructuration can significantly improve the thermoelectric efficiency [5,6]. This efficiency of thermoelectric materials is given by the dimensionless figure of merit $ZT = S^2T\sigma/k$, where S is the Seebeck coefficient, σ the electrical conductivity, and k the thermal conductivity. If we focus only on the thermal properties, ZT will be increased by reducing the phonon thermal transport. This reflects the fact that the heat source and the cold source must be as thermally isolated as possible to prevent too much heat leaking, as that will degrade the overall performances of the thermoelectric modules.

For electrons, the thermal and the electronic properties are coupled through the Wiedemann–Franz law. Thus, the only way of reducing the thermal transport is to reduce the *phonon* thermal conductivity. Two major directions are available to act on the phonon properties: incoherent and coherent effects. On the one hand, incoherent effects are ruled by the phonon mean free path (MFP), then the reduction is obtained by adding scattering centers, by reducing the size, having rough surface or by adding nano-inclusions. On the other hand, coherent effects will manifest themselves through the reduction of the group velocity (band flattening), opening of band gaps or having destructive interferences. Two significant length scales govern phonon physics, involving incoherent or coherent effects: the phonon mean free path (Λ) and the dominant phonon wavelength given by:

$$\lambda_{\mathrm{dom}} = \frac{h v_s}{2.82 k_B T} \tag{1}$$

where h the Planck constant, k_B the Boltzmann constant and v_s is the speed of sound. This length is indeed temperature dependent, increasing as the temperature decreases (see Fig. 1).

Here, we will focus our attention on the experimental attempts to reduce the phonon mean free path in single-crystal semiconducting materials by playing with the geometry of its surface or with its internal structure. Other means based on coherent effects will be discussed at the end of the paper. There are actually two complementary approaches to realizing an efficient phonon engineering at the nanoscale: the top–down one based on e-beam lithography to make small structures like nanowire and membrane, and the second one, the bottom–up, generally based on specific growth of nanostuctured materials (bulk or nanowire) using for instance molecular beam epitaxy (MBE).

These two important limits will be experimentally addressed in this paper summarizing the recent findings of our group: the low-temperature one set by boundary scattering limit where both important lengths (Λ and λ_{dom}) play a role and the room temperature limit, where for the time being only the mean free path can be engineered efficiently.

2. Towards the ballistic limit: thermal transport in Si nanowires

In low-dimensional systems, the surface scattering of phonons plays a crucial role in the understanding of thermal transport [7–9]. The so-called Casimir regime occurs when the bulk phonon MFP is much bigger than the actual size of the

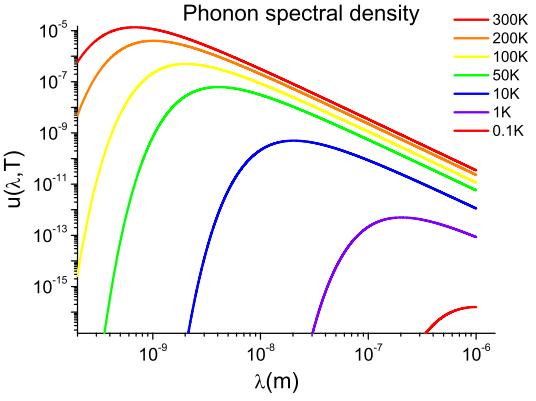

Fig. 1. Phonon spectral density as a function of the wavelength for different equilibrium temperatures of a black body. The dominant phonon wavelength for each temperature corresponds to the maximum of the curves. Typically, the dominant phonon wavelength is of the order of 1 nm at 300 K and 100 nm around 1 K.

Please cite this article in press as: O. Bourgeois et al., Reduction of phonon mean free path: From low-temperature physics to room temperature applications in thermoelectricity, C. R. Physique (2016), http://dx.doi.org/10.1016/j.crhy.2016.08.008

relevant length scales	transport regime	models	relevant formulae
λ_{dom} (T) < Λ_{ph} (T) < L	Diffusive regime (incoherent)	Kinetic model	$K = \frac{1}{3} C \upsilon_s \Lambda_{ph}$
λ_{dom} (T) < L ~ Λ_{ph} < $\Lambda_{ph\text{-}bulk}$	Casimir regime (incoherent)	Casimir model	$K_{Cas} = \beta \Lambda_{Cas} T^3$
λ_{dom} (T) ~ L < Λ_{ph}	Ziman regime (partly coherent)	Ziman model	$\Lambda_{ph} = \frac{1+p}{1-p} \Lambda_{Cas}$
L < λ_{dom} (T) < Λ_{ph}	Ballistic regime (coherent)	Landauer model	$T = \frac{1}{1 + 3L/4\Lambda_{eff}}$

Fig. 2. Classification of the different regimes of phonon transport in nanoscaled systems at low enough temperature, typically below 30 K for silicon. L is the sample length, Λ_{ph} is the inelastic phonon mean free path, and λ_{dom} the dominant phonon wavelength. Concerning the Landauer limit, the parameter T denotes the transmission coefficient between a nanowire and its heat reservoir. Other important lengths are explained in the text.

nanosystem under study. In that case, the phonon MFP is only set by the scattering on the surfaces. This limit is reached at low enough temperature when other scattering mechanisms do not dominate (phonon–phonon interaction, electron–phonon interaction, scattering on impurities etc.). As a result, effects linked to surface roughness have a significant impact on phonon transport [10,11]. These effects can be simple incoherent scattering when the phonon wavelength is much bigger than the mean asperity or, as the temperature is lowered, may become wavelength dependent. Indeed, if the wavelength is bigger than the mean roughness, specular reflections of phonons may occur on the surface. If elastic scattering is involved, the energy is conserved, leading to an increase in the MFP.

2.1. Normal phonon transport in Si nanowires at low temperature

In order to understand the thermal transport at low temperature, a summary of the Casimir and Ziman models is necessary. In the Casimir model, [7,9], the thermal conductance is given by:

$$K_{\mathrm{Cas}} = 3.2 \times 10^3 \left(\frac{2\pi^2 k_{\mathrm{B}}^4}{5\hbar^3 v_{\mathrm{s}}^3} \right)^{(2/3)} \frac{e \times w \Lambda_{\mathrm{Cas}}}{L} T^3 = \beta_{\mathrm{Cas}} T^3 \tag{2}$$

where k_{B} is the Boltzmann constant, $\hbar$ the Planck constant and v_{s} refers to the sound velocity. $\Lambda_{\mathrm{Cas}} = 1.12\sqrt{e \times w}$ is the Casimir MFP of the phonons in a nanowire having a rectangular section, e refers to the thickness and w to the average width of the nanowire; L is its length. This formula is obtained when the mean free path of phonons is only limited by the cross-section of the wire, i.e. by boundary scattering. Indeed, in this limit, each phonon hitting the rough surface is assumed to be absorbed an re-emitted in all direction and energy following the black body radiation law (see Fig. 1). In other words, in this Casimir limit, the surface is considered as infinitely rough whatever the phonon wavelength.

As the temperature is lowered, the dominant phonon wavelength actually grows (see Eq. (1)) and becomes eventually larger than the roughness amplitude; then specular reflections become more probable and cannot be neglected like in the Casimir model. To take this trend into account, the Casimir mean free path should be replaced in Eq. (2) by an effective MFP Λ_{eff}, as proposed by Ziman and colleagues [8,9]:

$$\Lambda_{\mathrm{eff}} = \frac{1+p}{1-p} \Lambda_{\mathrm{Cas}} \tag{3}$$

where p is the parameter describing the probability for a phonon to be specularly reflected at the surfaces. The value of this parameter will depend on both the wavelength of the phonons and the roughness of the wire surface. The Casimir purely diffusive case is given by $p = 0$ and the purely specular one, when $p = 1$, will be referred to as the ballistic limit; the MFP is diverging to infinite. The Ziman model takes into account a value for p that is different from zero; as the temperature is lowered, the phonon mean free path can be bigger than the section of the nanowire. The different phonon transport regimes and their associated models are summarized in the Table given in Fig. 2.

As a conclusion, the thermal transport in silicon nanowires having a section of 100 nm will be well described by the Casimir model, and then at lower temperature by the Ziman model, as it will be seen in the next section. Indeed, the length L is smaller than the bulk phonon mean free path $\Lambda_{\mathrm{ph-bulk}}$ in Si, and on the same order of magnitude as the dominant phonon wavelength. At even lower temperature, the fully ballistic limit should be described by a Landauer-type model where the thermal transport is given by transmission coefficients between the nanowire and the heat bath. This goes clearly beyond our focus in this paper; there is currently no experimental data in this regime.

Please cite this article in press as: O. Bourgeois et al., Reduction of phonon mean free path: From low-temperature physics to room temperature applications in thermoelectricity, C. R. Physique (2016), http://dx.doi.org/10.1016/j.crhy.2016.08.008

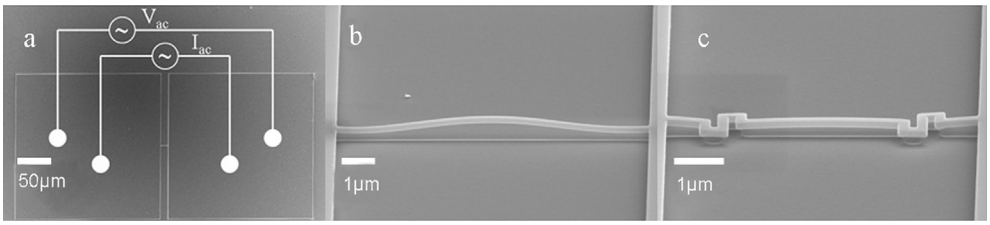

Fig. 3. A SEM images of: a) a suspended nanowire linked to the two pads where the electrical connections permit the 3ω measurements; b) a straight nanowire c) corresponds to the side view of a S-shaped nanowire.

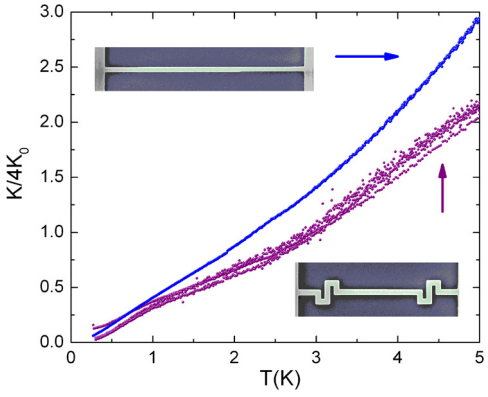

Fig. 4. Thermal conductance of 5 µm long nanowires normalized to four times the universal value of thermal conductance versus temperature. The thermal conductance of the straight nanowire is much bigger than the thermal conductance of the S-shape nanowires. The presence of the serpentine section stops the transmission of ballistic phonons, reducing the overall phonon mean free path.

2.2. Phonon blocking with S-shaped chicanes in Si nanowires

We will illustrate in the following section these different scatterings and phonon transport regimes in three situations: firstly the thermal transport in a normal straight silicon nanowire, secondly in a Si nanowire having S-shaped chicanes, and thirdly in Si nanowires with engineered surfaces. The nanowire thermal conductance has been measured using longitudinal 3ω technique with a highly sensitive thermometry based on niobium nitride (NbN) [12,10,11,13]. The Si nanowires are fabricated from silicon on insulator (SOI) substrates by e-beam lithography. The total length of each structure has been purposely set to 10 µm in order to easily compare the thermal measurement of all kinds of nanowires (see Fig. 3). The section of the nanowires is 100 nm by 200 nm. The central symmetry of the structures is necessary for the 3ω method employed to measure the thermal conductance [12].

The temperature profile looks like a parabola with the hottest point located at the center of the nanowire. The heat generated at each points of the suspended structure flows from the center to the heat bath on both sides. The thermal conductance is generally measured using a power of a few tens of femtowatts dissipated in the niobium nitride transducer deposited on top of the nanowires. This power creates on average a temperature gradient smaller than 1 mK. The values of the measured thermal conductance are around a few universal value of thermal conductance $K_0 = \pi^2 k_B^2 T/3h \sim 10^{-12} T$ W/K^2; a value used to normalized the data.

Equation (2) gives the correct order of magnitude for the thermal conductance, since a K value close to 10^{-11} W/K is predicted at 3 K and a value of 1.5×10^{-11} W/K is measured on a straight nanowire. For the explanation of the temperature variation of the thermal conductance, it is needed to take into account the contribution of specular reflection by introducing the Ziman mean free path, and hence the parameter p. This has been described in details in the past [10,11,14]. We would like to highlight here that the contribution of ballistic phonons to the thermal transport is significant. We have proposed a solution for thermal management that will not perturb diffusive transport but will affect only the ballistic one. Specific suspended nanowires have been made, including a double-bend chicane structures 400 nm in length; the total extended length of the S-shaped nanowire itself being identical to the one of the straight nanowire (see Fig. 3c and Fig. 4).

In recent works [14,15], we have shown that the S-shaped nanowires have a much lower thermal conductance than the straight one, as it can be seen in Fig. 4. If transport were only diffusive, this constriction would have no effect at all on thermal conductance. Actually, the severe reduction observed (reduction by more than 30 %) demonstrates two significant facts: first, this illustrates the contribution of ballistic phonons to thermal transport and second, including a chicane in a thermal conductor is a very efficient way of reducing thermal transport. Phonons having long mean free path (bigger than the Casimir mean free path Λ_{Cas}) will be blocked and reflected by the chicane acting like a mirror for the long-wavelength acoustic plane waves. Conversely, short-wavelength phonons that are more scattered by the nanowire surfaces will not be much affected by the chicane, their mean free path being already set by the section of the nanowire like in the Casimir

Please cite this article in press as: O. Bourgeois et al., Reduction of phonon mean free path: From low-temperature physics to room temperature applications in thermoelectricity, C. R. Physique (2016), http://dx.doi.org/10.1016/j.crhy.2016.08.008

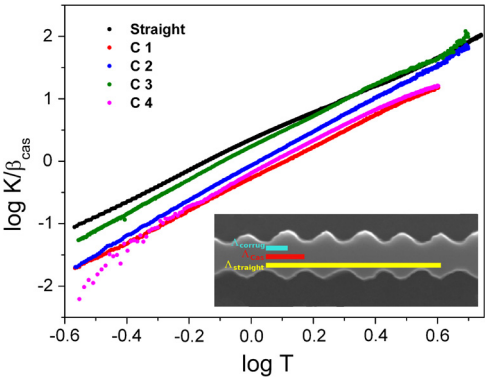

Fig. 5. Normalized thermal conductance versus temperature for a straight nanowire (Straight) and four corrugated nanowires (C1 to C4) in a log–log plot. The normalization coefficient β_{Cas} corresponds to the Casimir limit value of the thermal conductance at 1 K. The corrugated nanowire C_i can have much lower thermal conductance that smooth nanowire. The phonon MFP is reduced severely, even below the Casimir limit. As an illustration, in insert we compare the average phonon mean free path in the straight nanowire (in yellow), in the Casimir limit (in red), and as measured in corrugated nanowire (in blue). The corrugations reduce significantly the phonon mean free path.

regime. This concept has been successfully used to thermally isolate a suspended platform dedicated to sensitive thermal measurements [16].

2.3. Reduced thermal transport in corrugated nanowires

In the previous section, we have seen how a macroscopic constriction can act as a phonon filter. In this section, we will illustrate how phonon backscattering or multiple scatterings can be introduced by using nano-engineered surfaces. In this respect, phononic crystals, defined as a regular modulation of the geometry of a phonon waveguide, have attracted significant attention in the past decade as a promising means to reduce phonon transport. In the present samples, periodic nanostructurations are used (see Fig. 5) to induce phonon backscattering and reduce incoherently the thermal conductance, not coherently like in a real thermocrystal. We have reported that in that kind of engineered corrugated nanowires, phonon transport can be decreased even below the Casimir limit [15,17].

In order to compare thermal transport between various geometries of nanowires, the thermal conductances have to be normalized to a geometrical factor called the Casimir coefficient β_{Cas}, according to Eqs. (2) and (3). Fig. 5 reports the thermal conductance plotted as K/β_{Cas}.

This normalization yields the temperature power law and allows a direct comparison between the thermal transport of each nanowire. Indeed, from Eqs. (2) and (3), the normalized conductance can be expressed as:

$$\log(K/\beta_{Cas}) = a + b\,\log(T) \tag{4}$$

where

$$(K/\beta_{Cas}) = \frac{1+p}{1-p}\,T^b \tag{5}$$

From these two equations, we can extract the power-law factor b of the temperature variation of the thermal conductance, the value of the MFP Λ_{eff} and the parameter p [15,17].

The thermal conductance of the corrugated nanowires is clearly below the thermal conductance of straight nanowires, even if the power law has not been changed; it is very close to 3 ($b \approx 2.6$). The presence of artificial periodic nanostructuration increases phonon scattering (backscattering, phonon trapping etc.). Surface roughness is not changed, but the mean free path is clearly reduced. This can be depicted by ray-tracing Monte Carlo numerical simulations. Indeed, the multiple scattering of ballistic phonons can be seen through a corpuscular picture explaining the fact that the phonons are somehow trapped in the core of the nanowire. As a consequence, the phonon MFP that can be even smaller than the Casimir limit, i.e. smaller than the mean diameter of the nanowire. This is characterized by the necessity of putting a negative p parameter to fit the data. Even if this special result does not involve phonon band engineering like in a real phononic crystal, it gives however a fantastic way of turning a single-crystal semiconductor into a phonon glass.

3. In the diffusive limit: nano-inclusions limit thermal conductivity in semiconductors

After having shown in details the different ways of affecting the thermal transport in the presence of ballistic phonons, we will focus now on room-temperature effects where the diffusive regime is governing the thermal conductivity. We will show that engineering the phonon thermal properties is also possible with a semiconductor at room temperature (RT). As

Please cite this article in press as: O. Bourgeois et al., Reduction of phonon mean free path: From low-temperature physics to room temperature applications in thermoelectricity, C. R. Physique (2016), http://dx.doi.org/10.1016/j.crhy.2016.08.008

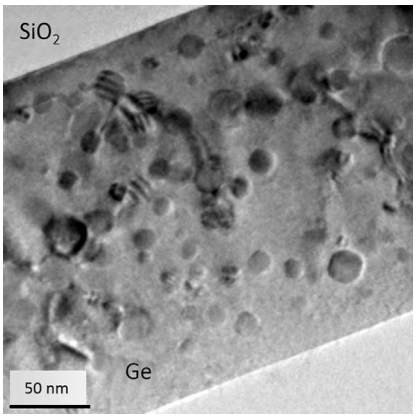

Fig. 6. TEM image of the germanium matrix with GeMn spherical nano-inclusions at 8 % of Mn. The presence of numerous inclusions will significantly increase the phonon scattering without perturbing the electronic transport. The scale bar represents 50 nm. The distance between the nano-inclusions is indeed smaller than the average phonon mean free path.

compared to the ballistic limits, working at RT in the diffusive limit will have significant implications for real applications in managing heating, cooling, or harvesting energy.

The great challenges mostly rely on our capacity to improve the performances of semiconductor materials. As, on the one hand, a semiconductor is by far too thermally conductive (around 100 W/mK), on the other hand its Seebeck coefficient is generally quite high (above 200 μV/K). Then, obtaining an efficient thermoelectric material having a high ZT based on a semiconductor is possible by decreasing significantly its thermal conductivity.

The increase in the thermoelectric efficiency is feasible thanks to the difference of mean free path existing between phonons (∼100 nm at 300 K) and electrons (∼1 nm at 300 K). By introducing in a given material a structural disorder at the nanometer scale, it is possible to induce phonon diffusion without affecting charge carriers, justifying the innovative concept of *electron crystal–phonon glass* material.

Indeed, in a semiconducting matrix, phonons contribute the most to heat transport, having an average mean free path of ∼100 nm at room temperature and a dominant wavelength of 1 nm at RT. With the objective of manipulating and controlling phonon transport in a SC, the engineering of materials can then follow the two different approaches mentioned in the introduction: either by playing with phonon wavelength [18–21] or with phonon mean free path [17,20,21]. At room temperature, the most efficient effect will be the reduction in the phonon mean free path using a geometrical scattering approach. Indeed, as it has been recently experimentally demonstrated, the phonon wavelength is far two small at RT for the nanostructuration to create sizable effects [20,21].

The best large-scale applicability is expected from bulk 3D SC material that has been engineered at the low dimension for thermal management. One of the most important concepts is the *electron crystal–phonon glass*, being an inclusion-embedded semiconducting system, which shows great advantages and potentials [22]. For crystalline semiconductors, the ideal model would be a defect-free highly crystalline matrix containing nanoscaled inclusions with a wide diameter distribution. It can be theoretically predicted that as the inter-distance of the inclusions is comparable to the phonon mean free path in the matrix, the nano-inclusions can prohibit efficiently phonon transport. Indeed, by introducing more phonon scattering processes, we expect to get a germanium based *electron crystal–phonon glass* material.

The materials of interest here are thin films of a single-crystalline germanium matrix embedded with randomly distributed Ge_3Mn_5 nano-inclusions grown by epitaxy on a germanium substrate (see Fig. 6). The nano-inclusions are found to be nearly spherical with a diameter distribution from 5 to 50 nm, depending on the growth parameters. Furthermore, manganese atoms act as p-type dopant in the Ge matrix, which ensures a good electrical conductivity of the material.

The experimental measurements of the thermal conductivities of the Ge:Mn materials have been done using a highly sensitive differential 3ω technique [23]. Experimental results of 3ω measurements revealed strong reductions in the thermal conductivity, compared to the Ge bulk at room temperature, for Ge:Mn thin films containing different Mn concentrations.

The major experimental finding is a reduction by more than a factor of ten with respect to the bulk value when there are 8 % of Mn in the Ge matrix. A thermal conductivity below 8 W/mK has been measured, which has to be compared to the bulk thermal conductivity, i.e. 65 W/mK. The reduction is fully ascribed to the presence of evenly distributed phonon scatterers that significantly reduce the phonon mean free path.

4. Conclusions

Different concepts of phonon thermal transport reduction have been shown experimentally, from the ballistic limit to the diffusive limit. These new paradigms will be fruitfully applied for the development of new materials or devices in thermoelectricity and energy harvesting in general. It seems that now, we are facing a kind of intrinsic limit in that reduction by non-coherent effects, a lower limit close to the value of the alloy's thermal conductivity. Unfortunately, engineering the

Please cite this article in press as: O. Bourgeois et al., Reduction of phonon mean free path: From low-temperature physics to room temperature applications in thermoelectricity, C. R. Physique (2016), http://dx.doi.org/10.1016/j.crhy.2016.08.008

phonon band by opening gaps like in a phononic crystal seems inappropriate for room-temperature thermal management, because phonon wavelengths are far too small as compared to the length accessible by current fabrication methods.

Other technological solutions may be found in playing also on the electrical properties of semiconductor-based systems to improve the Seebeck coefficient. Indeed, as proposed by Hicks and Dresselhaus [5], it could be possible to increase the Seebeck coefficient by playing with the electronic density of state at the Fermi level. Then, engineering the electronic properties by various means (nanostructuration, adding quantum dots, etc.) seems absolutely necessary if one wants to boost the performances of future thermoelectric materials.

Acknowledgements

We acknowledge technical supports from Nanofab, the Cryogenic and the Electronic facilities and the “Pôle Capteur thermométrique et Calorimétrie” of the Institut Néel for these experiments. Funding for this project was provided by a grant from the “Région Rhône-Alpes” (Cible), by the “Agence nationale de la recherche” (ANR) through the project QNM No. 0404 01 and Mesophon grant No. 15-CE30-0019 by the European Projects: MicroKelvin FP7 low-temperature infrastructure, Grant No. 228464, and MERGING Grant No. 309150.

References

[1] D.G. Cahill, W.K. Ford, K.E. Goodson, G.D. Mahan, A. Majumdar, H.J. Maris, R. Merlin, S.R. Phillpot, J. Appl. Phys. 93 (2003) 793.
[2] A. Shakouri, Annu. Rev. Mater. Res. 41 (2011) 399.
[3] D.G. Cahill, P.V. Braun, G. Chen, D.R. Clarke, S.H. Fan, K.E. Goodson, P. Keblinski, W.P. King, G.D. Mahan, A. Majumdar, H.J. Maris, R. Merlin, S.R. Phillpot, E. Pop, L. Shi, J. Appl. Phys. 1 (2014) 011305.
[4] S. LeBlanc, S.K. Yee, M.L. Scullin, C. Dames, K.E. Goodson, Renew. Sustain. Energy Rev. 32 (2014) 313.
[5] L.D. Hicks, M.S. Dresselhaus, Phys. Rev. B 47 (1993) 16631.
[6] M.S. Dresselhaus, G. Chen, M.Y. Tang, R.G. Yang, H. Lee, D.Z. Wang, R.F. Ren, J.P. Fleurial, P. Gogna, Adv. Mater. 19 (2007) 1.
[7] H.B.G. Casimir, Physica 5 (6) (1938).
[8] J.M. Ziman, Electrons and Phonons, Clarendon Press, Oxford, UK, 2001.
[9] R. Berman, E.L. Foster, J.M. Ziman, Proc. R. Soc. Lond. Ser. A 231 (1955) 130.
[10] J.S. Heron, T. Fournier, N. Mingo, O. Bourgeois, Nano Lett. 9 (2009) 1861.
[11] J.S. Heron, T. Fournier, N. Mingo, O. Bourgeois, Nano Lett. 10 (2010) 2288.
[12] O. Bourgeois, T. Fournier, J. Chaussy, J. Appl. Phys. 101 (2007) 016104.
[13] O. Bourgeois, E. André, C. Macovei, J. Chaussy, Rev. Sci. Instrum. 77 (2006) 126108.
[14] J.S. Heron, C. Bera, T. Fournier, N. Mingo, O. Bourgeois, Phys. Rev. B 82 (2010) 155458.
[15] C. Blanc, J.-S. Heron, T. Fournier, O. Bourgeois, Appl. Phys. Lett. 105 (2014) 043106.
[16] S. Alaie, D.F. Goettler, K. Abbas, M.F. Su, C.M. Reinke, I. El-Kady, Z.C. Leseman, Rev. Sci. Instrum. 84 (2013) 105003.
[17] C. Blanc, A. Rajabpour, S. Volz, T. Fournier, O. Bourgeois, Appl. Phys. Lett. 103 (2013) 043109.
[18] N. Zen, T.A. Puurtinen, T.J. Isotalo, S. Chaudhuri, I.J. Maasilta, Nat. Commun. 5 (2014) 3435.
[19] M. Nomura, J. Nakagawa, Y. Kage, J. Maire, D. Moser, O. Paul, Appl. Phys. Lett. 106 (2015) 143102.
[20] J. Maire, R. Anufriev, H. Han, S. Volz, M. Nomura, arXiv:1508.04574.
[21] M.R. Wagner, B. Graczykowski, J.S. Reparaz, A. El Sachat, M. Sledzinska, F. Alzina, C.M. Sotomayor Torres, arXiv:1511.07398.
[22] W. Kim, J. Zide, A. Gossard, D. Klenov, S. Stemmer, A. Shakouri, A. Majumdar, Phys. Rev. Lett. 96 (2006) 045901.
[23] Y.Q. Liu, D. Tainoff, M. Boukhari, J. Richard, A. Barski, P. Bayle-Guillemaud, E. Hadji, O. Bourgeois, IOP Conf. Ser., Mater. Sci. Eng. 68 (2014) 012005.

Please cite this article in press as: O. Bourgeois et al., Reduction of phonon mean free path: From low-temperature physics to room temperature applications in thermoelectricity, C. R. Physique (2016), http://dx.doi.org/10.1016/j.crhy.2016.08.008